1
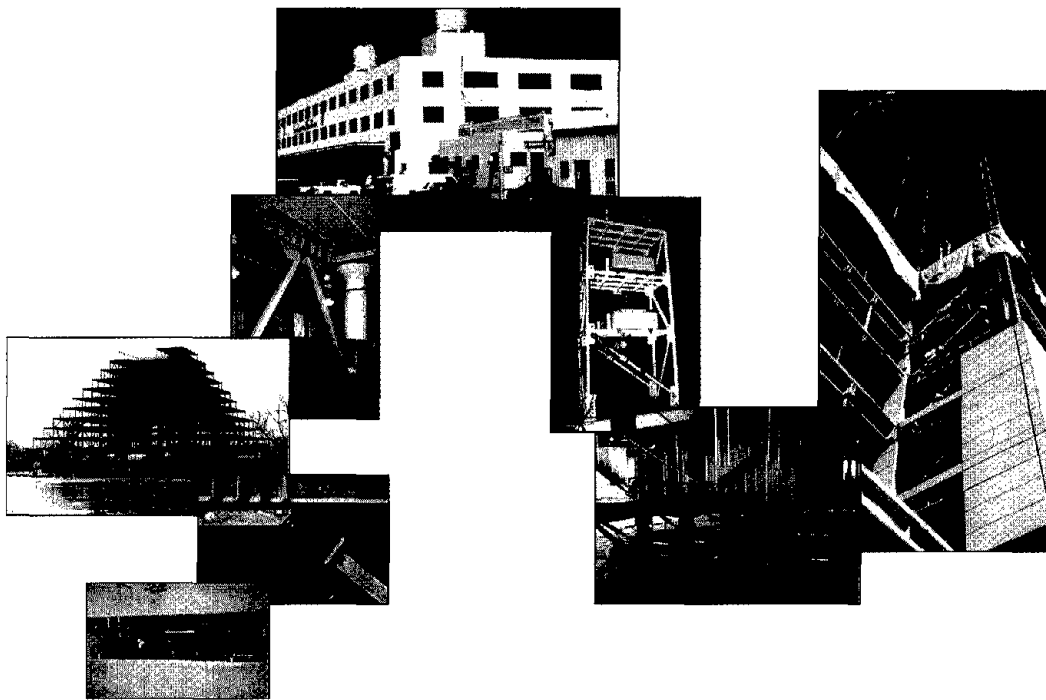
Passive Energy Dissipation Systems for Structural Design and Retrofit

M. C. Constantinou
T. T. Soong
G. F. Dargush

Monograph Series

Multidisciplinary Center for Earthquake Engineering Research
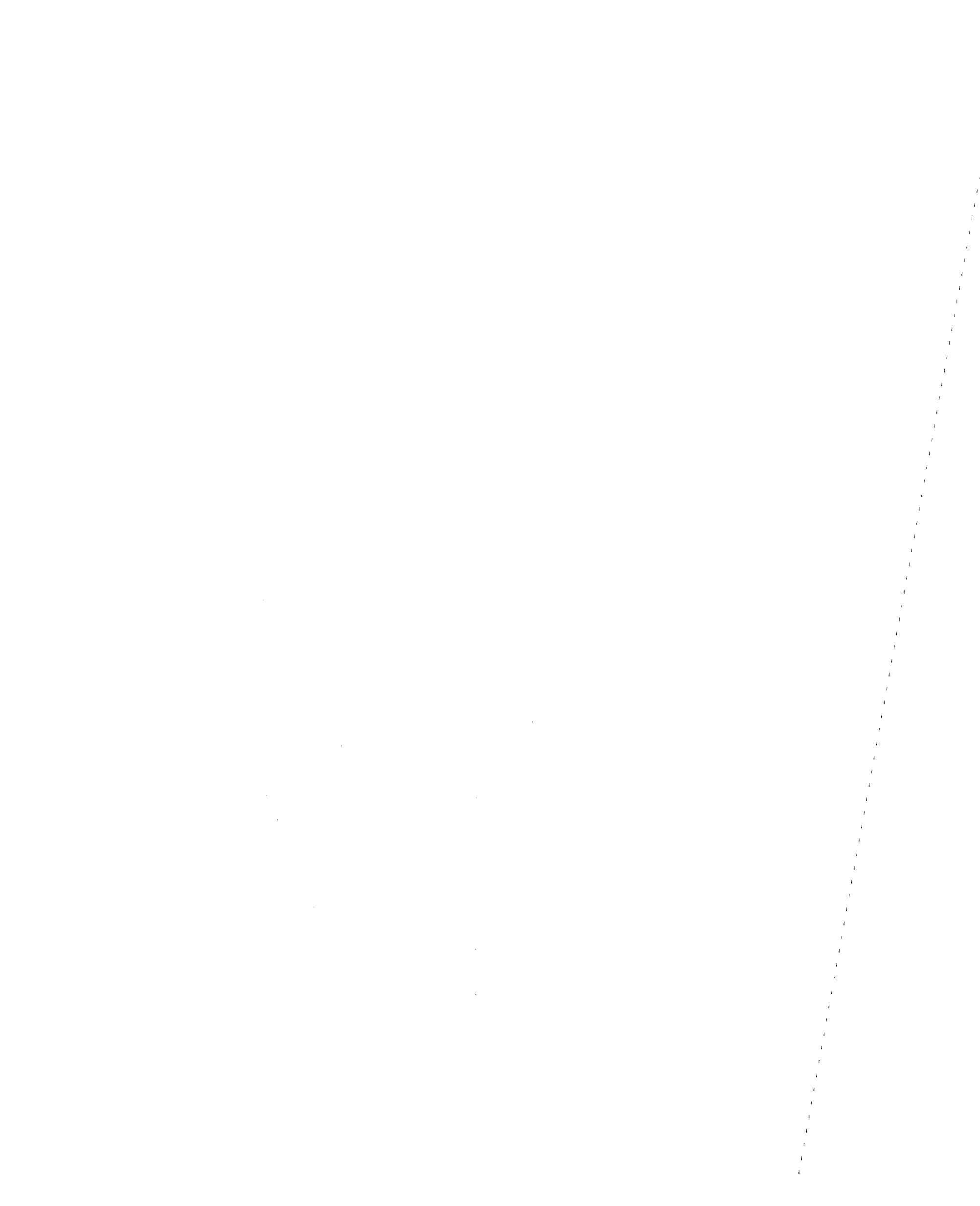A National Center of Excellence in Advanced Technology Applications

■ The Multidisciplinary Center for Earthquake Engineering Research

The Multidisciplinary Center for Earthquake Engineering Research (MCEER) is a national center of excellence in advanced technology applications that is dedicated to the reduction of earthquake losses nationwide. Headquartered at the State University of New York at Buffalo, the Center was originally established by the National Science Foundation (NSF) in 1986, as the National Center for Earthquake Engineering Research (NCEER).

Comprising a consortium of researchers from numerous disciplines and institutions throughout the United States, the Center's mission is to reduce earthquake losses through research and the application of advanced technologies that improve engineering, pre-earthquake planning and post-earthquake recovery strategies. Toward this end, the Center coordinates a nationwide program of multidisciplinary team research, education and outreach activities.

Funded principally by NSF, the State of New York and the Federal Highway Administration (FHWA), the Center derives additional support from the Federal Emergency Management Agency (FEMA), other state governments, academic institutions, foreign governments and private industry.

Passive Energy Dissipation Systems for Structural Design and Retrofit

PASSIVE ENERGY DISSIPATION SYSTEMS FOR STRUCTURAL DESIGN AND RETROFIT

by Michael C. Constantinou
Tsu T. Soong
Gary F. Dargush

F O R E W O R D

Earthquakes are potentially devastating natural events which threaten lives, destroy property, and disrupt life-sustaining services and societal functions. In 1986, the National Science Foundation established the National Center for Earthquake Engineering Research to carry out systems integrated research to mitigate earthquake hazards in vulnerable communities and to enhance implementation efforts through technology transfer, outreach, and education. Since that time, our Center has engaged in a wide variety of multidisciplinary studies to develop solutions to the complex array of problems associated with the development of earthquake-resistant communities.

Our series of monographs is a step toward meeting this formidable challenge. Over the past 12 years, we have investigated how buildings and their nonstructural components, lifelines, and highway structures behave and are affected by earthquakes, how damage to these structures impacts society, and how these damages can be mitigated through innovative means. Our researchers have joined together to share their expertise in seismology, geotechnical engineering, structural engineering, risk and reliability, protective systems, and social and economic systems to begin to define and delineate the best methods to mitigate the losses caused by these natural events.

Each monograph describes these research efforts in detail. Each is meant to be read by a wide variety of stakeholders, including academicians, engineers, government officials, insurance and financial experts, and others who are involved in developing earthquake loss mitigation measures. They supplement the Center's technical report series by broadening the topics studied.

As we begin our next phase of research as the Multidisciplinary Center for Earthquake Engineering Research, we intend to focus our efforts on applying advanced technologies to quantifying building and lifeline performance through the estimation of expected losses; developing cost-effective, performance-based rehabilitation technologies; and improving response and recovery through strategic planning and crisis management. These subjects are expected to result in a new monograph series in the future.

I would like to take this opportunity to thank the National Science Foundation, the State of New York, the State University of New

York at Buffalo, and our institutional and industrial affiliates for their continued support and involvement with the Center. I thank all the authors who contributed their time and talents to conducting the research portrayed in the monograph series and for their commitment to furthering our common goals. I would also like to thank the peer reviewers of each monograph for their comments and constructive advice.

It is my hope that this monograph series will serve as an important tool toward making research results more accessible to those who are in a position to implement them, thus furthering our goal to reduce loss of life and protect property from the damage caused by earthquakes.

GEORGE C. LEE

DIRECTOR, MULTIDISCIPLINARY CENTER

FOR EARTHQUAKE ENGINEERING RESEARCH

C O N T E N T S

P R E F A C E

Historically, aseismic design has been based upon a combination of strength and ductility. For small, frequent seismic disturbances, the structure is expected to remain in the elastic range, with all stresses well below yield levels. However, it is not reasonable to expect that a traditional structure will respond elastically when subjected to a major earthquake. Instead, the design engineer relies upon the inherent ductility of buildings to prevent catastrophic failure, while accepting a certain level of structural and nonstructural damage. This philosophy has led to the development of aseismic design codes featuring lateral force methods and, more recently, inelastic design response spectra. Ultimately, with these approaches, the structure is designed to resist an 'equivalent' static load. Results have been reasonably successful. Even an approximate accounting for lateral effects will almost certainly improve building survivability.

However, by considering the actual dynamic nature of environmental disturbances, more dramatic improvements can be realized. As a result of this dynamical point of view, new and innovative concepts of structural protection have been advanced and are at various stages of development. Modern structural protective systems can be divided into three major groups:

- **Seismic Isolation**
    Elastomeric Bearings
    Lead Rubber Bearings
    Combined Elastomeric and Sliding Bearings
    Sliding Friction Pendulum Systems
    Sliding Bearings with Restoring Force

- **Passive Energy Dissipation**
    Metallic Dampers
    Friction Dampers
    Viscoelastic Solid Dampers
    Viscoelastic or Viscous Fluid Dampers
    Tuned Mass Dampers
    Tuned Liquid Dampers

- **Semi-active and Active Systems**
  Active Bracing Systems
  Active Mass Dampers
  Variable Stiffness and Damping Systems
  Smart Materials

These groups can be distinguished by examining the approaches employed to manage the energy associated with transient environmental events.

The technique of seismic isolation is now widely used in many parts of the world. A seismic isolation system is typically placed at the foundation of a structure. By means of its flexibility and energy absorption capability, the isolation system partially reflects and partially absorbs some of the earthquake input energy before this energy can be transmitted to the structure. The net effect is a reduction of energy dissipation demand on the structural system, resulting in an increase in its survivability.

On the other end of the spectrum are semi-active and active control systems. Semi-active and active structural control is an area of structural protection in which the motion of a structure is controlled or modified by means of the action of a control system through some external energy supply. However, semi-active systems require only nominal amounts of energy to adjust their mechanical properties and, unlike fully active systems, they cannot add energy to the structure. Considerable attention has been paid to semi-active and active structural control research in recent years, with particular emphasis on the alleviation of wind and seismic response. The technology is now at the stage where actual systems have been designed, fabricated and installed in full-scale structures.

While all these technologies are likely to have an increasingly important role in structural design, the scope of the present monograph is limited to a discussion of passive energy dissipation systems, and, to a limited extent, semi-active devices. Research and development of passive energy dissipation devices for structural applications have roughly a 25-year history. The basic function of passive energy dissipation devices when incorporated into the superstructure of a building is to absorb or consume a portion of the input energy, thereby reducing energy dissipation demand on primary structural members and minimizing possible structural damage. Unlike seismic isolation, however, these devices can be effective against wind induced motions as well as those due to earthquakes. Contrary to active control systems, there is no need for an external supply of power.

In recent years, serious efforts have been undertaken to develop the concept of energy dissipation or supplemental damping into a workable technology, and a number of these devices have been installed in

structures throughout the world. This monograph introduces the basic concepts of passive energy dissipation, and discusses current research, development, design and code-related activities in this exciting and fast expanding field. At the same time, it should be emphasized that this entire technology is still evolving. Significant improvements in both hardware and design procedures will certainly continue for a number of years to come.

ACKNOWLEDGMENTS

ABBREVIATIONS

AC	Active Control
ADAS	Added Damping and Stiffness
AMD	Active Mass Damper
ATC	Applied Technology Council
ATMD	Active Tuned Mass Damper
AVD	Active Variable Damping
AVS	Active Variable Stiffness
BF	Bare Frame
BMR	Braced Moment Resisting
BOCA	Building Officials and Code Administrators
BSCLIM	Base Shear Coefficient Limit
CC	Control Computer
CDMG	California Division of Mines and Geology
DOF	Degree-of-Freedom
DTMD	Doubly-Tuned Mass Damper
DUOX	Dual-Mass System
EDR	Energy Dissipating Restraint
EDS	Energy Dissipation Systems
FDB	Frictional Damped Braced
FEM	Finite Element Method
FEMA	Federal Emergency Management Agency
HD	Passive High Damping Viscous System
HMD	Hybrid Mass Damper
ICBO	International Conference of Building Officials
IMSS	Mexican Institute of Social Security
LD	Passive Low Damping Viscous System

MDOF	Multiple-Degree-of-Freedom
MR	Moment Resisting
MTMD	Multiple Tuned Mass Dampers
NEHRP	National Earthquake Hazards Reduction Program
OPT	Optimal Control Algorithm
PED	Passive Energy Dissipation Systems
RMS	Root Mean Square
S/A	Semi-Active
SBC	Slotted Bolted Connection (Chapter 4)
SBC	Standard Building Code (Chapter 6)
SDOF	Single-Degree-of-Freedom
SEAONC	Structural Engineers Association of Northern California
SMA	Shape Memory Alloy
SMC	Sliding Mode Control Algorithm
SME	Shape Memory Effect
SRSS	Square Root of Sum of Squares
TLCD	Tuned Liquid Column Damper
TLD	Tuned Liquid Damper
TMD	Tuned Mass Damper
UBC	Uniform Building Code
USGS	United States Geological Survey
VDW	Viscous Damping Wall
VE	Viscoelastic

1

INTRODUCTION

1.1

SEISMIC DESIGN

In conventional seismic design, acceptable performance of a structure during earthquake shaking is based on the lateral force resisting system being able to absorb and dissipate energy in a stable manner for a large number of cycles. Energy dissipation occurs in specially detailed ductile plastic hinge regions of beams and column bases, which also form part of the gravity load carrying system. Plastic hinges are regions of concentrated **damage** to the gravity frame, which often is irreparable. Nevertheless, this design approach is acceptable because of economic considerations provided, of course, that structural collapse is prevented and life safety is ensured.

Situations exist in which the conventional design approach is not applicable. When a structure must remain functional after an earthquake, as is the case of important structures (hospitals, police stations, etc.), the conventional design approach is inappropriate. For such cases, the structure may be designed with sufficient strength so that inelastic action is either prevented or is minimal; an approach that is very costly. Moreover, in such structures, special precautions need to be taken in safeguarding against damage or failure of important secondary systems, which are needed for continuing serviceability. The recent experience with two of the newest hospital facilities in the Northridge earthquake (Earthquake Engineering Research Institute, 1995) demonstrates problems that may occur with such a design approach.

Moreover, a large number of older structures have insufficient lateral strength and lack the detailing required for ductile behavior. Seismic retrofitting of these structures is necessary and may be achieved by conventional seismic design, although often

at significant cost and with undesirable disruption of architectural features. The latter is a significant consideration in the seismic retrofit of historic structures with important architectural features.

Alternate design procedures have been developed which incorporate **earthquake protective systems** in the structure. These systems may take the form of seismic isolation systems or supplemental energy dissipation devices. An examination of the behavior and effects of these systems may begin with the consideration of the distribution of energy within a structure. During a seismic event, a finite quantity of energy is input into a structure. This input energy is transformed into both kinetic and potential (strain) energy which must be either absorbed or dissipated through heat. If there were no damping, vibrations would exist for all time. However, there is always some level of inherent damping which withdraws energy from the system and therefore reduces the amplitude of vibration until the motion ceases. The structural performance can be improved if a portion of the input energy can be absorbed, not by the structure itself, but by some type of supplemental "device". This is made clear by considering the conservation of energy relationship (Uang and Bertero, 1988):

$$E = E_k + E_s + E_h + E_d \qquad (1\text{-}1)$$

where E is the absolute energy input from the earthquake motion, E_k is the absolute kinetic energy, E_s is the recoverable elastic strain energy, E_h is the irrecoverable energy dissipated by the structural system through inelastic or other forms of action, and E_d is the energy dissipated by supplemental damping devices. The absolute energy input E, represents the work done by the total base shear force at the foundation on the ground (foundation) displacement. It, thus, contains the effect of the inertia forces of the structure.

In the conventional design approach, acceptable structural performance is accomplished by the occurrence of inelastic deformations. This has the direct effect of increasing energy E_h. It also has an indirect effect. The occurrence of inelastic deformations results in softening of the structural system which itself modifies the absolute input energy. In effect, the increased flexibility acts as a filter which reflects a portion of the earthquake energy.

The significant result is that it leads to reduced accelerations and reduced strains in regions away from the plastic hinges.

The technique of seismic isolation accomplishes the same task by the introduction, at the foundation of a structure, of a system which is characterized by flexibility and energy absorption capability. The flexibility alone, typically expressed by a period of the order of 2 seconds, is sufficient to reflect a major portion of the earthquake energy so that inelastic action does not occur. Energy dissipation in the isolation system is then useful in limiting the displacement response and in avoiding resonances. However, in earthquakes rich in long period components, it is not possible to provide sufficient flexibility for the reflection of the earthquake energy. In this case, energy absorption plays an important role.

Modern seismic isolation systems incorporate energy dissipating mechanisms. Examples are high damping elastomeric bearings, lead plugs in elastomeric bearings, mild steel dampers, fluid viscous dampers, and friction in sliding bearings.

Another approach to improving earthquake response performance and damage control is that of supplemental energy dissipation systems. In these systems, mechanical devices are incorporated into the frame of the structure and dissipate energy throughout the height of the structure. The means by which energy is dissipated is either yielding of mild steel, sliding friction, motion of a piston or a plate within a viscous fluid, orificing of fluid, or viscoelastic action in polymeric materials.

In addition to increasing the energy dissipation capacity per unit drift of a structure, some energy dissipation systems also increase the strength and stiffness. Such systems include the following types of energy dissipation devices: metallic-yielding, friction, and viscoelastic. Energy dissipation systems utilizing fluid viscous dampers will not generally increase the strength or stiffness of a structure unless the excitation frequency is high. For example, Figure 1.1 shows force-deformation curves of a simple one-story structure with and without energy dissipation systems (EDS). The curves are shown to extend well into the inelastic range, as expected to be the case in applications of seismic hazard mitigation. The addition of energy dissipation systems increases the strength and/or stiffness of the structure. In general, the addition of an energy dissipation system will result in a reduction in drift and, therefore, reduction of damage (due to energy dissipa-
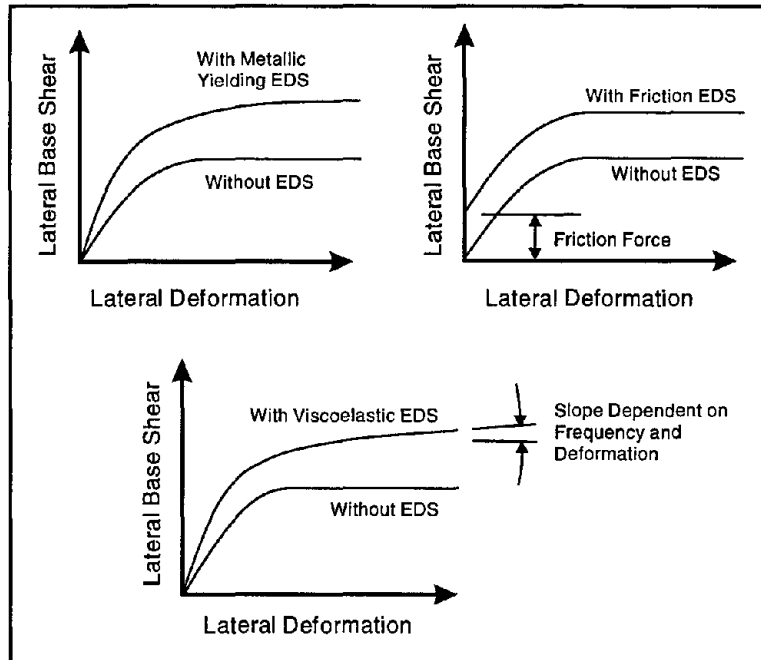
■ Figure 1.1 Effect of Energy Dissipation Systems on Force-Deformation Curves of a Structure

tion) and an increase in the total lateral force exerted on the structure (due to increased strength and/or stiffness). Reduction of both drift and total lateral force may be achieved only when deformations are reduced to levels below the elastic limit.

1.2

MOTION CONTROL SYSTEMS

Seismic isolation and energy dissipation systems are classified as earthquake protection systems since their function is to mitigate earthquake hazard. Mitigation is defined as the action taken to reduce the consequences of earthquakes, such as seismic strengthening or upgrading, installation of a seismic isolation or energy dissipation system, etc. However, energy dissipation systems are also useful in reducing dynamic response under wind and other types of service loads. Thus in general, seismic isolation and energy dissipation systems may be termed motion control systems.

The subject of this monograph is passive and, to a lesser extent, semi-active control systems. The term control systems denotes what was previously termed energy dissipation systems, whereas the terms passive and semi-active denote, respectively, systems that require no externally supplied power and systems that require minimal externally supplied power to operate. The latter may be considered as rather natural modifications of certain passive systems. Moreover, this monograph briefly describes dynamic vibration absorbers which are motion control systems, whose application is restricted to certain elastic structures under service and wind loading.

Dynamic vibration absorbers are oscillators which, when attached to a structure and tuned to a frequency close to that of a vibrating mode, cause an increase in damping of this mode as a result of transfer of kinetic energy among vibrating modes. Dynamic vibration absorbers may take the form of tuned mass dampers, tuned liquid dampers, tuned liquid column dampers as well as the form of arrays of such devices, each one tuned at a different frequency (Den Hartog, 1956; International Association for Structural Control, 1994; Sakai, 1989; Kareem, 1994; Soong and Constantinou, 1994).

Dynamic vibration absorbers have been used for the reduction of response of structures subjected to wind excitation, occupant activity and machine vibration. Typically, the application is restricted to structures which remain in the elastic range. Many of the applications are in tall modern buildings with very small inherent damping. In these cases, dynamic vibration absorbers can enhance damping by a small amount (typically, less than about 5% of critical), which is sufficient to suppress wind induced motion for the comfort of occupants. The effectiveness of dynamic vibration absorbers is significantly reduced when the structural system undergoes inelastic action. The reasons for this reduction in effectiveness are (a) de-tuning of the absorbers when inelastic action occurs, and (b) the enhancement of damping is insignificant in comparison to that generated by inelastic action.

The distinction between passive and active control systems is shown in Figures 1.2 and 1.3, which depict the elements of these systems. A passive control system, whether an energy dissipation system or a dynamic vibration absorber (or even a seismic isolation system), develops motion control forces at the points of attachment of the system. The power needed to generate these
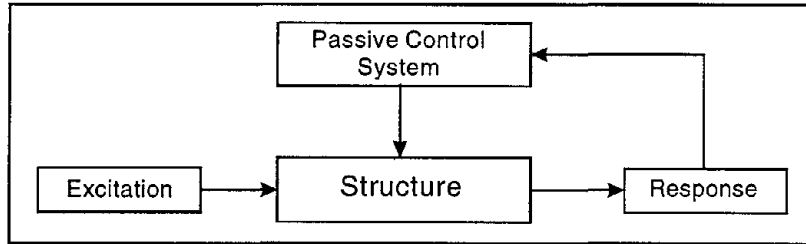
■ Figure 1.2 Elements of a Passive Control System

forces is provided by the motion of the points of attachment during dynamic excitation. The relative motion of these points of attachment determine the amplitude and direction of the control forces. For example, the seismic isolation system of the San Bernardino County Medical Center (Soong and Constantinou, 1994) includes 184 passive fluid viscous dampers, each capable of delivering 1400 kN force at velocity of 1.5 m/s and stroke of ±0.6 m. The power needed to operate each of these devices is 2100 kW or about 2800 hp. This power is provided by the relative motion of the isolation basemat and foundation to which these devices are attached.
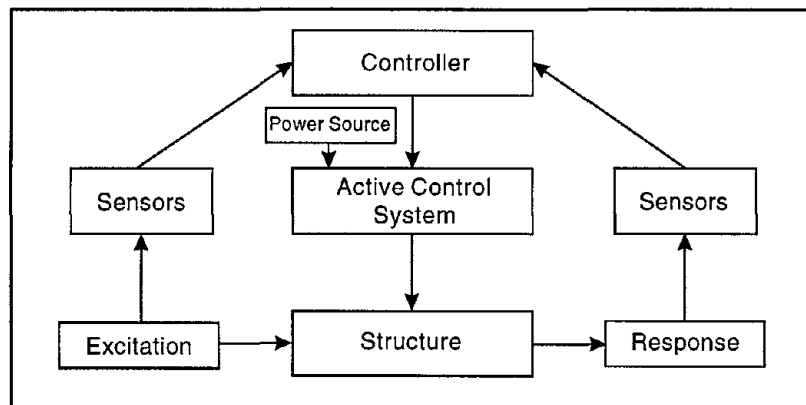
■ Figure 1.3 Elements of an Active Control System

An active control system also develops motion control forces as shown in Figure 1.3. However, the magnitude and direction of these forces are determined by a controller based on information from sensors and a control strategy (algorithm), and supplied by the active control system. For an active system, the forces may be developed by electro-hydraulic actuators (Soong, 1990; Reinhorn et al., 1992; International Association for Struc-

tural Control, 1994), which need to be fully powered by a hydraulic power source. Depending on the application, the power demand may be large. However, an active control system should, in principle, provide for better or more versatile response control.

Semi-active control systems generally originate from passive control systems which have been modified to allow for adjustment of their mechanical properties. Specifically, energy dissipation devices which operate through shearing of viscous fluid, orificing of fluid, or sliding friction have been modified to behave in a semi-active manner (International Association for Structural Control, 1994; also Symans and Constantinou, 1995 for a review).

The mechanical properties of semi-active control systems may be adjusted by a controller in the manner depicted in Figure 1.3 (per active control systems). However, the control forces are developed as a result of motion of the points of attachment of the semi-active devices (per passive control systems). Semi-active control systems require a power source for the adjustment of the mechanical properties of the system. The power demand is typically very small and remotely related to the power output of the system. For example, direct-drive servovalves have been used by Symans and Constantinou, 1995 in semi-active fluid dampers. These servovalves could adjust the flow characteristics of devices capable of delivering an output force of about 150 kN at velocities of about 350 mm/s (power of 52 kW or 70 hp). The servovalves only required 3.5 W power to operate, which could be supplied by a battery. An introduction to semi-active control is provided in Chapter 7.

The primary focus of this monograph, however, is on passive energy dissipation systems. The material spans basic principles and methods of analysis (Chapter 2), mathematical modeling of these systems together with analysis of structures equipped with passive energy dissipation systems (Chapter 3), recent analytical and experimental developments (Chapter 4), a review of recent applications (Chapter 5), and code development (Chapter 6). The objective is to provide the reader with a sound working knowledge of passive energy dissipation systems and their structural applications, in terms of both new design and retrofit. The reader is referred to Soong and Dargush (1997) for a more in-depth treatment of the theory and applications of passive energy dissipation.

2

BASIC PRINCIPLES

This chapter presents the principles of operation of passive energy dissipation systems. The presentation starts with illustrative examples of application of these systems on a structural frame. Through qualitative arguments, some general conclusions are established for the range of applicability of these systems and for the effects they have on the response of the frame. Subsequently, a treatment of linear viscoelastically damped structures (that is, linear elastic structures with viscoelastic energy dissipation systems) is presented. The lack of nonlinearity in these structures allows for a formal treatment of the problem and prepares the ground for presentation of simplified nonlinear methods of analysis, which are presented next.

Finally, the use of energy dissipating devices as elements of seismic isolation systems and the use of seismic isolation bearings to primarily absorb seismic energy rather than to lengthen the period are briefly discussed.

2.1

CLASSIFICATION

Passive energy dissipation systems are classified herein as hysteretic, viscoelastic and others. Examples of hysteretic systems include devices based on yielding of metals or through sliding friction. Figure 2.1 shows typical force-displacement loops of hysteretic energy dissipation systems. The simplest models of hysteretic behavior involve algebraic relations between force and displacement. Hence, hysteretic systems are often called displacement-dependent (e.g. FEMA, 1997). In this respect, shape memory alloy devices are also classified as hysteretic (or displacement-dependent) systems despite the fact that their force-displacement loops resemble those of Figure 2.3 for other systems, rather than those of Figure 2.1 for hysteretic systems.
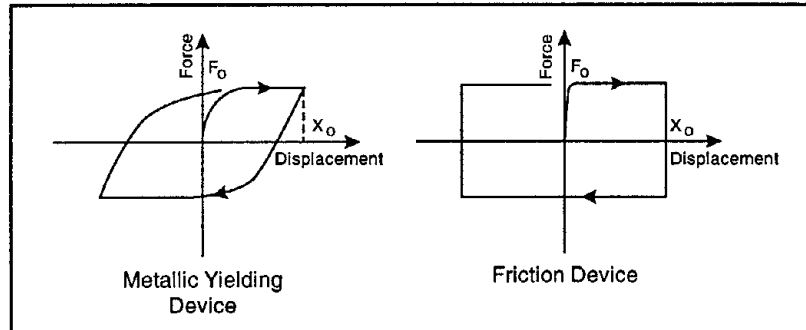
■ Figure 2.1 Idealized Force-Displacement Loops of Hysteretic Energy Dissipation Devices

Viscoelastic energy dissipation systems include devices consisting of viscoelastic solid materials, devices operating on the principle of fluid orificing (e.g. viscous fluid dampers) and devices operating by deformation of viscoelastic fluids. Figure 2.2 shows force-displacement loops of these devices. Typically, these devices exhibit stiffness and damping coefficients which are frequency dependent. Moreover, the damping force in these devices is proportional to velocity, that is, the behavior is viscous. Accordingly, they are classified as viscoelastic systems. A purely viscous device is a special case of a viscoelastic device with zero stiffness and frequency independent properties.
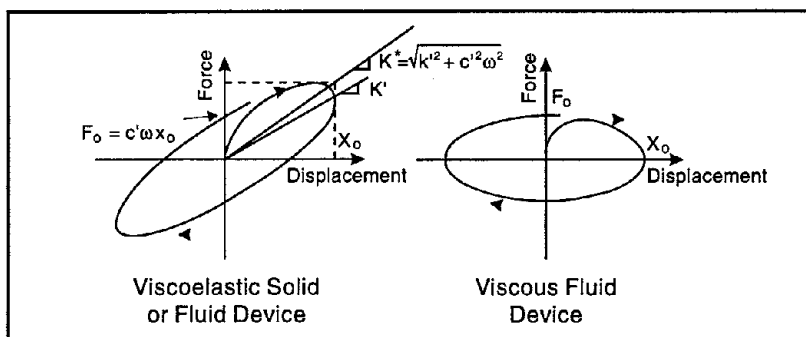
■ Figure 2.2 Idealized Force-Displacement Loops of Viscoelastic Energy Dissipation Devices

Energy dissipation systems which cannot be classified by one of the basic types depicted in Figure 2.1 and 2.2 are classified as other systems. Examples are friction-spring devices with re-
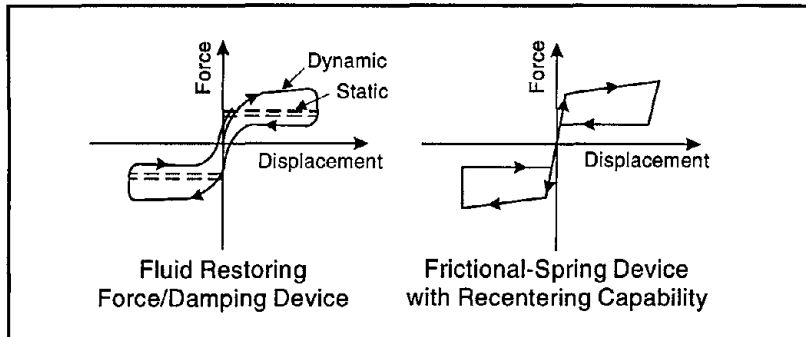
Figure 2.3 Idealized Force-Displacement Loops of Other Energy Dissipating Devices

centering capability and fluid restoring force and damping devices. Figure 2.3 illustrates the behavior of these devices. While the illustrated loops appear very different from those of Figures 2.1 and 2.2, in reality these devices originate from either hysteretic devices (a friction device with an innovative re-centering mechanism) or fluid viscous devices (a pressurized device to develop preload and re-centering capability, together with fluid orificing for energy dissipation).

2.2

ILLUSTRATIVE EXAMPLES OF APPLICATION

2.2.1 ELASTIC STRUCTURES

The frame of Figure 2.4 has been designed to remain elastic for the design earthquake. The so-called pushover (or capacity) curve of the frame is essentially linear. This curve is a plot of the sum of inertia forces on the structure (or base shear force) versus the top floor displacement (e.g., FEMA, 1997). Similarly, the corresponding force-displacement hysteresis loop depicts linear behavior and limited ability to absorb energy.

Consider the case when energy dissipating devices are added to the frame as shown in Figure 2.4. It is assumed that the
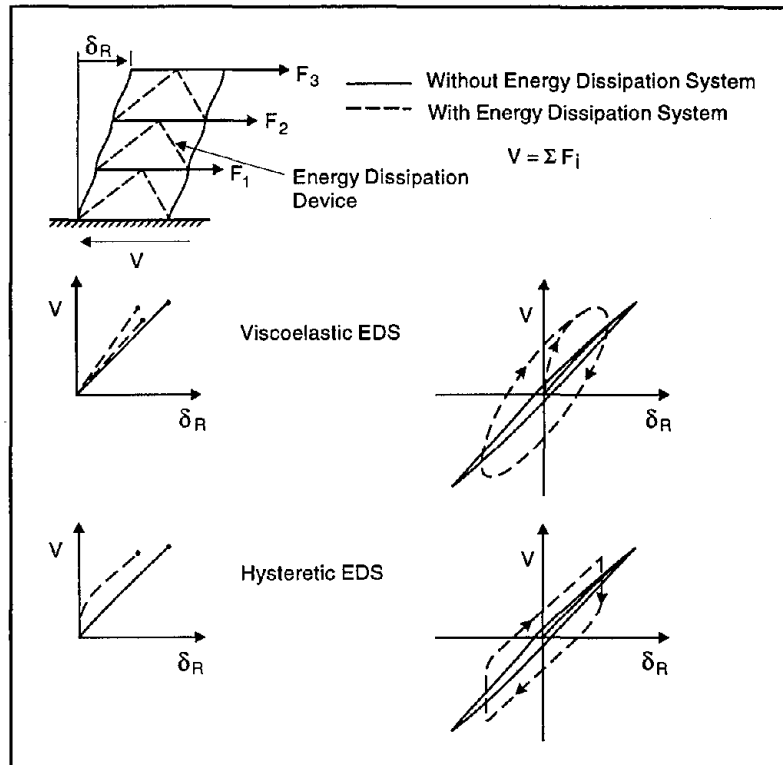
■ Figure 2.4 Pushover Curves and Force-Displacement Hysteresis Loops of an Elastic Structure Without and With Energy Dissipation Systems

connection details of the devices are such that neither inelastic action nor damage occurs in the frame at the points of attachment during seismic excitation. It is also assumed that the design of the energy dissipation system is such that it functions properly and dissipates energy throughout the height of the frame. This is particularly important in hysteretic energy dissipation systems, where an improper distribution of strength may result in concentration of inelastic action at a specific story level rather than over the entire height.

The ability of the frame to dissipate energy is substantially increased as demonstrated in the force-displacement hysteresis loops of the frame which are shown in Figure 2.4. Accordingly, the frame undergoes a considerably reduced amplitude of vibration in comparison to the frame without the energy dissipation system under the same earthquake motion.

While the energy dissipation system can achieve a considerable reduction in displacement response, it can also achieve a reduction in the total force exerted on the structure. In general, reduction in force will not be as much as reduction in displacement. This is due to the increased strength or increased stiffness provided by the energy dissipation system. Comparable reductions in displacement and force can be achieved with systems that do not increase the strength or stiffness of the structure to which they are attached. It should also be recognized that it is possible to have increases in force when the energy dissipation system causes substantial increases in either the strength or stiffness of the frame.

Most of the experimental work on energy dissipation systems has so far been performed with structures remaining in the elastic range (Lin et al., 1988; Whittaker et al., 1989; Aiken and Kelly, 1990; Chang et al., 1991; Constantinou and Symans, 1992; Seleemah and Constantinou, 1997). In general, these studies confirm the qualitative predictions of the illustrative example.

2.2.2 Yielding Structures with Proper Plastic Hinge Formation

Consider the frame of Figure 2.5 to have been designed for ductile behavior following the capacity design approach (e.g., Paulay and Priestley, 1992). As shown in Figure 2.5, plastic hinges develop in all the beams, a situation that results in stable hysteresis loops which resemble ideal hysteresis loops. Moreover, the frame undergoes substantial inelastic action under the design earthquake, which, as illustrated in the pushover curve of Figure 2.5, corresponds to global ductility of about 3.

The yielding frame has substantial ability to dissipate energy. Approximately, one can determine an effective damping ratio of at least 30% of critical for this frame. With such ability to dissipate energy, an increase in this ability due to the added energy dissipation system will not be very effective in further reducing the displacement of the frame. To approximately quantify this further response reduction, Figure 2.6 was prepared from data in FEMA, 1997. The figure presents plots of the displacement response ratio of a structure in which an energy dissipating system caused an increase in the damping ratio by either 10 or 20 or 30%
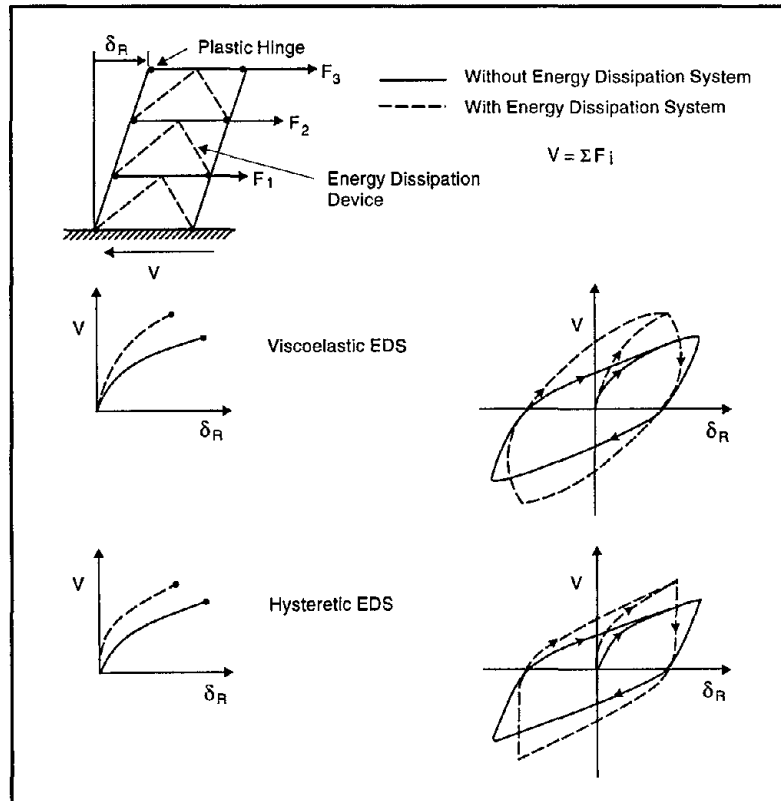
Figure 2.5 Pushover Curves and Force-Displacement Hysteresis Loops of a Yielding Structure Having Proper Plastic Hinge Formation Without and With Energy Dissipation Systems

of critical. The damping ratio of the structure without the energy dissipation system is shown to be in the range of 1 to 30% of critical. The response ratio shown here is valid for the so-called velocity domain of the response spectrum (long period range).

As shown in Figure 2.6, a structure with a damping ratio of 1 to 3% of critical (this has been the case in the experimental studies of Lin et al., 1988; Whittaker et al., 1989; Aiken and Kelly 1990; Chang et al., 1991; and Constantinou and Symans, 1992) will have its response reduced to approximately one half (reduction by 50%) when an energy dissipating system enhances damping by 20 to 30% of critical. However, when the structure has a damping ratio of 30%, an increase of damping by 20 to 30% of critical will cause a reduction of response to approximately 0.85 of the value without the energy dissipation system (reduction by 15%).
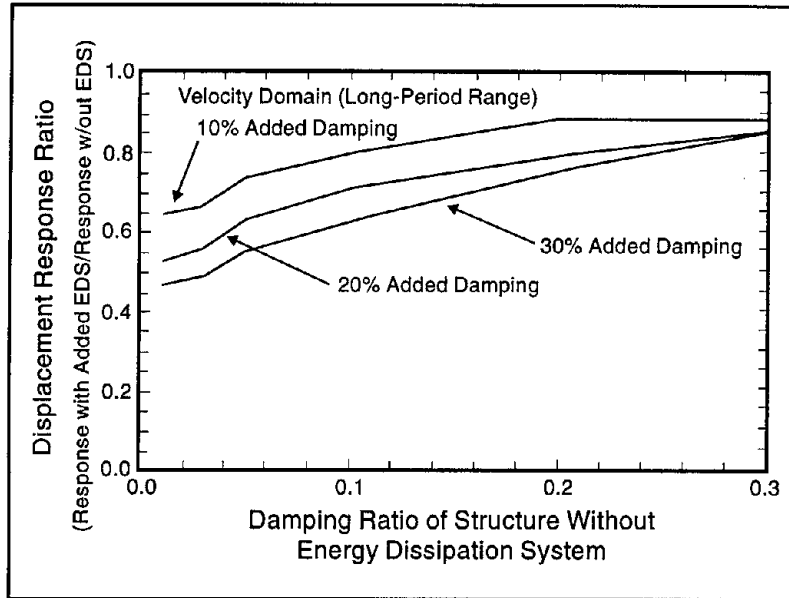
■ Figure 2.6 Response Reduction of Structure with Added Damping of 10, 20 or 30% of Critical

Actually, the reduction in response will be larger due to the increased effective stiffness of the structure, which is caused (a) by the reduction in drift, and (b) by the addition of stiffness in certain energy dissipation systems.

It should be noted that, as shown in Figure 2.5, the base shear force response of the structure with energy dissipation systems is larger than that of the structure without these systems. This would be the case when the pushover curve of the structure without an energy dissipation system exhibits essentially elastoplastic behavior. It is possible to have reduction in base shear force when the pushover curve exhibits significant post-yielding stiffness. This issue will be further discussed later in this chapter when examples of analysis are presented.

2.2.3 Yielding Structures with Improper Plastic Hinge Formation

Structures designed for low lateral forces without proper distribution of stiffness and detailing for ductility typically develop
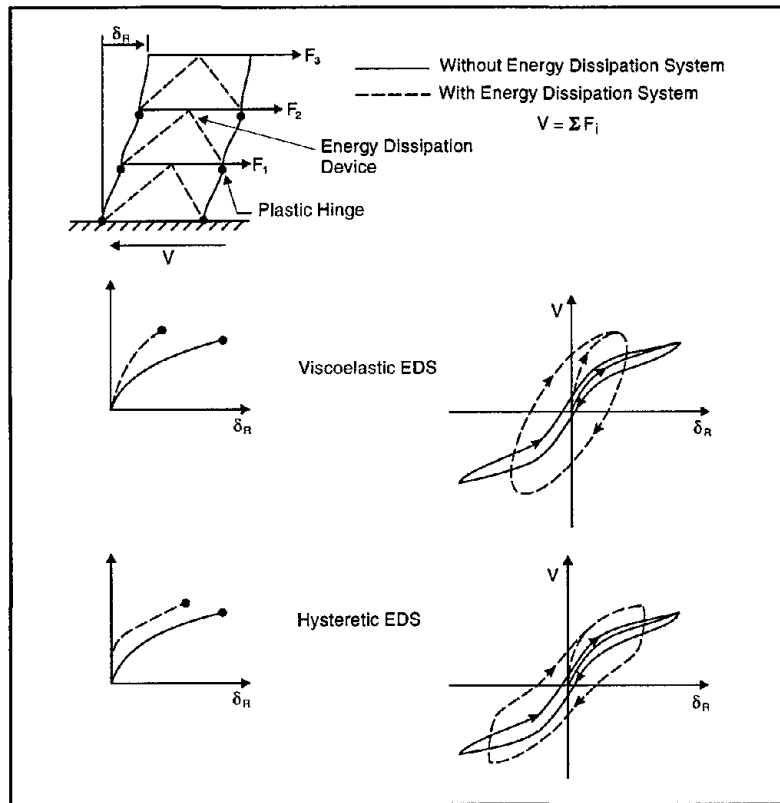
■ Figure 2.7 Pushover Curves and Force-Displacement Hysteresis Loops of a Yielding Structure Having Improper Plastic Hinge Formation Without and With Energy Dissipation Systems

improper plastic hinge mechanisms and undesirable modes of deformation. Figure 2.7 shows a frame with such characteristics, where plastic hinges can form in the columns and lead to hysteresis loops with low energy absorption capability. Such a mechanism may lead to excessive hinge rotations which cannot be accommodated, resulting in deterioration of strength and stiffness and eventually failure. Figure 2.7 depicts a case in which neither significant deterioration nor failure has occurred.

The addition of an energy dissipation system to this frame results in significant improvement in energy absorption capability and large reduction in displacement. This reduction in displacement is associated with reduction in plastic hinge rotation and possible elimination of some plastic hinges. However, the total force on the frame may be increased as a result of the increase in stiffness and/or strength provided by the energy dissipation sys-

tem. As discussed in Section 2.2.2, this is generally the case for structures with nearly elastoplastic pushover curves.

Experimental studies of seismic retrofit of a reinforced concrete frame with energy dissipation systems (Lobo et al., 1993a; Reinhorn et al., 1995) demonstrated behavior similar to that depicted in Figure 2.7. It is apparent that energy dissipation systems are most useful in applications of seismic retrofit.

2.3

ANALYSIS OF LINEAR VISCOELASTIC STRUCTURES

This section presents some readily obtained results on the dynamic properties of linear viscoelastically damped structures, that is, linear elastic structures with viscoelastic energy dissipation systems. The results are useful in quantifying the effect that these systems have on the structure to which they are attached and provide a basis for simplified methods of analysis for inelastic structures.

Viscoelastic energy dissipation systems may take the form of viscoelastic solid, viscoelastic fluid and viscous devices. In general, such devices exhibit mechanical properties which are frequency and temperature dependent, and under certain conditions strain (or deformation) dependent. Mathematical models capable of describing the frequency and temperature dependency of the properties of these devices are described in Chapter 3. Herein the analysis is restricted to the simplest possible model for these devices, that is, the Kelvin model. The force in each of these devices is described as a function of relative displacement, x, and relative velocity

$$F = k'(\omega)x + c'(\omega)\dot{x} \qquad (2\text{-}1)$$

where k' and c' are, respectively, the storage stiffness and damping coefficient of the device. These quantities are, in general, frequency dependent. However, it is assumed that a representative frequency has been selected so that in the following analysis k' and c' are constants. For example, frequency ω should be the frequency of free vibration when modal properties of the damped

structure are determined. Application of this simplified modeling approach to structures with viscoelastic fluid devices (Makris and Constantinou, 1990 and 1991) produced results in very good agreement with exact analytical results.

Of interest is the determination of the frequencies of free vibration, mode shapes and damping ratios of the damped structure. While the structure is linear elastic and added stiffness and damping are provided by elements obeying the simple constitutive relation of Eq. (2.1), the resulting structural system is not amenable to easy solution of its eigenvalue problem. The problem is that of a nonclassically damped structure (the interested reader is referred to Liang and Lee, 1991, for a general exposition of nonclassical damping and to Constantinou and Symans, 1992 for application of exact methods of analysis to structures with viscous energy dissipation systems).

Herein, an approximate method, which is based on energy considerations, is utilized. The method starts with the assumption that the frequencies and mode shapes of the nonclassically damped structure are identical to those of the original structure with the added effect of storage stiffness but not damping (i.e., C in Eq. (2.1) is zero) from the energy dissipation system. Thus, the frequencies and mode shapes can be determined by standard eigenvalue analysis.

The damping ratio in the kth mode of vibration may be expressed as (Chopra 1995)

$$\zeta_k = \frac{W_k}{4\pi L_k} \tag{2-2}$$

where W_k is the energy dissipated in a single cycle of motion and L_k is the maximum strain energy. To evaluate W_k and L_k, it is assumed that the structure undergoes vibration in the kth mode with frequency ω_k and mode shape vector Φ. Concentrating only on the energy dissipated by the viscoelastic devices, W_k can be expressed (Constantinou and Symans, 1992; FEMA, 1997) as

$$W_k = \pi \omega_k \sum_j c_j' \cos^2 \theta_j \phi_{rj}^2 \tag{2-3}$$

where c'_j is the damping coefficient of device j, θ_j is angle of inclination and ϕ_{rj} is the device relative modal displacement as depicted in Figure 2.8.
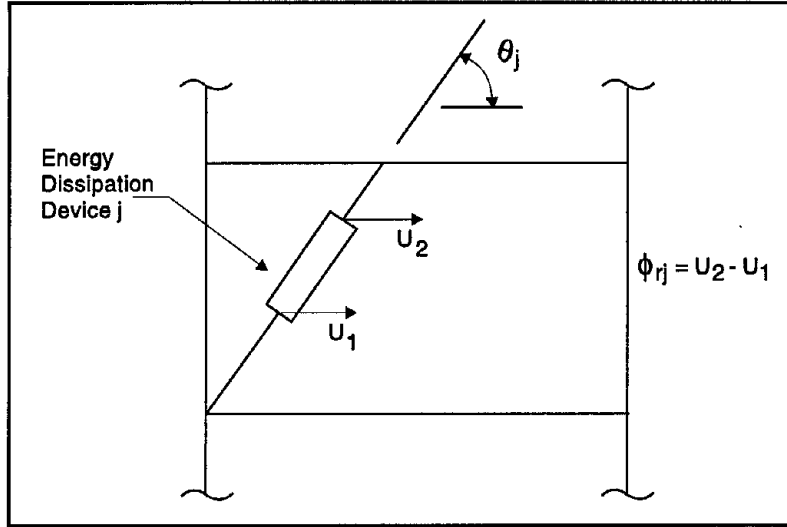
■ Figure 2.8 Definition of Relative Displacement and Angle of Inclination of Energy Dissipation Device

Energy L_k may be expressed either as the maximum strain energy or as the maximum kinetic energy (Chang et al., 1991; Constantinou and Symans, 1992)

$$L_k = \frac{1}{2}\Phi^T K\Phi = \frac{1}{2}\omega_k^2\sum_i m_i\phi_i^2 \qquad (2-4)$$

where **K** is the stiffness matrix of the structure including the effect of storage stiffness of the viscoelastic devices, m_i is ith lumped mass of the structure and φ_i is the modal displacement of mass m_i. The damping ratio is

$$\zeta_k = \frac{1}{2}\frac{\sum\limits_j c'_j \cos^2\theta_j \phi_{rj}^2}{\omega_k \sum\limits_i m_i\phi_i^2} \qquad (2-5)$$

where summation j extends over the energy dissipation devices and summation i extends over lumped masses.

Evaluation of frequencies and damping ratios requires an iterative procedure. First the storage stiffness of the energy dissi-

pation devices is determined at an assumed frequency (i.e. an estimate of the frequency of free vibration in the selected vibration mode). An eigenvalue analysis of the structure with the effect of added storage stiffness is performed. Calculated and assumed frequencies are then compared and the process is repeated until the two frequencies are sufficiently close. With the frequency and mode shape established, the damping coefficient is determined and direct application of Eq. (2.5) gives the damping ratio. The entire calculation process needs to be repeated for each mode of vibration which is of interest. This iterative procedure would approximately account for the effect of the frequency dependency of properties of the viscoelastic devices. To account for the effects of temperature and strain (or deformation) dependencies, analysis should be performed with the applicable mechanical properties. The procedure described is simplified (iteration is avoided) when the energy dissipation system exhibits linear viscous behavior, that is, $k' = 0$ and c' is independent of frequency.

An alternative form of Eq. (2.5), which is applicable only to systems with non-zero storage stiffness, exploits the relation between damping coefficient and storage stiffness:

$$c' = \frac{\eta k'}{\omega} \qquad (2\text{-}6)$$

where η is the loss factor. The result is

$$\zeta_k = \frac{\eta}{2} \left(\frac{\sum_j k_j' \cos^2\theta_j \phi_{rj}^2}{\Phi^T K \Phi} \right) \qquad (2\text{-}7)$$

The significance of Eq. (2.7) is that the loss factor for typical viscoelastic solid materials (e.g. Chang et al., 1991) is only marginally dependent on frequency, temperature or strain, whereas the storage stiffness and damping coefficient exhibit significant dependence on these parameters. Typically, the loss factor for these materials has a value close to unity. The quantity in parenthesis in Eq. (2.7) is recognized as the contribution to the strain energy from the energy dissipation system divided by the total strain energy of the structure.

An example is presented to demonstrate the procedure. A single-story structure has a frequency of 2 Hz and a lumped weight of 27000 N. Two energy dissipation devices are diagonally attached through rigid braces at an angle of 36°. First consider that these devices are linear viscous fluid dampers with damping coefficient $c' = 15.5$ Ns/mm (this is the case of the devices tested by Constantinou and Symans, 1992 at a temperature of about 20°C). When modeling the structure as a single-degree-of-freedom system, $\phi_i = 1$ and $\phi_{rj} = 1$ ($i = 1, j = 1$). Moreover, since the devices lack storage stiffness, the frequency of the damped frame is unchanged. Direct application of Eq. (2.5) result in $\zeta = 0.29$.

Consider now that two viscoelastic solid energy dissipation devices are attached to the frame. The devices are made of the material tested by Chang et al., 1991, of which the mechanical properties are shown in Figure 2.9. These properties are normalized so as to represent the mechanical properties of the material rather than the device. The presented properties are the shear storage (G') and loss moduli (G''), and loss factor η, which are related to the storage stiffness and damping coefficient through the bonded area A_b and total thickness h of the material (see Chapter 3 for a detailed presentation):

$$k' = G' \frac{A_b}{h} \quad , \quad c' = \frac{G''}{\omega} \frac{A_b}{h} \quad , \quad \eta = \frac{G''}{G'} \qquad (2\text{-}8)$$

Figure 2.9 shows the dependency of properties on frequency, temperature and strain amplitude γ_o, which is defined as the shear deformation amplitude divided by the thickness of each layer of material. For each device, temperature of about 20°C and strain of about 0.2 and dimensional properties $A_b = 2600$ mm^2 and $h = 28$ mm is considered. For a frequency of 2Hz, $G'' = 2.1$ MPa so that c' at this frequency is 15.5 Ns/mm, thus identical to that of the viscous fluid damper. However, the storage stiffness of the devices will cause an increase in frequency so that the effective c' will be less. For the calculation, it is assumed that the frequency increased to a value between 2.25 and 2.50 Hz. Approximately then, $G' = 1.74$ MPa, $G'' = 2.20$ MPa and $\eta = 1.27$. The added stiffness is $2k' \cos^2\theta = 211.5$ N/mm and the total stiffness is 646 N/mm (the stiffness of the undamped structure is 434.5 N/mm). For this total stiffness, the frequency is 2.44 Hz, thus the assumed
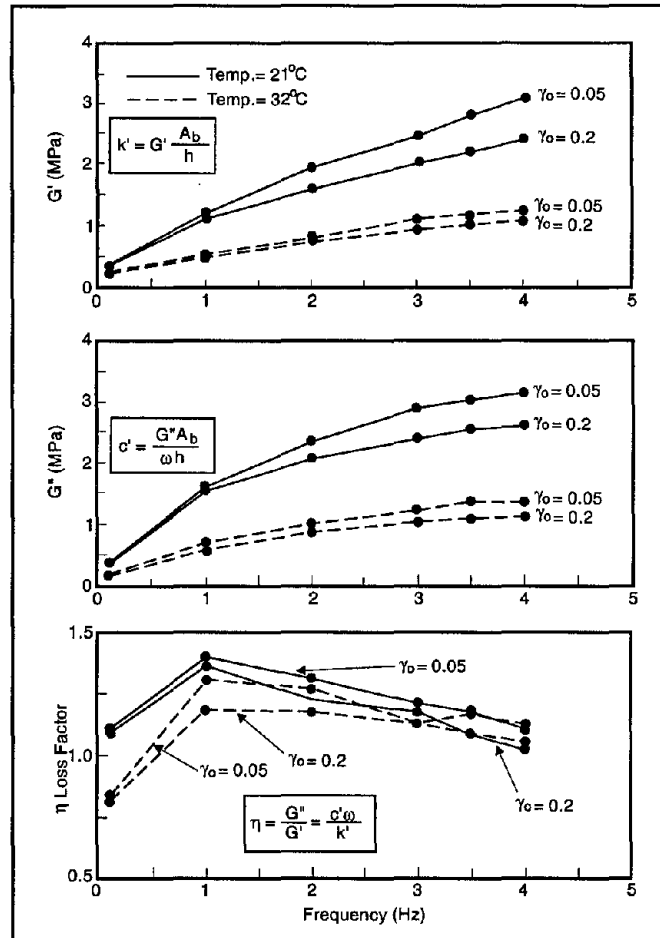
■ Figure 2.9 Properties of a Viscoelastic Solid Energy Dissipation Device

values of properties are valid. It follows that at a frequency of 2.44 Hz, $c' = 13.3$ Ns/mm and from Eq. (2.5) the damping ratio is determined to be 0.21. Alternatively, (2-7) yields $\zeta = (1.27/2)$ $(211.5/646) = 0.21$.

With the modal properties of the viscoelastically damped structure determined, analysis of seismic response can be performed by the response spectrum approach. In this approach, the peak dynamic response is determined for each significant mode of vibration. The structure is represented in mode k as a single degree of freedom system with frequency ω_k, damping ratio ζ_k and modal mass equal to

$$M_k = \frac{\left(\sum_i m_i \phi_{ik}\right)^2}{\sum_i m_i \phi_{ik}^2} \qquad (2\text{-}9)$$

where ϕ_{ik} is the amplitude of the kth mode shape at lumped mass m_i. The peak acceleration and displacement response of the single-degree-of-freedom system, S_{ak} and S_{dk}, respectively, are determined from response spectra which have been modified to account for the increased damping ratio ζ_k. The base shear V_k and displacement of degree of freedom i, δ_{ik}, are then obtained from

$$V_k = M_k S_{ak} \;,\; \delta_{ik} = \phi_{ik} \Gamma_k S_{dk} \qquad (2\text{-}10)$$

where Γ_k is the kth modal participation factor:

$$\Gamma_k = \frac{\sum_i m_i \phi_{ik} S_i}{\sum_i m_i \phi_{ik}^2} \qquad (2\text{-}11)$$

where S_i in Eq. (2.11) is the horizontal displacement of lumped mass i corresponding to unit horizontal ground displacement. $S_i = 1$ for a two-dimensional model of the structure.

2.4 MODIFICATION OF RESPONSE SPECTRUM FOR HIGHER DAMPING

The 5%-damped response spectra represents the usual seismic loading specification. For structures with enhanced damping provided by an energy dissipation system, the 5%-damped spectra needs to be modified.

The 1994 NEHRP Recommended Provisions (Federal Emergency Management Agency, 1995) and FEMA, 1997 describe procedures for constructing smooth, elastic, free-field and 5%-damped response spectra. These spectra are based on site coefficients C_a and C_v, which are related to the effective peak acceleration and
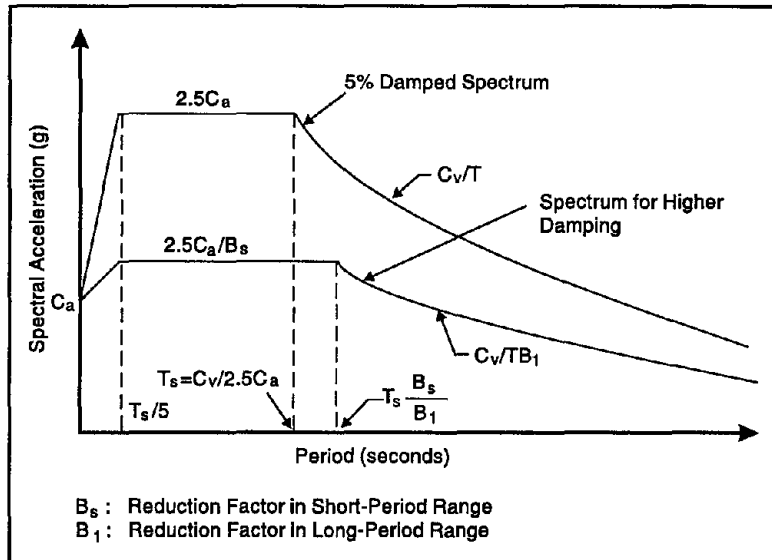
■ Figure 2.10 Modification of Elastic Response Spectrum for Damping Different than 5% of Critical

effective peak velocity coefficients (which describe the ground shaking hazard), and the soil profile type. Figure 2.10 shows the form of the response spectrum.

A number of studies determined spectral amplification factors that can be used for response modification due to increased damping (i.e., Newmark and Hall, 1982). Herein, modification factors from FEMA, 1997 are presented which are in general agreement with the aforementioned studies. Table 2.1 lists these factors and Figure 2.10 demonstrates their application.

■ Table 2.1 Factor for Modification of Response

Damping Ratio (% of Critical)	Factor B_s for Short-period Range	Factor B_l for Long-period Range
≤ 2	0.8	0.8
5	1.0	1.0
10	1.3	1.2
20	1.8	1.5
30	2.3	1.7
40	2.7	1.9
≥ 50	3.0	2.0

It should be noted that the spectral acceleration shown in Figure 2.10 is actually the so-called pseudo acceleration S_{pa}, which is exactly the acceleration at maximum displacement. Figure 2.11 compares pseudo acceleration and maximum acceleration response spectra for the 1940 El Centro earthquake (S00E) where it is demonstrated that, for large values of damping (i.e, 30% of critical and larger), the pseudo acceleration is typically less than the maximum acceleration.

It is possible to obtain an approximate relation between maximum and pseudo accelerations by assuming that during the cycle of maximum response, the analyzed single-degree-of-free-
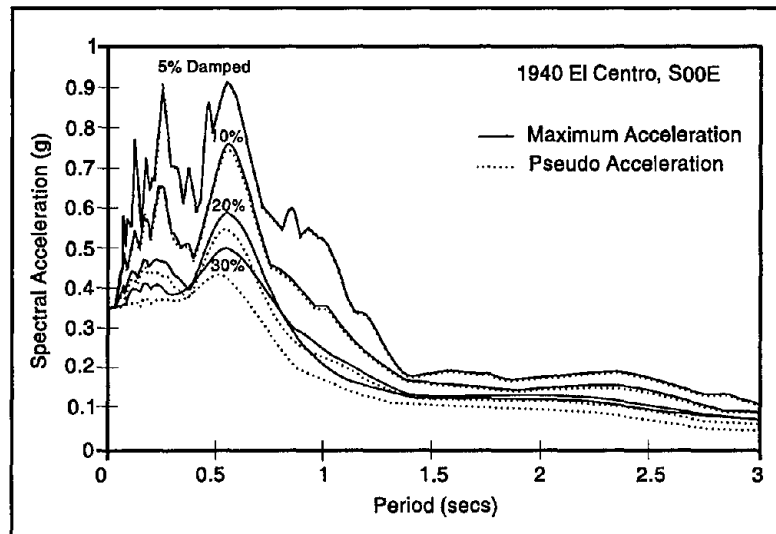
■Figure 2.11 Response Spectra of Maximum and Pseudo Acceleration

dom system undergoes harmonic motion of frequency ω ($\omega = 2\pi/$ T, T being the period). It is easily shown that

$$S_a = \left(f_1 + 2\zeta f_2 \right) S_{pa} \qquad (2\text{-}12)$$

where

$$f_1 = \cos\left[\tan^{-1}(2\zeta) \right], \, f_2 = \sin\left[\tan^{-1}(2\zeta) \right] \qquad (2\text{-}13)$$

and ζ is the damping ratio.

It should be noted that the maximum acceleration occurs at a time in which the displacement is less than the maximum displacement. Moreover, the pseudo acceleration is the acceleration response at maximum displacement. It may be easily shown that, approximately, the displacement at maximum acceleration is equal to f_1 times the maximum displacement. Also, factors f_1 and f_2 represent useful combination factors for obtaining member forces for design. That is, at the instant of maximum acceleration, member forces may be obtained as the linear combination of forces at the instant of maximum drift times f_1 and of forces at the instant of maximum velocity (equal to maximum drift multiplied by frequency ω) times f_2.

2.5

CONSIDERATIONS IN DESIGN AND ANALYSIS

2.5.1 DISSIPATION OF ENERGY

The amount of energy dissipated in a cycle of motion of an energy dissipation device is needed in the calculation of effective damping ratios for simplified analysis. Consider that the device is subjected to sinusoidal motion

$$x = x_o \sin\omega t \qquad (2-14)$$

and the device resists this motion with force F. For hysteretic devices, the force-displacement loops will be of the form shown in Figure 2.1. The loops are characterized by the force at zero displacement, F_o, which is often called the characteristic strength. The energy dissipated per cycle is

$$W_d = 4F_o x_o f \qquad (2-15)$$

where $f = 1$ for friction devices and $f < 1$ for metallic yielding devices. The actual value of factor f depends on the characteristics of the device.

For viscoelastic solid or fluid devices, the force-displacement loops will be of the form shown in Figure 2.2. Force F can be described by equation Eq. (2.1) where parameters k' and

c' have the physical interpretation depicted in Figure 2.2. The energy dissipated per cycle is

$$W_d = \pi c' \omega x_o^2 \qquad (2\text{-}16)$$

Viscous fluid dampers can be designed to produce an output force in the form (see Chapter 3)

$$F = c_v |\dot{x}|^a \text{sgn}(\dot{x}) \qquad (2\text{-}17)$$

where c_v is a generalized damping coefficient and α may take values in the range of about 0.25 to 2. That is, the damper may exhibit nonlinear viscous behavior (the case $\alpha = 1$ is that of a linear device). The energy dissipated per cycle (see Soong and Constantinou, 1994 for more information) is

$$W_d = \lambda c_v x_o^{1+\alpha} \omega^\alpha = \lambda F_o x_o \qquad (2\text{-}18)$$

where

$$\lambda = 4 \cdot 2^\alpha \cdot \frac{\Gamma^2\left(1 + \dfrac{\alpha}{2}\right)}{\Gamma(2+\alpha)} \qquad (2\text{-}19)$$

In the above, F_o is the force at zero displacement and Γ is the gamma function. Note that for $\alpha = 1$, $\lambda = \pi$ and Eq. (2.18) is identical to Eq. (2.16).

2.5.2 EFFECT OF BRACING

Energy dissipating devices are typically attached to a structure through bracing, which may take the form of a diagonal or a chevron brace. For example, Figure 2.12 illustrates the installation of a fluid viscous damper on top of a chevron brace. The energy dissipation assembly of this story and bay of the structure consists of the chevron brace and fluid viscous damper installed in series. When the brace has infinite stiffness, the force exerted by the damper on the top girder is related to the relative velocity between the top and bottom girders, $\dot{x}$, that is, $F = c_v \dot{x}$ (for linear viscous behavior). In this case, analysis of the damped structure may be performed by the procedures of Section 2.3.
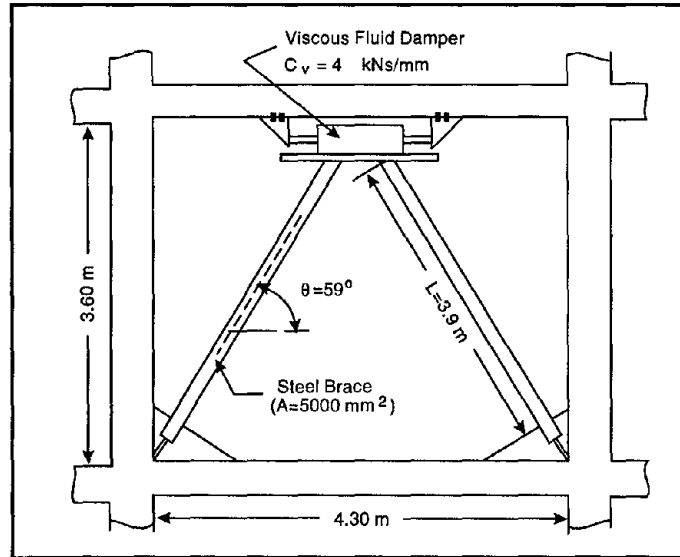
Figure 2.12 Viscous Fluid Damper Installed on Top of Chevron Brace In a Structure

In general, bracing has finite stiffness so that the behavior of the energy dissipation assembly is that of a spring in series with a viscous damper. The behavior of this assembly is best described by the Maxwell model (see Chapter 3) for which the force, F, exerted on the top girder is described by

$$F + \frac{c_v}{k_b} \frac{dF}{dt} = c_v \dot{u} \tag{2-20}$$

where k_b is the stiffness of the bracing (= $2AE \cos^2 \theta/L$ for the bracing of Figure 2.12). The force may also be described by the familiar form of Eq. (2.1) with storage stiffness $k'(\omega)$ and damping coefficient $c'(\omega)$:

$$k'(\omega) = \frac{c_v \tau \omega^2}{1 + \tau^2 \omega^2} \quad , \quad c'(\omega) = \frac{c_v}{1 + \tau^2 \omega^2} \tag{2-21}$$

where $\tau = c_v / k_b$ is the so-called relaxation time.

Eqs. (2.21) are valid for harmonic motion of frequency ω. When ω is the natural frequency of the structure, (2-21) reveals the effect of bracing on the damped structure. For infinitely stiff

bracing, $\tau = 0$, $k' = 0$ and which describes the case of linear viscous damper with $c' = c_v$ (see Section 2.3). For any other case, the energy dissipation assembly exhibits viscoelastic behavior. For the particular case of Figure 2-12, $k' = 136$ kN/mm, $c_v = 4$ kNs/mm and $\omega = 14$ rad/s. It follows that $c' = 0.855\, c_v = 3.42$ kNs/mm. Thus, the effect of bracing is to reduce the added damping by approximately 15%. Note that the natural frequency was calculated with the added effect of storage stiffness k', as described in Section 2.3.

2.5.3 Axial Forces in Columns

Energy dissipation devices will typically be attached to moment frames in configurations similar to that depicted in Figure 2.12. While the energy dissipation system can result in significant reduction in drift (and, thus, reduction in column bending moment and/or reduction in inelastic deformation), it also affects load paths. Specifically, the change from a moment frame to a braced configuration can result in substantial increase in column axial forces.

For example, Figure 2.13 shows a frame with a friction energy dissipation system which was tested on a shake table (Aiken and Kelly, 1990). The friction devices were installed on top of chevron braces (configuration of Figure 2.12) and, on sliding, they could develop the forces depicted in Figure 2.13. Assuming that all friction devices slide, the resulting additional column axial forces were calculated and are shown in the figure. It may be seen that the interior column carries 56.9 kN (12.75 kips) gravity axial load and a combined gravity and seismic axial load of 131.4 kN (29.46 kips) (the latter figure does not include the effect of lateral inertia load, which was assumed to be negligible for interior columns in this simplified calculation).

The preceding example demonstrates that substantial additional axial loads can develop in the columns of the energy dissipation assembly. In hysteretic energy dissipation systems, the peak column axial force occurs simultaneously (in-phase) with the peak column drift. However, in viscoelastic energy dissipation systems, the peak column axial force occurs at a time in which the drift is less than maximum. Particularly, for linear viscous energy dissipation systems, the additional column axial force is
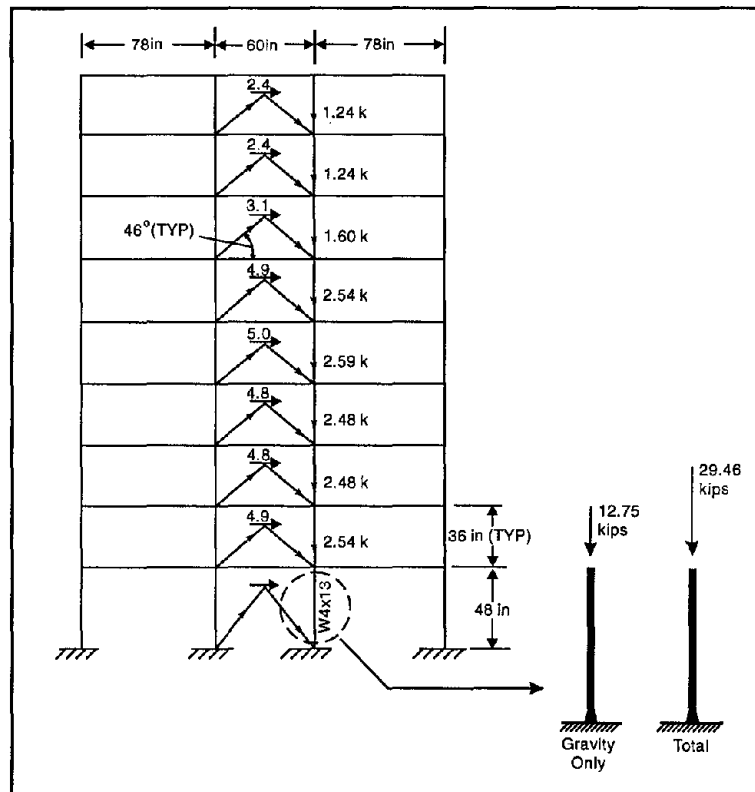
■ Figure 2.13 Gravity and Additional Axial Load in Interior Column of 9-Story Model Structure with Friction Energy Dissipation Devices

out-of-phase with the column drift. That is, peak column axial forces occur when the drift is zero.

SIMPLIFIED NONLINEAR ANALYSIS OF STRUCTURES WITH PASSIVE ENERGY DISSIPATION SYSTEMS

Nonlinear response time history analyses of structures with energy dissipation systems will, in general, provide the most realistic indication of global structural response and of demands on individual structural components. However, the results of such analysis tend to be highly sensitive to small changes in the as-

sumptions regarding the behavior of components and in the ground motion histories used in the analysis. The FEMA, 1997 guidelines recognize this problem and recommend the use of nonlinear response time history analysis with a multitude of ground motions (independent review provided by qualified experts should also be used).

Simplified nonlinear methods of analysis permit a direct evaluation of inelastic response by utilizing design demand spectra, which are established from the 5%-damped pseudo-acceleration response spectra after adjustment for the effective damping in the structure. However, the results are approximate since these methods are based on a representation of the nonlinear global characteristics of the structure by effective linear and viscous representations. A significant difference between these methods of analysis and linear methods of analysis is that the latter make use of the elastic properties of the structure, whereas the former make use of the effective properties at the calculated displacements.

Simplified nonlinear methods of analysis have been utilized in the development of the static lateral response procedure for seismic-isolated structures (e.g., ICBO, 1994) and one such method is explicitly described in FEMA, 1997. In this section, simplified nonlinear methods of analysis are presented that are largely based on the FEMA, 1997 approach, although alternative approaches will be highlighted.

Simplified nonlinear methods of analysis usually follow the approach of replacing the nonlinear system by an "equivalent" linear system utilizing modal analysis procedures. Since these procedures are valid for elastic structures, their use for inelastic or nonlinear structures represent an approximation. Moreover, simplified nonlinear methods of analysis require the use of response spectra that are constructed from the 5%-damped response spectra based on the level of inelastic action and added damping in the structural system. The construction of these spectra also represents an approximation. That is, simplified nonlinear methods of analysis involve several approximations such that their application requires understanding of structural behavior, knowledge of structural dynamics and prudent use of engineering judgment.

2.6.1 General Description of Simplified Nonlinear Methods of Analysis

Simplified nonlinear methods of analysis contain a number of steps or procedures as explained below and illustrated in Figure 2.14.

1. A mathematical representation of the structure, including all important characteristics of the seismic framing system and energy dissipation system, is incrementally pushed by laterally applied loads. The pushover curve, that is, the base shear-roof displacement relation, is established. There are a number of important considerations in the pushover analysis:

    a. The pattern of lateral loads must be consistent with the distribution of inertia forces on the yielding structure. The most appropriate distribution is one in which the loads are related to story resistances, that is, the pattern of loads changes with increasing displacements (Reinhorn et al., 1995; Valles et al., 1997; Bracci et al., 1997). For example, the pattern may start as an inverted triangle (modal pattern) and progressively change towards a uniform load pattern (i.e., proportional to mass). In any case, modal and uniform load patterns may give upper and lower bound pushover curves and it is a good practice to perform calculations with both.

    b. Since the analysis is static, the velocity dependent characteristics of energy dissipation devices (e.g.,viscoelastic and viscous devices) cannot be accounted for. It is assumed that these characteristics affect only the effective damping of the system, which will be accounted for in the modification of the response spectrum.

    c. Certain characteristics of energy dissipation devices (e.g., stiffness of viscoelastic devices) are frequency dependent. They should be determined for the effective frequency of the structure at the actual displacements and accounted for in the pushover analysis.

Step 1   Pushover Analysis

δ_3 F_3

δ_2 F_2

δ_1 F_1

$V = \sum_i F_i$

V

Assumed
Displacement

δ_3

Pushover Curve

Step 2   Perform Eigenvalue Analysis Using Effective Member
          Stiffnesses at Assumed Displacement
Step 3   Establish Design Demand Spectrum Using Effective
          Damping in Fundamental Mode
Step 4   Convert Pushover Curve to Spectral Capacity Curve

V

δ_3

$S_a = \dfrac{V}{W_{s1}} g$

$S_d = \dfrac{\delta_3}{\varphi_{31}\Gamma_1}$

S_a

S_d

Step 5   Overlie Spectral Capacity Curve on Design Demand
          Spectrum and Calculate Response

S_a

A

Spectral
Capacity
Curve

Design
Demand
Curve

$V = \dfrac{A W_{s1}}{g}$

$\delta_3 = \varphi_{31}\Gamma_1 D$

D

S_d

Step 6   If Calculated $\delta_3 \neq$ Assumed Displacement, Repeat Steps 2 to 5
Step 7   Obtain Higher Mode Response

FEMA, 1997

■ Figure 2.14 Illustration of Simplified Nonlinear Method of Analysis

2. An eigenvalue analysis of the structure using the effective stiffness of the members at an assumed roof displacement is performed to determine effective frequencies (periods) and mode shapes.

3. For the fundamental mode of vibration, the effective damping at the assumed displacement is determined. This is used in the construction of the so-called design demand spectrum, that is, a graph of spectral acceleration versus spectral displacement as modified for the level of effective damping in the structure. The approach of FEMA, 1997 utilizes the effective damping (i.e., combined contribution by the energy dissipation system and yielding action in the structural frame) to construct the design demand spectrum. Other approaches have been proposed (e.g., Valles et al., 1997; Bracci et al., 1997) that construct the design demand spectrum by utilizing information on yielding action and viscous damp ing contributed by the viscous force component of the energy dissipation system (i.e., the two components are not combined but are used separately).

4. The pushover curve is converted to a spectral capacity curve, that is, a plot of spectral acceleration versus spectral displacement, using Eqs. (2.9) to (2.11) and the fundamental mode shape established in step (2).

5. The design demand spectrum is overlain on the spectral capacity curve to determine the spectral acceleration and spectral displacement response of the structure in its fundamental mode. Displacements and base shear at maximum displacement are then determined by use of Eqs. (2.9) to (2.11).

6. Steps (2) to (5) are repeated if the calculated and assumed roof displacements are not equal.

7. Response in higher modes is determined by means similar to those used for the response in the fundamental mode.

2.6.2 ESTIMATING RESPONSE OF YIELDING SIMPLE SYSTEMS WITH ENERGY DISSIPATING DEVICES

Important steps in the simplified nonlinear method of analysis is the establishment of the design demand spectrum (step 3) and the determination of response by overlaying this spectrum on

the spectral capacity curve (step 5). In essence, this approach is one of replacing the nonlinear system by an "equivalent" linear system. There are several methods of establishing equivalent linear systems (e.g., see Iwan and Gates, 1979). Of these systems, the one used in FEMA, 1997 and herein is the one based on the geometric stiffness approximation. That is, the effective period is determined from the secant (or effective) stiffness K_s at maximum displacement u, whereas the effective damping is determined from (2-3) with $L_k = \frac{1}{2}K_s u^2$. The validity of this approximation is investigated in this section.

In this study, a single-degree-of-freedom system with the characteristics shown in Figure 2.15 is analyzed. Note that the system is characterized by (a) elastic period T_{el}, (b) strength to elastic demand ratio e, (c) added linear viscous damping ratio β_v representing the energy dissipation devices, and (d) post-yielding to elastic stiffness ratio α. Moreover, the system is characterized by inherent viscous damping ratio β_i equal to 0.05 in both the elastic and inelastic ranges of displacement. This damping ratio is used to account for energy dissipation under elastic conditions and without the viscous energy dissipation system. Note that the structural framing system exhibits ideal bilinear hysteretic behavior.

Elastic Period $\qquad T_{el} = 2\pi\sqrt{\dfrac{D_y}{A_y}}$

Added Viscous Damping $\qquad \beta_v = \dfrac{C\,T_{el}}{4\pi m}$

Strength to Elastic Demand Ratio $\qquad e = \dfrac{A_y}{S_{ae}}$

(S_{ae} = Spectral Acceleration of Elastic System of Period T_{el} and 5% Damping)
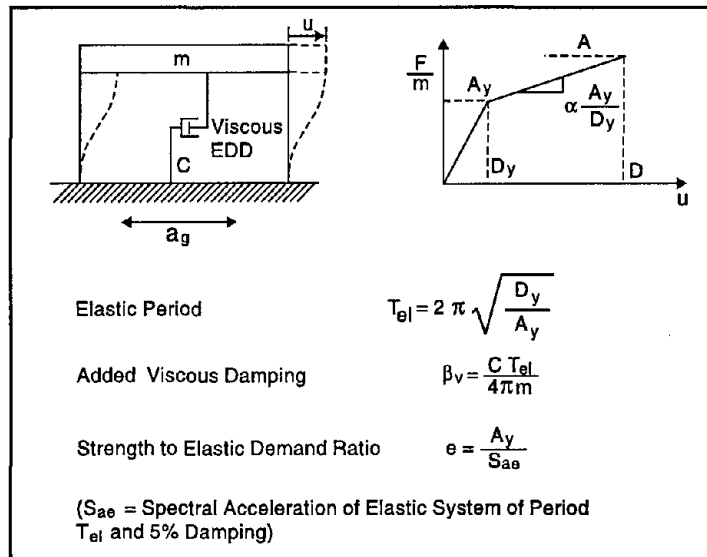
■ Figure 2.15 Analyzed SDOF Inelastic System with Linear Viscous Energy Dissipation System

The system was excited with the 20 horizontal components of the ten scaled earthquake motions of Table 2.2. Each of these earthquakes was selected to have a magnitude larger than 6.5, epicentral distance between 10 and 20 km and site conditions of soft rock to stiff soil. In accordance with the 1994 NEHRP Recommended Provisions, the Soil Type Profile is between C and D. The motions were scaled by the following procedure:

a. Each pair of ground accelerations was normalized by the SRSS (square root of sum of squares) of the peak ground velocities of the two components.

b. The SRSS spectra of each normalized pair were constructed.

c. The average of the ten SRSS spectra was constructed and raised by factor f to match at period of 1 second the 1.4 times the target response spectrum.

d. The scale factor of each pair was then determined as f times the SRSS of peak ground velocities of the pair (from step (a)).

■ Table 2.2 Motions Used in Analysis and Scale Factors

Earthquake	Station	Components	Scale Factor
1949 W. Washington	325 (USGS)	N04W, N86E	2.74
1954 Eureka	022 (USGS)	N11W, N79E	1.74
1971 San Fernando	241 (USGS)	N00W, S90W	1.96
1971 San Fernando	458 (USGS)	S00W,S90W	2.22
1989 Loma Prieta	Gilroy 2 (CDMG)	90,0	1.07
1989 Loma Prieta	Hollister (CDMG)	90,0	1.46
1992 Landers	Yermo (CDMG)	360,270	1.28
1992 Landers	Joshua (CDMG)	90,0	1.48
1994 Northridge	Moorpark CDMG)	180,90	2.61
1994 Northridge	Century (CDMG)	90,360	2.27

The target spectrum was the one for Soil Type Profile of C to D per the 1994 NEHRP Recommended Provisions. That is, $C_a = 0.4$ and $C_v = 0.6$ (see Figure 2.10). The scale factors are given in Table 2.2. Moreover, Figure 2.16 shows the average SRSS response spectra of the ten scaled pairs and the average response spectra of the 20 scaled components. It may be seen that the 20

scaled components represent well, on the average, the target spectrum to periods of about 3 seconds. Also, Figure 2.17 shows average damped response spectra of these 20 scaled components. Note that the spectra present the spectral acceleration, that is, spectral displacement times frequency squared. They are useful in directly obtaining the maximum displacement and acceleration at maximum displacement, but not the maximum acceleration.
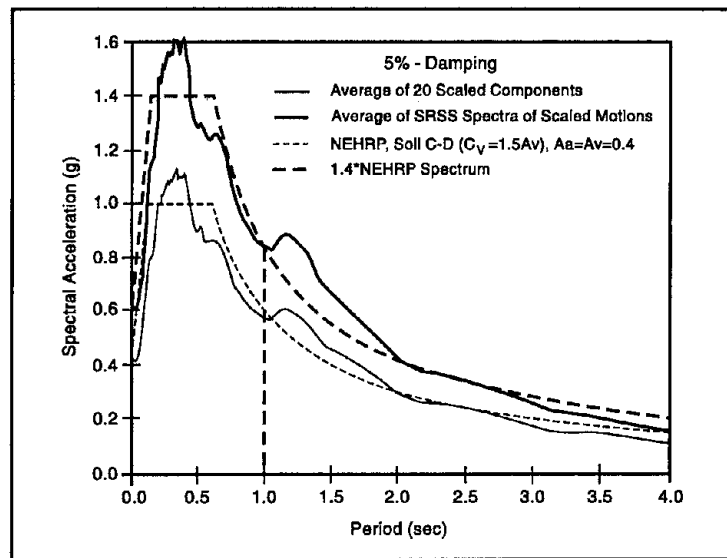
■ Figure 2.16 Response Spectra of Scaled Motions used in Analysis
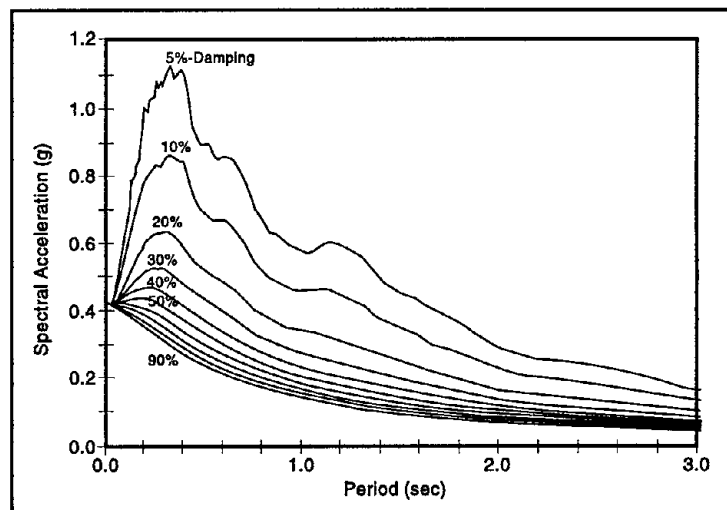
■ Figure 2.17 Average Damped Response Spectra of Scaled Motions

The spectra of Figure 2.17 may be used to obtain response modification factors (B_s and B_1 per Figure 2.10). This was done for the long.period range of the spectra of Figure 2.17 to obtain the following B_1 factors: for damping of 10% B_1 = 1.2, for 20% B_1 = 1.7, for 30% B_1 = 2.0, for 40% B_1 = 2.5 and for 50% B_1 = 3.0. Comparing these response modification factors to those of FEMA, 1997 (see Table 2.1), it is seen that the latter are generally conservative. Moreover, the response modification factors of FEMA, 1997 are limited to a damping ratio of 50%, so that when damping exceeds 50%, the factors are highly conservative.

In general, the use of the response modification factors of Table 2.1 (per FEMA, 1997) will lead to conservative estimation of maximum displacements in the long-period range (presumably, the range of effective period of most buildings). However, in viscous and viscoelastic energy dissipation systems, predictions of maximum velocities are of significance in determining forces in the energy dissipation devices. The maximum velocity in a simplified method of analysis is typically determined (e.g., FEMA, 1997) as pseudo-velocity. That is, it is determined as spectral acceleration divided by frequency. For example, the maximum velocity would be calculated for the NEHRP spectra of Figure 2.10 as $C_v g / 2\pi B_1$ in the long-period range.

Figure 2.18 presents maximum velocity spectra (average of 20 scaled motions) for damping ratio in the range of 0.05 to 0.50 that correspond to the spectral acceleration spectra of Figure 2.17. Directly on Figure 2.18 are shown dashed lines that represent pseudo-velocity spectra for damping ratio of 0.10, 0.20 and 0.50 (calculated for C_v = 0.6). It is seen that the pseudo-velocity represents a good approximation to maximum velocity in the long-period range.

Dynamic response time history analyses of the system of Figure 2.15 were conducted for the following range of parameters: T_{el} = 0.5 and 1.0 s, e = 0.025, 0.05, 0.1, 0.15, 0.2, 0.3 and 0.5, α = 1 (elastic), 0.5, 0.25, 0.15 and 0.05, β_v = 0.15 and 0.25 and β_i = 0.05. Note that spectral acceleration S_{ae} (see Figure 2.15) is taken as 1 g for systems with T_{el} = 0.5 s and as 0.6 g for systems with T_{el} equal to 1.0 s. Tables 2.3 to 2.6 present results on the average peak displacement (for 20 scaled earthquake components) for each analyzed system. The tables also present values
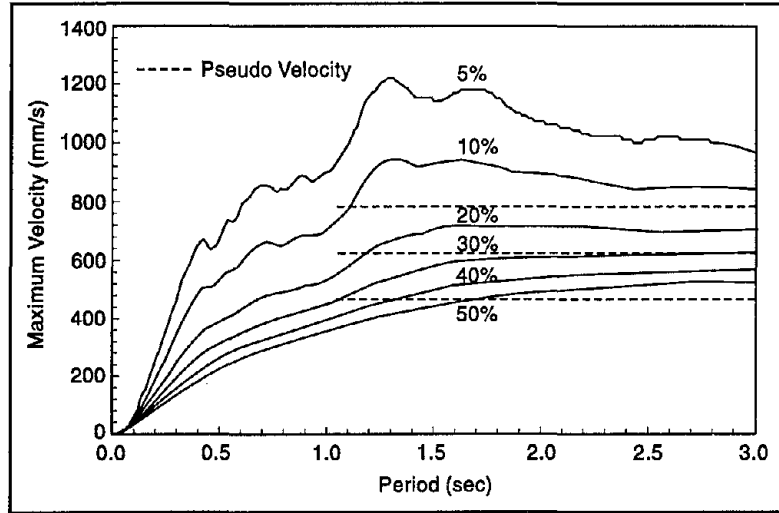
■ Figure 2.18 Average Maximum Velocity Spectra of Scaled Motions and Pseudo-Velocity Spectra for Damping Ratio of 0.1, 0.2 and 0.5 in the Long-Period Range

of effective period T_{eff} and effective damping β_{eff} for each system. These quantities were determined from the calculated average peak displacement D and the corresponding acceleration response A (see Figure 2.15). Based on the geometric stiffness approach for approximating the system by an equivalent linear one and use of Eq. (2.3), expressions for T_{eff} and β_{eff} are

$$T_{eff} = 2\pi \left(\frac{D}{A} \right)^{\frac{1}{2}} \qquad (2\text{-}22)$$

$$\beta_{eff} = \frac{2\left(A_y D - AD_y\right)}{\pi AD} + \beta_v \frac{T_{eff}}{T_{el}} + \beta_i \qquad (2\text{-}23)$$

Note that in Eq. (2.23), the first term represents the contribution from yielding of the framing system (assumed to be perfect bilinear hysteretic), the second term represents the contribution of viscous damping force associated with the energy dissipation devices and the third represents the inherent damping ($\beta_i = 0.05$). Of interest is to note that the contribution of viscous damping force increases with increases in inelastic action (i.e., when T_{eff} increases).

■ Table 2.3 Results of Analysis on Peak Displacements for System with T_{el} = 0.5 sec and β_V = 0.15

Strength Ratio e	Stiffness Ratio α	Average of Response History Analysis			Prediction by Simplified Method of Analysis		
		T_{eff} (sec)	β_{eff}	Displ. (mm)	T_{eff} (sec)	β_{eff}	Displ. (mm)
Elastic	1.00	0.50	0.20	32.6	0.50	0.20	32.6
0.025	0.50	0.70	0.28	43.7	0.70	0.28	44.8
0.025	0.25	0.96	0.39	54.9	0.96	0.39	56.1
0.025	0.15	1.21	0.49	63.6	1.21	0.49	65.9
0.025	0.05	1.88	0.80	71.2	1.89	0.80	73.1
0.05	0.50	0.68	0.30	41.7	0.68	0.30	42.6
0.05	0.25	0.92	0.42	50.3	0.92	0.42	50.8
0.05	0.15	1.13	0.53	56.5	1.13	0.53	57.9
0.05	0.05	1.59	0.83	61.0	1.59	0.83	60.4
0.1	0.50	0.66	0.32	38.2	0.66	0.32	39.0
0.1	0.25	0.84	0.47	43.5	0.83	0.47	42.0
0.1	0.15	0.97	0.58	46.1	0.97	0.58	45.4
0.1	0.05	1.23	0.81	51.5	1.19	0.80	46.5
0.15	0.50	0.63	0.34	36.1	0.63	0.34	35.5
0.15	0.25	0.76	0.48	38.9	0.75	0.48	37.2
0.15	0.15	0.85	0.58	40.7	0.83	0.58	37.3
0.15	0.05	1.00	0.75	44.6	0.95	0.73	38.7
0.2	0.50	0.61	0.34	34.9	0.61	0.34	34.0
0.2	0.25	0.70	0.47	36.3	0.69	0.47	33.3
0.2	0.15	0.76	0.56	37.6	0.73	0.54	33.1
0.2	0.05	0.86	0.68	40.6	0.79	0.64	33.2
0.3	0.50	0.57	0.32	33.3	0.56	0.32	31.5
0.3	0.25	0.62	0.42	34.3	0.60	0.39	30.9
0.3	0.15	0.64	0.47	34.9	0.61	0.42	30.3
0.3	0.05	0.68	0.54	36.3	0.62	0.45	29.8
0.5	0.50	0.51	0.22	32.6	0.50	0.21	32.0
0.5	0.25	0.51	0.23	32.7	0.51	0.22	32.3
0.5	0.15	0.51	0.23	32.7	0.51	0.23	31.6
0.5	0.05	0.51	0.24	32.7	0.50	0.24	30.1

■ Table 2.4 Results of Analysis on Peak Displacements for System with $T_{ef} = 1.0$ sec and $\beta_v = 0.15$

Strength Ratio e	Stiffness Ratio α	Average of Response History Analysis			Prediction by Simplified Method of Analysis		
		T_{eff} (sec)	β_{eff}	Displ. (mm)	T_{eff} (sec)	β_{eff}	Displ. (mm)
Elastic	1.00	1.00	0.20	85.4	1.00	0.20	85.5
0.025	0.50	1.39	0.28	106.3	1.39	0.28	109.0
0.025	0.25	1.91	0.39	114.8	1.91	0.39	118.0
0.025	0.15	2.38	0.50	122.0	2.39	0.50	125.0
0.025	0.05	3.58	0.81	126.8	3.58	0.81	126.0
0.05	0.50	1.37	0.30	100.9	1.37	0.29	105.0
0.05	0.25	1.82	0.43	106.6	1.82	0.42	109.0
0.05	0.15	2.20	0.54	111.1	2.20	0.54	110.0
0.05	0.05	3.00	0.83	115.4	2.93	0.83	107.0
0.1	0.50	1.31	0.32	92.7	1.31	0.32	93.8
0.1	0.25	1.65	0.47	95.6	1.64	0.47	92.4
0.1	0.15	1.89	0.58	97.9	1.85	0.59	88.6
0.1	0.05	2.33	0.80	105.1	2.15	0.78	84.7
0.15	0.50	1.26	0.34	86.9	1.26	0.34	86.5
0.15	0.25	1.51	0.48	89.0	1.49	0.48	83.1
0.15	0.15	1.67	0.58	91.0	1.60	0.57	79.2
0.15	0.05	1.95	0.74	99.1	1.73	0.69	74.6
0.2	0.50	1.21	0.34	83.3	1.21	0.34	82.3
0.2	0.25	1.39	0.47	84.1	1.37	0.47	78.0
0.2	0.15	1.50	0.55	86.0	1.43	0.53	74.6
0.2	0.05	1.67	0.67	91.9	1.50	0.60	71.9
0.3	0.50	1.13	0.32	80.7	1.13	0.32	78.4
0.3	0.25	1.23	0.41	80.6	1.19	0.39	74.4
0.3	0.15	1.28	0.46	82.1	1.22	0.42	73.3
0.3	0.05	1.35	0.53	85.5	1.24	0.46	71.5
0.5	0.50	1.02	0.23	82.3	1.04	0.23	82.1
0.5	0.25	1.03	0.24	81.4	1.03	0.24	81.4
0.5	0.15	1.04	0.25	81.7	1.03	0.24	81.4
0.5	0.05	1.05	0.26	82.3	1.02	0.26	76.8

Note: Prediction by simplified method is not reported when β_{eff} exceeds 0.9

■ Table 2.5 Results of Analysis on Peak Displacements for System with T_{eI} = 0.5 sec and β_V = 0.25

Strength Ratio e	Stiffness Ratio α	Average of Response History Analysis			Prediction by Simplified Method of Analysis		
		T_{eff} (sec)	β_{eff}	Displ. (mm)	T_{eff} (sec)	β_{eff}	Displ. (mm)
Elastic	1.00	0.50	0.30	27.1	0.50	0.30	27.1
0.025	0.50	0.69	0.42	35.1	0.69	0.42	35.4
0.025	0.25	0.95	0.59	43.5	0.95	0.58	44.2
0.025	0.15	1.19	0.74	47.9	1.19	0.74	49.2
0.025	0.05	1.78	1.17	51.5	--	—	—
0.05	0.50	0.68	0.44	33.5	0.68	0.44	33.9
0.05	0.25	0.90	0.61	40.0	0.90	0.61	40.2
0.05	0.15	1.09	0.77	43.0	1.09	0.77	44.0
0.05	0.05	1.48	1.12	45.5	--	--	--
0.1	0.50	0.65	0.46	31.1	0.65	0.46	31.2
0.1	0.25	0.81	0.64	34.9	0.80	0.64	33.7
0.1	0.15	0.92	0.77	36.8	0.92	0.77	36.0
0.1	0.05	1.13	1.02	40.1	--	--	--
0.15	0.50	0.62	0.46	29.6	0.62	0.46	29.4
0.15	0.25	0.73	0.63	31.7	0.72	0.62	30.0
0.15	0.15	0.80	0.73	33.0	0.78	0.72	30.5
0.15	0.05	0.92	0.90	36.2	--	--	--
0.2	0.50	0.59	0.45	28.5	0.59	0.45	27.9
0.2	0.25	0.67	0.59	29.8	0.65	0.58	27.3
0.2	0.15	0.71	0.67	30.7	0.69	0.65	27.9
0.2	0.05	0.78	0.79	33.0	--	--	—
0.3	0.50	0.55	0.41	27.5	0.54	0.40	26.2
0.3	0.25	0.58	0.48	28.1	0.56	0.45	25.9
0.3	0.15	0.60	0.52	28.4	0.57	0.48	25.6
0.3	0.05	0.62	0.58	29.4	0.58	0.50	25.6
0.5	0.50	0.50	0.30	27.2	0.50	0.30	27.1
0.5	0.25	0.50	0.30	27.2	0.50	0.30	27.1
0.5	0.15	0.50	0.30	27.2	0.50	0.30	27.1
0.5	0.05	0.50	0.30	27.2	0.50	0.30	27.1

Note: Prediction by simplified method is not reported when β_{eff} exceeds 0.9

■ Table 2.6 Results of Analysis on Peak Displacements for System with T_{el} = 1.0 sec and β_V = 0.25

Strength Ratio e	Stiffness Ratio α	Average of Response History Analysis			Prediction by Simplified Method of Analysis		
		T_{eff} (sec)	β_{eff}	Displ. (mm)	T_{eff} (sec)	β_{eff}	Displ. (mm)
Elastic	1.00	1.00	0.30	68.9	1.00	0.30	68.9
0.025	0.50	1.38	0.42	82.8	1.38	0.42	84.0
0.025	0.25	1.89	0.59	89.2	1.89	0.59	90.3
0.025	0.15	2.33	0.75	94.1	2.33	0.75	94.0
0.025	0.05	3.40	1.16	96.8	--	--	--
0.05	0.50	1.35	0.44	79.4	1.35	0.44	79.7
0.05	0.25	1.78	0.62	83.6	1.77	0.62	82.2
0.05	0.15	2.12	0.77	86.0	2.11	0.77	83.8
0.05	0.05	2.78	1.10	89.1	--	--	--
0.1	0.50	1.29	0.46	74.1	1.29	0.46	73.8
0.1	0.25	1.59	0.64	75.6	1.57	0.64	71.8
0.1	0.15	1.78	0.76	76.6	1.74	0.76	69.9
0.1	0.05	2.14	0.99	83.6	--	--	--
0.15	0.50	1.23	0.46	70.3	1.23	0.46	69.9
0.15	0.25	1.44	0.62	71.5	1.41	0.61	66.8
0.15	0.15	1.56	0.72	72.7	1.50	0.70	64.6
0.15	0.05	1.77	0.88	78.9	--	--	--
0.2	0.50	1.18	0.45	67.9	1.18	0.45	67.4
0.2	0.25	1.32	0.58	68.8	1.29	0.57	64.0
0.2	0.15	1.40	0.66	70.1	1.34	0.63	52.0
0.2	0.05	1.52	0.77	74.4	--	--	--
0.3	0.50	1.09	0.41	66.8	1.09	0.40	65.3
0.3	0.25	1.16	0.48	67.6	1.13	0.46	63.0
0.3	0.15	1.19	0.52	68.5	1.15	0.48	62.8
0.3	0.05	1.24	0.58	70.8	1.16	0.51	61.1
0.5	0.50	1.00	0.30	67.9	1.00	0.30	68.9
0.5	0.25	1.00	0.30	67.9	1.00	0.30	68.9
0.5	0.15	1.00	0.30	68.0	1.00	0.30	68.9
0.5	0.05	1.00	0.30	68.3	1.00	0.30	68.9

Tables 2.3 to 2.6 also include predictions of displacement, effective period and effective damping by the simplified method of analysis. In this analysis, the displacement D was assumed, acceleration A was calculated from the characteristics of the system (see Figure 2.15) and Eqs. (2.22) and (2.23) were used to obtain the effective period and damping. These values were then used to obtain the response directly from the damped spectra of Figure 2.17. Iteration was required to achieve convergence of assumed and calculated response.

The results of Tables 2.3 to 2.6 demonstrate that the simplified method of analysis predicts well the average of peak displacement response, although it occasionally under predicts the response by as much as 20%. Under prediction of displacement response typically occurs in situations where the contribution of hysteretic damping (i.e., first term in Eq. (2.23)) is significant.

Note that predictions based on the simplified method used the actual spectra of Figure 2.17. Generally, such spectra are not available, nor is common in practice to generate them. FEMA, 1997 recommends the use of response modification factors to account for higher damping as demonstrated in Figure 2.10. This method was applied in the prediction of response of some of the analyzed systems and results are presented in Table 2.7. The table includes average and average plus one standard derivation (1σ) results of dynamic analysis for the displacement and the average of peak acceleration. The displacement prediction of the simplified method is typically conservative and in most cases in between the average and average $+1\sigma$ results of dynamic analysis. Predictions on peak acceleration were based on Eqs. (2.12) and (2.13) where S_{pa} is the acceleration at maximum displacement and ζ is the viscous damping component of effective damping (i.e., second and third terms in Eq. (2.23)). It is seen that the prediction for peak acceleration is good.

2.6.3 Estimating Response in Higher Modes

In a simplified nonlinear method of analysis, response in the higher modes may be determined by application of the response spectrum method using the effective stiffness properties of the structure at the actual displacements of the structure. Under

■ Table 2.7 Results of Analysis and Prediction of Simplified Method, Case of System with T_{ef} = 1.0 sec and β_V = 0.15

Strength Ratio e	Stiffness Ratio α	Average Pk. Displ. (mm)	Average +1σ Pk. Displ. (mm)	Average Pk. Accel. (g)	Simplified Method	
					Displ. (mm)	Peak Accel. (g)
Elastic	1.00	85.45	109.29	0.37	99.40	0.43
0.1	0.50	92.73	120.82	0.27	114.91	0.29
0.1	0.25	96.62	128.67	0.21	132.01	0.21
0.1	0.15	97.86	133.12	0.19	154.82	0.18
0.15	0.50	86.86	111.72	0.27	109.24	0.29
0.15	0.25	88.99	118.36	0.22	121.07	0.22
0.15	0.15	91.00	122.59	0.21	139.28	0.19
0.2	0.50	83.27	105.38	0.27	104.74	0.30
0.2	0.25	84.12	108.98	0.24	112.29	0.23
0.2	0.15	86.00	112.50	0.23	125.72	0.21
0.3	0.50	80.66	99.99	0.30	98.89	0.32
0.3	0.25	80.56	100.53	0.27	100.06	0.26
0.3	0.15	82.09	103.50	0.27	103.73	0.24
0.3	0.05	85.47	109.70	0.26	115.18	0.22
0.5	0.50	82.27	102.47	0.34	96.29	0.37
0.5	0.25	81.42	101.19	0.33	94.69	0.35
0.5	0.15	81.69	101.74	0.32	94.06	0.34
0.5	0.05	82.31	103.07	0.32	93.44	0.33

Note: Effective damping in all cases is about equal to or less than 0.5

certain conditions, which may exist in buildings having a complete vertical distribution of viscous energy dissipation devices, the damping ratio in higher modes may be very large and can reach critical or over critical values. The origin of this interesting phenomenon may be found in Eq. (2.5) where for higher modes, the device relative modal displacements φ_{rj} assume large values. It should be noted that this phenomenon cannot, generally, occur in structures having viscoelastic energy dissipation devices since such devices contribute stiffness and, therefore, cause an increase in the strain energy (see Eq. (2.7) which has the strain energy in the denominator of the equation describing modal damping).

The existence of highly damped, and particularly over critically damped modes, represents a theoretical complexity since modal analysis procedures are invalid. Under these conditions, it is known that a single-degree-of-freedom structure behaves as a "rigid body" with maximum acceleration approximately equal to

the peak ground acceleration. For example, Figure 2.19 presents spectra of peak response quantities of a single-degree-of-freedom viscously damped system subjected to the 20 scaled motions of Table 2.2. The spectra demonstrate that despite the high damping (concentrating on the case of the critically damped system, that is, damping ratio of 1.0) the system responds with a non-zero maximum velocity, which is of significance in determining forces in the viscous energy dissipation devices.

The typical approach for determining the maximum velocity (e.g., FEMA, 1997) is to calculate the maximum velocity as the maximum displacement times frequency (= 2π/period), where the maximum displacement is determined from the spectral acceleration of the 5%-damped spectrum at the relevant period divided by factor B of Table 2.3 (that is, maximum velocity is calculated as pseudo-velocity). For the short-period range, this factor is limited to 3.0 for damping ratio equal to or more than 0.50. Figure 2.19 shows, in dashed lines, predictions of acceleration at maximum displacement, pseudo-velocity and maximum displacement by the FEMA, 1997 procedure for this particular case. Evidently, the procedure results in conservative estimates of maximum velocity for damping ratio larger than or equal to 0.50.

2.6.4 EXAMPLE OF APPLICATION OF SIMPLIFIED NONLINEAR METHOD OF ANALYSIS

Building and Energy Dissipation System

The example structure consists of several three-story, three-bay frames as shown in Figure 2.20. It is assumed that diaphragms are flexible at each floor level so that analysis of a single frame without regard for torsion is appropriate. Each frame has a complete vertical distribution of fluid viscous dampers. All dampers have identical properties, which are described by the simple dashpot model, that is, damper force $F = c_v \dot{x}$ where c_v is the damping coefficient and $\dot{x}$ is the damper axial velocity. The frame is modeled as a shear-type structure with story shear-story drift relations as shown in Figure 2.20. Floor seismic weights, determined on the basis of tributary area, are shown in Figure 2.20.
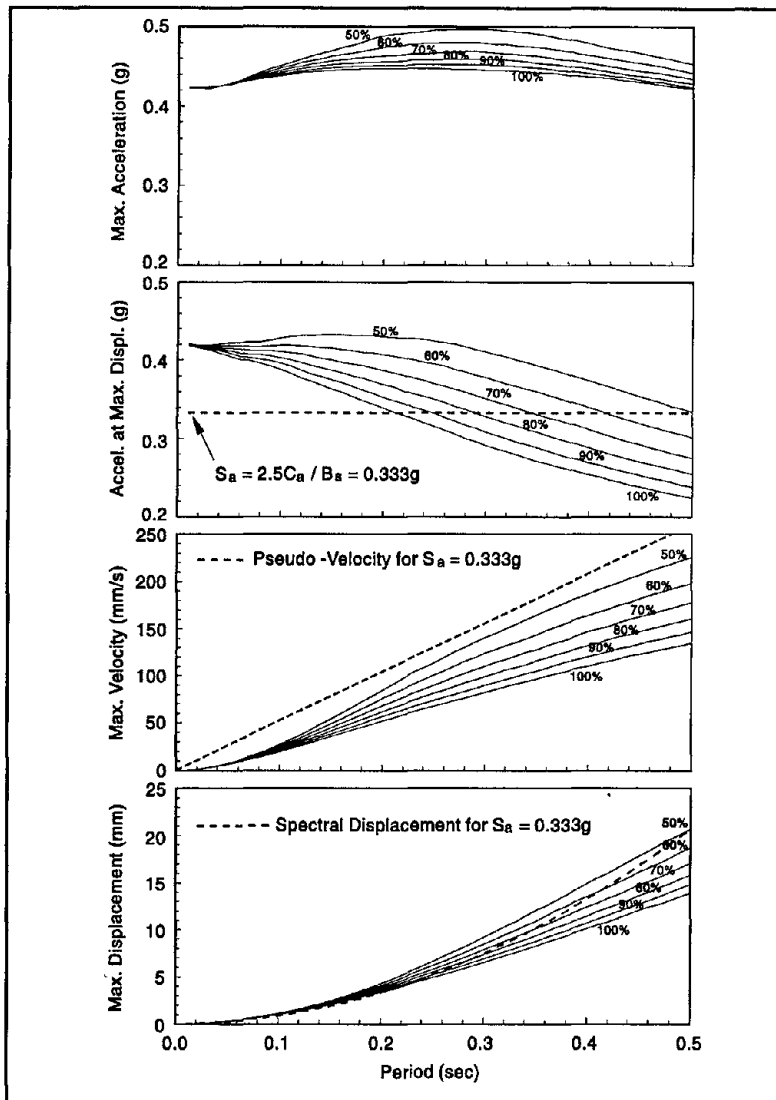
Figure 2.19 Average Response Spectra of Scaled Motions in the Short-Period Range and for High Damping

The seismic shaking is described by the 1994 NEHRP Recommended Provisions, 5%-damped spectrum of Figure 2.10 with $C_a = 0.4$, $C_v = 0.6$ and $T_s = 0.6$ sec.

The properties of the dampers are selected on the basis of providing added damping ratio in the fundamental mode and under elastic conditions equal to 0.20. That is, using Eq. (2.5) with $\theta_j = 33.7°$, $\phi_3 = 1$, $\phi_2 = 0.6440$, $\phi_1 = 0.2894$ and $\omega_1 = 8.378$ r/s
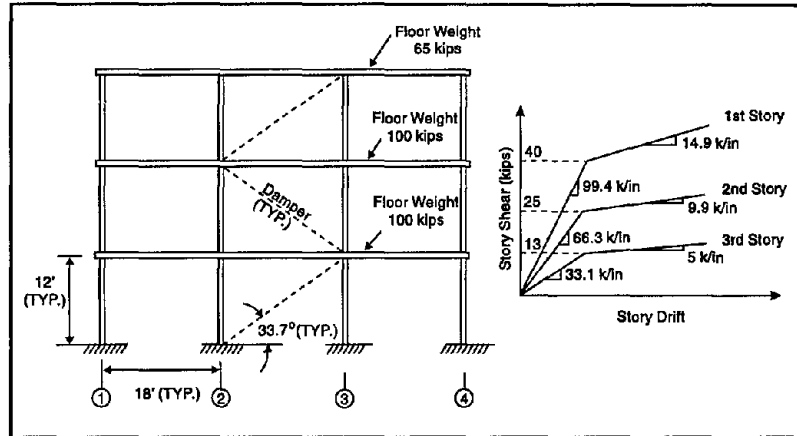
■Figure 2.20 Example Building

(period = 0.75 sec) , the result for ζ_1 = 0.20 is $c'_j = c_v = 4.28$ k-sec/in (j = 1, 2 and 3).

Analysis of the structure is performed without consideration to dependencies, if any, of the properties of the dampers on excitation frequency, temperature, bi-lateral load, and other effects. These effects should be considered by performing multiple analyses.

Dampers in this analysis are assumed to have linear viscous behavior. However, when connected to braces, they effectively behave as spring-dashpot systems in series. The effect of bracing has been discussed in Section 2.5.2, where Eqs. (2.21) are provided for evaluating the significance of brace flexibility. In this example, braces are selected to be square tubing, F_y = 46 ksi, 6 x 6 x 5/16. This section can safely carry a compressive force of over 70 kips for length L = 21.6 feet. The stiffness of this brace k_b = AE/L is 768 k/in. Using Eqs. (2.21), the storage stiffness and damping coefficient of the brace-damper assembly are 1.7 k/in and 4.27 k-s/in, respectively. Thus, the brace-damper assembly behaves essentially as purely viscous (note that damping coefficient of 4.27 k-s/in is essentially identical to the damper coefficient). Accordingly in this case, the brace flexibility is neglected as being insignificant.

Pushover Curves

Pushover curves for the example structure are established for two patterns of lateral loads, one for uniform pattern (that is,
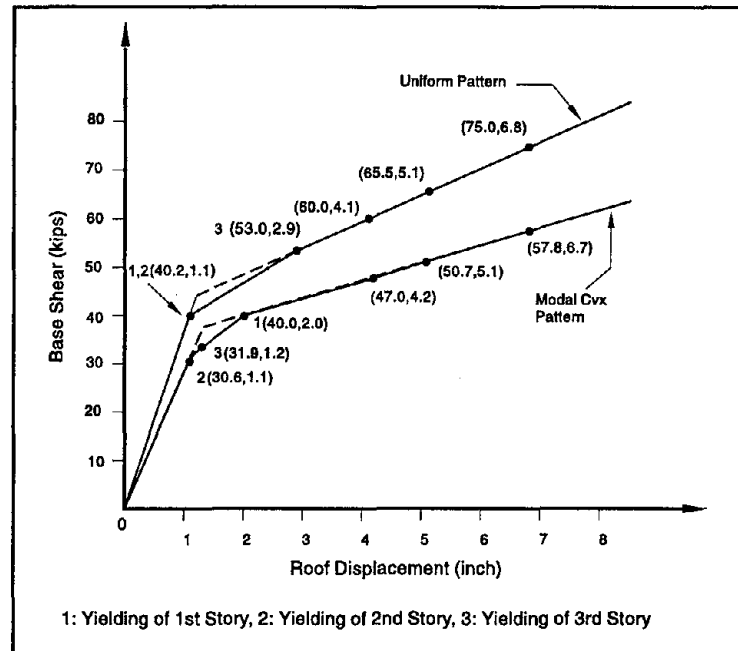
Figure 2.21 Pushover Curves of Example Building

lateral loads proportional to floor seismic weight) and one for modal pattern. The latter follows the approach of FEMA, 1997 in which the loads are proportional to the vertical distribution factors of the linear static procedure (C_{v3}= 0.4129, C_{v2}= 0.4025, C_{v1} = 0.1846).

Figure 2.21 shows the pushover curves in the two cases of lateral load patterns. The two pushover curves are different and, as it will be seen in the sequel, the modal properties of the structure at various stages of pushover by the two patterns are also different. This demonstrates the significance of the assumed lateral load pattern. It is believed, but not confirmed with a sufficient number of studies, that both patterns (uniform and modal) should be used in obtaining bounds of response. Other studies (e.g., Reinhorn, et al., 1995; Bracci et al., 1997; Valles et al., 1997) favor the use of patterns in which the lateral loads do not monotonically increase but rather depend on the structural member resistances as the members progressively yield during pushover.

Roof Displ (in)		Mode 1 $k=1$	Mode 2 $k=2$	Mode 3 $k=3$
4.2	T_k (sec)	1.189	0.542	0.345
	ω_k (r/s)	5.284	11.593	18.212
	$\{\Phi_k\}$	1	1	1
		0.6011	-0.9198	-3.7502
		0.1937	-0.4945	8.2873
	W_{sk} (kips)	199.0	33.7	32.3
	Γ_k	1.3775	0.4391	0.0622
5.1	T_k (sec)	1.258	0.573	0.368
	ω_k (r/s)	4.995	10.965	17.074
	$\{\Phi_k\}$	1	1	1
		0.6086	-0.8858	-3.5782
		0.2095	-0.5231	7.2985
	W_{sk} (kips)	202.5	33.8	28.7
	Γ_k	1.3794	0.4442	0.0655
	ζ_k	0.388 (+0.055)	1.210	0.970
6.1	T_k (sec)	1.322	0.602	0.389
	ω_k (r/s)	4.753	10.437	16.152
	$\{\Phi_k\}$	1	1	1
		0.6151	-0.8571	-3.4544
		0.2228	-0.5449	6.6240
	W_{sk}	205.4	33.7	25.9
	Γ_k	1.3803	0.4472	0.0677

Notes: $W_{sk} = M_k g$, M_k determined by Eq. (2.9)
   Γ_k is determined by Eq. (2.11)
   ζ_k is determined by Eq. (2.5)

Modal Properties at Various Stages of Pushover

Modal properties of the structure were determined at various stages of pushover and are presented in Tables 2.8 and 2.9 for the two patterns of lateral loads. These properties were determined by eigenvalue analysis of the building using the effective story stiffnesses at various stages of roof displacement. One should note the significant differences in mode shapes among the two load patterns for the same roof displacement. This indicates that calculations of story drifts and damper forces can be significantly affected by the assumed lateral load pattern.

Tables 2.8 and 2.9 contain also, for the case of roof displacement of 5.1 inch (this is approximately the roof displacement calculated in the simplified nonlinear method of analysis), calculations of damping ratios in each mode. The damping ratio was calculated by Eq. (2.5) using the mode shapes and frequencies calculated on the basis of effective story stiffness at roof displacement of 5.1 inch. Note that higher modes are near critically or over critically damped.

The damping ratio shown in Tables 2.8 and 2.9 is the one provided by the energy dissipation system. Additional effective damping is provided by inelastic action in the structural frame

■ Table 2.9 Modal Properties of Example Building in Various Stages of Pushover Analysis by the Uniform Pattern

Roof Displ (in)		Mode 1 k = 1	Mode 2 k = 2	Mode 3 k = 3
4.2	T_k (sec)	1.223	0.478	0.359
	ω_k (r/s)	5.138	13.145	17.502
		1	1	1
	$\{\Phi_k\}$	0.7781	-0.4549	-1.5804
		0.3538	-0.8327	1.6424
	W_{sk} (kips)	230.0	26.3	8.7
	Γ_k	1.2907	0.4113	0.1216
5.1	T_k (sec)	1.304	0.527	0.386
	ω_k (r/s)	4.820	11.932	16.295
		1	1	1
	$\{\Phi_k\}$	0.7512	-0.5243	-1.8431
		0.3407	-0.7477	2.1599
	W_{sk} (kips)	228.1	26.1	10.8
	Γ_k	1.3093	0.4192	0.1110
	ζ_k	0.309 (+0.056)	0.948	1.160
6.1	T_k (sec)	1.390	0.568	0.408
	ω_k (r/s)	4.522	11.056	15.392
		1	1	1
	$\{\Phi_k\}$	0.7463	-0.5168	-1.9403
		0.3568	-0.7370	2.2410
	W_{sk}	230.4	25.0	9.6
	Γ_k	1.3139	0.4135	0.1007

exclusive of the dampers. This portion of damping has been calculated by the following procedure (per FEMA, 1997). The pushover curve has been approximated by a bilinear representation (see Figure 2.21) and converted to spectral capacity curve. Spectral acceleration and displacement at yield, A_y and D_y respectively, and spectral acceleration and displacement at roof displacement of 5.1 inch, A and D respectively, were calculated. The effective damping ratio provided by the frame exclusive of the dampers was calculated as

$$\beta_{eff} = \frac{2q\left(A_y D - A D_y\right)}{\pi A D} \qquad (2\text{-}24)$$

where q is an efficiency factor that is equal to the actual area enclosed by the loop divided by the loop area of a perfect bilinear hysteretic system. Note that for $q = 1$ (perfect hysteresis loop), Eq. (2.24) is identical to the first term in Eq. (2.23). Also note that Eq. (2.24) is based on the geometric stiffness approach for approximating the system by an equivalent linear one (see Section 2.6.2). A factor $q = 0.2$ was assumed that would represent a system with small ability to dissipate energy during inelastic action. Calculated values of effective damping ratio (accounted for only in the fundamental mode) were approximately equal to 0.055 (included in Tables 2.8 and 2.9 in parenthesis).

Response Calculations

Response calculations are presented in detail for the case of modal pattern of lateral loads. Calculation of response in the fundamental mode starts with an assumption on the roof displacement. In this case, the assumption $\delta_3 = 4.2$ inch was made and calculations as illustrated in Figure 2.14 resulted in a roof displacement of 5.1 inch. Calculations were then repeated for an assumed roof displacement of 5.1 inch. These calculations are presented now in some detail.

The pushover curve for modal pattern of Figure 2.21 is converted to spectral capacity curve by use of Eqs. (2-10) and using the modal properties for roof displacement of 5.1 inch of Table 2.8 (note that $W_{sk} = M_k$ g). This curve is shown in Figure 2.22 overlying the spectral capacity curve which was determined
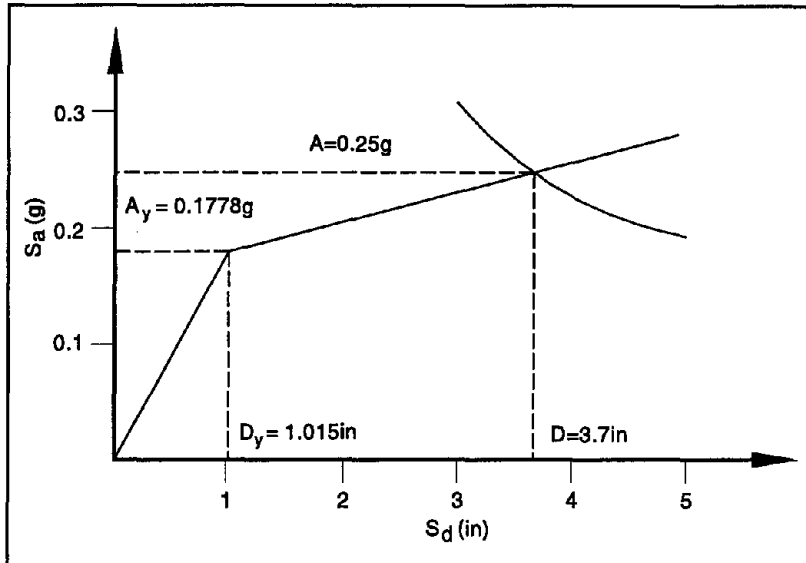
■ Figure 2.22 Overlying of Spectral Capacity Curve and Design Demand Spectrum for Response Calculation in Fundamental Mode, Case of Modal Pattern

from the response spectrum of Figure 2.10 for damping ratio of 0.443 (0.388 + 0.055 per Table 2.8). Since the period of the structure is 1.258 sec (see Table 2.8), that is in the long-period range, the spectral capacity curve was established for a response modification factor $B = B_1 = 1.943$ per Section 2.4 and Table 2.1. The calculated spectral response is $A = 0.25$ g and $D = 3.7$ inch, which upon conversion to base shear and roof displacement (Eqs. (2.10)) give $V_1 = 50.6$ kips and $\delta_3 = 5.1$ inch. That is, convergence of assumed and calculated roof displacements is achieved.

Floor displacements and story drifts in the fundamental mode are then obtained from the results of pushover analysis at the calculated roof displacement of 5.1 inch. They are presented in Table 2.10 together with results on damper axial displacements (= story drift times cos θ_j) and damper axial force (= damper displacement times ω_1, where $\omega_1 = 4.995$ r/s is the frequency of the structure in the fundamental msode at roof displacement of 5.1 inch - see Table 2.8).

Calculation of response in the higher modes follows standard modal analysis procedures using the effective modal properties of the structure established at roof displacement of 5.1 inch. Since both modes have periods in the short-period range and damping exceeds 0.50, a response modification factor $B = B_S = 3.0$ (per

■ Table 2.10 Response of Example Structure for Modal Pattern of Lateral Loads

Response Quantity	Floor or Story	Mode 1	Mode 2	Mode 3	SRSS
Lateral Loads (kips)	3	20.9	9.6	1.4	
	2	20.4	-13.1	-7.8	
	1	9.3	-7.8	15.9	
Floor Displacement (in)	3	5.110	0.476	0.029	5.132
	2	3.137	-0.421	-0.104	3.167
	1	1.114	-0.249	0.211	1.161
Story Drift (in)	3	1.973	0.897	0.133	2.171
	2	2.023	0.172	0.315	2.055
	1	1.114	0.249	0.211	1.161
Damper Axial Displacement (in)	3	1.641	0.746	0.110	1.806
	2	1.683	0.143	0.262	1.709
	1	0.927	0.207	0.176	0.966
Damper Axial Force (kips)	3	35.1	35.0	8.1	50.2
	2	36.0	6.7	19.1	41.3
	1	19.8	9.7	12.8	25.5
Actions in 1st Story Column 3 (P:kips, M:k-ft)	Max. Drift	P=13.6 M=76.0	P=0 M=17.0	P=0 M=14.3	P=13.6 M=79.2
	Max. Veloc.	P=50.4	P=10.3	P=1.0	P=51.5
	Max. Accel.	P=41.6 M=60.1	P=10.3 M=17.0	P=1.0 M=14.3	P=42.9 M=64.1

Table 2.1) is used. Results are presented in Table 2.10. Combined responses by the SRSS rule are also presented in the same table. It should be noted that the calculation of response in the higher modes presents complexities when the energy dissipation devices have nonlinear behavior. The interested reader is referred to Seleemah and Constantinou (1997) for details.

Table 2.10 also presents results on actions in a selected member (first story column 3). These actions are calculated at three stages: (a) at maximum drift, (b) at maximum velocity (i.e., when drift is zero), and (c) at maximum acceleration. The latter is determined as a linear combination of actions for stage (a) times factor f_1 and for stage (b) times factor f_2, where factors f_1 and f_2 are given by Eq. (2.13). Note that Eq. (2.13) is used with ξ equal to the viscous component of damping ratio (Eq. (2.5)). Moreover, for high values of damping, as those of the higher modes, factors f_1 and f_2 are conservatively assumed to be equal to unity. Figure 2.23 illustrates loads and member actions on the structure at the various considered stages.
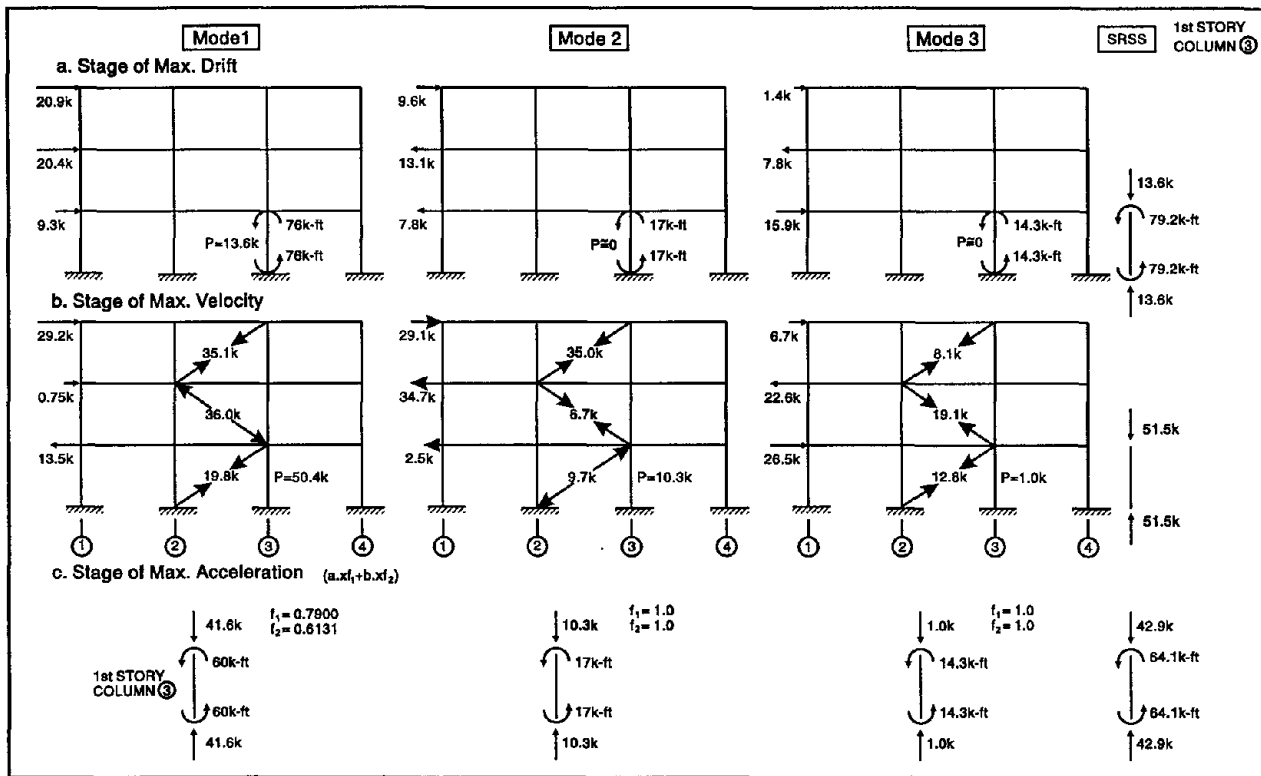
Figure 2.23 Illustration of Forces Acting on Example Structure for Modal Pattern of Lateral Loads and Actions in Selected Member

Calculations were repeated for the uniform pattern of loads and results are presented in Table 2.11. A comparison of Tables 2.10 and 2.11 reveals differences in the calculated responses among the two assumed patterns of lateral loads. It is believed that the use for design of the maximum calculated response quantities among the two assumed patterns of loads is appropriate and it is required in FEMA, 1997.

■Table 2.11 Response of Example Structure for Uniform Pattern of Lateral Loads

Response Quantity	Floor or Story	Mode 1	Mode 2	Mode 3	SRSS
Lateral Loads (kips)	3	15.7	9.1	2.4	
	2	24.2	-7.3	-6.8	
	1	24.2	-10.5	8.0	
Floor Displacement (in)	3	4.835	0.379	0.054	4.850
	2	3.902	-0.199	-0.099	3.908
	1	2.020	-0.284	0.116	2.043
Story Drift (in)	3	0.933	0.578	0.153	1.108
	2	1.882	0.085	0.216	1.896
	1	2.020	0.284	0.116	2.043
Damper Axial Displacement (in)	3	0.776	0.481	0.127	0.922
	2	1.566	0.071	0.179	1.578
	1	1.681	0.236	0.097	1.700
Damper Axial Force (kips)	3	16.0	24.6	8.9	30.7
	2	32.3	3.6	12.5	34.8
	1	34.7	12.1	6.7	37.4
Actions in 1ˢᵗ Story Column 3 (P:kips, M:k-ft)	Max. Drift	P=13.5 M=96.2	P=1 M=13.1	P≈0 M=5.4	P=13.6 M=97.2
	Max. Veloc.	P=46.1	P=8.9	P=1.7	P=47.0
	Max. Accel.	P=35.7 M=81.8	P=9.9 M=13.1	P=1.7 M=5.4	P=37.1 M=83.0

2.6.5 NONLINEAR DYNAMIC ANALYSIS OF EXAMPLE BUILDING

Nonlinear dynamic analysis of the example building of Section 2.6.4 has been performed using the 20 scaled motions of Table 2.2. Note that this group of motions is compatible with the response spectrum used in the simplified analysis of the building (see Section 2.6.2).

The building was modeled as shear-type with bilinear hysteretic characteristics consistent with the story-shear-story drift relations of Figure 2.20 and the assumed inherent damping capability of the frame in the simplified analysis. For example, Figure 2.24 shows calculated story shear-story drift loops of the first story for one of the scaled motions of Table 2.2. The figure includes the
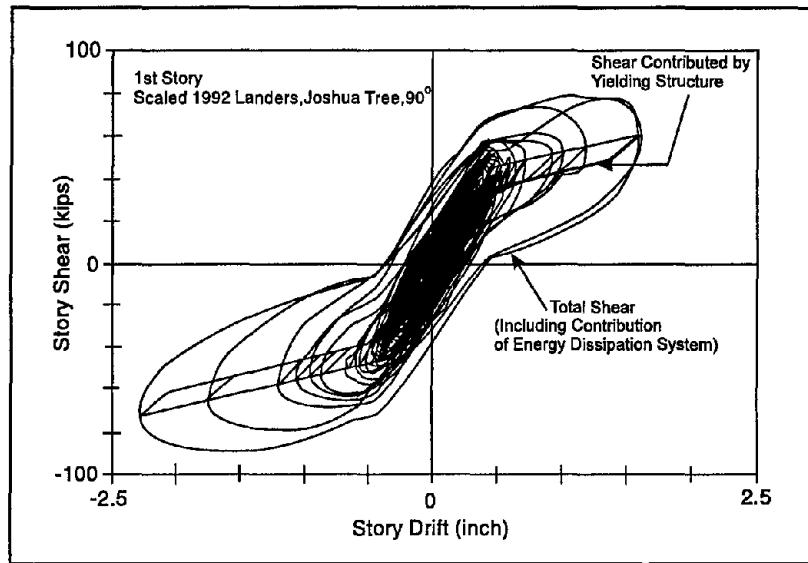
Figure 2.24 Calculated First Story Shear-Drift Loops In Nonlinear Dynamic Analysis of Example Building

loop for the total story shear (shear in columns plus horizontal component of damper force) and the portion of that loop contributed by the columns alone). Of interest is to note in Figure 2.24 that the maximum story (base) shear is 1.24 times larger than the shear at maximum displacement (that is, the shear contributed by the columns alone). Considering harmonic response in the maximum drift cycle, Eq. (2.12) may be used to estimate the ratio of maximum shear force to shear at maximum drift (as $f_1 + 2\zeta f_2$). Since ζ is, approximately, in the range 0.31 to 0.39 (see Tables 2.8 and 2.9), the shear force ratio is predicted to be in the range 1.18 to 1.27, thus in good agreement with dynamic analysis results.

Table 2.12 presents a summary of the results of dynamic analysis and a comparison to the results of the simplified method of analysis. Results of the nonlinear dynamic analysis are presented in terms of minimum, maximum, average, and average plus one standard deviation (1σ) responses of the 20 sets of results.

Table 2.12 demonstrates a significant scatter in results obtained by the nonlinear dynamic analysis method. Moreover, the maximum among modal and uniform pattern results of the simplified nonlinear method compare well with the average plus one standard deviation results of dynamic analysis for displacements, and with the average results of dynamic analysis for damper forces. That is, the displacement prediction is conservative in comparison to the average, whereas the damper force prediction is about at the average of dynamic analysis results. This represents a confirmation of the usefulness of simplified nonlinear methods of analysis, however, limited to a single example. More studies are certainly needed with a variety of structural system properties and configurations, and energy dissipation systems in order to validate simplified nonlinear methods of analysis.

■ Table 2.12 Comparison of Results of Nonlinear Dynamic and Simplified Nonlinear Methods of Analysis

Response Quantity		Simplified Nonlinear Method		Nonlinear Dynamic Method			
		Modal Pattern	Uniform Pattern	Min.	Avg.	Avg. +1σ	Max.
Roof Displ. (in)		5.132	4.850	1.235	3.562	4.947	6.658
Story Drift (in)	3	2.171	1.108	0.332	0.679	0.930	1.289
	2	2.055	1.896	0.513	1.452	2.001	2.664
	1	1.161	2.043	0.466	1.514	2.129	2.824
Damper Axial Displ. (in)	3	1.806	0.922	0.276	0.565	0.774	1.073
	2	1.709	1.578	0.427	1.208	1.665	2.216
	1	0.966	1.700	0.388	1.259	1.771	2.350
Damper Axial Force (kip)	3	50.2	30.7	11.5	21.8	28.4	37.7
	2	41.3	34.8	17.2	44.1	58.3	70.3
	1	25.5	37.4	15.1	39.4	53.5	60.7

ENERGY DISSIPATION DEVICES AS ELEMENTS OF SEISMIC ISOLATION SYSTEMS

Seismic isolation systems typically contain a mechanism for energy dissipation, such as specially compounded rubber for high damping, lead-plugs in rubber bearings and friction in sliding isolation systems (Kelly, 1993; Skinner et al., 1993, Soong and Constantinou, 1994). Moreover, a number of devices have been developed for enhancing energy dissipation in isolation systems. These include yielding steel devices and lead extrusion dampers used in a number of bridges and one building in New Zealand (Skinnner et al., 1993), and a variety of yielding steel, lead, friction and viscoelastic fluid dampers used in a large number of buildings in Japan (Kelly, 1988; Skinner et al., 1993). Application of these hybrid (seismic isolation and energy dissipation) systems was discontinued in Japan and New Zealand since approximately 1990 in favor of the use of lead-rubber and high damping rubber bearings.

More recently, considerations for the effects of near fault, high velocity seismic pulses and the recordings of such motions in the 1994 Northridge and 1995 Kobe earthquakes prompted engineers in the United States to return to hybrid systems in an attempt to mitigate their effects. Since expected displacements and required damper force output in this type of earthquake are large, the energy dissipation devices of choice are fluid viscous dampers. Moreover, the use of viscous devices in the isolation system provides benefits in the distribution of story shear forces as compared to comparable hysteretic devices. For example, Figure 2.25 compares the distribution of story shear over height in an 8-story building with an isolation system consisting of either hysteretic isolators or essentially linear isolators (such as low damping rubber bearings) and linear viscous dampers. Both systems are designed to have the same isolation period, T_I, and effective damping, β, per definition of the Uniform Building Code (International Conference of Building Officials, 1994). The seismic input consists of nine pairs of actual earthquakes scaled to be representative of Seismic Zone 4, soil type S_2 in accordance with the Uniform Building Code. Presented results are mean values of story
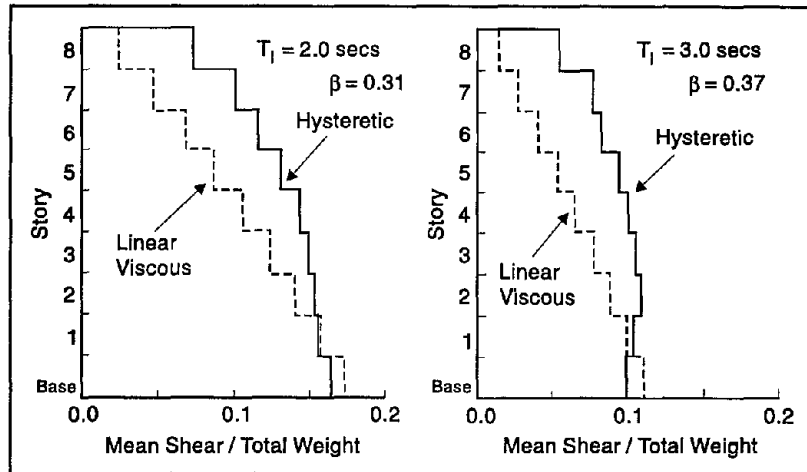
■ Figure 2.25 Comparison of Distribution of Shear Force with Height in 8-story Structure with Hysteretic and Linear Viscous Isolation Systems. Seismic Input Representative of Seismic Zone 4, Soil type S_2 per 1994 UBC

shear forces (each pair of earthquakes resulted in maximum shears in two orthogonal directions; the maximum shear among the two was used in the calculation of the mean). The two isolation systems resulted in nearly the same isolation system displacement and base shear. However, the distribution of story shear with height of the viscous system is more favorable than that of the hysteretic system. The results clearly indicate significant higher mode participation and large upper floor accelerations in the hysteretic system.

An important recent application of viscous dampers within an isolation system is in the new San Bernardino County Medical Center Replacement Project in Colton, California (see Chapter 5 for further details). Scheduled to be completed in 1998, this roughly 80,000 square meters complex consists of five interconnected buildings supported on 392 high damping rubber bearings with 184 fluid dampers used for enhanced energy dissipation (Hussain et al., 1993; Engineering News-Record, 1995). The complex is situated nine miles from the San Andreas and two miles from the San Jacinto faults. It has been designed for a maximum considered earthquake having spectral acceleration of 0.66 g and 0.44 g at periods of 2.0 and 3.0 seconds, respectively.

The viscous dampers have an installed length of 3.75 m, stroke of ±0.6 m and output force of 1400 kN at velocity of 1.5 m/

sec. The behavior of these dampers is nonlinear viscous as de-
scribed by Eq. (2.17) with exponent α equal to approximately 0.4.
Cyclic testing of these devices at full scale was not possible. Rather,
full scale drop hammer testing was conducted (Taylor and Con-
stantinou, 1995) based on comparative drop hammer and cyclic
testing conducted on reduced-scale prototypes. Figure 2.26 shows
the force-velocity relation established by cyclic testing of a re-
duced-scale prototype device at three different ambient tempera-
tures. Drop hammer test data were within ±5% of the cyclic test
data. The insensitivity of properties of the device to ambient tem-
perature, which was a requirement for this project, was accom-
plished by proper selection of materials and material volumes so
that changes in the physical and mechanical properties of the fluid
were compensated by volume changes so that fluid pressures were
practically unaffected.

The nonlinear viscous behavior of the dampers for this
project was desirable for the following reasons: (a) force output
increments are small at large velocities, (b) energy dissipation per
cycle is more than that of comparable linear viscous dampers (see
eq. (2.18) and (2.19)), and (c) such devices are suitable for attenu-
ating the effects of high velocity pulses and have been used in the
military for attenuating weapon's grade shock and blast effects.
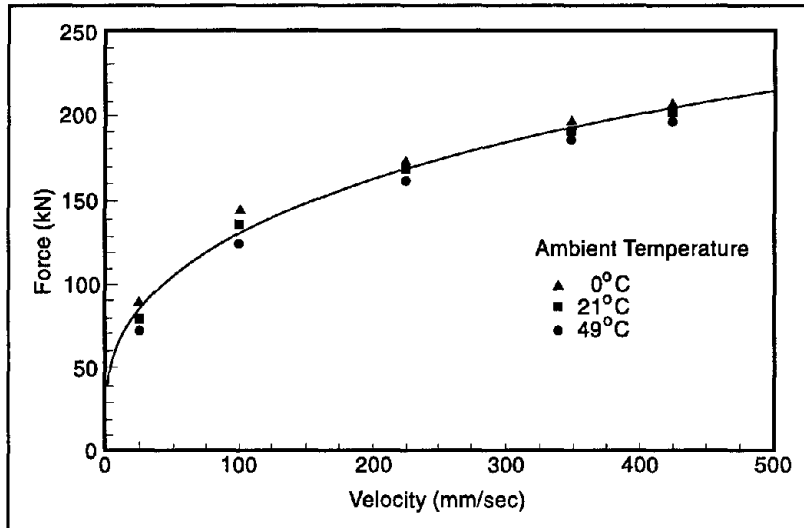
■ Figure 2.26 Force-Velocity Relation of Reduced-Scale Prototype Fluid Damper of San Bernardino
County Medical Center Replacement Project

MENSHIN DESIGN

Menshin is a design strategy used in Japan for bridges. The strategy utilizes seismic isolation bearings as elements to dissipate energy and to distribute the lateral forces to elements of the substructure, rather than as elements to primarily lengthen the period and reflect, thus, seismic energy.

The reason for using this design approach is related to the particular design criteria for bridges utilized in Japan (Kawashima and Unjoh, 1994; Civil Engineering Research Center, 1992). Figure 2.27 presents the level 2 bridge design spectra for Japan. They are characterized by a constant spectral acceleration region that extends up to between 1.4 sec and 2.0 sec period, depending on the ground conditions. Evidently, for effective seismic isolation, it is necessary to lengthen the period to values beyond 3.0 sec, which is very difficult, if at all possible, to achieve with elastomeric isolation systems given that bearing loads are light for typical highway bridges. Moreover, such an isolation system would have resulted in large bearing displacements, which are undesirable due to concerns for safety and requirements for large expansion joints, with their related problems of cost, maintenance, driving discomfort and noise pollution.
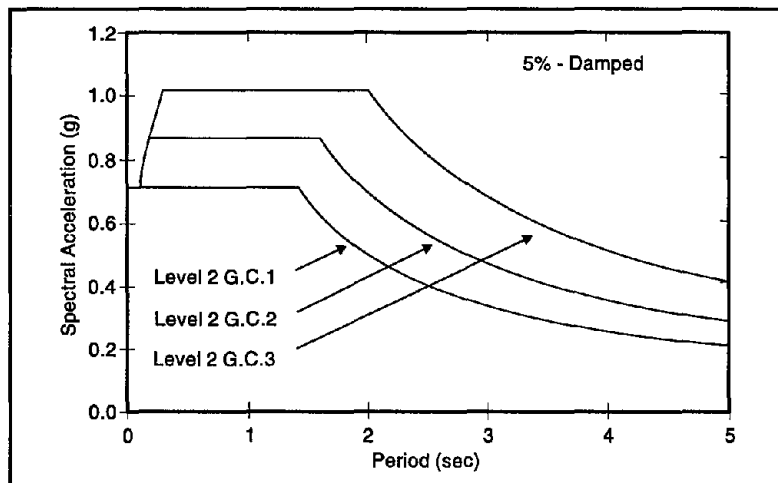
■ Figure 2.27 Level 2 Bridge Design Spectra for Japan (Ground Condition 1 = Stiff Soil; Ground Condition 3 = Deep Alluvium Soil)

Given these constraints, Japanese engineers opted for the use of stiff elastomeric bearing systems (period of the order of 1.0 sec) and utilization of the energy dissipation capability of the bearings for further, though limited in comparison to seismic isolation, reduction of displacement and acceleration response. Moreover, by proper selection of stiffness characteristics and strength (for lead-rubber bearings) they could achieve a desirable distribution of lateral forces to elements of the substructure. It may be viewed as a conservative application of seismic isolation bearings, in which the element of flexibility is not fully utilized. Rather, Menshin design appears to be the use of seismic isolation bearings as elements of an energy dissipation system.

Recently, isolation systems characterized by considerable flexibility have been developed and tested for application in Japan (Tsopelas et al., 1996). These systems utilize flexible isolation bearings and fluid viscous dampers for significant enhancement of energy dissipation capability, so that bearing displacements for all ground conditions in Japan can be limited to less than 160 mm and isolation system shear force can be limited to less than 1/3 of the supported weight. These systems should be classified as hybrid seismic isolation-energy dissipation systems.

MATHEMATICAL MODELING

Passive energy dissipation systems utilize a wide range of materials and technologies as a means to enhance the damping, stiffness and strength characteristics of structures. The basic principles involved in determining the overall performance and design of these systems were presented in the previous chapter. In this chapter, a more detailed discussion of the behavior of individual passive devices and systems is provided, with emphasis on the development of appropriate mathematical models. This information is needed to better understand the principal assumptions employed in the simplified design procedures and to better appreciate the capabilities and limitations of the various devices.

The performance-based classification scheme, introduced in Chapter 2 and summarized in Table 3.1, is employed to categorize passive energy dissipation systems. Broadly speaking, dissipation may be achieved either by the conversion of kinetic energy to heat or by the transferring of energy among vibrating modes. The first mechanism incorporates both **hysteretic devices** that dissipate energy with no significant rate dependence, and **viscoelastic devices** that exhibit considerable rate (or frequency) dependence. Included in the former group are devices that operate on principles such as yielding of metals and frictional sliding, while the latter group consists of devices involving deformation of viscoelastic solids or fluids and those employing fluid orificing. A third classification consists of **re-centering devices** that utilize either a preload generated by fluid pressurization or internal springs, or a phase transformation to produce a modified force-displacement response that includes a natural re-centering component. An idealized single-degree-of-freedom (SDOF) structure is shown in Figure 3.1a with a passive hysteretic, viscoelastic or re-centering device operating in parallel. A macroscopic model defining the stiffness and damping characteristics of the device is needed in order to determine the overall structural response.

■Table 3.1 Passive Energy Dissipation Systems

Classification	Principles of Operation	Materials and Technologies	Performance Objectives
Hysteretic Devices	Yielding of metals Friction	Steel or lead Metal-to-metal or non-metal contact	Energy dissipation, strength enhancement
Viscoelastic Devices	Deformation of viscoelastic solids Deformation of viscoelastic fluids Fluid orificing	Viscoelastic polymers Highly viscous fluids Fluids; advanced orifice designs and fluid sealing	Energy dissipation, stiffness enhancement
Re-centering Devices	Fluid pressurization and orificing Friction-spring action Phase transformation in metals	Compressible fluids, high pressure sealing Metal-to-metal or non-metal contact Shape memory alloys, superelastic behavior	Energy dissipation, strength enhancement, re-centering capability
Dynamic Vibration Absorbers	Tuned mass oscillators Tuned liquid oscillators	Mass-spring-fluid damper Water tanks, U-shaped liquid containers	Damping enhancement

The second mechanism mentioned above, pertaining to the transfer of energy between modes, is utilized in **dynamic vibration absorbers**. In these systems, supplemental oscillators involving mass, stiffness and damping are introduced, as illustrated in Figure 3.1b. In order to significantly enhance performance, the dynamic characteristics of the supplemental oscillators must be tuned to those of the primary structure. Tuned mass dampers and tuned liquid dampers are included in this category.

In the following sections, each major type of passive system will be examined in some detail. Emphasis will be placed on the physical basis for their behavior and on the mathematical models appropriate for characterization of their response. In many cases, models with varying levels of sophistication will be provided. For preliminary design and analysis, rather simple
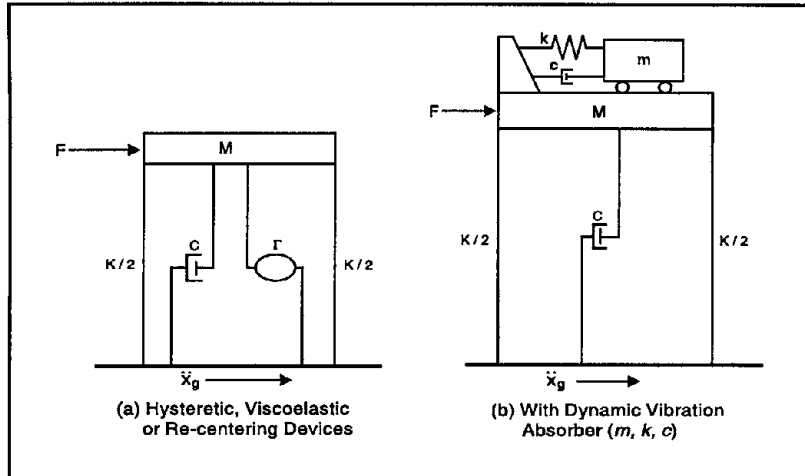
■ Figure 3.1 Idealizations for Passively Damped SDOF Structures (M, K, C)

(a) Hysteretic, Viscoelastic or Re-centering Devices

(b) With Dynamic Vibration Absorber (m, k, c)

approximations are often desirable, while for final detailed design, more precise representations may be required.

3.1
HYSTERETIC SYSTEMS

Hysteretic systems, by definition, dissipate energy through a mechanism that is independent of the rate of load application. Included in this group are **metallic dampers** that utilize the yielding of metals as the dissipative mechanism, and **friction dampers** that generate heat through dry sliding friction. Typical force-displacement responses for these devices obtained under constant amplitude, displacement-controlled cyclic conditions are displayed in Figure 3.2. The quantities F and x represent the overall device force and displacement, respectively. For cyclic loading at displacement amplitude x_0 and circular frequency ω, the displacement at time t can be written

$$x(t) = x_o \sin \omega t \qquad (3.1)$$

Notice from Figure 3.2 that for both metallic and friction devices, the response remains essentially unchanged at various

(a) Metallic Dampers   (b) Friction Dampers
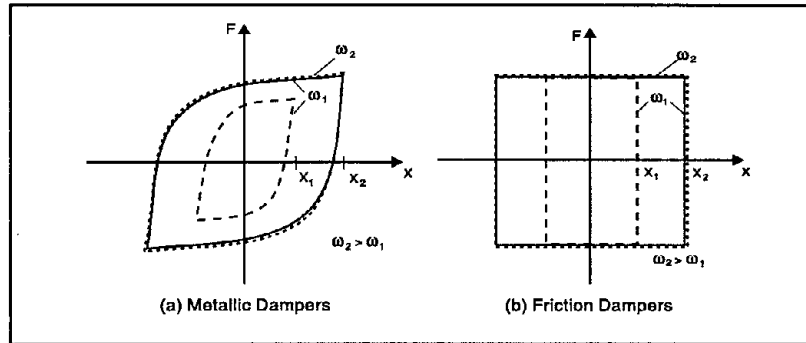
■ Figure 3.2 Idealized Force-displacement Response of Hysteretic Devices

excitation frequencies, thus demonstrating rate independence. However, the devices are inherently nonlinear. The force output clearly does not scale with the displacement, and significant path dependence is apparent. This nonlinearity of hysteretic devices must be considered in both structural analysis and design. It should also be noted that in all cases, energy dissipation occurs only after a certain threshold force is exceeded. Consequently, hysteretic dampers are intended primarily for seismic applications.

3.1.1 METALLIC DAMPERS

One of the most effective mechanisms available for the dissipation of energy, input to a structure during an earthquake, is through the inelastic deformation of metallic substances. In traditional steel structures, aseismic design relies upon the post-yield ductility of structural members to provide the required dissipation. However, the idea of utilizing supplemental metallic hysteretic dampers within the superstructure to absorb a large portion of the seismic energy began with the conceptual and experimental work by Kelly et al., (1972) and Skinner et al., (1975). During the ensuing years, considerable progress has been made in the development of metallic dampers and many new designs have been proposed.

Examples of metallic dampers that have received significant attention in recent years include the X-shaped and triangular plate dampers illustrated in Figure 3.3. These parallel plate devices are typically installed within a frame bay between a chevron brace and the overlying beam. As a result, the dampers primarily resist the horizontal forces associated with interstory drift via flex-

(a) X-shaped Plate Damper   (b) Triangular Plate Damper
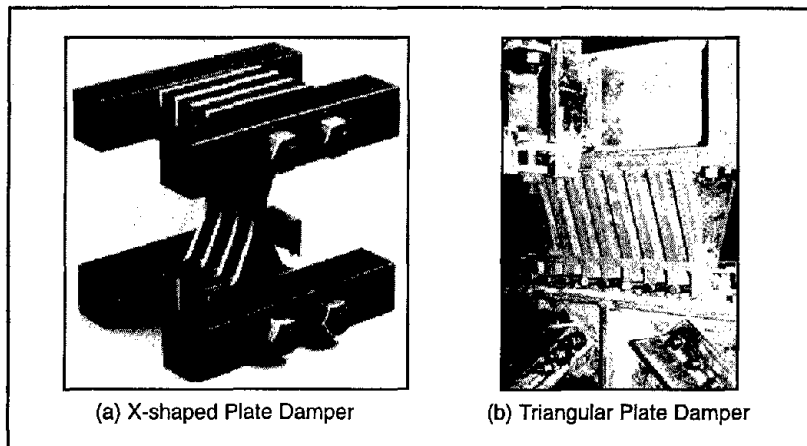
a. Courtesy of CounterQuake Corp.   b. Tsai et al., 1993
■ Figure 3.3 Metallic Damper Geometries

ural deformation of the individual plates. Beyond a certain level of force, the plates yield and thus provide a supplemental amount of energy dissipation. The tapered shape of the plates promotes nearly uniform yielding throughout their length.

Despite differences in the geometric configuration of various metallic devices, the underlying dissipative mechanism in all cases results from the inelastic deformation of a metal. Usually that metal is mild steel, although sometimes lead is employed. In any case, in order to effectively employ a metallic damper for improved aseismic structural design, one must construct a reasonable mathematical model of its relevant force-deformation characteristics. Since this overall response is intimately linked with the cyclic stress-strain behavior of the metal, it is beneficial at this point to briefly review the typical inelastic stress-strain response of structural steel.

The response of an annealed mild steel specimen, subjected to monotonic uniaxial loading, is illustrated in Figure 3.4a. This is a very familiar picture which includes the appearance of upper and lower yield stresses, a stress-strain plateau, and then a strain hardening regime. However, under constant amplitude strain-controlled cycling, the response depicted in Figure 3.4b results. At any given amplitude, a stabilized curve is eventually obtained that is independent of the prior loading history (Cofie and Krawinkler, 1985). Notice in Figure 3.4b that the knee is now rounded and that the plateau has disappeared. Logically one would expect that the overall force-displacement response of steel damp-

(a) Monotonic **(b) Cyclic**
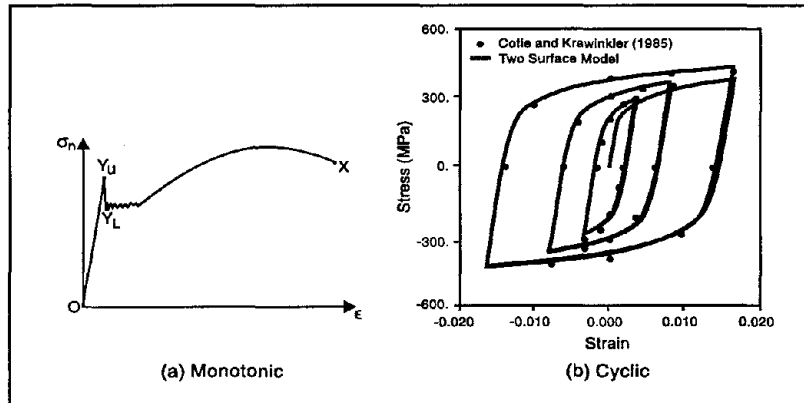
■Figure 3.4 Stress-strain Response of Structural Steel

ers will have a similar appearance. Indeed, this is generally the case, as indicated in the experimental results shown in Figure 3.5 for the X-shaped plate damper (Whittaker et al., 1991).

There are at least two different approaches that can be taken to construct a force-displacement damper model. The first approach involves the direct use of experimental data obtained from component testing of the metallic damper. The basic form of the force-displacement model is selected, usually based upon an analogy with plasticity theory, and then the model parameters are determined via a curve fitting procedure. This experiment-based modeling is discussed in more detail below. In the second approach, the force-displacement model is instead constructed from an appropriate constitutive relationship for the metal by applying the principles of mechanics. This latter approach can often provide additional insight into the behavior of the device, while reducing the requirements for component testing. Details concerning the development of these mechanics-based models, which are beyond the present scope, can be found inTsai andTsai (1995) and Dargush and Soong (1995).

The first serious attempt to develop a rational force-displacement relationship for a metallic damper can be found in the work conducted by Özdemir (1976). The focus in that study was on torsion beam dampers, however the formulations developed have more general applicability. The response of any metallic damper is a function of its geometry and the mechanical characteristics of the metal from which it is manufactured. Consequently, as mentioned above, it is quite logical to utilize force-displace-

(a) Displacement Amplitude 0.45 in   (b) Displacement Amplitude 1.5 in
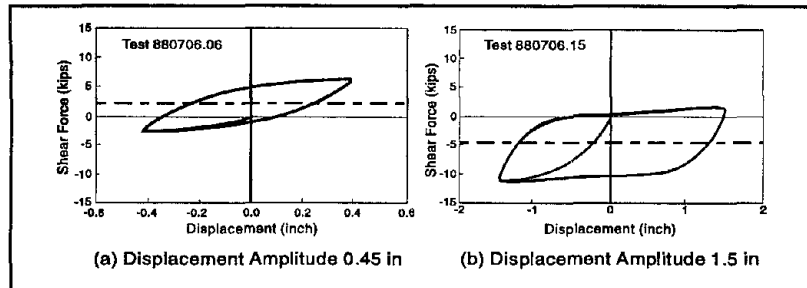
Whittaker et al., 1991

■ **Figure 3.5 Force-displacement Response of X-shaped Plate Damper**

ment models that have a form similar to those employed for constitutive modeling of that metal. This is exactly the approach taken by Özdemir. The structure of his damper models is based upon those frequently used in state-variable viscoplasticity.

For example, consider a generic metallic damper deflecting under the action of an applied force. The Özdemir model for the device can be written:

$$\dot{F} = k_o \dot{x} - k_o |\dot{x}| \left(\frac{F - B}{F_o} \right)^n \tag{3.2a}$$

$$\dot{B} = \alpha k_o |\dot{x}| \left(\frac{F - B}{F_o} \right)^n \tag{3.2b}$$

with damper force F, displacement x, and the internal variable B representing a backforce. The superposed dot represents differentiation with respect to time or a pseudotime quantity. Four parameters k_o, F_o, n, and α are required to define the damper response. The exponent n in Eqs. (3.2) is restricted to odd integers, although the form of the equations can be easily generalized to permit n as any real number (Graesser and Cozzarelli, 1991a).

Note that the integration of Eqs. (3.2) in time is required for determination of damper response. This is most easily accomplished numerically using, for example, a high order Runge-Kutta formula with adaptive step size (Press et al., 1992). As an illustration of the potential behavior encompassed in Eqs. (3.2), consider the response shown in Figure 3.6 due to a sinusoidal variation of enforced displacement. Notice from Figure 3.6a that the response is indeed independent of the displacement rate, as desired. The

F

LEGEND

—— $\dot{x}=\dot{x}_0$

--- $\dot{x}=10\dot{x}_0$

x

(a) Variation of Displacement
Rate

F

LEGEND

—— n = 1

— — n = 7

--- n = 49

x

(b) Variation in Sharpness
of Knee

F

LEGEND

—— α = 0.00

— — α = 0.02

--- α = 0.05

x

(c) Variation of Strain
Hardening
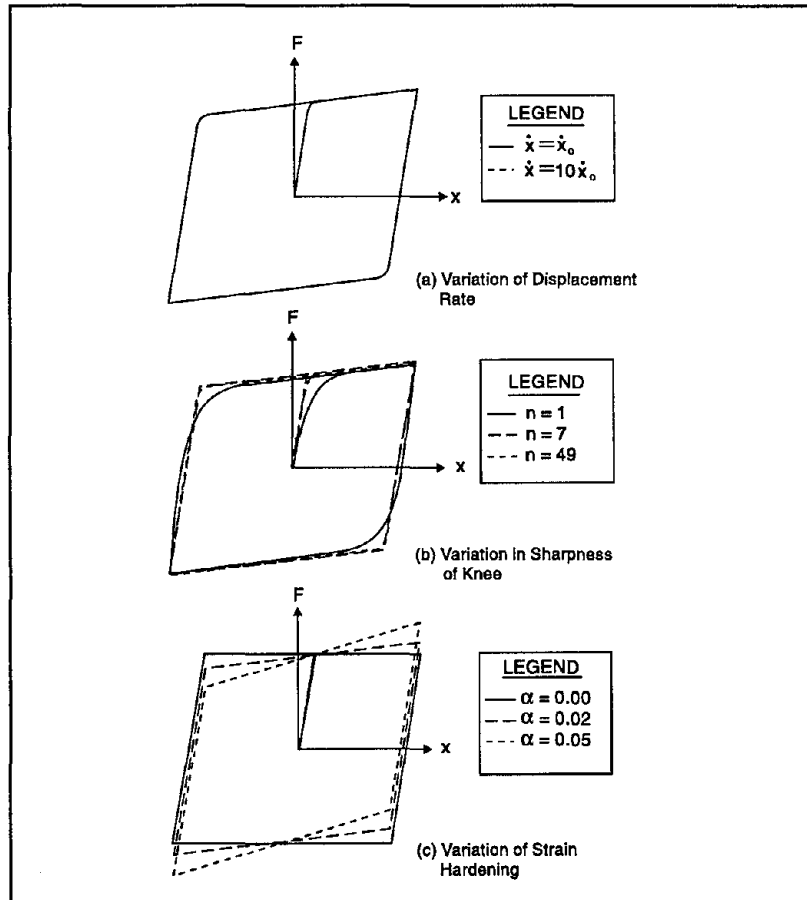
■ Figure 3.6 Özdemir Rate-independent Model

parameter k_0 represents the initial elastic device stiffness. Furthermore, it is evident from Figure 3.6b that the parameter n controls the sharpness of the knee, while α determines the slope in the inelastic range as indicated in Figure 3.6c. For $n \to \infty$, the response approaches an elastic-linear strain hardening idealization. Additionally, with $\alpha = 0$, the classical elastic-perfectly plastic model is recovered. It should be noted that the amount of energy dissipated by the passive device modeled by Eqs. (3.2) can be determined easily at any instant via numerical integration.

In the original work by Özdemir (1976), the damper parameters k_0, F_0, n, and α were selected to provide a best fit with experimental results for a displacement-controlled sinusoidal loading. The model was subsequently verified via comparisons involving

random displacement-controlled excitations, and found to be in good overall agreement for moderate displacement magnitudes.

Extensions of Eqs. (3.2) are also possible in order to model more complicated cyclic responses. In particular, Özdemir examined models that include the deterioration of yield strength, elastic modulus, and hardening characteristics by introducing additional internal state variables. These extended versions, with perhaps slight variations, have direct applicability to many of the metallic dampers presently in existence. However, some caution is needed, since the structure of the Özdemir rate-independent model is closely related to early versions of endochronic plasticity theory (Valanis, 1971). As a result, this model suffers from the same theoretical defects present in the initial Valanis formulations (e.g., Rivlin, 1981). Although stable results are typically obtained, careful control of the numerics is advised to ensure that accurate solutions are obtained for rate-independent applications.

Alternatively, one can develop a model based upon an analogy with the popular two-surface plasticity models (Dafalias and Popov, 1975; Krieg, 1975). Consider, for example, the following uniaxial version written in force-displacement space. Two distinct, but nested, yield surfaces are defined in force space, as illustrated in Figure 3.7. The inner or loading surface, which separates the elastic and inelastic response regimes, is characterized by its center and radius represented by the backforce B and inner yield force F_y^L, respectively. On the other hand, the outer or bounding surface, which completely contains the smaller inner surface, is always centered at the origin of force space with radius equal to a variable outer yield F_y^B. Translation of the inner surface corresponds to kinematic hardening, while expansion of the outer surface produces isotropic hardening of the device.
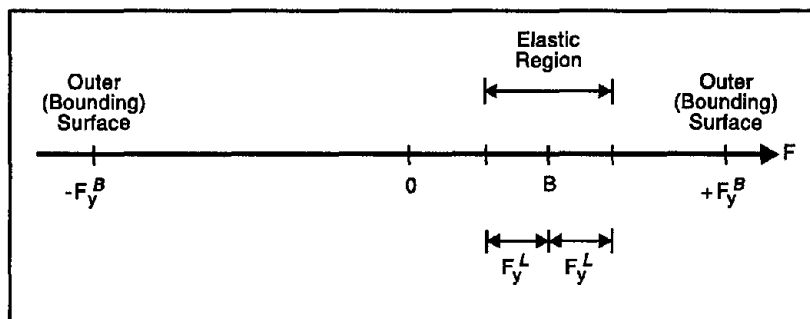
■ Figure 3.7 Two Surface Force-Displacement Model

■ Table 3.2 Uniaxial Two-Surface Device Model

If $|F - B| < F_y^L$ or $(F - B)\dot{x} \le 0$, then

    Elastic loading or unloading

    $\dot{F} = k\dot{x}$

    $\dot{B} = 0$

    $\dot{F}_y^B = 0$

Else if $|F| < F_y^B$, then

    Inelastic loading inside outer surface

    $\dot{F} = [k^P / (k + k^P)]k\dot{x}$

    $\dot{B} = \dot{F}$

    $\dot{F}_y^B = 0$

        where

        $k^P = h^B (\beta / \gamma)^n$

        $h^B = h_0^B + h_1^B F_y^B$

        $\beta = F_y^B + F\,sgn(\dot{x})$

        $\gamma = 2F_y^B$

Else

    Inelastic loading on outer surface

    $\dot{F} = [k^P / (k + k^P)]k\dot{x}$

    $\dot{B} = \dot{F}$

    $\dot{F}_y^B = |\dot{F}|$

        where

        $k^P = h^B$

        $h^B = h_0^B + h_1^B F_y^B$

End if

The yield criteria, flow rules, and hardening rule are established to ensure that the current force F always lies on or within both surfaces, that all transitions during loading are smooth, and that infinitesimal deformation cycles do not cause anomalous behavior. The model, which requires the determination of six device parameters $(k, F_y^L, F_{y0}^B, h_0^B, h_1^B,$ and $n)$ is defined in Table 3.2. Note that F_{y0}^B corresponds to the initial value of F_y^B. Parameter values can be obtained from cyclic force-displacement damper response data by using the Marquardt (1963) algorithm for nonlinear least-squares curve fitting. A similar approach, based upon a two surface model, is described in Pong et al., (1994).

Most of the recent metallic damper modeling efforts reported in the literature have employed more simplistic representations. For example, one finds numerous applications of elastic-perfectly plastic or Ramberg-Osgood idealizations (e.g., Su and Hanson, 1990; Xia and Hanson, 1992). The Ramberg-Osgood model essentially establishes a power law relationship between stress and inelastic strain, and consequently is effective in modeling the response of a variety of metals under monotonic loading. Another approach that has appeared involves formulations in which the inelastic behavior is converted into equivalent linear viscous damping on the basis of energy dissipation per cycle (e.g., Hanson, 1993; Scholl, 1993). These simplified approaches may be appropriate for preliminary design.

3.1.2 Friction Dampers

The mechanism involved in energy dissipation in metallic dampers can be categorized as one form of internal friction. On the other hand, attention will now shift to dampers that utilize the mechanism of friction between two solid bodies sliding relative to one another to provide the desired energy dissipation. An examination of the effects of frictional damping on the response of building structures was conducted by Mayes and Mowbray (1975), however it appears that Keightley (1977) was the first to consider frictional devices for building applications. Subsequently, based primarily upon an analogy to the automotive brake, Pall et al., (1980) then continued the development of passive frictional dampers to improve the seismic response of structures. The objective is to slow down the motion of buildings "by braking rather than breaking" (Pall and Marsh, 1982).

There has been considerable progress during the intervening years, and a number of devices have been developed. Two representative types of friction dampers are illustrated in Figure 3.8. Figure 3.8a displays a design proposed by Pall and Marsh

(a) X-braced Friction Damper

(b) Uniaxial Friction Damper
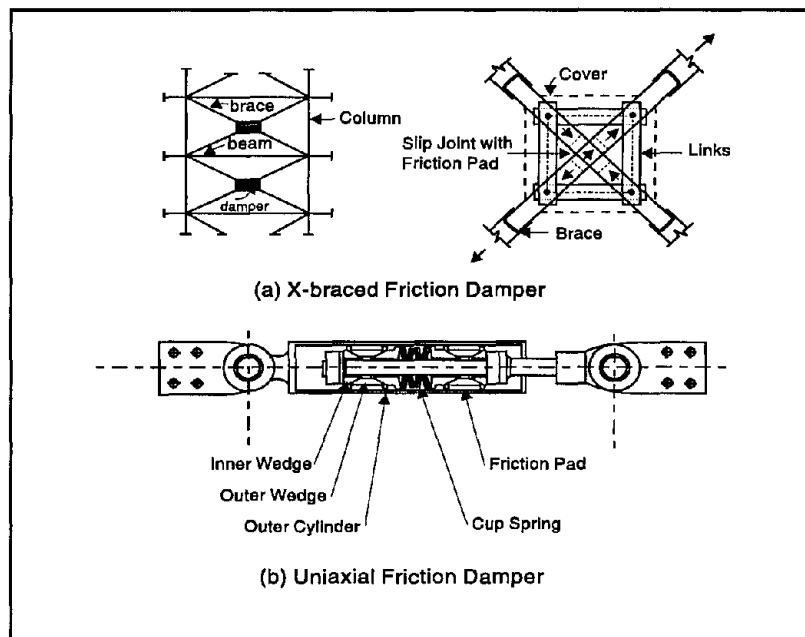
a. Pall and Marsh, 1982   b. Aiken and Kelly, 1990

■ Figure 3.8   Representative Friction Dampers

(1982) for application in conjunction with cross-bracing in framed structures. Brake lining pads are utilized for the sliding surfaces. Another friction device, based upon an industrial damper, is shown in Figure 3.8b. In this uniaxial device, which was recently tested by Aiken and Kelly (1990), copper alloy friction pads slide along the inner surface of the cylindrical steel casing. The required normal force is provided through the action of the spring against the inner and outer wedges.

While there are numerous forms of friction that can be effectively used to mitigate damage to structures during environmental disturbances, all of the devices to be discussed in this section employ solid sliding friction as their basic dissipative mechanism. Thus, in friction dampers, irrecoverable work is done by the tangential force required to slide one solid body across the surface of another. It is naturally of paramount importance that a consistent, predictable frictional response be maintained throughout the life of the damper. However, this response depends to a considerable extent on surface conditions, which may in turn be affected by environmental factors.

The scientific study of dry friction has a long history dating to the illustrious work of daVinci, Amontons, and Coulomb. The basic theory is founded upon the following hypotheses, which were initially inferred from physical experiments involving planar sliding of rectilinear blocks:

1. The total frictional force that can be developed is independent of the apparent surface area of contact.
2. The total frictional force that can be developed is proportional to the total normal force acting across the interface.
3. For the case of sliding with low relative velocities, the total frictional force is independent of that velocity.

As a result of these assumptions, at the instant of impending slippage or during sliding itself, one can write

$$F_t = \mu F_n \qquad (3.3)$$

where F_t and F_n represent the frictional and normal forces, respectively, and μ is the coefficient of friction. Since it is frequently observed that the coefficient of friction is somewhat higher when slippage is imminent than it is during sliding, separate static (μ_s) and kinetic (μ_k) coefficients are often introduced. In either case,

the frictional force F_t acts tangentially within the interfacial plane in the direction opposing the motion or impending motion.

In order to extend the theory to more general conditions, involving non-uniform distributions or non-planar surfaces, these basic assumptions are often abstracted to the infinitesimal limit. Thus, total forces are replaced by surface tractions, and the generalization of Eq. (3.3) becomes

$$\tau_t = \mu \tau_n \qquad (3.4)$$

in terms of the tangential τ_t and normal τ_n tractions. This form is also useful for determining the nominal contact stresses that are often required for proper design. Note that an integration of Eq. (3.4) over a planar contact area recovers Eq. (3.3).

The concept of Coulomb friction, as described above, provides the theoretical basis for most of the work that has appeared concerning friction dampers. However, it should be emphasized that frictional processes are seldom all that simple. In practice, the Coulomb theory is only approximately true. Furthermore, the coefficient of friction μ, which appears in Eqs. (3.3) and (3.4), must not be viewed as a constant. Instead, μ is a variable parameter that depends not only upon the selection of sliding materials, but also on the present condition of the sliding interface. This latter dependency greatly increases the complexity of the modeling problem, since surfaces are often the site of numerous ongoing physical and chemical processes. These processes may change the physical and chemical character of the surfaces, and consequently produce a significant impact on the frictional response through a change in the true area of contact. In particular, the use of galvanic couples (e.g., mild steel and brass) must be avoided, and additional protective measures must be employed in aggressive environments to prevent corrosion.

Considerable effort has been directed toward the development of a modern mechanistic approach to solid friction, which has led to an improved qualitative understanding of the process, however a quantitative assessment of frictional response from first principles is not yet possible. More importantly, since there is still no theory for sliding friction comparable to the well-established theory of metal plasticity, there is a need for much more reliance on physical testing. With that in mind, Pall et al., (1980) began

their development of friction dampers by conducting static and dynamic tests on a variety of simple sliding elements having different surface treatments. The goal was not necessarily to obtain maximum energy dissipation, but rather to identify a system that possesses a consistent, predictable response. For these tests, contact was maintained between the faying surfaces by pretensioning high strength bolts. The resulting load-displacement curves obtained under constant amplitude displacement-controlled cyclic loading are displayed in Figure 3.9.

(a) Mill scale   (b) Sand blasted

(c) Inorganic Zinc-Rich paint   (d) Metalized

(e) Brake Lining Pads   (f) Polyethylene Coating
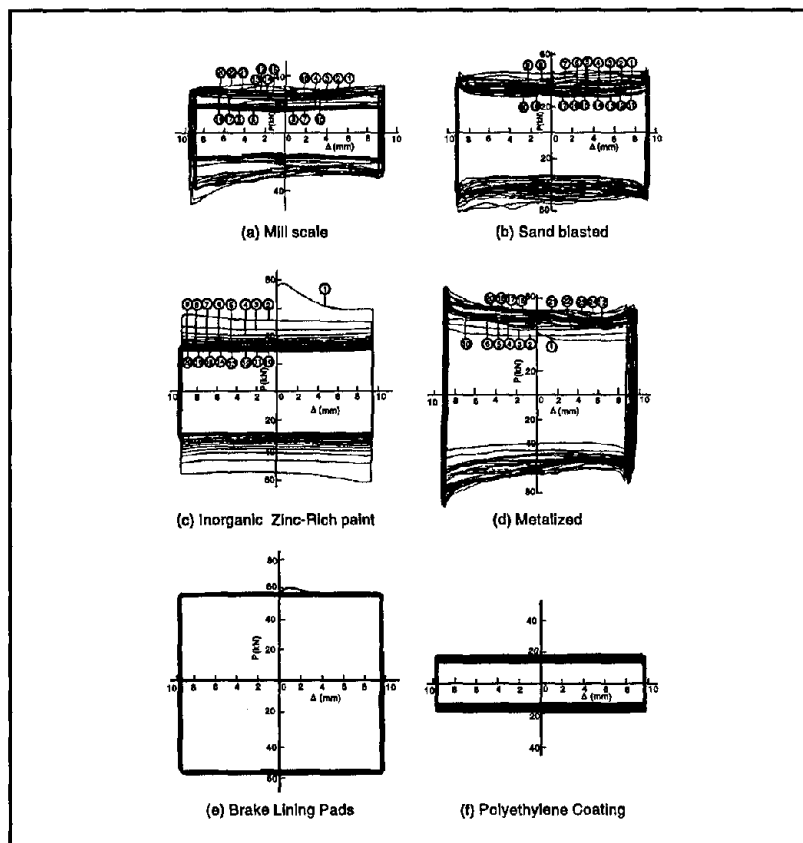
Pall et al., 1980
■ Figure 3.9 Hysteresis Loops of Limited Slip Bolted Joints

Of the surfaces considered by Pall et al., (1980), the systems containing heavy duty brake lining pads inserted between steel plates did provide a consistent, predictable response. Based upon the behavior obtained by Pall et al., (1980) and illustrated in Figure 3.9e, characterization of their simple brake lining frictional

system in terms of an elastic-perfectly plastic model is quite appropriate. Either a limiting form of the Özdemir model can be utilized as explained above or the simple single-surface plasticity model defined in Table 3.3 can be adopted, where k_0 and F_s represent the elastic stiffness and slip load, respectively.

■ Table 3.3 Elastic-Perfectly Plastic Device Model

If $|F| < F_s$ or $F\dot{x} \leq 0$ then

        Elastic

        $\dot{F} = k_0\dot{x}$

Else

        Slippage

        $\dot{F} = 0$

End if

■ Table 3.4 Hysteric Device Model with Symmetric Bearing Stops

If $|F| < F_s$ or $(F\dot{x} \leq 0$ and $|x| \leq x_b)$ then

        Elastic

        $\dot{F} = k_0\dot{x}$

Else if $|x| < x_b$ then

        Slippage

        $\dot{F} = 0$

Else

        Bearing

        $\dot{F} = k_2\dot{x}$

End if

In some friction dampers, however, a stiff bearing stage occurs for displacements beyond a given slip length. A suitable hysteretic model for that case is defined in Table 3.4, where the additional parameters x_b and k_2 represent the total displacement at first contact with the bearing surface and the bearing stiffness, respectively. The model, which assumes zero stiffness during slippage (i.e., $k_1 = 0$), is specified in rate form in order to properly address arbitrary loading-unloading histories. A typical result for displacement controlled cycling at two different amplitudes is displayed in Figure 3.10, where all of the model parameters are detailed.
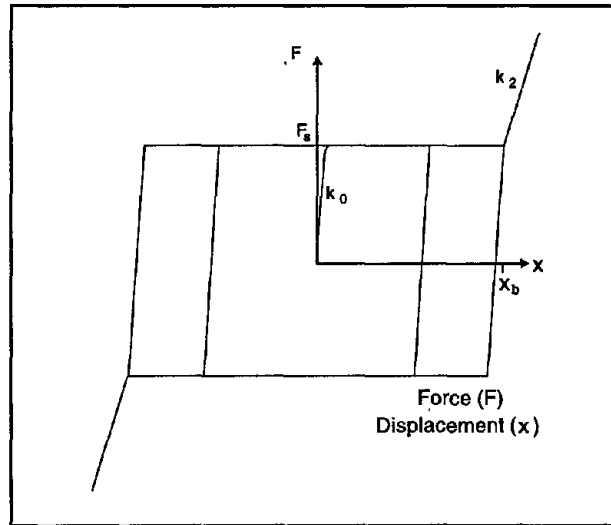
Figure 3.10 Coulomb Friction Element

3.2

VISCOELASTIC SYSTEMS

A range of passive systems that dissipate energy in a rate dependent manner will be discussed in this section. As indicated in Table 3.1, this grouping includes **viscoelastic solid dampers** and **viscoelastic fluid dampers**, with the latter expanded to incorporate devices based upon both fluid deformation and orificing. Typical force-displacement responses obtained for these devices under constant amplitude, displacement-controlled cyclic conditions are provided in Figure 3.11a. In general, these devices exhibit both damping and stiffness, although the important case of a purely viscous damper in which force and displacement are 90° out-of-phase is illustrated in Figure 3.11b. Notice that for viscoelastic devices, the response is dependent upon frequency. However, in Figure 3.11 and in many applications, the behavior is confined to the linear range. This often greatly simplifies the required analysis procedures as discussed in Chapter 2. Furthermore, since energy dissipation occurs even for infinitesimal deformations, viscoelastic devices have potential application for both wind and seismic protection.
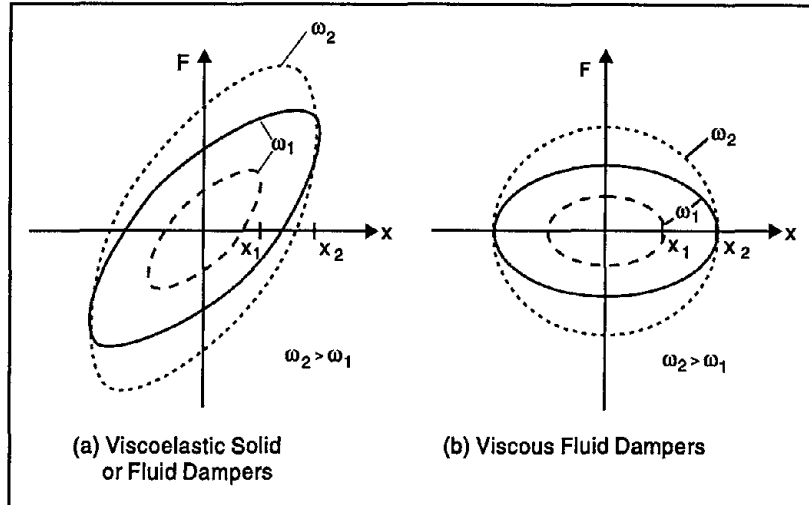
■ Figure 3.11 Idealized Force-displacement Response of Viscoelastic Devices

3.2.1 VISCOELASTIC SOLID DAMPERS

Viscoelastic solid materials used in civil engineering structural applications are usually copolymers or glassy substances that dissipate energy when subjected to shear deformation. A typical viscoelastic (VE) damper, which consists of viscoelastic layers bonded with steel plates, is shown in Figure 3.12. When mounted in a structure, shear deformation and hence energy dissipation takes place when the structural vibration induces relative motion between the outer steel flanges and the center plate.

The response of these viscoelastic materials under dynamic loading depends upon the frequency of vibration, the level of strain, and the ambient temperature. Under infinitesimal harmonic excitation with frequency ω, the relationship between shear stress $\tau(t)$ and shear strain $\gamma(t)$ can be expressed as (Zhang et al., 1989)

$$\tau(t) = G'(\omega)\gamma(t) + \frac{G''(\omega)}{\omega}\dot{\gamma}(t) \tag{3.5}$$

where $G'(\omega)$ and $G''(\omega)$ are the shear storage and loss moduli, respectively. The loss factor is then defined by $\eta(\omega) = G''(\omega) / G'(\omega)$. For more general excitation, Boltzmann's superposition principle
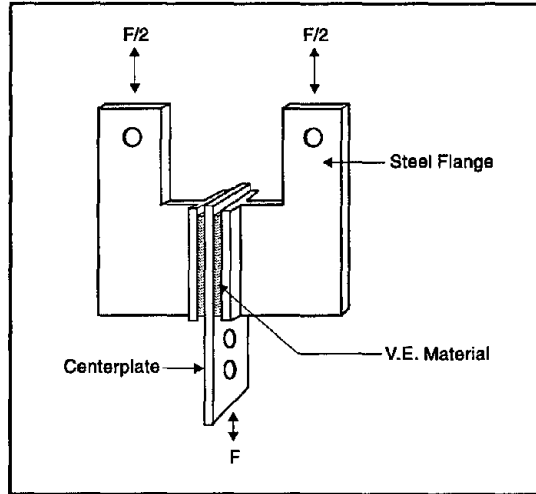
■ Figure 3.12 Typical Viscoelastic Solid Damper Configuration

can be invoked to provide the following constitutive relation for polymeric materials (e.g., Ferry, 1980)

$$\tau(t) = \int_{o+}^{t} G(\xi)\, \dot{\gamma}\, (t - \xi)\, d\xi + G(t)\gamma(0) \qquad (3.6)$$

For the usual case of zero initial strain $\gamma(0)$, this reduces to simply

$$\tau(t) = \int_{o}^{t} G(\xi)\, \dot{\gamma}\, (t - \xi)\, d\xi \qquad (3.7)$$

In the above, $G(t)$ represents the stress relaxation modulus, which is defined as the ratio of stress to strain at constant deformation. Thus, $G(t)$ can be determined experimentally for a given material. Results for one particular copolymer are shown in Figure 3.13. Many different expressions can be assumed for the stress relaxation modulus, including those associated with the classical Kelvin and Maxwell models. However, in order to capture the viscoelastic behavior over a sufficiently broad frequency range, more sophistication is often required. The following four-parameter model originally developed by Williams (1964) has proved to be particularly effective for representing viscoelastic materials in passive energy dissipation systems (Shen and Soong, 1995):

$$G(t) = G_e + \frac{G_g - G_e}{\left[1 + t / t_o\right]^\alpha}$$

(3.8)

where G_e is the rubbery modulus, G_g is the glassy modulus, t_o is the relaxation time, and α is a real constant giving the slope of the relaxation curve through the transition region between glassy and rubbery behavior. The stress relaxation modulus $G(t)$ as given in Eq. (3.8) predicts a bounded modulus for all non-negative time and has been found to be reasonably accurate for most VE materials. Initially, $G(t)$ coincides with the glassy modulus, but then smoothly approaches the rubbery modulus with increasing time.
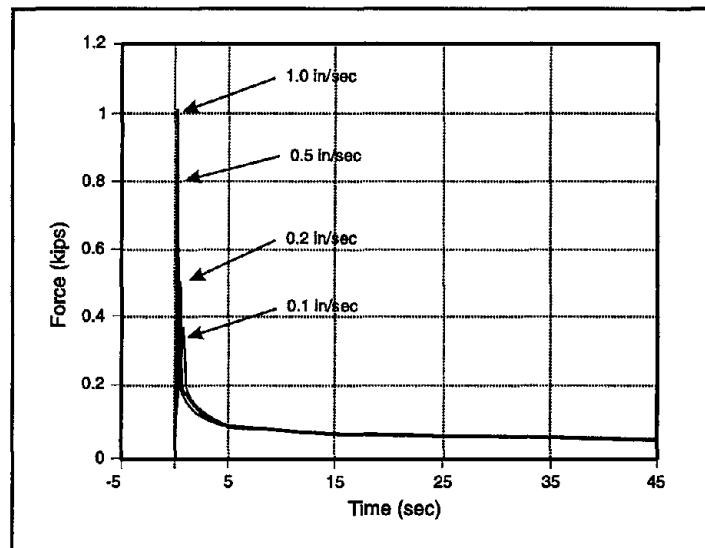
Shen and Soong, 1995

■ Figure 3.13 Stress Relaxation Tests at Different Strain Rates

By performing a Laplace transform of Eq. (3.8), the above model parameters can be related to the storage and loss moduli. The resulting expressions can be written:

$$G'(\omega) = G_e + \left(G_g - G_e\right) \Gamma \left(1 - \alpha\right) \left(\omega t_o\right)^\alpha \cos\left(\frac{\alpha\pi}{2} + \omega t_o\right)$$

(3.9a)

$$G''(\omega) = \left(G_g - G_e\right) \Gamma (1 - \alpha) \left(\omega t_o\right)^\alpha \sin\left(\frac{\alpha\pi}{2} + \omega t_o\right)$$

(3.9b)

where $\Gamma(\xi)$ represents the gamma function. In Shen and Soong

(1995), material parameters were first determined by curve fitting stress relaxation data, and then checked against measurements involving sinusoidal excitations. Figure 3.14 provides a typical comparison between the moduli calculated from Eqs. (3.9) versus those determined from the sinusoidal tests. A good correlation is obtained throughout the range from 1 Hz to 3 Hz.
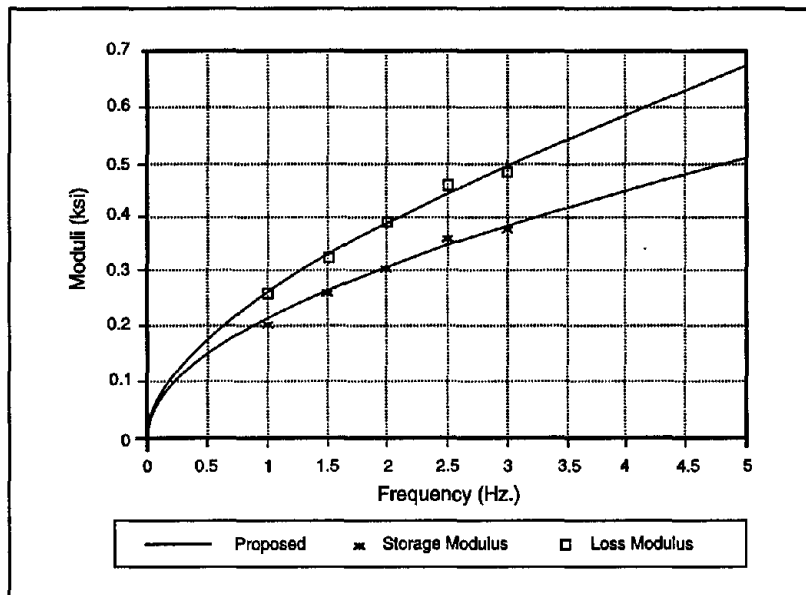
Shen and Soong, 1995

■ Figure 3.14 Comparison of Storage and Loss Moduli Between Simulation and Test

Alternative VE material models based upon fractional derivatives have also appeared in the literature (Gemant, 1936; Bagley and Torvik, 1983), including some recent applications to viscoelastic solid dampers (Kasai et al., 1993; Tsai and Lee, 1993). A further discussion of these fractional derivative models will be postponed until the following section on viscoelastic fluid dampers.

As mentioned previously, the typical materials used in viscoelastic solid dampers are also temperature dependent. However, for a large class of polymers, the shape of the dynamic moduli versus frequency curves is similar when evaluated at various temperatures. This led to the development of the method of reduced variables (e.g., Ferry, 1980), which affords a convenient simplification in separating the two principal variables, frequency and

temperature. By using this method, the temperature dependence of the VE moduli can be obtained by plotting

$$G'_{T0}(\omega) = G'_T(\omega)\rho_0 T_0 \ / \ \rho T \ vs. \ \omega\beta_T$$

$$G''_{T0}(\omega) = G''_T(\omega)\rho_0 T_0 \ / \ \rho T \ vs. \ \omega\beta_T \qquad (3.10)$$

$$G_{T0}(t) = G_T(t)\rho_0 T_0 \ / \ \rho T \ vs. \ t \ / \ \beta_T$$

where T is the ambient temperature of interest, T_0 is an arbitrarily selected reference temperature at which the measurements are made and ρ is the density of the VE material. All temperatures must be measured on an absolute scale. The remaining function in Eq. (3.10), β_T is a shift factor of time or frequency, which is determined experimentally. Often a plot of $\log \beta_T$ versus temperature produces nearly a straight line, as indicated by the experimental data shown in Figure 3.15. Consequently, the parameters a and b in the following regression can be determined with minimal testing:

$$\log\beta_T = aT + b \qquad (3.11)$$

An application of the method to VE damper materials is provided in Shen and Soong (1995).

Once the constitutive model has been established for the response of the damper material in shear, the overall force-deformation model for the damper can be constructed. Due to the geometric simplicity of the typical damper possessing shear area A and thickness δ, the following force-displacement relationship is obtained for response under time harmonic excitation:

$$F(t) = k'(\omega)\,x(t) + c'(\omega)\dot{x}(t) \qquad (3.12)$$

where

$$k' = \frac{AG'(\omega)}{\delta} \qquad c' = \frac{AG''(\omega)}{\omega\delta} \qquad (3.13\text{a, b})$$
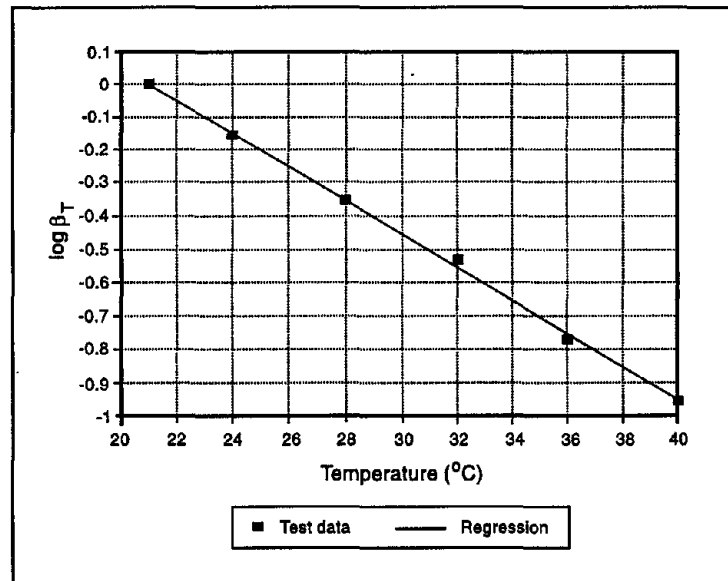
■ Figure 3.15 Regression of Scale Factor, β_T

The analogy with Eq. (3.5) is obvious. It should be noted that this expression is exact only for harmonic excitation. For more general response, an integral form based upon Eq. (3.6) could be developed. However, in many structural applications, the approximations involved in adopting the Kelvin model defined in Eq. (3.12) are quite reasonable provided that one selects a proper value for ω. For example, in multi-degree-of-freedom (MDOF) structural systems, Soong and Lai (1991) have proposed the use of the modal strain energy method to establish the modal damping ratios and modified modal frequencies due to added VE dampers. Further details are provided in Chapter 4.

3.2.2 VISCOELASTIC FLUID DAMPERS

All of the passive devices described to this point utilize the action of solids to enhance the performance of structures subjected to transient environmental disturbances. However, fluids can also be effectively employed in order to achieve the desired level of passive control. Significant effort has been directed in recent years toward the development of viscous fluid dampers for

(a) Cylindrical Pot Fluid Damper

(b) Viscous Damping Wall

(c) Orificed Fluid Damper
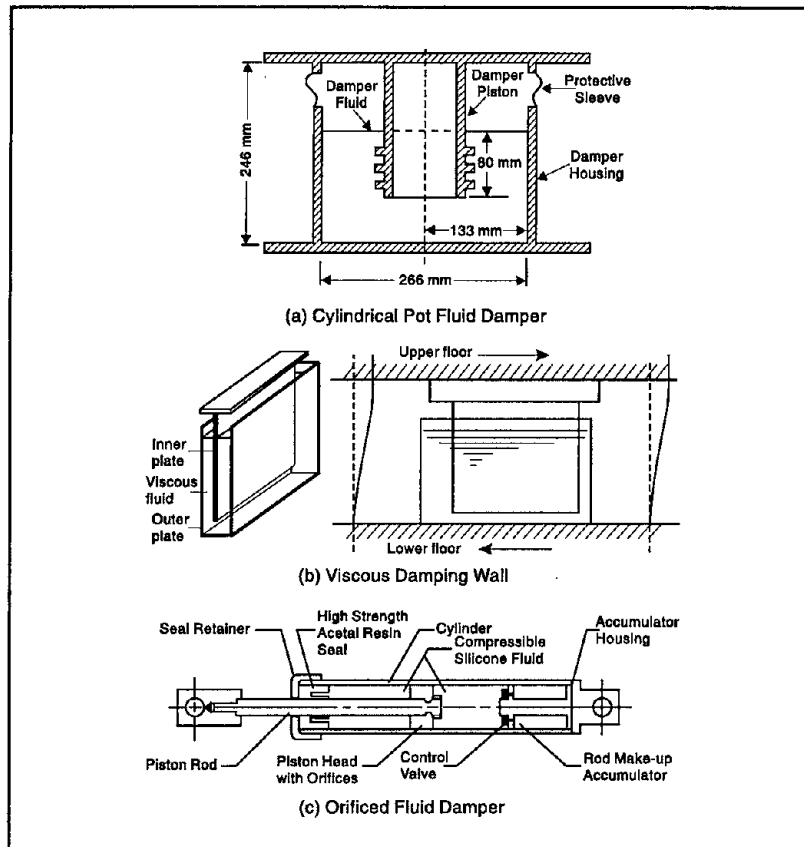
a. Makris and Constantinou, 1991; b. Miyazaki and Mitsusaka, 1992; c. Constantinou et al., 1993

■ **Figure 3.16 Viscoelastic Fluid Dampers**

structural applications, primarily through the conversion of technology from the military and heavy industry. Several examples of fluid dampers are shown in Figure 3.16.

One straightforward design approach is patterned directly after the classical dashpot. In this case, dissipation occurs via conversion of mechanical energy to heat as a piston deforms a thick, highly viscous substance, such as a silicone gel. Figure 3.16a depicts one such damper, which has found application as a component in seismic base isolation systems (Huffmann, 1985; Makris and Constantinou, 1990). While these devices could also be deployed within the superstructure, an alternative, and perhaps more effective, design concept involves the development of the viscous damping wall (VDW) illustrated in Figure 3.16b (Arima

et al., 1988). In this design, the piston is simply a steel plate constrained to move in its plane within a narrow rectangular steel container filled with a viscous fluid. For typical installation in a frame bay, the piston is attached to the upper floor, while the container is fixed to the lower floor. Relative interstory motion shears the fluid and thus provides energy dissipation.

Both of the devices discussed above accomplish their objectives through the deformation of a viscous fluid residing in an open container. In order to maximize the energy dissipation density of these devices, one must employ materials with large viscosities. Typically, this leads to the selection of materials that exhibit both frequency and temperature dependent behavior.

There is, however, another class of fluid dampers that rely instead upon the flow of fluids within a closed container. In these designs, the piston acts now, not simply to deform the fluid locally, but rather, to force the fluid to pass through small orifices. As a result, extremely high levels of energy dissipation density are possible. However, a correspondingly high level of sophistication is required for proper internal design of the damper unit.

A typical orificed fluid damper for seismic application is illustrated in Figure 3.16c (Constantinou et al., 1993; Constantinou and Symans, 1993). This cylindrical device contains a compressible silicone oil which is forced to flow via the action of a stainless steel piston rod with a bronze head. The head includes a fluidic control orifice design. In addition, an accumulator is provided to compensate for the change in volume due to rod positioning. Alternatively, the device may be designed with a run-through piston rod to prevent volume changes. High strength seals are required to maintain closure over the design life of the damper. These uniaxial devices, which were originally developed for military and harsh industrial environments, have recently found application in seismic base isolation systems as well as for supplemental damping during seismic and wind-induced vibration.

While viscoelastic fluid damper construction varies considerably from each other and from the viscoelastic solid damper counterparts, mathematical models suitable for overall force-displacement response have a similar form. In general, the devices are both frequency and temperature dependent, and in some cases amplitude dependence is also evident. Over the years, numerous

constitutive models have been proposed for such viscoelastic fluids. A particularly effective class is based upon the generalization of classical models to incorporate fractional derivative operators. As noted in the previous section, this was first suggested by Gemant (1936). More recently, Makris and Constantinou (1991) applied fractional derivative Maxwell models to represent the behavior of viscoelastic fluid dampers, and then extended those models by incorporating complex order derivatives (Makris and Constantinou, 1993).

Consider, for example, the complex-derivative Maxwell constitutive model that has been used to characterize a particular polybutane fluid over a broad frequency and temperature range (Makris et al., 1995). At some reference temperature T_0, under the assumption of infinitesimal incompressible deformation, the proposed model can be written in terms of shear stress τ and shear strain γ as:

$$\tau + \left[\lambda(T_o)\right]^v \frac{d^v \tau}{dt^v} = \mu(T_o)\frac{d\gamma}{dt} \qquad (3.14)$$

where $\lambda=\lambda_1+i\lambda_2,$ $v=v_1+iv_2,$ and $\mu = \mu_1 + i\mu_1$ are complex-valued material parameters. As indicated, both λ and μ are functions of temperature. The symbol d^v/dt^v denotes a generalized derivative of order v with respect to time (Oldham and Spanier, 1974). For $v=1$, Eq. (3.14) reduces to the classical Maxwell model.

The storage modulus G' and loss modulus G'' corresponding to the above model can be obtained by performing a Fourier transform. Using the relationship for the Fourier transform of a generalized derivative (Erdelyi et al., 1954; Makris, 1992)

$$F\left\{\frac{d^v f(t)}{dt^v}\right\} = \left[i\omega\right]^v F\left[f(t)\right] \qquad (3.15)$$

one obtains

$$G'\left(\omega,T_o\right) = \Re\left(G*\left(\omega,T_o\right)\right) \qquad (3.16a)$$

$$G''\left(\omega,T_o\right) = \Im\left(G*\left(\omega,T_o\right)\right) \qquad (3.16b)$$

with dynamic modulus

$$G^*(\omega, T_o) = \frac{i\omega\mu(T_o)}{1 + \left[i\omega\lambda(T_o)\right]^\nu}$$ (3.17)

In Eq. (3.16), $\Re$ and $\Im$ extract the real and imaginary part of their argument, respectively. The material parameters are then obtained from experimental data by employing a nonlinear regression algorithm in the complex space, with an additional causality constraint to ensure non-negative phase lag (Makris et al., 1995).

Having established the material parameters in the complex-derivative Maxwell model, the frequency dependence is completely characterized at the reference temperature T_0. It remains to determine the temperature dependence of the response. Once again the method of reduced variables can often be applied. In that case, the frequency shift function β_T characterizes the temperature dependence.

A plot of the reduced dynamic modulus versus reduced angular frequency, $\beta_T\omega$, is shown in Figure 3.17 for a polybutane fluid. This experimental data, obtained at three different temperatures, clearly delineates a pair of master curves for the storage and loss moduli, and thus validates the use of the method of reduced variables for this material. Also displayed in that figure are the dynamic shear moduli obtained from the complex-derivative Maxwell model. The correlation is quite good over a broad frequency range. The only noticeable deviation occurs in the storage modulus at low frequency. However, in that range, the loss modulus is
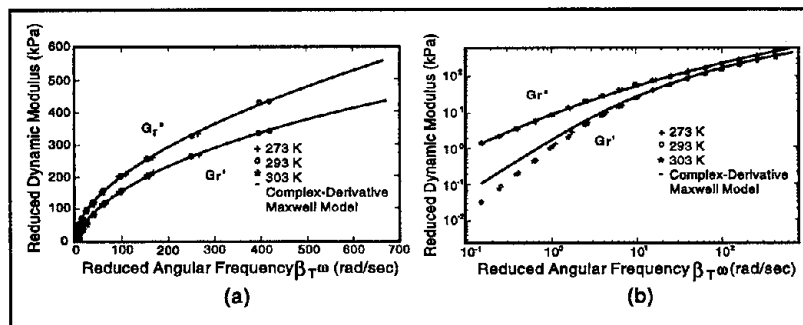
Makris et al., 1995

■ Figure 3.17 Dynamic Modulus for Polybutane Fluid

an order of magnitude greater, thus reducing the significance of the deviation.

In many cases, one would expect that the overall force-deformation response of fluid dampers closely follows the constitutive behavior, as defined above. Such is the case for the cylindrical pot fluid dampers. In Makris and Constantinou (1991) and Makris et al., (1993), the following fractional derivative Maxwell force-displacement model was utilized to model overall damper response:

$$F(t) + \lambda^{\nu} \frac{d^{\nu} F(t)}{dt^{\nu}} = C_o \frac{dx(t)}{dt} \tag{3.18}$$

with F as the force applied to the piston and x as the resulting piston displacement. Furthermore, the damper parameters C_0, λ, and ν represent the zero-frequency damping coefficient, the relaxation time, and the order of fractional derivative, respectively. In Makris and Constantinou (1991), the damper parameters are determined directly from experimental data, while in Makris et al., (1993) the parameters are estimated from material data and a simplified analytical model. A typical result is shown in Figure 3.18. It should be noted that for sufficiently low frequencies, inertia effects are unimportant, and one finds that the macroscopic parameters λ and ν coincide with those obtained from constitutive modeling. Thus, only C_0 is a function of the damper geometry.
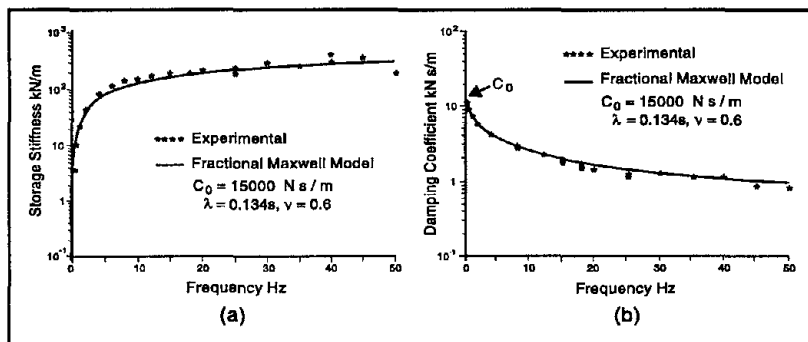
Makris and Constantinou, 1991

■ Figure 3.18 Macroscopic Model for Cylindrical Pot Fluid Damper Response

Modeling of the orificed fluid damper, illustrated in Figure 3.16c, is developed in Constantinou and Symans (1993). Typical experimentally measured room temperature force-displacement loops are shown in Figure 3.19. For this damper, the frequency dependence is much less dramatic, and a classical Maxwell model is adequate throughout the frequency range of interest. Thus, Eq. (3.18) reduces to the following:

$$F(t) + \lambda \frac{dF(t)}{dt} = C_o \frac{dx(t)}{dt} \qquad (3.19)$$

with real parameters λ and C_o representing the relaxation time and zero frequency damping coefficient, respectively. Comparisons of the model with the experimentally determined storage stiffness, damping coefficient and phase angle are displayed in
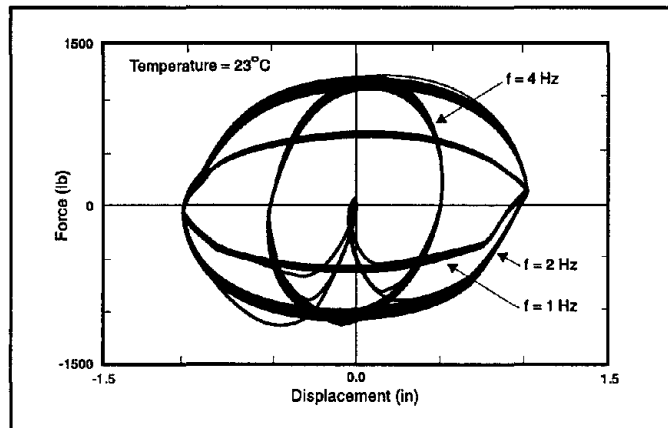
Constantinou and Symans, 1993

■ Figure 3.19 Force-displacement Response of Orificed Fluid Damper

Figure 3.20. Notice that the relaxation time, $\lambda = 0.006$ s, is quite small. This indicates that, below a cut-off frequency of approximately 4 Hz, Eq. (3.19) can be simplified further by neglecting the second term on the left hand side which becomes insignificant. One is then left with the linear, purely viscous dashpot model

$$F(t) = C_o \frac{dx(t)}{dt} \qquad (3.20)$$

which greatly simplifies the subsequent structural analysis.

(a) Storage Stiffness and Damping Coefficient   (b) Phase Angle
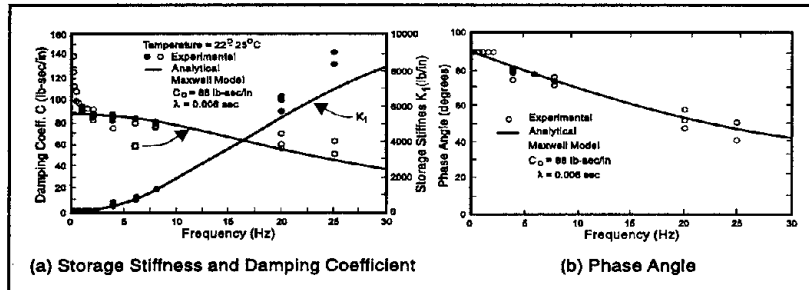
Constantinou and Symans, 1993

■ Figure 3.20 Comparison of Experimental and Analytically-derived Values for Orificed Fluid Damper at Room Temperature

It should be noted that frequency dependencies in orificed fluid dampers result from the use of accumulators or similar parts that involve the operation of valves. Valves themselves have dynamic characteristics and typically may not be compatible with the dynamic movement of the damper piston rod at high frequency. This results in restricted fluid flow to the accumulator and, thus, reduction in fluid volume. If desired, this phenomenon can be entirely prevented via the use of a run-through piston rod. This type of construction has been used in all of the applications of orificed fluid dampers in structural systems (see Chapter 5).

3.3

RE-CENTERING SYSTEMS

The mechanical behavior of hysteretic and viscoelastic devices have been examined in the previous two sections and is illustrated schematically in Figs. 3.2 and 3.11, respectively. There exists, however, another class of dampers referred to here as re-centering devices that possess distinctly different force-displacement characteristics. Included in this grouping are **pressurized fluid dampers, preloaded spring-friction dampers**, and **phase transformation dampers**. The first of these displays some rate-dependence due to the presence of the fluid, while the response of the remaining devices tends to be rate independent. All of these devices retain very little residual deformation upon removal of the applied load, and thus provide an inherent re-centering capability.

3.3.1 Pressurized Fluid Dampers

A pressurized fluid restoring device was recently employed by Tsopelas and Constantinou (1994) to provide both damping and re-centering capability for a base isolation system. This double-acting preloaded device is illustrated in Figure 3.21. The resistance
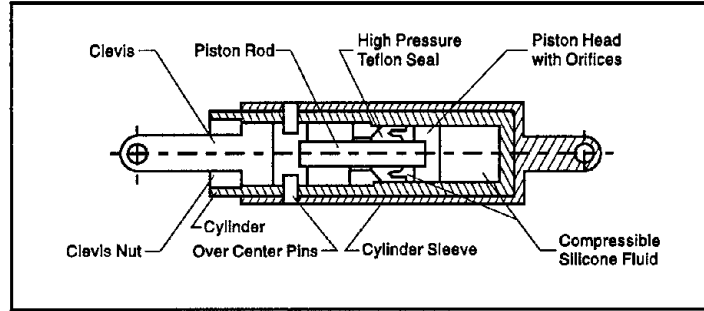
Tsopelas and Constantinou, 1994

■ Figure 3.21 Pressurized Fluid Restoring Device

is provided by several different physical phenomena, including the preload due to initial pressurization, the device stiffness associated with the compressibility of the silicone oil, seal friction, and damping due to the passage of fluid through the orifices. As a result, the following mathematical model was developed to represent the macroscopic response:

$$F = F_o \left[1 - \exp\left(- \delta |x|\right) \right] \text{sgn}(x) + k_o x +$$
$$\left[F_{min} + \alpha k_o |x| \right] Z + F_d \, \text{sgn}(\dot{x})$$

(3.21)

with the four individual terms on the right-hand-side corresponding, in order, to the mechanisms defined above. In this equation, F_o is the preload, k_o is the stiffness, F_{min} is the seal friction at zero displacement, and F_d is the fluid damping force. Additionally, one needs the following evolution equation for the internal variable Z,

$$x_y \dot{Z} + \gamma |\dot{x}| Z |Z| + \beta \dot{x} Z^2 - \dot{x} = 0$$

(3.22)

along with the definitions:

$$F_d = \begin{cases} F_{dp}\left[1 - \exp\left(-\varepsilon_p|\dot{x}|\right)\right] & \text{for } x\dot{x} > 0 \\ F_{dm}\left[1 - \exp\left(-\varepsilon_m|\dot{x}|\right)\right] & \text{for } x\dot{x} < 0 \end{cases} \qquad (3.23)$$

$$\delta = \delta_o \exp\left(-\delta_1|\dot{x}|\right) \qquad (3.24)$$

Model parameters include F_o, k_o, F_{min}, F_{dp}, F_{dm}, x_y, α, β, γ, δ_o, δ_1, ε_p, and ε_m. It should be noted that the device contains a bias in the damping force, as modeled in Eq. (3.23). High damping is provided on loading, while low damping is obtained during unloading. Some comparisons between analytical and experimental response, obtained by Tsopelas and Constantinou (1994), using this model are shown in Figure 3.22. The correlation is quite good during both static and dynamic testing.
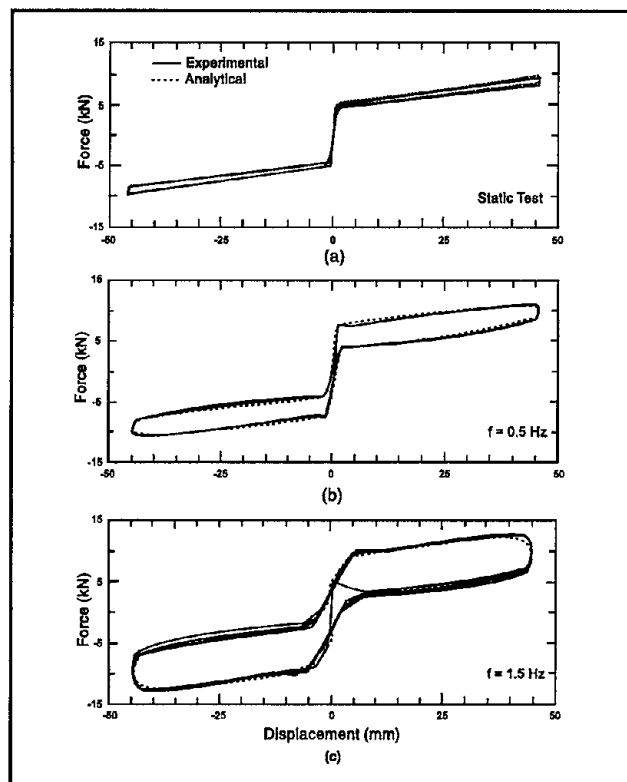
Tsopelas and Constantinou, 1994

■ Figure 3.22 Comparison of Experimental and Analytical Response of Pressurized Fluid Restoring Device

Next, consider the fluid device shown in Figure 3.23 that utilizes the orificed flow of a pressurized compressible silicone-based elastomer in order to enhance stiffness and damping (Pekcan et al., 1995). Figure 3.24 presents typical force-displacement loops obtained experimentally for the device. Until the internal preload is overcome, the device remains quite stiff. However, beyond that
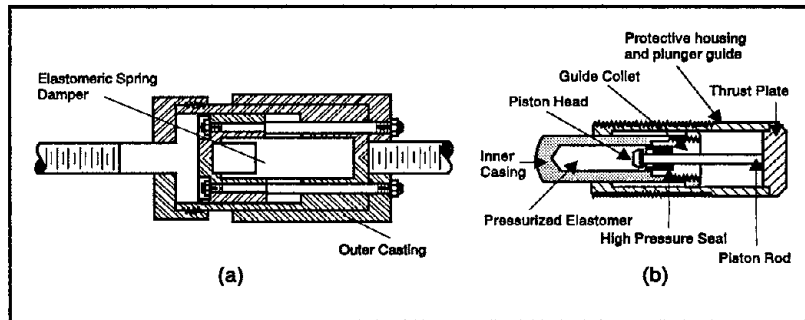
Pekcan et al., 1995

■ Figure 3.23 Elastomeric Spring Damper
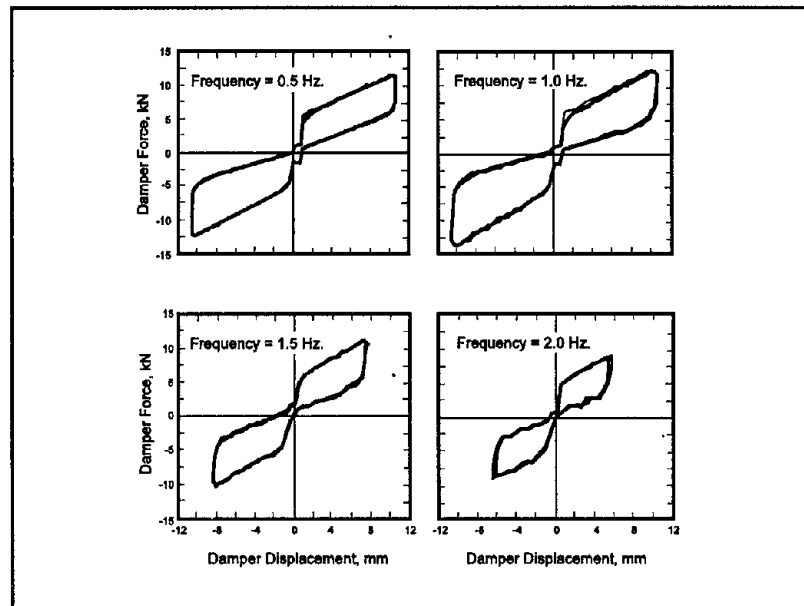
Pekcan et al., 1995

■ Figure 3.24 Experimental Response of Elastomeric Spring Damper

level of axial force, the piston compresses the elastomer and forces it to flow through the orifice provided between the piston head and the inner casing. Thus, one obtains both a stiffness and damping component in the response. Upon removal of the external loading, the device tends toward its undeformed state due to the initial internal elastomer pressure. The following mathematical model was developed in Pekcan et al., (1995) to describe the response under general conditions:

$$F = k_2 x + \frac{(k_1 - k_2)x}{\left[1 + (k_1 x / F_y)^2 \right]^{1/2}}$$

$$+ C \, sgn(\dot{x}) \left| \dot{x} x / x_{max} \right|^\alpha$$

(3.25)

where F_y, k_1 and k_2 represent the damper static prestress force, the initial damper stiffness and the elastomeric damper stiffness, respectively. Meanwhile, the remaining model parameters C, x_{max} and α define the damping constant, the maximum device stroke and the velocity exponent, respectively. A typical result obtained with Eq. (3.25), provided in Figure 3.25, is in general agreement with the experimental response. It is expected that the model defined in Eqs. (3.21)-(3.24) could also be used to describe this response.

a) Standard Solution   b) Variation of Frequency

Legend: --- f = 0.01 Hz. ···· f = 0.1 Hz. —— f = 2.5 Hz. – – f = 10 Hz.
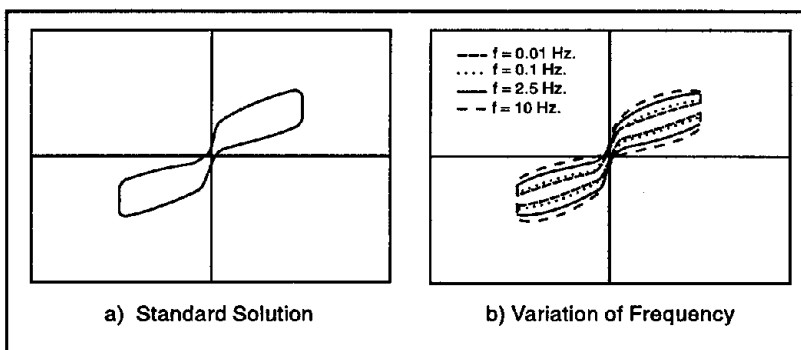
Pekcan et al., 1995

■ Figure 3.25 Elastomeric Spring Damper Model

3.3.2 PRELOADED SPRING-FRICTION DAMPERS

A similar force-displacement response has also been ob-
tained in a cylindrical device that employs frictonal wedges, along
with a preloaded internal spring (Richter et al., 1990). A sche-
matic of the damper is shown in Figure 3.26, while the typical
experimentally measured response is presented in Figure 3.27 for
two different configurations. The force-displacement loops gener-
ated by the device in Figure 3.27a have the characteristic double
flag shape associated with a preloaded device, while Figure 3.27b
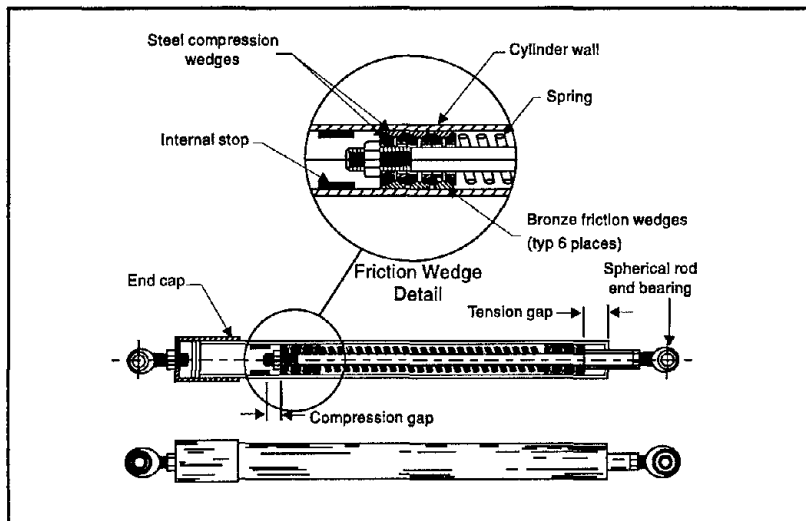
Nims et al., 1993a

■ Figure 3.26 Spring-friction Damper

illustrates the behavior when the preload is zero. In either case,
energy dissipation occurs due to frictional sliding, and consequently
the response is frequency independent. Further details on the
behavior of this device are provided in Nims et al., (1993a), and
in the following chapter.

3.3.3 PHASE TRANSFORMATION DAMPERS

In recent years, a new class of materials referred to as shape
memory alloys (SMA) have been considered for application in
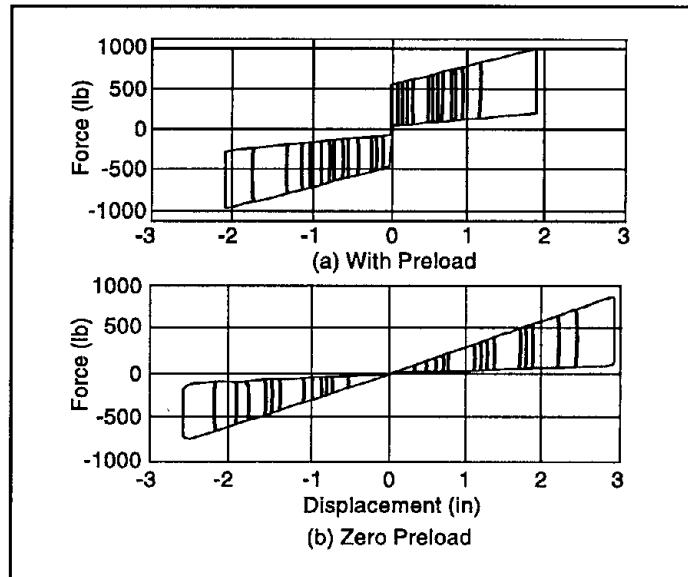
Nims et al., 1993a

■ Figure 3.27 Experimental Response of Spring-friction Damper

passive dampers. These metals collectively exhibit somewhat counter-intuitive behavior as a result of reversible temperature or stress induced transformations between martensitic and austenitic crystalline phases. Consider, for example, the shape memory effect. An SMA specimen in its low temperature martensitic phase is first distorted in an apparently permanent manner. The temperature of the specimen is then elevated above a critical level, inducing a transformation to the austenitic phase. As a consequence, the specimen returns to its original undistorted shape.

Of more direct interest for passive energy dissipation, however, is the characteristically large hysteresis loop that is obtained during cyclic loading of SMA materials in the martensitic phase, and the so-called superelastic behavior that occurs for loading above the critical temperature. A typical hysteresis curve for the former case is displayed in Figure 3.28a. In the latter case, the material is initially in the austenitic phase and behaves in an elastic manner. Once a critical stress level is reached, a reverse transformation is induced converting austenite into martensite. This transformation takes place at a greatly reduced modulus, thus resembling plastic behavior in ordinary metals, although the

microstructural mechanism is quite different. After the material is completely transformed into martensite, further loading results in elastic deformation with a significantly increased modulus. Unloading induces the reverse transformation back to the austenitic phase, but at a reduced critical stress level. At zero applied stress, the material is once again elastic with virtually no residual stress. This superelastic behavior is depicted in Figure 3.28b.

a) Response in Martensitic Phase   b) Superelastic Response
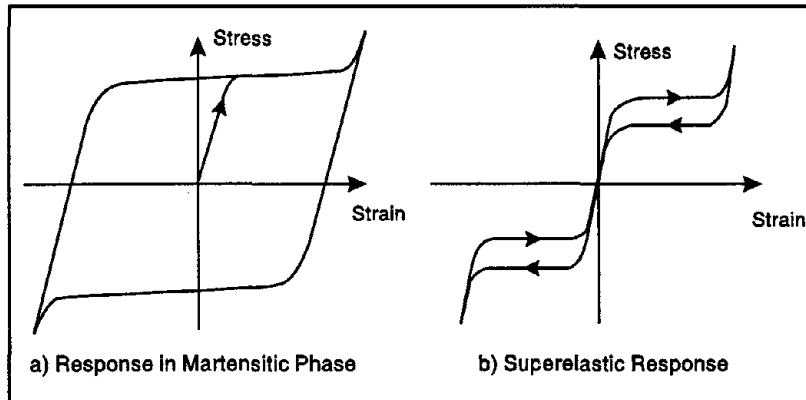
Graesser and Cozzarelli, 1989

■ Figure 3.28 Stress-strain Response of Shape Memory Alloys

In an effort to represent the entire range of this behavior, Graesser and Cozzarelli (1989) extended the rate-independent Özdemir hysteretic model. Their one-dimensional formulation in terms of damper force F and displacement x can be written:

$$\dot{F} = k_o |\dot{x}| \left(\frac{F - B}{F_o} \right)^n \tag{3.26a}$$

$$B = \alpha k_o \left[x_{in} + g_T |x|^c H(-x\dot{x}) erf(ax) \right] \tag{3.26b}$$

where k_0, F_0, n, α, g_T, c and a are device constants, and $H(x)$ and $erf(x)$ represent the Heaviside step function and the error function, respectively. Additionally, x_{in} denotes the inelastic displacement, while B is again a backforce. An example of superelastic behavior obtained with this model is shown in Figure 3.29.

50.0

α = 0.0197
n = 3
a = 2500   c = .001 g_T = .07

25.0

F   0.0

-25.0

-50.0

-0.020   0.000   0.020

X
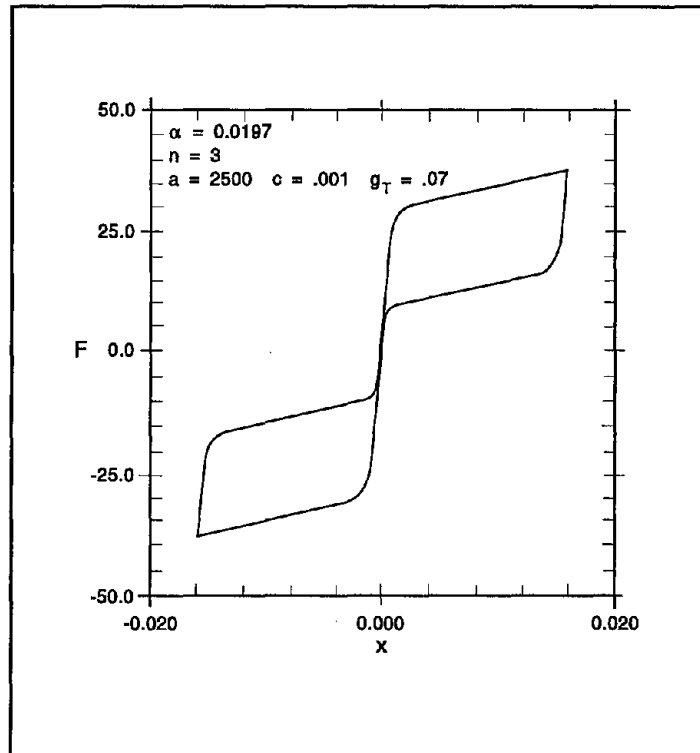
Graesser and Cozzarelli, 1989

■ Figure 3.29 Force-displacement Response for SMA Hysteretic Model Exhibiting Superelastic Behavior

3.4

DYNAMIC VIBRATION ABSORBERS

The final class of passive systems to be considered involves the use of dynamic vibration absorbers in a structure as illustrated in Figure 3.1b. The objective of incorporating a dynamic vibration absorber into a structure is basically the same as that associated with all of the other passive devices discussed previously, namely, to reduce energy dissipation demand on the primary structural members under the action of external forces. The reduction, in this case, is accomplished by transferring some of the structural vibrational energy to the absorber. Two basic types of dynamic vibration absorbers are prevalent in practice. The first is the **tuned**

mass damper which, in its simplest form, consists of an auxiliary mass-spring-dashpot system anchored or attached to the main structure. The second type is labeled **tuned liquid dampers**, and generally involves the dissipation of energy either through the sloshing of liquids in a container or via the passage of liquids through orifices. Although tuned mass dampers and tuned liquid dampers have been proposed for aseismic design, the primary applications to date have been for alleviation of vibrations due to wind loading. The present limitations for seismic application include detuning that occurs as the primary structure yields, the high levels of damping that are normally required, and an inability to effectively control higher mode response often associated with transient or impulsive excitations.

3.4.1 TUNED MASS DAMPERS

The modern concept of tuned mass dampers for structural applications has its roots in dynamic vibration absorbers studied as early as 1909 by Frahm (Den Hartog, 1956). A schematic representation of Frahm's absorber is shown in Figure 3.30, which consists of a small mass m and a spring with spring stiffness k attached to the main mass M with spring stiffness K. Under a simple harmonic load, one can show that the main mass M can be kept
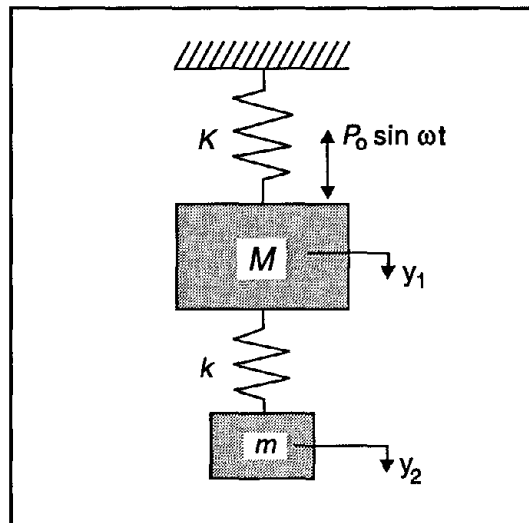
■Figure 3.30 Undamped Absorber and Main Mass Subject to Harmonic Excitation (Frahm's Absorber)

completely stationary when the natural frequency ($\sqrt{k/m}$) of the attached absorber is chosen to be (or tuned to) the excitation frequency.

Much of the early development as described above has been limited to the use of dynamic absorbers in mechanical engineering systems in which one operating frequency is in resonance with the fundamental frequency of a machine. Building structures, however, are subjected to environmental loads, such as wind and earthquakes, which possess many frequency components. The performance of a dynamic vibration absorber, frequently referred to as a tuned mass damper (TMD), in complex multi-degree-of-freedom damped building structures, is expected to be different.

Consider first the response of a single-degree-of-freedom (SDOF) structural system subjected to a vibratory force $f(t)$ as shown in Figure 3.31a. The response of the structural system can be re-
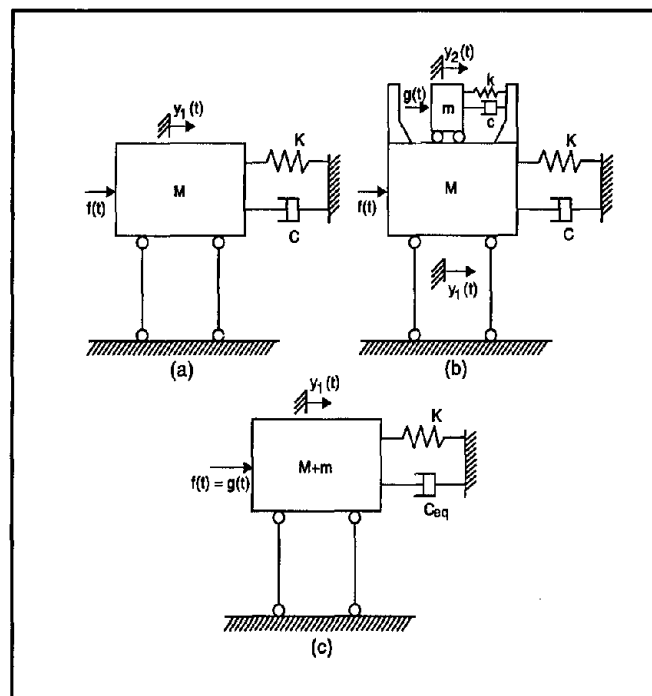
■ Figure 3.31 Models of SDOF Structure and TMD

duced in some circumstances by adding a secondary mass, or a TMD, which has motion relative to the system as shown in Figure 3.31b. The equations of motion for the structure/TMD system are, using the notation given in that figure,

$$M\ddot{y}_1(t) + C\dot{y}_1(t) + Ky_1(t) = c\dot{z}(t) + kz(t) + f(t) \qquad (3.27a)$$

$$m\ddot{z}(t) + c\dot{z}(t) + kz(t) = -m\ddot{y}_1(t) + g(t) \qquad (3.27b)$$

where $y_1(t)$ is the displacement of the structural system and $z(t)$ is the relative displacement of the added mass with respect to the structure. The damping coefficients and stiffnesses are denoted by c and k for the added mass and C and K for the structural system, respectively. The external force on the structure is represented by $f(t)$, while $g(t)$ equals zero for wind excitation and equals $\mu f(t)$ for earthquake loading, $\mu = m/M$ being the mass ratio.

Summation of Eqs. (3.27a) and (3.27b) leads to

$$(M + m)\ddot{y}_1(t) = C\dot{y}_1(t) + Ky_1(t) = f(t) + g(t) - m\ddot{z}(t) \qquad (3.28)$$

It is seen that the net effect of the added small mass (m) on the structure, aside from a slight decrease in natural frequency and a slight increase in external force from $f(t)$ to $f(t) + g(t)$, is the addition of a 'force term' $[-m\ddot{z}(t)]$.

When $f(t)$ is considered as a harmonic force or a stationary random input, Eq. (3.28) can be rewritten in the form of energy or power balance as

$$\begin{aligned} (M + m) < \ddot{y}_1\dot{y}_1 > + C < \dot{y}_1^2 > +K < y_1\dot{y}_1 > \\ = < (f + g)\,\dot{y}_1 > -m < \ddot{z}\dot{y}_1 > \end{aligned} \qquad (3.29)$$

in which $< \bullet >$ is the mathematical expectation for the case of stochastic input and the time average in one cycle for the case of harmonic excitation. For steady-state response, $<\ddot{y}_1\dot{y}_1> = <\dot{y}_1y_1> = 0$. Equation (3.29) is thus changed into the simple power balance equation:

$$C < \dot{y}_1^2 > = < (f + g)\dot{y}_1 > -m < \ddot{z}\dot{y}_1 > \qquad (3.30)$$

in which $C<\dot{y}_1^2>$ is the dissipated power due to structural damping and $<(f+g)\dot{y}_1>$ is the input power from the external force which is always positive.

The power flow $(m<\ddot{z}\dot{y}_1>)$ from the structural system to the secondary mass plays a basic role in the use of TMDs in struc-

tures and thus is an appropriate measure of TMD effectiveness, i.e., the larger the power flow, the smaller the mean-square velocity response of the structural system. Maximum power flow is obtained when the relative displacement of the secondary mass lags that of the structural system by a phase angle of 90°. In this case, the relative acceleration of the secondary mass is in phase with the velocity response in the structural system and the power flow is equivalent to an effective dissipative power which increases the total effective damping (C_{eq}) in the structural system as shown in Figure 3.31c, where

$$C_{eq} = C + m \frac{<\ddot{z}\dot{y}_1>}{<\dot{y}_1^2>}$$ (3.31)

It is worth noting here that input power from the external force varies with TMD parameters. However, this variation is small compared to the power flow and, in fact, the magnitude of the input power may decrease to produce a change which is favorable to TMD efficiency.

An appreciation of TMD efficiency in reducing structural response can be gained by following the basic development of Den Hartog for the simple case when the structural system is undamped $(C = 0)$ and is subject to a sinusoidal excitation with frequency ω (i.e., $f(t) = P_o \sin \omega t$ and $g(t) = 0$). In this procedure, the dynamic effect of a TMD is measured in comparison with the static deflection produced by the maximum force applied statically to the structure. This static deflection is $y_{st} = P_o / K$, while the dynamic amplification factor for an undamped structural system, R, is

$$R = \frac{y_{max}}{y_{st}}$$ (3.32)

$$= \sqrt{\frac{\left(\alpha^2 - \beta^2\right)^2 + \left(2\zeta_a \alpha \beta\right)^2}{\left[\left(\alpha^2 - \beta^2\right)\left(1 - \beta^2\right) - \alpha^2 \beta^2 \mu\right]^2 + \left(2\zeta_a \alpha \beta\right)^2 \left(1 - \beta^2 - \beta^2 \mu\right)^2}}$$

where
$\beta = \omega / \omega_s$ = forced frequency ratio
$\alpha = \omega_a / \omega_s$ = frequency ratio (natural frequencies)

$\omega_a^2 = k / m =$ squared natural frequency of TMD

$\omega_s^2 = K / M =$ squared natural frequency of structural system

$\zeta_a = c / c_c = c / 2m\omega_a =$ damping ratio of TMD

The amplification factor is a function of the four essential variables: μ, ζ_a, α, and β. Figure 3.32 shows a plot of R as a function of the frequency ratio β for $\alpha = 1$ (tuned case), $\mu = 0.05$, and for various values of the damping ratio ζ_a.
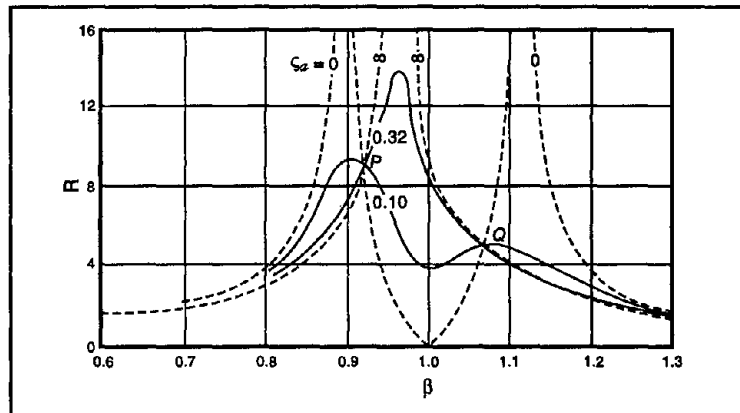
■ Figure 3.32 Amplification Factor as a Function of β

Observe what happens with increased damping in TMD. Without structural damping, the response amplitude is infinite at two resonant frequencies of the combined structure/TMD system. When the TMD damping becomes infinite, the two masses are virtually fused to each other and the result is a SDOF system with mass 1.05 M so that the amplitude at resonant frequency becomes infinite again. Therefore, somewhere between these extremes there must be a value of ζ_a for which the peak becomes a minimum.

An objective in adding the TMD is to bring the resonant peak of the amplitude down to its lowest possible value so that smaller amplifications over a wider frequency bandwidth, with β close to unity, can be achieved. The minimum peak amplitude can be obtained by properly choosing α to adjust the two fixed points (P and Q) to reach equal heights and by choosing ζ_a to adjust the system amplification curve to pass with a horizontal tangent through one of those two points. The optimum frequency ratio α following this procedure is determined as

$$\alpha_{opt} = \frac{1}{1+\mu}$$

(3.33)

which gives the amplitude at P or Q:

$$R = \sqrt{1 + \frac{2}{\mu}}$$

(3.34)

A good estimate for ζ_{opt} can be determined as the average of two values which make the fixed points P and Q maxima on an R vs. β plot, respectively (Brock, 1946), i.e.,

$$\zeta_{opt} = \sqrt{\frac{3\mu}{8(1+\mu)}}$$

(3.35)

From Eq. (3.30), one can easily observe that an increase in damper mass always reduces the maximum amplification factor for the optimally-designed TMD. This maximum amplification and optimum absorber parameters are summarized in Table 3.5.

Equation (3.32) can also be established when damping is present in the structural system; however, now the invariant points P and Q no longer exist. Hence, one must resort to numerical means in order to determine the optimum values of α and ζ_a. A detailed analysis was carried out by Warburton (1982) to determine optimum damper parameters for both harmonic and random excitations, with random excitation being applied as a force to the structure (as in the case of wind) or as base acceleration (as in the case of earthquake). A low damping ratio ζ_s of the main structure was assumed in this analysis.

For harmonic excitations, the optimization criterion was to minimize response amplitude R, given by

$$R_j = \sqrt{\frac{A_j^2 + B_j^2}{C^2 + D^2}}$$

(3.36)

where j is case number as defined in Table 3.6, A and B are given in the same table, and

■Table 3.5 Optimum Absorber Parameters Attached to Undamped SDOF Structure

Case	Excitation		Optimized Response		Optimized Absorber Parameter	
	Type	Applied to	Parameter Optimized (R)	R_{opt}	α_{opt}	ζ_{opt}
1	Force $P_o e^{i\omega t}$	Structure	$\dfrac{Ky_1}{P_o}$	$\left(1+\dfrac{2}{\mu}\right)^{1/2}$	$\dfrac{1}{1+\mu}$	$\sqrt{\dfrac{3\mu}{8(1+\mu)}}$
2	Force $P_o e^{i\omega t}$	Structure	$\dfrac{M\ddot{y}_1}{P_o}$	$\left(\dfrac{2}{\mu(1+\mu)}\right)^{1/2}$	$\left(\dfrac{1}{1+\mu}\right)^{1/2}$	$\sqrt{\dfrac{3\mu}{8(1+\mu/2)}}$
3	Acceleration $\ddot{X}_g e^{i\omega t}$	Base	$\dfrac{\omega_s^2 y_1}{\ddot{X}_g}$	$\left(\dfrac{2}{\mu}\right)^{1/2}(1+\mu)$	$\dfrac{(1-\mu/2)^{1/2}}{1+\mu}$	$\sqrt{\dfrac{3\mu}{8(1+\mu)(1-\mu/2)}}$
4	Acceleration $\ddot{X}_g e^{i\omega t}$	Base	$\dfrac{\ddot{X}_g+\ddot{y}_1}{\ddot{X}_g}$	$\left(1+\dfrac{2}{\mu}\right)^{1/2}$	$\dfrac{1}{1+\mu}$	$\sqrt{\dfrac{3\mu}{8(1+\mu)}}$
5	Random Force	Structure	$\dfrac{<y_1^2> K^2}{2\pi S_o \omega_s}$	$\left(\dfrac{1+3\mu/4}{\mu(1+\mu)}\right)^{1/2}$	$\dfrac{(1+\mu/2)^{1/2}}{1+\mu}$	$\sqrt{\dfrac{\mu(1+3\mu/4)}{4(1+\mu)(1+\mu/2)}}$
6	Random Acceleration	Base	$\dfrac{<y_1^2> \omega_s^3}{2\pi S_o}$	$(1+\mu)^{3/2}\left(\dfrac{1}{\mu}-\dfrac{1}{4}\right)^{1/2}$	$\dfrac{(1-\mu/2)^{1/2}}{1+\mu}$	$\sqrt{\dfrac{\mu(1-\mu/4)}{4(1+\mu)(1-\mu/2)}}$

Notes: $<y_1^2>$ is the mean-square value of $y_1(t)$
S_o is force intensity in case 5 and acceleration intensity in case 6

Warburton, 1982

Table 3.6 Values of A_j and B_j for Various Excitations and Response Parameters

Case	Excitation	Response Parameter Considered	Response Amplitude R_j	A_j	B_j
1	$P_o e^{i\omega t}$	y_1	$\dfrac{K y_1}{P_o}$	$\alpha^2 - \beta^2$	$2\zeta_a \alpha\beta$
2	$P_o e^{i\omega t}$	$\dot{y}_1$	$\dfrac{K \dot{y}_1}{P_o \omega_s}$	$-2\zeta_a \alpha\beta^2$	$\beta(\alpha^2 - \beta^2)$
3	$P_o e^{i\omega t}$	$\ddot{y}_1$	$\dfrac{M \ddot{y}_1}{P_o}$	$-\beta^2(\alpha^2 - \beta^2)$	$-2\zeta_a \alpha\beta^3$
4	$P_o e^{i\omega t}$	Force at base	$\dfrac{F}{P_o}$	$\alpha^2 - \beta^2 - 4\zeta_s\zeta_a\alpha\beta^2$	$2\zeta_a\alpha\beta + 2\zeta_s\beta(\alpha^2 - \beta^2)$
5	$\ddot{X}_g e^{i\omega t}$	y_1	$\dfrac{\omega_s^2 y_1}{\ddot{X}_g}$	$\alpha^2(1+\mu) - \beta^2$	$2\zeta_a\alpha\beta(1+\mu)$
6	$\ddot{X}_g e^{i\omega t}$	$\ddot{y}_1 + \ddot{X}_g$	$\dfrac{\ddot{y}_1 + \ddot{X}_g}{\ddot{X}_g}$	As Case 4	As Case 4
7	$\ddot{X}_g e^{i\omega t}$	$y_1 + X_g$	$\dfrac{\omega_s^2(y_1 + X_g)}{\ddot{X}_g}$	$-\dfrac{A_4}{\beta^2}$	$-\dfrac{B_4}{\beta^2}$

Notes: F = Force at base
$P_o e^{i\omega t}$ is the excitation applied to main mass
$\ddot{X}_g e^{i\omega t}$ is the excitation applied at base

Warburton, 1982

$$C = \left(\alpha^2 - \beta^2\right)\left(1 - \beta^2\right) - \mu\alpha^2\beta^2 - 4\zeta_a\zeta_s\alpha\beta^2 \qquad (3.37a)$$

$$D = 2\zeta_a\alpha\beta\left(1 - \beta^2 - \mu\beta^2\right) + 2\zeta_s\beta\left(\alpha^2 - \beta^2\right) \qquad (3.37b)$$

The optimum values of α and ζ_a can again be found by setting $\partial R_j / \partial\alpha$ and $\partial R_j / \partial\zeta_a$ equal to zero and solving the resulting equations. However, these equations are generally nonlinear in α and ζ_a, and thus require numerical solutions, some of which are presented in Warburton (1982).

3.4.2 Tuned Liquid Dampers

The basic principles involved in applying a tuned liquid damper (TLD) to reduce the dynamic response of structures is quite similar to that discussed above for the tuned mass damper. In particular, a secondary mass is introduced into the structural system and tuned to act as a dynamic vibration absorber. In the case of tuned liquid dampers, generally the response of the secondary system is highly nonlinear due either to liquid sloshing or the presence of orifices. As a consequence of this inherent nonlinearity, most of the work related to characterizing response of tuned liquid dampers has been based directly upon physical experiments. However, some mathematical models have been developed for tuned liquid dampers, under the assumption of moderate amplitude sloshing with no wave breaking. All of these efforts utilize extensions of the classical theories by Airy and Boussinesq for shallow water gravity waves of finite amplitude, which are detailed in Mei (1983). The model employed by Lepelletier and Raichlen (1988) is briefly summarized below.

Consider the two-dimensional idealization of a rectangular tank of length L and width b, as shown in Figure 3.33, containing water of nominal depth h. The following differential equations governing motion of the fluid can be written in terms of the wave elevation $\eta(x,t)$ and the depth-averaged horizontal velocity $u(x,t)$:

$$\eta_{,t} + \left[(h + \eta)u\right]_{,x} = 0 \qquad (3.38a)$$

$$u_{,t} + uu_{,x} + g\eta_{,x} - \frac{h^2}{3} u_{,xxt}$$

$$+ \frac{1}{h}\left(\frac{v\omega}{2}\right)^{1/2}\left(1 + \frac{2h}{b} + C\right)u + \ddot{x}_b = 0 \qquad (3.38b)$$

where subscripts following commas denote partial differentiation with respect to time t and space x. Additionally, in Eq. (3.38b), v, ω, g and $\ddot{x}_b$ represent the kinematic viscosity of the fluid, a characteristic frequency of the fluid motion, the gravitational acceleration and the acceleration of the tank base, respectively. Notice that nonlinearities appear in the second terms in both equations. Meanwhile, the fourth term in Eq. (3.38b) involving $u_{,xxt}$ provides dispersion, and the fifth term models dissipation associated with the boundary layer on the tank bottom and side walls. Dissipation due to free surface contamination is also included via the parameter C, which is usually assigned a unit value.
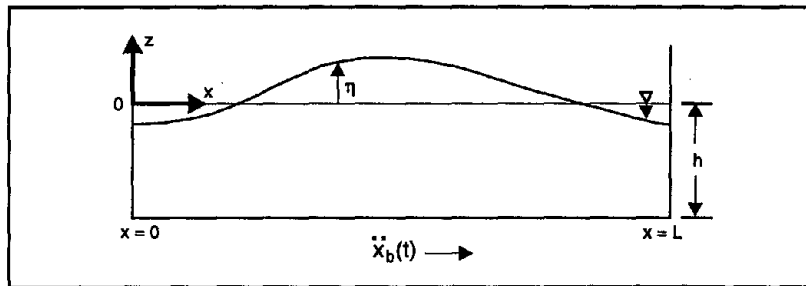
Lepelletier and Raichlen, 1988

■ Figure 3.33 Tuned Liquid Damper Geometric Definition

The relative contributions of nonlinearity and dispersion can be determined by considering the Stokes parameter defined by $U_s = \eta_0\lambda^2 / h^3$, where η_0 represents the wave amplitude and λ is the horizontal wavelength. For small values of U_s, dispersion dominates, while for large values of the Stokes parameter the response becomes significantly nonlinear. The latter regime is characterized by the appearance of progressive solitary waves and frequency bifurcations near resonance of the liquid. These resonant frequencies can be determined approximately by considering the dispersion relations for linearized response without dissipation. The resulting natural frequency for the kth mode can be written:

$$\omega_k = \left(2k - 1\right)\pi \frac{\left(gh\right)^{1/2}}{L}\left[1 - \frac{1}{6}\left(2k - 1\right)^2 \pi^2 \left(\frac{h}{L}\right)^2\right] \qquad (3.39)$$

Lepelletier and Raichlen (1988) solved Eqs. (3.38a,b) numerically using a finite element approach, and also conducted physical experiments to better understand the response under harmonic base excitation at frequency ω. Typical time histories of the free surface near the lowest resonance are shown in Figure 3.34. Peak amplitudes occur at a frequency slightly above that determined from the linearized conditions defined in Eq. (3.39).
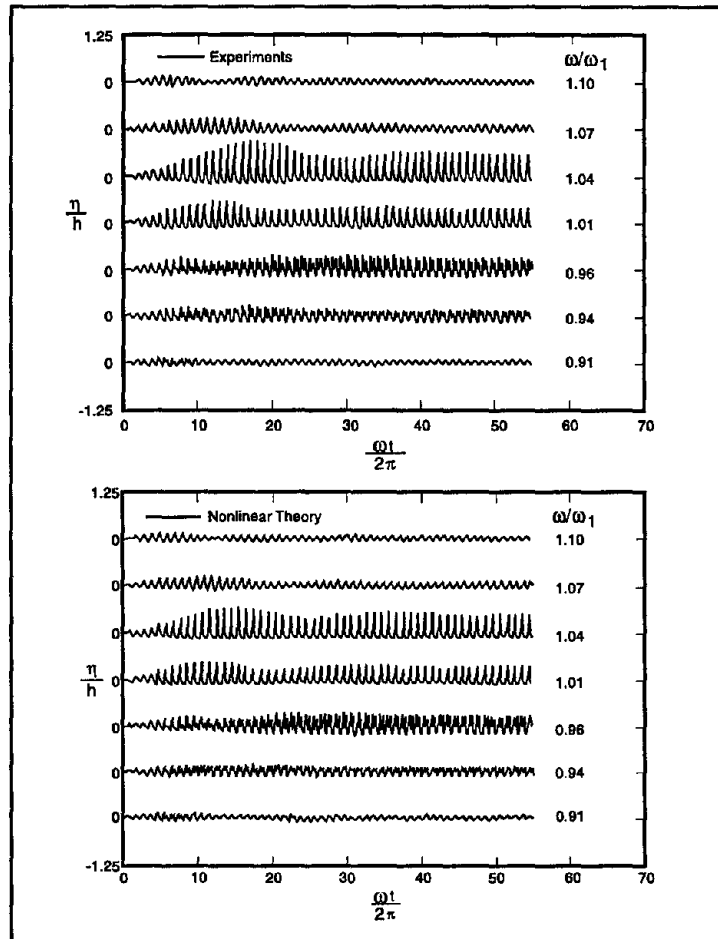
Lepelletier and Raichlen, 1988

■ Figure 3.34 Free Surface Time Histories Near Lowest Resonance

At somewhat lower frequencies, a bifurcation occurs that is a consequence of the nonlinearities along with low dispersion. In all cases, a good correlation was obtained between the experiments and the finite element solutions.

Similar numerical and experimental results have been obtained by other researchers. For example, Shimizu and Hayama (1987) developed a formulation which attempts to relax some of the shallow water assumptions inherent in Eq. (3.38). The authors then utilize a finite difference method to solve the resulting boundary value problem, and compare results with those obtained via physical experiments on a rectangular tank. Response time histories of surface elevation are provided in Figure 3.35. The numerical
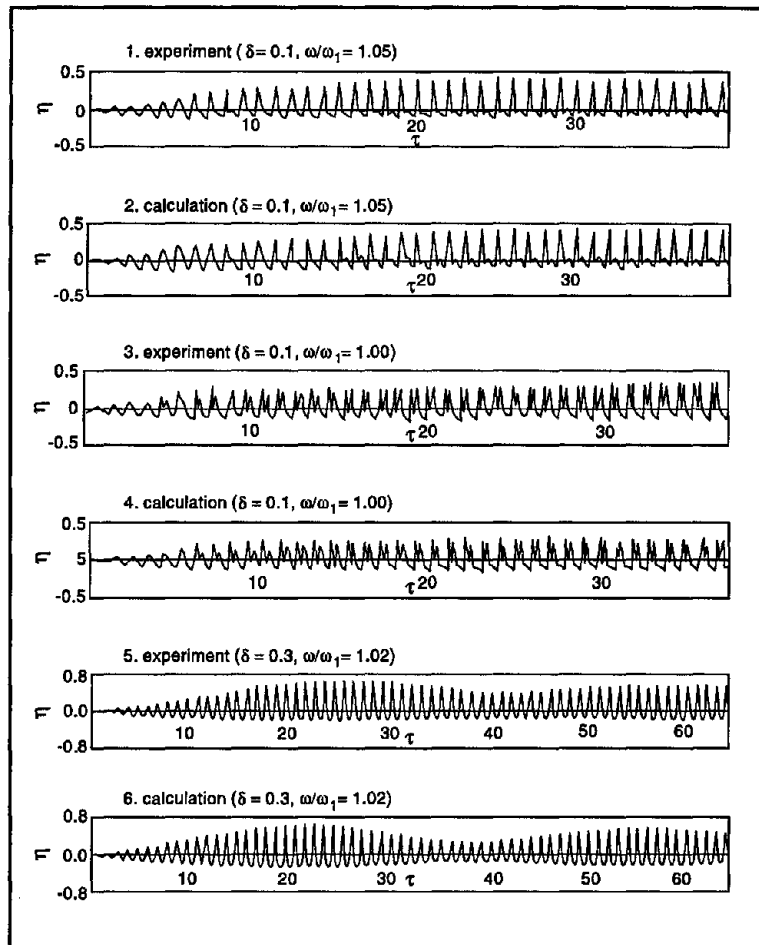
Shimizu and Hayama, 1987

■ Figure 3.35 Free Surface Time Histories Near Lowest Resonance

algorithm again provides quite accurate solutions, and the response is similar to that obtained by Lepelletier and Raichlen (1988). Application of this latter formulation to tuned liquid dampers is considered in Sun et al., (1989). These authors also attempt to establish a rational means to determine dissipation during sloshing motion. Typical time histories for the surface elevation and the base shear force are presented in Figure 3.36, while force-displacement hysteresis loops are shown in Figure 3.37.
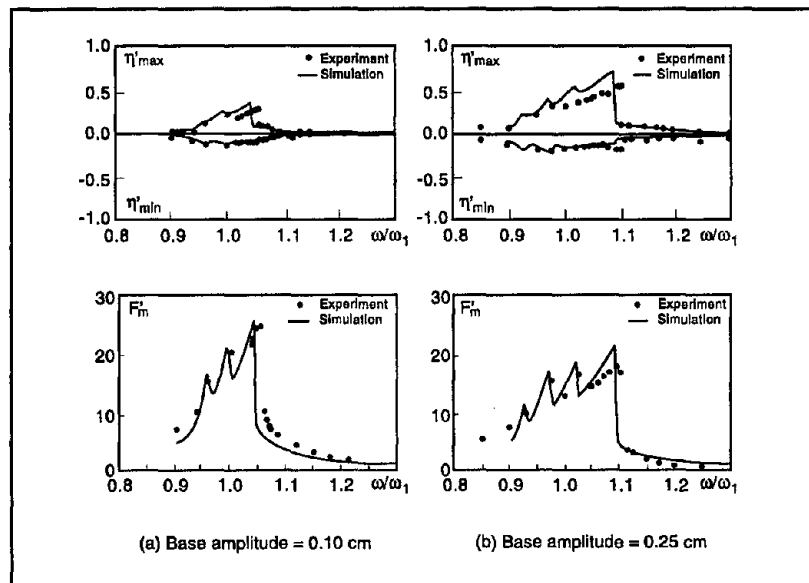
Fujino et al., 1992
■ Figure 3.36 Tuned Liquid Damper Surface Elevation Extrema and Base Shear Force Response
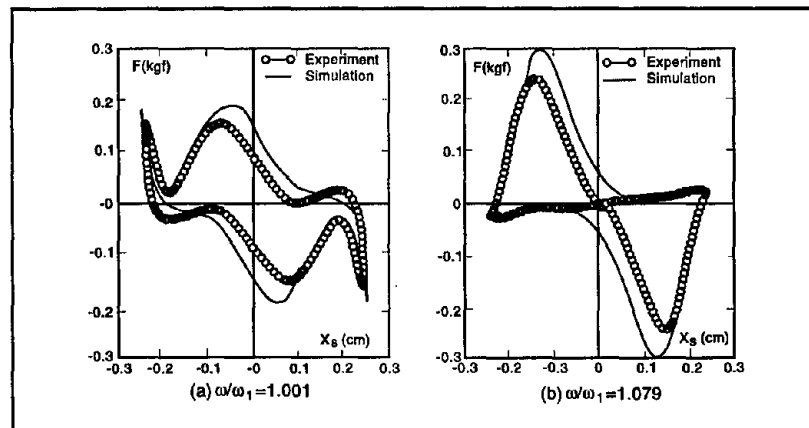
Fujino et al., 1992
■ Figure 3.37 Tuned Liquid Damper Force-displacement Response

In the above shallow water approximations, the dimensionality of the governing equations is reduced by integrating or averaging through the depth of the fluid. Alternatively, one can directly model the entire fluid domain by utilizing, for example, a finite element formulation. Efforts employing this latter approach for the analysis of sloshing include works by Su et al., (1982), Huerta and Liu (1988) and Okamoto and Kawahara (1990).

Once the characteristics of the sloshing liquid are established, the behavior of the overall structural system can be determined to some extent based upon the theory provided in Section 3.4.1 for tuned mass dampers (TMD). For example, an analogy between tuned liquid dampers and TMD parameters is provided in Sun et al., (1995). However, it must be remembered that TLD response is nonlinear. Stiffness and damping are frequency and amplitude dependent.

3.5

ANALYSIS OF STRUCTURES WITH PASSIVE MOTION CONTROL SYSTEMS

3.5.1 GENERAL FORMULATION

After having obtained a suitable mathematical model for a particular passive device, it is often necessary to perform a detailed analysis of the overall structural system under the action of dynamic loads. In the current section, several formulations for dynamic analysis of a structure incorporating passive elements are briefly outlined. The most effective approach will often depend upon the specific type of passive element employed. For example, an approach based upon modal superposition is appropriate for the linear analysis of structures with supplemental viscoelastic devices, while direct time domain procedures are applicable to a wide range of nonlinear analysis including those associated with the response of structures with hysteretic dampers.

The finite element method (e.g., Zienkiewicz and Taylor, 1989; Bathe, 1996) currently provides the most general basis for this formulation. From a purely physical viewpoint, each indi-

vidual structural member can be represented mathematically by one or more finite elements having the same mass, stiffness, and damping characteristics as the original member. Beams and columns are represented by one dimensional elements, while shear walls and floor slabs are idealized by employing two dimensional finite elements. Alternatively, a less detailed traditional structural engineering approach can be adopted in which story masses and stiffnesses are defined. Many reliable general-purpose finite element software packages currently exist to solve the structural dynamics problem, including ABAQUS, ADINA, ANSYS, and MSC/ NASTRAN. While some of these programs may not specifically address the special formulations needed to characterize all passive energy dissipation devices, most permit generic user-defined elements. Alternatively, one can utilize packages geared exclusively toward civil engineering structures, such as ETABS, DRAIN, and IDARC, which in some cases can already accommodate typical passive elements.

Via any of the above-mentioned methods and programs, the displacement response of the structure is ultimately represented by a discrete set of variables, which can be considered the components of a generalized relative displacement vector $x(t)$ of dimension N. Then, the N equations of motion for the discretized structural system, subjected to uniform base excitation and time varying forces, can be written

$$\mathbf{M}\ddot{x} + \mathbf{C}\dot{x} + \mathbf{K}x + \mathbf{\Gamma}x = -\left(\mathbf{M} + \overline{\mathbf{M}}\right)\ddot{x}_g + \mathbf{p} \qquad (3.40)$$

where $\mathbf{M}$, $\mathbf{C}$, and $\mathbf{K}$ represent the mass, damping, and stiffness matrices, respectively, while $\mathbf{\Gamma}$ symbolizes a matrix of operators which model the passive dampers present in the structure. Meanwhile, the vector $\ddot{x}_g$ contains the rigid body contribution of the seismic ground displacement to each degree of freedom, and $\mathbf{p}$ includes the forces due to aerodynamic loading. The matrix $\overline{\mathbf{M}}$ represents the mass of the passive dampers.

There are several approaches that can be taken to solve Eq. (3.40). The preferred approach, in terms of accuracy and efficiency, depends upon the form of the various terms in that equation. It is first supposed that the passive dampers can be modeled as

direct linear functions of the acceleration, velocity, and displacement vectors. That is,

$$\Gamma x = \overline{M}\ddot{x} + \overline{C}\dot{x} + \overline{K}x \qquad (3.41)$$

Then, Eq. (3.40) can be rewritten as

$$\hat{M}\ddot{x} + \hat{C}\dot{x} + \hat{K}x = -\hat{M}\ddot{x}_g + p \qquad (3.42)$$

in which

$$\hat{M} = M + \overline{M} \qquad (3.43a)$$

$$\hat{C} = C + \overline{C} \qquad (3.43b)$$

$$\hat{K} = K + \overline{K} \qquad (3.43c)$$

Equation (3.42) is now in the form of the classical matrix structural dynamic analysis problem. In the simplest case, which is now assumed, all of the matrix coefficients associated with the primary structure and the passive elements are constant. As a result, Eq. (3.42) represents a set of N linear second-order ordinary differential equations with constant coefficients. These equations are, in general, coupled. Thus, depending upon N, the solution of Eq. (3.42) throughout the time range of interest could become computationally demanding. This required effort can be reduced considerably if the equation can be uncoupled via a transformation; that is, if $\hat{M}, \hat{C},$ and $\hat{K}$ can be diagonalized. Unfortunately, this is not possible for arbitrary matrices $\hat{M}, \hat{C},$ and $\hat{K}$. However, with certain restrictions on the damping matrix $\hat{C}$, the transformation to modal coordinates accomplishes the objective, as shown below.

3.5.2 MODAL SUPERPOSITION METHOD

Consider the generalized eigenvalue problem associated with the undamped free vibration of the MDOF structure. That is

$$\left(\hat{K} - \omega_o^2 \hat{M}\right)\phi = 0 \qquad (3.44)$$

where ω_o represents an undamped natural frequency of the structure including passive elements and ϕ is the associated mode shape vector. The present undamped system will have N such natural frequencies and mode shapes labeled ω_{oi} and ϕ_i respectively, for $i = 1,2,...,N$. Usually, the natural frequencies are ordered by increasing numerical value, with the lowest (ω_{o1}) referred to as the fundamental frequency. Additionally, the mode shapes satisfy the following orthogonality conditions

$$\phi_i^T \hat{M} \phi_j = \begin{cases} 1 & for\ i=j \\ 0 & for\ i \neq j \end{cases} \tag{3.45a}$$

$$\phi_i^T \hat{K} \phi_j = \begin{cases} \omega_{oi}^2 & for\ i=j \\ 0 & for\ i \neq j \end{cases} \tag{3.45b}$$

and form a complete set spanning the N-dimensional vector space. Consequently, this set provides the basis for a suitable transformation that can be applied to the original system defined in Eq. (3.42). In Eqs. (3.45a) and (3.45b), superscript T indicates vector or matrix transpose.

There are numerous methods available to solve the generalized eigenvalue problem defined in Eq. (3.44). The choice depends largely upon the size and structure of the matrices $\hat{M}$ and $\hat{K}$. Nearly all of the structural analysis codes noted above contain efficient and robust eigenvalue extraction routines that require little user intervention. Routines are also available through the LAPACK (Anderson, et al., 1992) or IMSL implementations.

For notational convenience, the natural frequencies are placed in a diagonal matrix ω_o. The corresponding mode shape vectors form the columns of a square matrix Φ, which functions as the transformation matrix. Thus, any relative displacement vector x can be represented by

$$x = \Phi y \tag{3.46}$$

where y is the vector of modal (or normal) coordinates. Utilizing Eq. (3.46), along with Eq. (3.45), in Eq. (3.42) leads to the following equations of motion expressed in terms of the modal coordinates,

$$\ddot{y} + \Phi^T \hat{C} \Phi \dot{y} + \omega_o^2 y = -\ddot{y}_g + \Phi^T p \tag{3.47}$$

where

$$\ddot{y}_g = \Phi^T \hat{M} \ddot{x}_g \qquad (3.48)$$

In general, Eq. (3.47) still represents a coupled set of ordinary differential equations. The equations uncouple only when $\Phi^T \hat{C} \Phi$ is also a diagonal matrix. This occurs for the case of proportional (or Rayleigh) damping, in which

$$\hat{C} = \alpha_0 \hat{M} + \alpha_1 \hat{K} \qquad (3.49)$$

for scalar constants α_0 and α_1. From Eqs. (3.45) and (3.49), one obtains

$$\Phi^T \hat{C} \Phi = \alpha_0 I + \alpha_1 \omega_o^2 \qquad (3.50)$$

which is diagonal. The form of $\hat{C}$ can actually be generalized to the Caughey series

$$\hat{C} - \hat{M} \sum_{j=0}^{N-1} \alpha_j \left[\hat{M}^{-1} \hat{K} \right]^j \qquad (3.51)$$

while still permitting diagonalization. Eq. (3.51) is seldom used to compute $\hat{C}$ from a given set of α_j. Instead, modal viscous damping ratios ζ_j are specified, such that

$$\Phi^T \hat{C} \Phi = 2\zeta\omega_o \qquad (3.52)$$

with ζ representing a diagonal matrix containing the ζ_j. With this assumed, Eq. (3.47) becomes

$$\ddot{y} = 2\zeta\omega_o \dot{y} + \omega_o^2 y = -\ddot{y}_g + \Phi^T p \qquad (3.53)$$

Since the equations are now uncoupled, it is possible to write a scalar equation, for each mode i, as

$$\ddot{y}_i = 2\zeta_i \omega_{oi} \dot{y}_i + \omega_{oi}^2 y_i = -\ddot{y}_{gi} + q_i \qquad (3.54)$$

in which

$$q_i = \phi_i^T \mathbf{p} \qquad (3.55)$$

Equation (3.54) has the form of an SDOF system, and can be readily solved by numerical means. Thus, the solution of the original problem expressed in Eq. (3.52) is greatly simplified. The major computational task in this whole process is the determination of the natural frequencies and mode shapes. Even this task is not as onerous as it first appears, since for most physical problems only a small percentage of the N modes actually participate significantly in the system response. As a result, only the structural modes within a certain frequency range need be calculated.

The price paid for this simplicity is the initial restriction to system matrices with constant coefficients, and the further constraint on the damping matrix specified in Eq. (3.51). If the latter condition is relaxed, it still may be advantageous to use this approach based upon the undamped modes. The governing equations in modal coordinates, Eq. (3.47), remain coupled. However, it is often still possible to utilize a set much smaller than N, since typically only a small portion of the undamped modes will participate. For a more thorough treatment of the modal superposition method, the textbook by Clough and Penzien (1975) is recommended.

3.5.3   DIRECT TIME DOMAIN ANALYSIS

For analysis of structures that involve nonlinear response, superposition is of course no longer valid, and a direct time domain approach is generally adopted. While many methods are available to perform the required time integration numerically, the Newmark algorithm is most often selected, providing a reasonable balance between stability and accuracy. The implicit Newmark algorithm begins with a discretization of the time axis into intervals of duration Δt. At any instant, the equations of motion given in Eq. (3.42) can be recast in the form:

$$\mathbf{g}\left(\mathbf{x}^t\right) = \hat{\mathbf{M}}\ddot{\mathbf{x}}^t + \hat{\mathbf{C}}^t\dot{\mathbf{x}}^t + \hat{\mathbf{K}}^t\mathbf{x}^t + \hat{\mathbf{M}}\ddot{\mathbf{x}}_g^t - \mathbf{p}^t = 0 \qquad (3.56)$$

where the superscripts denote evaluation at time t. It is assumed that this solution is known, and that the role of the analysis is to determine a solution at time $t + \Delta t$. That is, one needs to solve

$$
\begin{aligned}
\mathbf{g}\left(\mathbf{x}^{t+\Delta t}\right) &= \hat{\mathbf{M}}\ddot{\mathbf{x}}^{t+\Delta t} + \hat{\mathbf{C}}^{t+\Delta t}\dot{\mathbf{x}}^{t+\Delta t} \\
&+ \hat{\mathbf{K}}^{t+\Delta t}\mathbf{x}^{t+\Delta t} + \hat{\mathbf{M}}\ddot{\mathbf{x}}_g^{t+\Delta t} - \mathbf{p}^{t+\Delta t} = 0
\end{aligned}
\tag{3.57}
$$

With the Newmark parameters chosen in the usual manner, the trapezoidal rule is then invoked to relate quantities at time $t + \Delta t$ to those at time t. Thus,

$$
\mathbf{x}^{t+\Delta t} = \mathbf{x}^t + \frac{\Delta t}{2}\left(\dot{\mathbf{x}}^t + \dot{\mathbf{x}}^{t+\Delta t}\right)
\tag{3.58a}
$$

$$
\dot{\mathbf{x}}^{t+\Delta t} = \dot{\mathbf{x}}^t + \frac{\Delta t}{2}\left(\ddot{\mathbf{x}}^t + \ddot{\mathbf{x}}^{t+\Delta t}\right)
\tag{3.58b}
$$

After substituting Eq. (3.58) into Eq. (3.57), one obtains

$$
\mathbf{g}\left(\mathbf{x}^{t+\Delta t}\right) = \tilde{\mathbf{K}}^{t+\Delta t}\mathbf{x}^{t+\Delta t} - \tilde{\mathbf{f}}^{t+\Delta t} = 0
\tag{3.59}
$$

where

$$
\tilde{\mathbf{K}}^{t+\Delta t} = \tilde{\mathbf{K}}^{t+\Delta t} + \frac{2}{\Delta t}\hat{\mathbf{C}}^{t+\Delta t} + \frac{4}{\left(\Delta t\right)^2}\hat{\mathbf{M}}
\tag{3.60a}
$$

$$
\begin{aligned}
\tilde{\mathbf{f}}^{t+\Delta t} &= -\hat{\mathbf{M}}\ddot{\mathbf{x}}_g^{t+\Delta t} + \mathbf{p}^{t+\Delta t} \\
&+ \left[\frac{4}{(\Delta t)^2}\hat{\mathbf{M}} + \frac{2}{\Delta t}\hat{\mathbf{C}}^{t+\Delta t}\right]\mathbf{x}^t \\
&+ \left[\frac{4}{(\Delta t)}\hat{\mathbf{M}} + \hat{\mathbf{C}}^{t+\Delta t}\right]\dot{\mathbf{x}}^t + \hat{\mathbf{M}}\ddot{\mathbf{x}}^t
\end{aligned}
\tag{3.60b}
$$

In general, Eq. (3.59) represents a set of nonlinear equations in the variables $\mathbf{x}^{t+\Delta t}$. There are numerous iterative solution

techniques that are applicable, including full, modified, and quasi-Newton methods. For the full Newton- Raphson method, one solves the linearized system

$$\mathbf{K}_{(n)}^{t+\Delta t} \Delta \mathbf{x} = \mathbf{f}_{(n)}^{t+\Delta t} \tag{3.61}$$

at each iteration (n). In Eq. (3.61), the effective tangent stiffness matrix and force vector can be written

$$\mathbf{K}_{(n)}^{t+\Delta t} = \left(\frac{\partial \mathbf{g}}{\partial \mathbf{x}}\right)_{(n)}^{t+\Delta t} \tag{3.62a}$$

$$\mathbf{f}_{(n)}^{t+\Delta t} = -\mathbf{g}\left(\mathbf{x}_{(n)}^{t+\Delta t}\right) \tag{3.62b}$$

respectively. The solution of Eq. (3.61) is used to update the displacements via

$$\mathbf{x}_{(n+1)}^{t+\Delta t} = \mathbf{x}_{(n)}^{t+\Delta t} + \Delta \mathbf{x} \tag{3.63}$$

Iteration continues until a suitable norm of $\Delta\mathbf{x}$ is reduced below a specified small tolerance. Once convergence is obtained at a particular time step, the displacement is established from $\mathbf{x}^{t+\Delta t} = \mathbf{x}_{(n+1)}^{t+\Delta t}$, the velocity and acceleration vectors at $t + \Delta t$ are computed from Eq. (3.58), and member forces and moments are evaluated. Then, the time parameter t is incremented, a new time step size Δt is selected, and the analysis proceeds to the next step by assuming $\mathbf{x}_{(1)}^{t+\Delta t} = \mathbf{x}^t$ or by utilizing an extrapolation algorithm.

   Since Eq. (3.61) requires the formation and factorization of $\mathbf{K}_{(n)}^{t+\Delta t}$ at each iteration, in practice, the full Newton-Raphson algorithm is seldom employed. Instead, the system matrix is updated less frequently and acceleration techniques are often utilized. All major structural analysis codes include algorithms similar to the one outlined above. In many cases, the program adaptively determines appropriate time step size to maximize computational efficiency and to reduce the burden placed on the design engineer. The algorithm can also be enhanced by introducing line searches in the direction of the Newton step $\Delta\mathbf{x}$ in an effort to

obtain a globally-convergent scheme. Additional details concerning time domain numerical analysis can be found in Zienkiewicz and Taylor (1989) and Bathe (1996). It is expected that these nonlinear direct time approaches will play an increasingly important role in structural design, particularly for systems employing passive energy dissipation technology.

3.5.4 ALTERNATIVE FORMULATIONS FOR VISCOELASTIC SYSTEMS

Another alternative approach, for linear structures that include passive dampers employing the classical Maxwell force-displacement models of Eq. (3.19), was developed in Constantinou and Symans (1993). This formulation can be derived starting from Eq. (3.40). Assuming that the forces due to the passive devices are $\Gamma x = f_\Gamma$ and that $\overline{M} = 0$, one can write

$$M\ddot{x} + C\dot{x} + Kx + f_\Gamma = -M\ddot{x}_g + p \qquad (3.64)$$

For building models that employ one degree of freedom per floor, the passive damper force vector f_Γ contains the horizontal components of damper forces acting on the individual floors. That is,

$$f_\Gamma = \begin{pmatrix} n_1 F_1 - n_2 F_2 \\ n_2 F_2 - n_3 F_3 \\ \vdots \\ n_j F_j - n_{j+1} F_{j+1} \\ \vdots \\ n_N F_N \end{pmatrix} \qquad (3.65)$$

where n_j is the number of identical dampers installed in the jth story and F_j is the corresponding horizontal force from a single damper. For the classical Maxwell model under consideration,

$$F_j + \lambda \frac{dF_j}{dt} = C_0 \cos^2 \theta_j \left(\frac{dx_j}{dt} - \frac{dx_{j-1}}{dt} \right) \qquad (3.66)$$

with θ_j representing the placement angle from the horizontal for the jth floor dampers.

After performing a Fourier transform on Eqs. (3.64)-(3.66), one obtains

$$\tilde{\mathbf{K}}(\omega)\tilde{\mathbf{x}} = -\mathbf{M}\tilde{\ddot{\mathbf{x}}}_g + \tilde{\mathbf{p}} \qquad (3.67)$$

where the tilde symbolizes a Fourier transformed quantity, and

$$\tilde{\mathbf{K}}\left(\omega\right) = -\omega^2\mathbf{M} + i\omega\mathbf{C} + \mathbf{K} + \tilde{\Gamma}\left(\omega\right) \qquad (3.68)$$

represents the dynamic stiffness of the structure. The frequency dependent coefficient matrix $\tilde{\Gamma}$ in Eq. (3.67) can be readily obtained from

$$\tilde{\Gamma}\tilde{\mathbf{x}} = \tilde{\mathbf{f}}_\Gamma \qquad (3.69)$$

with

$$\tilde{F}_j = \left[\frac{i\omega C_0\cos^2\theta_j}{1 + i\omega\lambda}\right]\left(\tilde{x}_j - \tilde{x}_{j-1}\right) \qquad (3.70)$$

The time history response can then be obtained by utilizing the discrete Fourier transform method (e.g., Press et al., 1992). In essence, one solves Eq. (3.67) for $\tilde{x}(\omega)$ independently at a number of frequencies, and an inverse fast Fourier transform algorithm is subsequently employed to reconstruct the time domain response $x(t)$. The solid viscoelastic damper, cylindrical pot fluid damper and viscous damping wall models can also be accommodated with this approach. One only needs to replace Eq. (3.70) with the appropriate frequency domain macroscopic model.

A time history analysis can also be conducted by solving the set of first-order differential equations (Constantinou and Symans, 1993):

$$\mathbf{B}\dot{\mathbf{z}} + \mathbf{A}\mathbf{z} = \mathbf{f} \qquad (3.71)$$

directly in the time domain. From Eq. (3.66), the various matrices and vectors in Eq. (3.71) are defined as follows:

$$z = \begin{pmatrix} \dot{x} \\ x \\ f_\Gamma \end{pmatrix}$$

(3.72a)

$$B = \begin{bmatrix} M & 0 & 0 \\ 0 & I & 0 \\ 0 & 0 & \lambda I \end{bmatrix}$$

(3.72b)

$$A = \begin{bmatrix} C & K & I \\ -I & 0 & 0 \\ -D & 0 & I \end{bmatrix}$$

(3.72c)

$$f = \begin{pmatrix} -M\ddot{x}_g + p \\ 0 \\ 0 \end{pmatrix}$$

(3.72d)

Furthermore, complex eigenvalues and eigenvectors can be determined by solving the generalized eigenvalue problem

$$\left(A + \mu B\right)z = 0$$

(3.73)

The natural frequencies and damping ratios are then determined from

$$\omega_{oi} = |\mu_i|$$

(3.74a)

$$\zeta_{oi} = -\Re(\mu_i) / \omega_{oi}$$

(3.74b)

The approach defined in Eqs. (3.71)-(3.74) is specifically developed for structures with viscoelastic dampers, however similar state-space formulations are often quite attractive for other situations. For example, problems involving nonproportional damping, modal superposition and model reduction can be handled effectively via state space methods.

Another approach that is often taken in the finite element literature for solution of problems with viscoelastic materials involves the representation of the relaxation functions in terms of a series of exponentials (ABAQUS, 1997). This permits a computationally efficient treatment of the hereditary contributions, without restricting the behavior to classical Kelvin or Maxwell formulations.

Clearly from the above brief discussion, there are many different approaches that can be adopted for the analysis of structures with passive dampers, although in some cases typical structural analysis software packages do not presently provide these capabilities, except through user-defined formulations.

As discussed in the preceding chapters, passive energy dissipation systems encompass a range of materials and devices for enhancing damping, stiffness and strength, and can be used both for natural hazard mitigation and for rehabilitation of aging or deficient structures. In general, they are characterized by a capability to enhance energy dissipation in the structural systems in which they are installed. This may be achieved either by conversion of kinetic energy to heat or by transferring of energy among vibrating modes. The first method includes devices which operate on principles such as yielding of metals, frictional sliding, phase transformation in metals, deformation of viscoelastic solids or fluids and fluid orificing. The latter method includes supplemental oscillators which act as dynamic vibration absorbers.

In what follows, advances in this area in terms of research and development of some of these devices are presented and discussed. For the sake of completeness, tuned mass dampers and tuned liquid dampers are included in the discussion although they are primarily used for vibration control of structures against wind-induced vibrations.

4.1

M E T A L L I C   D A M P E R S

As indicated in Section 3.1.1, the idea of utilizing added metallic energy dissipators within a structure to absorb a large portion of the seismic energy began with the conceptual and experimental work of Kelly et al., (1972) and Skinner et al., (1975). Several of the devices considered included torsional beams, flexural beams and U-strip energy dissipators. During the ensuing years, a wide variety of such devices have been studied or tested (Tyler, 1985; Bergman and Goel, 1987; Whittaker et al., 1991; Tsai et al.,

1993). Many of these devices use mild steel plates with triangular or X-shaped plates so that yielding is spread almost uniformly throughout the material. A typical X-shaped plate damper or ADAS (Added Damping and Stiffness) device is shown in Figure 3.3a. As discussed in Section 3.1.1, force-displacement response of an ADAS device under constant amplitude displacement controlled cycles has been examined by Whittaker et al., (1991). A typical result is displayed in Figure 3.5, where the area within the hysteresis loops provides a measure of the amount of dissipated energy. Other materials, such as lead and shape-memory alloys, have also been evaluated (Sakurai et al., 1992; Aiken et al., 1992). Some particularly desirable features of these devices are their stable hysteretic behavior, low-cycle fatigue property, long term reliability, and relative insensitivity to environmental temperature. Hence, numerous analytical and experimental investigations have been conducted to determine the characteristics of individual devices.

Despite obvious differences in their geometric configuration, the underlying dissipative mechanism in all cases results from inelastic deformation of the metallic elements. Therefore, in order to effectively include these devices in the design of an actual structure, one must be able to characterize their expected hysteretic behavior under arbitrary cyclic loading. While mathematical models have been developed for this purpose as discussed in Section 3.1.1, this development has been based primarily upon experimentation at the macroscopic level. In this approach, a mathematical force-displacement model is first selected, generally based upon an analogy with existing constitutive relationships for metals. Model parameters are then determined via curve fitting procedures from force-displacement experimental data obtained for the particular damper.

While serious attempts have been made to develop a rational force-displacement relationship for a metallic damper, the trend in the more contemporary work is toward utilizing even simpler representations, based upon elementary plasticity theories. For example, one finds that metallic dampers have been characterized by an elastic-constant strain hardening model (e.g., Perry et al., 1993), by a so-called tri-linear model (e.g., Tsai et al., 1993), or by a cyclic Ramberg-Osgood model (e.g., Su and Hanson, 1990). More recently, Pong et al., (1994) employed a two-surface force-space model in order to simulate some important features of

damper response, such as cyclic hardening, which were not addressed in the elementary models.

However, it should be noted once again that, in all the work referenced above, a macroscopic approach is taken. The model describes only the overall force-displacement response of a specific damper configuration, with model parameters determined directly from physical testing of that damper. Recently, Dargush and Soong (1995) developed an inelastic constitutive model for the material of metallic yield dampers based on a microscopic mechanistic approach. This approach permits a better understanding of the damper behavior. For example, information concerning inelastic strain histories provided by the model can be used to estimate fatigue life of the damper material.

With the knowledge of damper characteristics, the response behavior of a structure with added metallic yield dampers can be analyzed based on the procedures developed in Chapters 2 and 3. An important aspect of the structural analysis that should be emphasized with regard to metallic yield dampers is related to the predicted response under earthquake excitations. While the insertion of metallic dampers into a structural system generally reduces response by dissipating a portion of the energy, the response may actually increase for some specific seismic inputs. For example, consider a one-degree-of-freedom system with mass m, stiffness k and a viscous damping ratio of 0.05 subjected to the 1940 El Centro S00E ground motion, with the added damper modeled as a massless rate-independent elastic-perfectly plastic element depicted in Figure 4.1. Plots of maximum acceleration and displacement re-
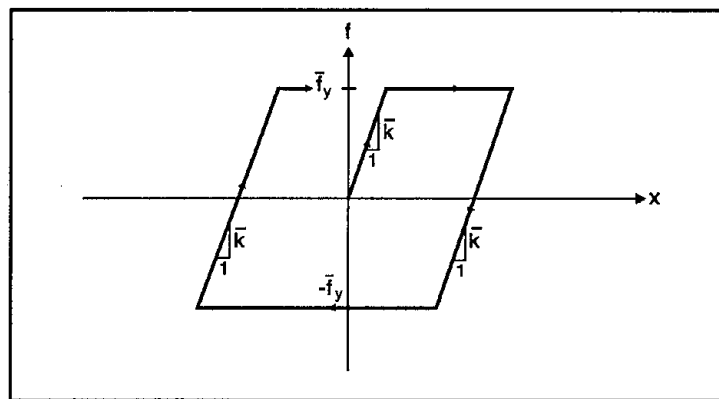
■ Figure 4.1 Force-displacement Relationship for Elastic-Perfectly Plastic Element

sponse versus elastic structural period T_o are shown in Figure 4.2, where

$$T_O = 2\pi\left(\frac{m}{k + \bar{k}}\right)^{1/2} \qquad (4.1)$$

and $\bar{k}$ is the initial stiffness. It is clear from these diagrams that there exist ranges of T_o in which the elastoplastic damper is either ineffective or even detrimental.
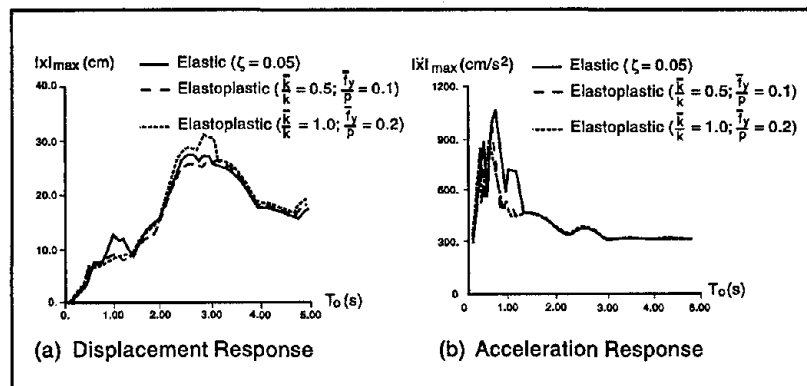
Figure 4.2 SDOF Response to 1940 El Centro (N-S Component)

The above results for the simple SDOF system certainly suggest that detailed nonlinear transient dynamic analyses are required to properly evaluate the effectiveness of any real structure employing metallic dampers for enhanced seismic protection. As mentioned in Section 3.5, the finite element method (FEM) currently provides the most suitable framework for a multi-degree-of-freedom (MDOF) analysis of an overall structure. The modified Newton-Raphson time domain approach, for example, is directly applicable for structures that include metallic dampers. This type of algorithm is typically available in most major FEM computer programs. Many of these programs also permit user-defined structural elements. Additionally, major codes include substructuring facilities, which permit separation of linear and nonlinear degrees of freedom. The effective tangent stiffness matrix for the linear case can be formed and eliminated once at the beginning of the analysis. The solution at each time step then involves the formation and decomposition of a relatively small system containing only the

nonlinear DOF. This type of partitioning was utilized by Özdemir (1976) for analysis of structures incorporating torsional beam dampers. Subsequently, the same methodology was used by Bhatti et al., (1978) to develop an optimal design approach for a base isolation system, which included the torsional beam damper. The method of feasible directions was employed in the latter work for the optimization of several simple structural systems. In light of the considerable advances in computing capabilities and optimization software that has occurred during the intervening years, it would be interesting to apply a similar approach for the design of metallic dampers positioned within the superstructure.

Recent applications of nonlinear structural analysis to building frames incorporating metallic dampers can be found in Xia and Hanson (1992), Jara et al., (1993), and Tsai et al., (1993). The first two references consider X-shaped plate dampers, while the last examines triangular plate dampers. All three works utilize the DRAIN-2D computer code (Kanaan and Powell, 1973) for the analyses.

As a final note in this section, it should be mentioned that there are several attractive alternatives to the modified Newton-Raphson algorithm. One of these involves rewriting the governing equations in the state-space form by introducing both displacement and velocity as primary unknowns (Soong and Grigoriu, 1993). This permits the use of very accurate and efficient first-order differential equation solvers.

4.2

FRICTION DAMPERS

Friction dampers utilize the mechanism of solid friction that develops between two solid bodies sliding relative to one another to provide the desired energy dissipation. As stated in Section 3.1.2, several types of friction dampers have been developed for the purpose of improving seismic response of structures.

As in the case of metallic dampers, the development of macroscopic force-displacement models for friction dampers has been dependent, to a considerable extent, on the results of experimental testing. Pall et al., (1980) began their development of friction dampers by conducting static and dynamic tests on a variety

of simple sliding elements having different surface treatments. The goal was not necessarily to obtain maximum energy dissipation, but rather to identify a system that possesses a consistent and predictable response. For these tests, contact was maintained between the sliding surfaces by pretensioning 12.7 mm diameter high strength bolts. The resulting load-displacement response under monotonic loading is shown in Figure 4.3, while Figure 3.9 details the hysteretic behavior under constant amplitude displacement-controlled cyclic loading.
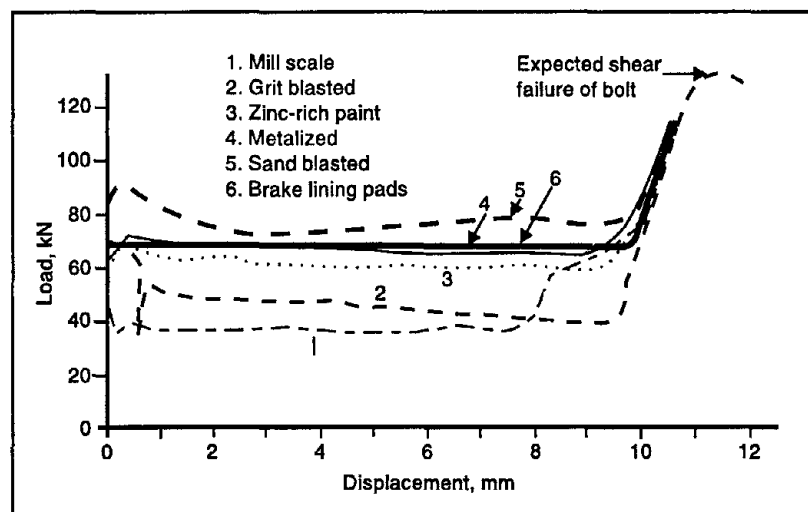
Pall et al., 1980

■ Figure 4.3 Load-displacement Response of Limited Slip Bolted Joints

Subsequently, Pall and Marsh (1982) proposed a system in which the braces in a moment resisting frame incorporated frictional devices. These devices utilize the same heavy duty brake lining pads. In a typical X-braced system, the braces are designed to buckle at relatively low compressive loads. As a result, the braces contribute only when subjected to tension. By installing uniaxial friction elements within each brace, slippage would only occur in the tensile direction and very little energy dissipation would result during cyclic loading. However, the special damper mechanism, devised by Pall and Marsh (1982), and depicted in Figure 3.8a, permits much more effective operation. During cyclic loading, the mechanism tends to straighten buckled braces and also enforces slippage in both tensile and compressive directions.

Initially, Pall and Marsh (1982) used a simple elastoplastic model to represent the behavior of this X-braced friction damper. However, Filiatrault and Cherry (1987) determined that this is only valid if the device slips during every cycle, and if the slippage is always sufficient to completely straighten any buckled braces. Otherwise, the Pall-Marsh model overestimates the energy dissipation. To remedy this situation, Filiatrault and Cherry (1987) proposed a more detailed macroscopic model for the device. A schematic is provided in Figure 4.4. Each member of the
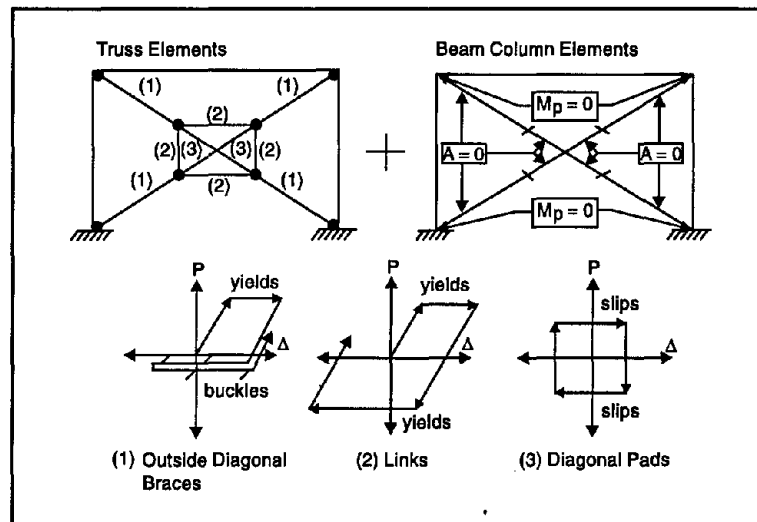
Filiatrault and Cherry, 1987

■ Figure 4.4 Refined Model for X-braced Friction Damper

bracing-damper system is represented by elements reflecting its individual axial and bending characteristics. Thus, the structural braces are assumed to yield in tension, but buckle elastically in compression. The device links are permitted to yield in both tension and compression, while the sliding brake pads are represented by a hysteretic model corresponding to the experimental results obtained by Pall et al., (1980). Bending stiffness is included to maintain stability of the damper mechanism.

In addition to developing the refined model, Filiatrault and Cherry (1987) conducted some physical experiments. In particular, they examined the response of the X-braced damper, with heavy duty asbestos brake lining pads, subjected to cyclic displacement-controlled loading along one diagonal. Results are shown in Figure 4.5. Notice that, although a consistent response
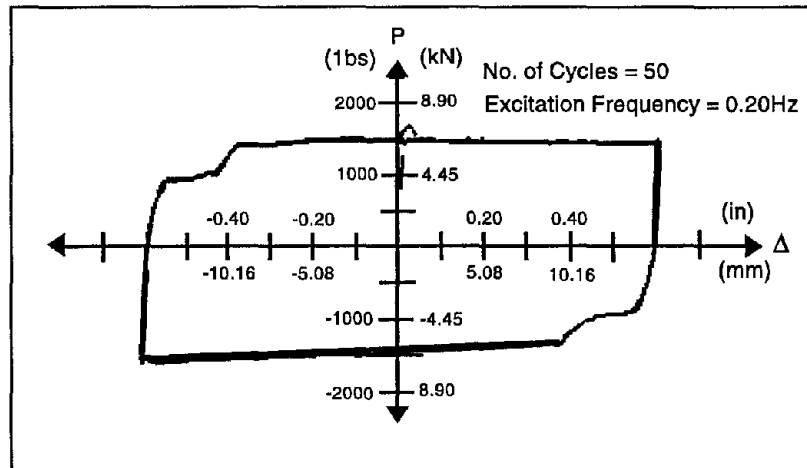
Filiatrault and Cherry, 1987

■ Figure 4.5 Experimental Hysteresis Loops for X-braced Friction Damper

is still maintained over a total of fifty cycles with a displacement amplitude of 15 mm, the hysteresis loops are no longer perfectly rectangular. The notches appearing in the two corners of the loops were attributed to the difference between the diameters of the bolts and bolt holes. In fact, the results shown in the figure were obtained after inserting steel bushings in the corner holes and slots of the device. From this investigation, it is clear that seemingly minor fabrication details can affect the overall performance of the friction damper. A hysteretic model can also be developed for this imperfect Coulomb friction element, which essentially involves multilevel bearing stops.

Several alternate friction damper designs have also been proposed in the recent literature. For example, Roik et al., (1988) discuss seismic control of structures through the use of three-stage friction-grip elements. Another simple design, the Slotted Bolted Connection (SBC), shown in Figure 4.6, was investigated by FitzGerald et al., (1989). Experimental results obtained under sizable displacement controlled loading are provided in Figure 4.7. In State 1, the gusset plate slips relative to the channel plates, while in State 2 there is also slippage between the channel and cover plates. It should be noted that the consistent experimental response present in Figure 4.7 is attributed by the authors to the inclusion of Belleville spring washers. On the other hand, Grigorian et al., (1993) also employ Belleville washers in an SBC design, but obtain much more erratic behavior as indicated in Figure 4.8.
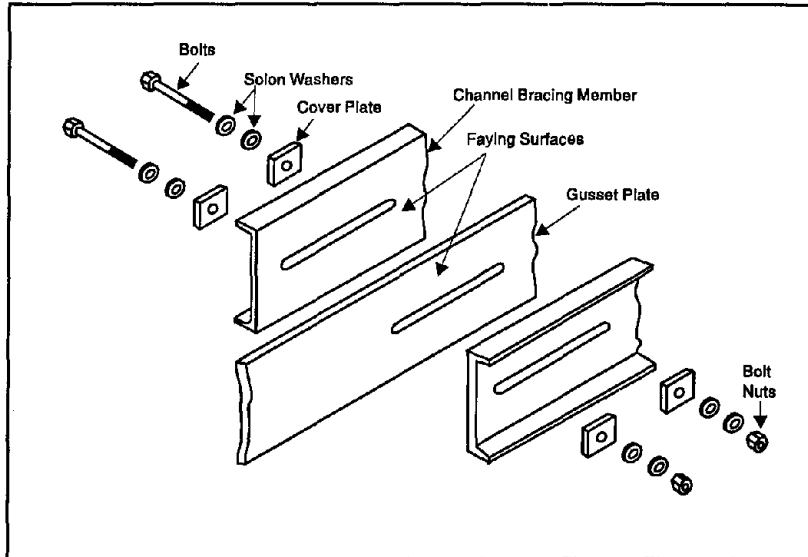
■Figure 4.6 Slotted Bolted Connection

Run 1. Deformation State 1

Run 2. Deformation State 2
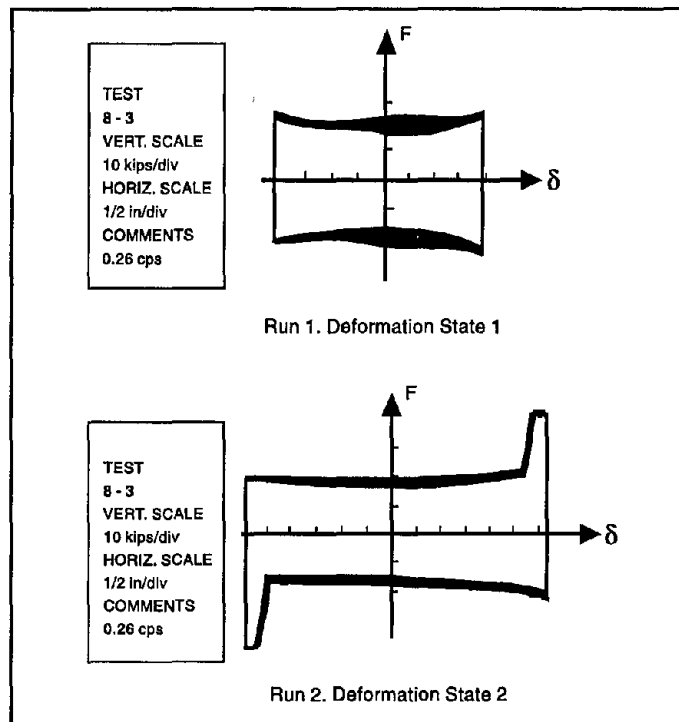
■ Figure 4.7 Typical Load Deformation Diagram for Slotted Bolted Connections

Steel on Steel Imposed Displacements · Steel on Brass Imposed Displacements

Steel on Steel Force Response · Steel on Brass Force Response

Steel on Steel Hysteresis Diagram · Steel on Brass Hysteresis Diagram

Steel on Steel Response · Steel on Brass Response
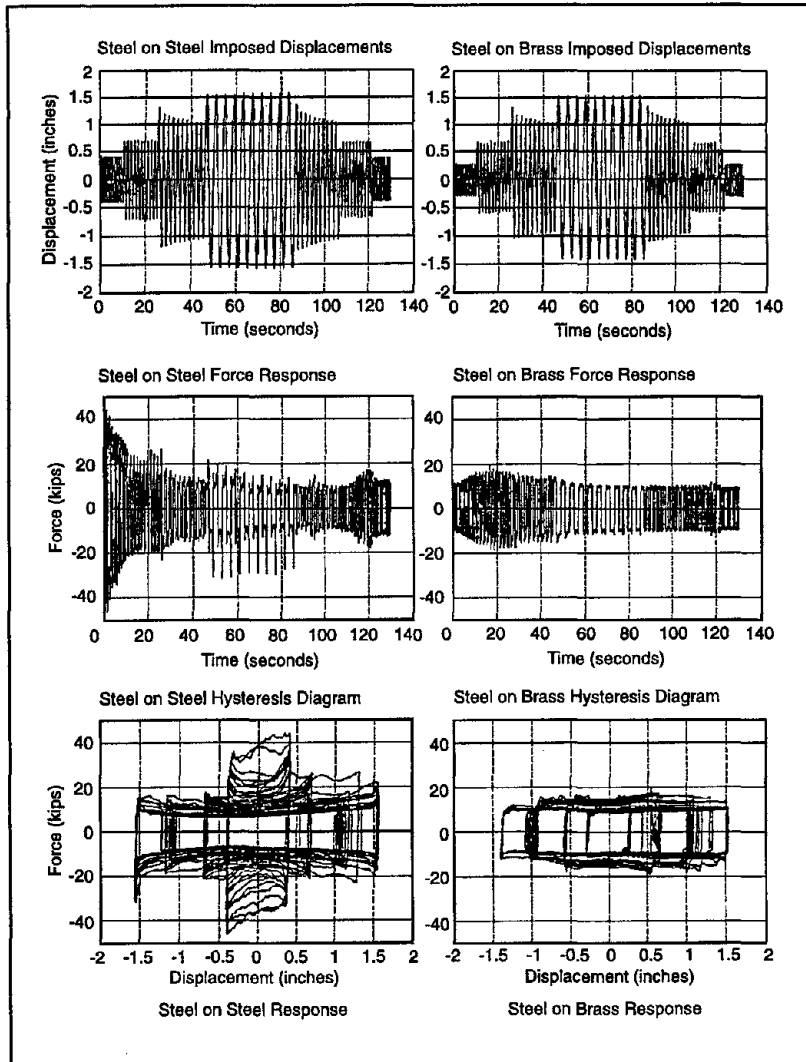
Grigorian et al., 1993

■ Figure 4.8 Cyclic Response of Slotted Bolted Connections

Clearly this latter type of response from a critical structural component must be deemed unacceptable.

The uniaxial friction damper illustrated in Figure 3.8b, manufactured by Sumitomo Metal Industries Ltd., utilizes a slightly more sophisticated design. The pre-compressed internal spring exerts a force that is converted through the action of inner and outer wedges into a normal force on the friction pads. These copper alloy friction pads contain graphite plug inserts, which pro-

vides dry lubrication. This helps to maintain a consistent coefficient of friction between the pads and the inner surface of the stainless steel casing. Aiken and Kelly (1990) indicate that the response of these dampers is extremely regular and repeatable with rectangular hysteresis loops. Furthermore, the effect of loading frequency and amplitude, number of cycles, or ambient temperature on damper response was reported to be insignificant. Although the supportive component test data is not available in the literature, it would seem that a simple elastic-perfectly plastic hysteretic model is also appropriate for structural analysis involving this device.

The final friction damper to be considered is the Energy Dissipating Restraint (EDR) manufactured by Fluor Daniel, Inc. and detailed in Figure 4.9. Superficially, the design is similar to the Sumitomo concept, since this device also includes an internal spring and wedges encased in a steel cylinder. However, there are several novel aspects of the EDR that combine to produce very different response characteristics. A detailed presentation of the design and its performance is provided in Nims et al., (1993a). As indicated in Figure 4.9, the EDR utilizes steel compression wedges and bronze friction wedges to transform the axial spring force into a normal pressure acting outward on the cylinder wall. Thus, the
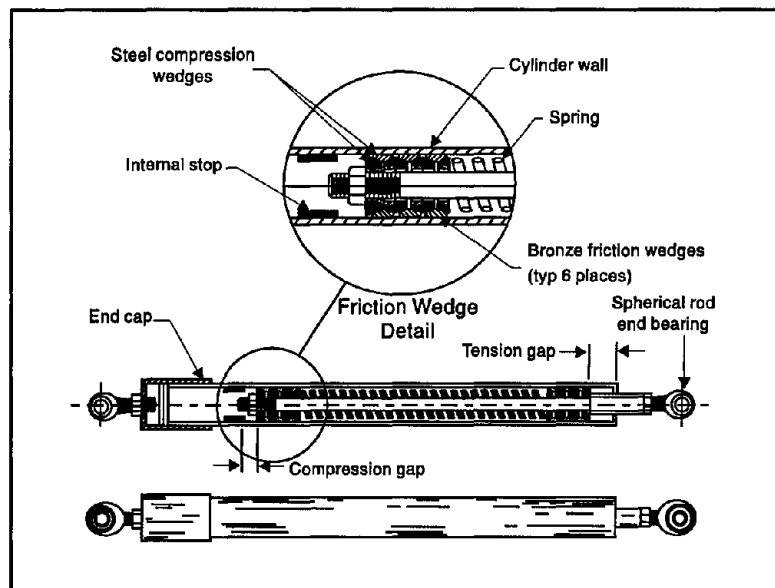
Nims et al., 1993a

■ **Figure 4.9 Energy Dissipating Restraint**

frictional surface is formed by the interface between the bronze wedges and the steel cylinder. Internal stops are provided within the cylinder in order to create the tension and compression gaps that are illustrated in Figure 4.9. Consequently, unlike the Sumitomo device, the length of the internal spring can be altered during operation, providing a variable frictional slip force. Typical experimental hysteretic behavior is displayed in Figure 4.10 for three different configurations. Figure 4.10a represents the response obtained with zero gaps and zero spring preload. Triangular shaped hysteresis loops result indicating slip force proportional to the device displacement. With non-zero spring preload, but no initial gaps, the flag-shaped hysteresis loops of Figure 4.10b are obtained. Finally, with a non-zero preload and very large gaps, the device acts as a standard Coulomb damper as indicated in Figure 4.10c. Clearly, from Figure 4.10, the response characteristics of the EDR are quite different from those of the other friction dampers.

Considerable experimental studies have also been performed at the structural level. The first such investigation was conducted by Filiatrault and Cherry (1987), who evaluated the performance of the cross-braced friction dampers. Two identical three-story, one-third scale steel frame structures were fabricated in a manner that readily permitted transformation between moment resisting (MR), braced moment resisting (BMR) and frictional damped braced (FDB) frame configurations. Natural frequencies and damping ratios were measured at low amplitude for all three configurations. Then the structures were mounted on a shaking table and subjected to a series of earthquake records with varying magnitude and frequency content. In general, the authors found that the friction-damped structures responded significantly better than the MR or BMR designs for high intensity signals.

The experimental program designed by Filiatrault and Cherry (1987), and described briefly above, was well conceived and quite comprehensive. However, one minor point must be made concerning the use of full scale cross-braced friction devices in a one-third scale structure. Even though slip loads were adjusted to appropriate levels, this scaling imbalance reduces the contribution of any geometric nonlinearities that may be associated with the device. It is difficult to determine the significance of that contribution without further testing or detailed modeling.
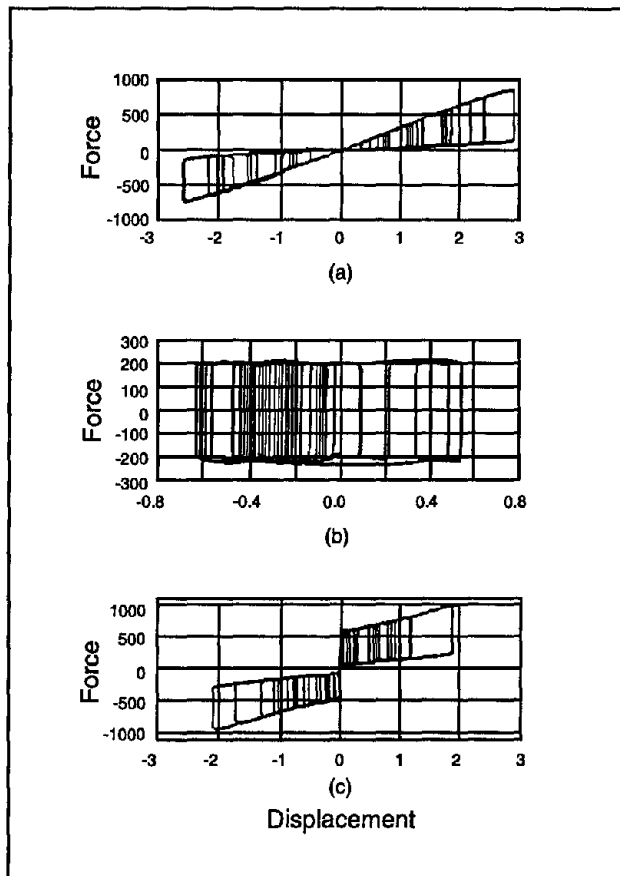
Richter et al., 1990

■ Figure 4.10 Experimental Data for EDR

An additional experimental study on the cross-braced dampers was conducted by Aiken et al., (1988). A three-bay, nine-story, one-quarter scale steel structure was extensively tested on an earthquake simulator, in both MR and FDB frame configurations. The dissipating elements in the FDB design utilized a brake lining pad/stainless steel frictional interface. Low amplitude natural frequencies and damping ratios were first determined for both configurations. The fundamental frequencies were 2.0 Hz and 2.23 Hz for the MR and FDB frames, respectively, while the corre-

sponding damping ratios were calculated at 2.4% and 5.6%. The structure was subjected to a total of ten different seismic signals with varying magnitude. As expected, for a given earthquake, an increase in magnitude was found to increase the effectiveness of the friction dampers. For example, the ratio of roof-to-ground acceleration dropped from 3.1 to 2.0 as the peak ground acceleration of an El Centro time history was elevated from 0.30 g to 0.84 g. At that highest intensity, the FDB structure had an estimated equivalent damping ratio of 32%.

In order to compare performance of the MR and FDB frames, Aiken et al., (1988) used temporal scaling of the 1985 Mexico City ground motion to achieve a quasi-resonance response for each configuration. The predominant signal frequency was adjusted to coincide with the fundamental frequency of the structure. For the MR frame, a peak ground acceleration of 0.25 g then produced a maximum displacement of 3.1 in., while a 0.65 g peak acceleration resulted in a displacement of only 2.8 in. for the friction-damped frame. Furthermore, in the latter case, approximately 70% of the input energy was dissipated by the frictional devices. The primary structural members remained in the elastic range.

More recently, using the same nine-story test frame, Aiken and Kelly (1990) performed a combined experimental and numerical investigation of uniaxial Sumitomo friction elements installed in conjunction with chevron bracing. A comprehensive test program was conducted, involving free vibration, random excitation, and pulse loadings, along with a total of fourteen different seismic ground motions. Only a brief summary can be provided here, but all test results are thoroughly documented in the referenced report. The authors note that the performance of the friction dampers was outstanding. The hysteresis loops indicated very consistent, nearly ideal Coulomb behavior throughout the duration of the test program. For example, the response at all ten friction damper locations, for the El Centro ground motion at 0.712 g peak acceleration, are reproduced in Figure 4.11. Approximately 60% of the input energy is dissipated in the dampers. Meanwhile, the corresponding floor accelerations, displacements, and interstory drifts are presented in Figure 4.12, along with those for the conventional MR and BMR frames. It is apparent from these profiles that the FDB structure nearly attains the benefits of the reduced displacement response of the BMR frame, combined
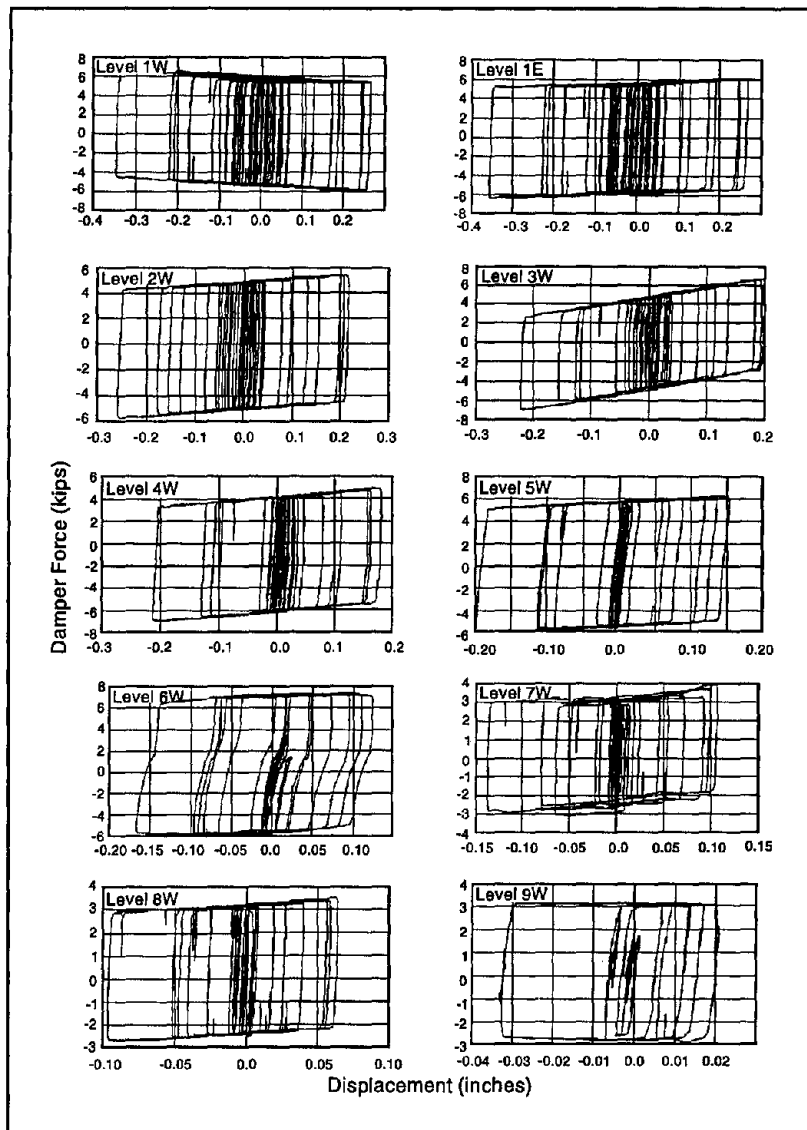
Aiken and Kelly, 1990

■ Figure 4.11 Response of Sumitomo Dampers in Nine-Story Frame for El Centro 0.712g Input

with the acceleration response of the MR frame. The report also contains details of a numerical study and comparisons with responses obtained using viscoelastic dampers in the same structural frame.

The final experimental study to be discussed in this section concerns the behavior of the EDR device. Richter et al., (1990) describe results from a series of over 400 shaking table tests con-
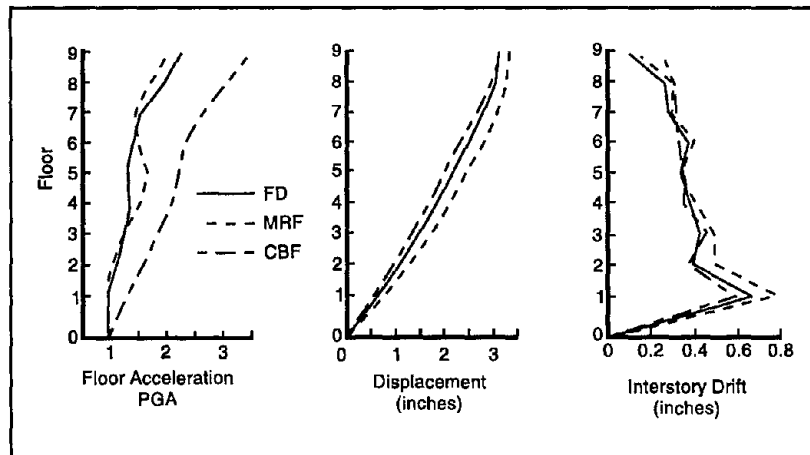
Aiken and Kelly, 1990

■ Figure 4.12 Overall Response Comparison in Nine-story Frame for El Centro 0.712g Input

ducted on a small, 6 ft. high, three-story steel frame structure. Although a number of different internal EDR damper configurations were considered, in all cases, two devices were mounted in each story. Typical hysteretic response of the dampers, configured with no gaps and an initial slip load of 200 lbs., is shown in Figure 4.13 for a scaled Zacatula ground motion. The flag-shaped loops are well-defined and quite consistent. Cumulative energy time histories are provided in Figures 4.14a,b for Zacatula and El Centro signals, respectively. In both cases, the frictional devices dissipate over 90% of the total input energy. However, as noted by the authors, hysteretic mechanisms do not respond quickly to sudden impulses. This is evident in these energy response curves. Additionally, higher modes were sometimes excited due to sudden stiffness changes associated with the frictional devices. Despite these limitations, the EDR device consistently provided reductions in displacements and interstory drifts, and increased the effective damping ratio of the test structure.

After a hysteretic model has been validated for a particular friction damper, it can be readily incorporated in an overall structural analysis. Although some attempts have been made to introduce the concepts of equivalent viscous damping (e.g., Scholl, 1993), in general, a full nonlinear time domain analysis is required. The finite element methodologies outlined in Chapter 3 are directly applicable, and in fact have been used in a number of detailed numerical investigations involving friction dampers. The
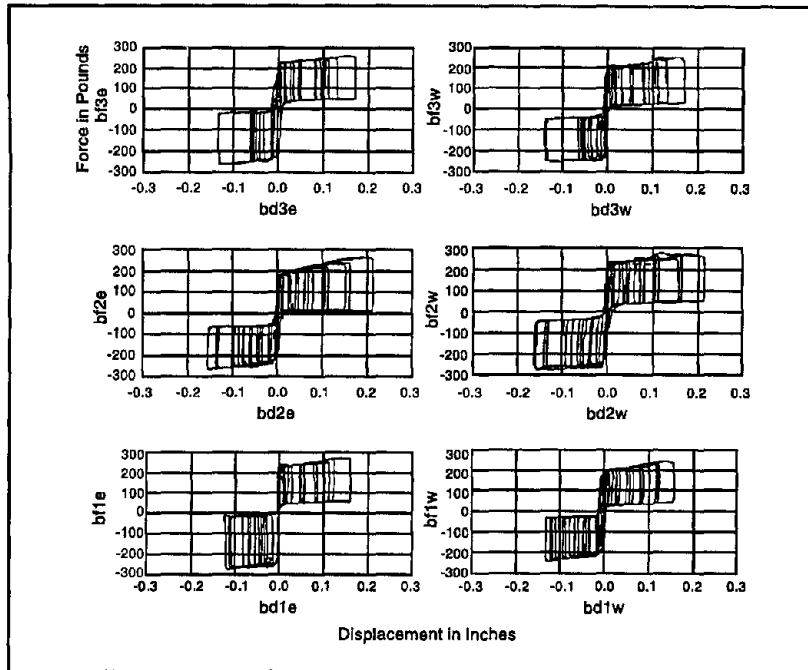
Richter et al., 1990
■ Figure 4.13 EDR Response in Three-story Test Frame for Zacatula Ground Motion

present section contains a review of the more prominent efforts, which attempt to highlight the benefits of incorporating various frictional devices into structural systems.

As a part of their initial work, Pall et al., (1980) performed parametric studies on a hypothetical panelized apartment building incorporating Limited Slip Bolted (LSB) joints. The nonlinear analysis utilized DRAIN-2D (Kanaan and Powell, 1973) to deter-

a) Zacatula Ground Motion   b) El Centro Ground Motion
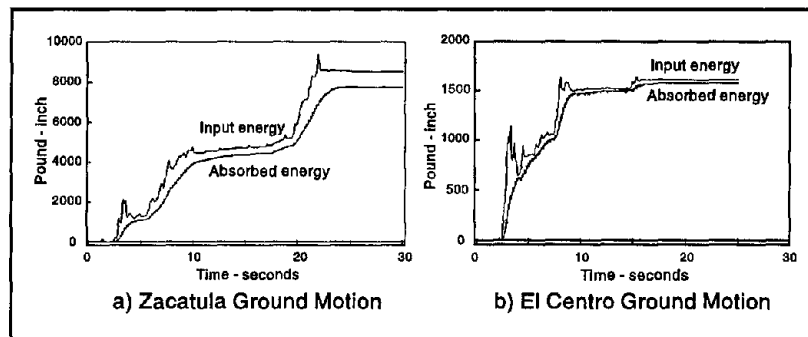
Richter et al., 1990
■ Figure 4.14 Cumulative Energy Time History for EDR Damped Three-story Test Frame

mine the response due to the 1940 El Centro S00E seismic ground motion scaled to various intensities. Results show that both building height and slip load had a major influence on seismic performance. For example, Figures 4.15a,b present the maximum wall normal stress at the base and the maximum displacement at the top, respectively, as a function of those two parameters. Ratios of less than unity indicate enhanced performance for the friction-damped structure. It is apparent that significant improvement is possible for the 15- and 20-story buildings, while the addition of LSB joints is not beneficial for the stiffer 5- and 10-story models. Unfortunately, this behavior is difficult to generalize, because the response is strongly influenced by the frequency content of the seismic signal.
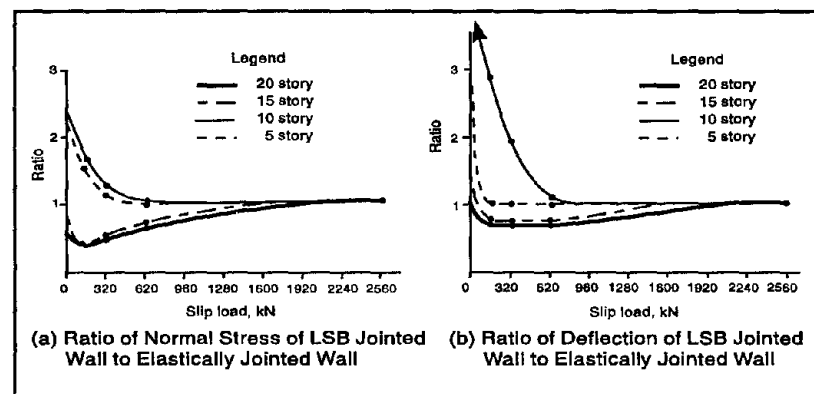
Pall et al., 1980

■ Figure 4.15 Numerical Results of LSB Joint for El Centro Ground Motion

Pall and Marsh (1982) presented similar numerical trends for a 10-story steel frame supported on a rigid foundation, again subjected to the 1940 El Centro earthquake. Results for three configurations, MR, BMR and FDB, were compared. The DRAIN-2D analysis included consideration of tensile yielding and compressive buckling of primary frame members, along with their simple hysteretic friction damper model. Zero viscous damping was assumed for the structure in all three configurations. Their results show that addition of friction dampers results in significant reductions in interstory drifts. Reduced column shear and bending moment are also apparent. On the other hand, axial forces are greater than those obtained for the moment resisting frame.

For the particular case considered, plastic hinges form in beam members of the MR and BMR designs, while the primary members in the FDB with optimal slip loads remain elastic. The authors note, however, that results obtained for a single seismic record may not be conclusive.

Similar studies were carried out by Filiatrault and Cherry (1987, 1988). In Filiatrault and Cherry (1988), a comparative numerical study was conducted of conventional, friction-damped, and base-isolated BMR steel frame structures. A typical ten-story building, with cross bracing in the even stories, was employed for the comparison. Optimal friction device slip loads were determined using DRAIN-2D for the 1940 El Centro S00E signal. In a similar manner, design parameters were established for the lead-rubber hysteretic bearing base isolation system. Mathematical models of all three systems were then subjected to signals from the 1977 Bucharest and 1985 Mexico City earthquakes, which have a very strong low frequency content. In terms of damage to structural members, results show that both base isolated (BIBMR) and frictional damped (FDB) frames performed well under the El Centro earthquake. However, only the FDB design was effective for the remaining two disturbances. However, it is difficult to draw general conclusions concerning the relative merits of FDB and BIBMR designs. It can be argued that the BIBMR system was simply not designed to respond favorably to strong low frequency content earthquakes. In that regard, this study by Filiatrault and Cherry (1988) highlights the importance of optimizing structural performance, not for a single seismic signal, but rather for the entire range of earthquake inputs that can be expected to occur at a particular site. The computational effort required for such an approach is not beyond that available with modern engineering workstations.

More recently, numerical and theoretical investigations on the response of structural systems incorporating EDR devices have appeared. Nims et al., (1993a) conducted parametric studies on idealized SDOF systems with added frictional elements that produce either the flag-shaped or triangular-shaped hysteresis loops discussed earlier. The parameters considered include the frequencies of the braced and unbraced structure, unbraced damping ratio ζ, EDR device initial slip load P_i as a percentage of the structural weight, and amplitude and frequency content of the seismic signal. Figure 4.16 provides a typical set of results for devices

a) Comparison for El Centro Input

b) Varying Slip Load for El Centro Input

c) Comparison for Zacatula Input

d) Varying Slip Load for Zacatula Input
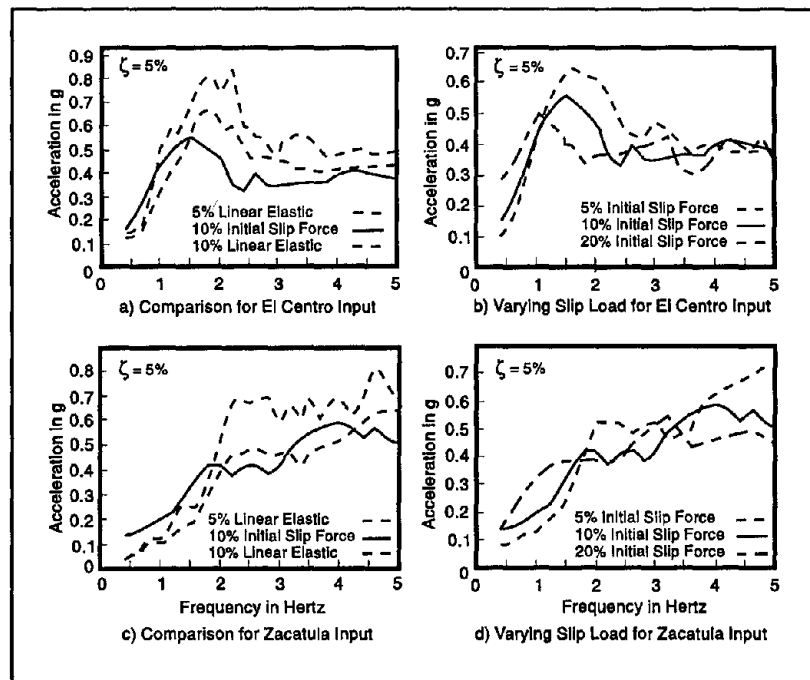
Nims et al., 1993a

■ Figure 4.16 Numerical Response of SDOF Structure with EDR

with flag-shaped hysteresis loops. In these plots, the acceleration response, due to the El Centro and Zacatula earthquakes, is plotted versus unbraced structural frequency with $\zeta = 0.05$. The frequency of the braced structure is assumed, in all cases, to equal twice the unbraced frequency. From Figures 4.16a,c, it is apparent that the addition of frictional devices reduces response, except for structures in the low frequency range. (Results for an unbraced structure with $\zeta = 0.10$ are also included in these figures to illustrate the effects of adding purely viscous damping mechanisms. The variation of response with initial slip load is quantified in Figures 4.16b,d.

The above EDR results are for a SDOF system. However, the response of a six-story, 0.3-scale steel MDOF structure, subjected to the El Centro and Zacatula ground motions, has been reported in Nims et al., (1993b). Comparisons made with the corresponding unbraced and conventionally braced frames indicate that the friction dampers effectively reduce displacements, while maintaining comparable acceleration levels.

Nonlinear analysis methods have been employed out of necessity in all of the efforts referred to in this section to describe the behavior of structural systems that incorporate friction dampers. In recent work, Inaudi et al., (1993b) have developed some interesting and potentially useful methods to approximate the response of systems that include EDR devices with triangular-shaped hysteresis loops. The authors note that although these frictional elements are nonlinear and the principle of superposition does not apply, the response is scale invariant. Thus, if a deformation history is scaled by a certain factor, the forces in the device are multiplied by that same factor. This permits the effective use of the techniques of harmonic linearization and statistical linearization (Inaudi et al., 1993b) to develop estimates of the actual nonlinear response. In general, very good results are obtained, indicating that these methods may be suitable for preliminary design calculations. It should be noted, however, that the use of discontinuous memory functions within a force-displacement model can lead to difficulties under arbitrary excitations which include partial unloading-reloading cycles.

4.3

VISCOELASTIC DAMPERS

While viscoelastic (VE) dampers have been applied to buildings for motion control against wind-induced vibrations for more than 25 years, research and development of VE dampers for seismic applications began only recently. Over the last few years, significant advances in this direction have been made through analyses and experimental tests. In order to assess seismic applicability of VE dampers, extensive experimental programs have been designed and carried out for steel frames in the laboratory (Ashour and Hanson, 1987; Su and Hanson, 1990; Lin et al., 1991; Fujita et al., 1992; Kirekawa et al., 1992; Aiken et al., 1993; Bergman and Hanson, 1993; Chang et al., 1993b, c; Chang et al., 1995), for lightly reinforced concrete frames in the laboratory (Foutch, et al., 1993; Lobo et al., 1993b; Chang et al., 1994; Shen et al., 1995), and for a full-scale steel frame structure in the field (Chang et al., 1993a; Lai et al., 1995). In what follows, two of these experiments are described and their results summarized.
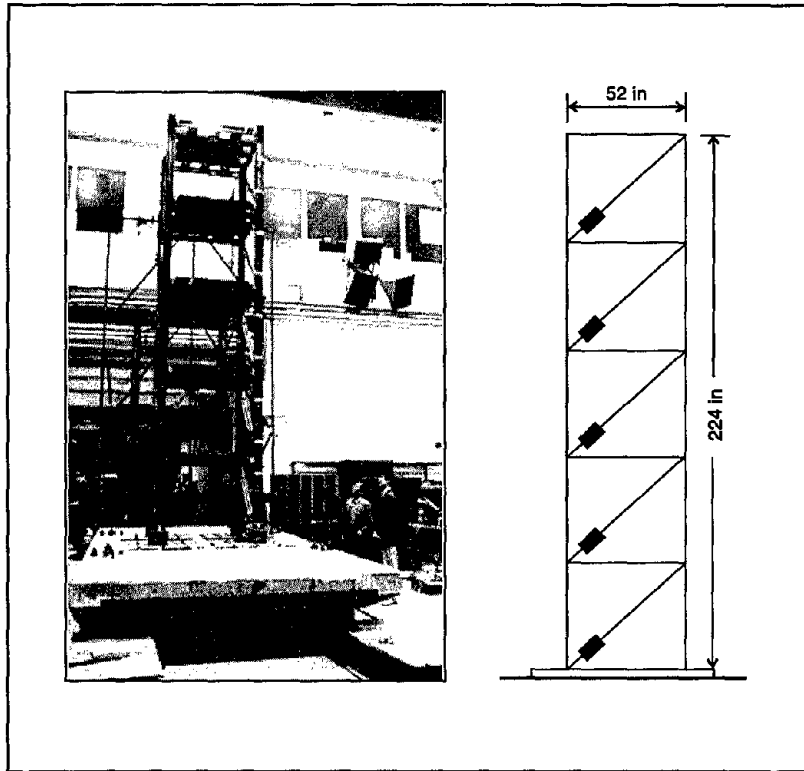
52 in

224 in

Chang et al., 1993a

■ Figure 4.17 The Five-story Test Structure

2/5-Scale Five-story Steel Frame

The test structure in this case is a 2/5-scale five-story steel frame of a prototype structure. Its overall dimensions are 52 in. × 52 in. in plan and 224 in. in height as shown in Figure 4.17 (Chang et al., 1993a). A lumped mass system simulating the dynamic properties of the prototype structure was accomplished by adding steel plates at each floor level. The weight at each floor is 1.27 kips for the first four floors and 1.31 kips for the top floor. All the girder-to-column joints are fully welded as rigid connections. The calculated fundamental frequency of the test structure without added dampers is 3.1 Hz and the first-mode damping ratio used in the analysis program is 1.0% of critical.

A pair of properly designed dampers was diagonally placed on the model structure at each floor as shown in Figure 4.17. The responses of the test structure with and without added VE dampers and with precisely controlled ambient temperatures were stud-

ied experimentally under simulated white noise and earthquakes of varying intensities.

The natural frequency of the viscoelastically damped model structure lies between 3.2 Hz and 3.7 Hz, depending on the ambient temperature. The VE dampers were designed to increase the damping ratio of the model structure to about 15% of critical at room temperature of about 25°C without significantly changing the structure's natural frequency.

As the ambient temperature of VE dampers increases, the VE material becomes softer and their efficiency decreases. Figure 4.18a,b shows the effect of ambient temperature on the structure's

(a) Measured Natural Frequency   (b) Measured Damping Ratio
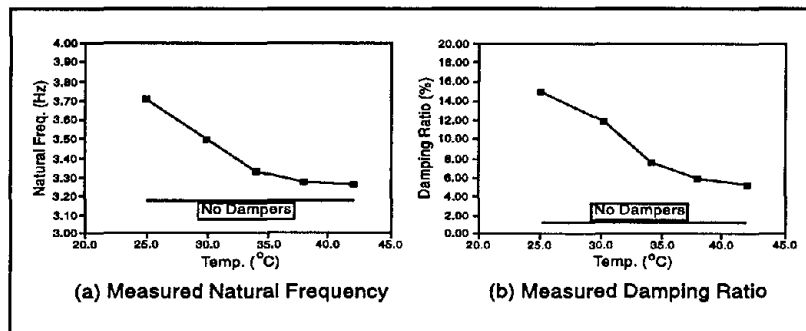
Chang et al., 1993a

■Figure 4.18   Effect of Ambient Temperature on Natural Frequency and Damping Ratio

natural frequency and damping ratio. Table 4.1 summarizes the effectiveness of the VE dampers under various ambient temperatures (Chang et al., 1992). A 0.12 g white noise excitation was used as the input motion for the comparison to eliminate the fluctuation in the input frequencies. Figure 4.19a-c shows displacement time histories at the roof of the model structure without added dampers ($\omega = 3.1$ Hz) and of the model structure with added dampers at ambient temperatures of 25°C ($\omega = 3.6$ Hz) and 42°C ($\omega = 3.26$ Hz), respectively, under 0.12 g Hachinohe earthquake. The damping ratios corresponding to these cases are given in Figure 4.18b. It is seen that, even at 42°C, due to extra damping provided by the VE dampers, the viscoelastically damped structure still achieves a significant reduction in seismic response as compared to the no-damper case. Similar observations can be made on story drifts and floor accelerations at all floor levels. The temperature increase during ground shaking in the VE material in this study was insignificant (below 2° C).

■Table 4.1 Summary of Dynamic Response Reduction Percentage under 0.12g White
Noise Excitation

Maximum Response	Floor Level	No Damper Reference	With Dampers (% Reduction of No-Damper Case)				
			T=25° C	T=30° C	T=34° C	T=38° C	T=42° C
Relative Floor Disp. (in)	5	0.696	81.9	81.3	76.4	70.7	66.7
	4	0.588	83.3	80.1	75.0	69.9	66.7
	3	0.484	84.3	80.8	75.6	71.1	68.6
	2	0.328	83.5	79.6	75.6	71.6	69.5
	1	0.116	76.7	73.3	70.7	65.5	63.8
Interstory Drift (in)	5	0.152	78.3	82.2	78.3	75.0	73.0
	4	0.164	86.0	84.1	78.7	73.2	70.1
	3	0.178	82.0	82.0	74.2	68.5	65.2
	2	0.214	85.0	82.7	77.1	72.4	68.2
	1	0.116	76.7	73.3	70.7	65.5	63.8
Maximum Floor Accel. (g)	5	1.222	85.7	85.1	81.1	77.0	73.9
	4	0.856	82.5	80.5	76.8	72.5	69.4
	3	0.988	86.5	85.2	81.5	78.7	77.8
	2	0.948	84.6	84.7	84.7	80.1	78.4
	1	0.658	74.6	75.2	77.4	75.2	76.4

Chang et al., 1992

Shaking table tests were also carried out on the viscoelastically damped structure at room temperature (25°C) under the time scaled El Centro earthquake with a peak acceleration of 0.6 g (Chang et al., 1995). Numerical studies using an inelastic analysis program DRAIN-2D (Kanaan and Powell, 1973) showed that, without added VE dampers, the model structure would undergo inelastic deformation under this strong ground motion. Therefore, under such severe ground motions, only analytical studies were conducted on the model structure without added dampers. The inelastic analysis results are used to assess the effectiveness of VE dampers under strong earthquake ground motions.

Figure 4.20a,b shows displacement time histories at the roof of the model structure without and with added VE dampers under the 0.6 g El Centro earthquake ground motion. The natural frequencies of the structure without and with added VE dampers are about 3.1 Hz and 3.7 Hz, respectively. It can be seen that VE dampers provide significant extra damping to the structure so that the structure behaved elastically and the seismic response was greatly reduced. Similar observations can be made for story drifts and floor accelerations at all floor levels. The effectiveness of VE

(a) No Damper Added

(b) With Dampers at 25°C

(c) With Dampers at 42°C
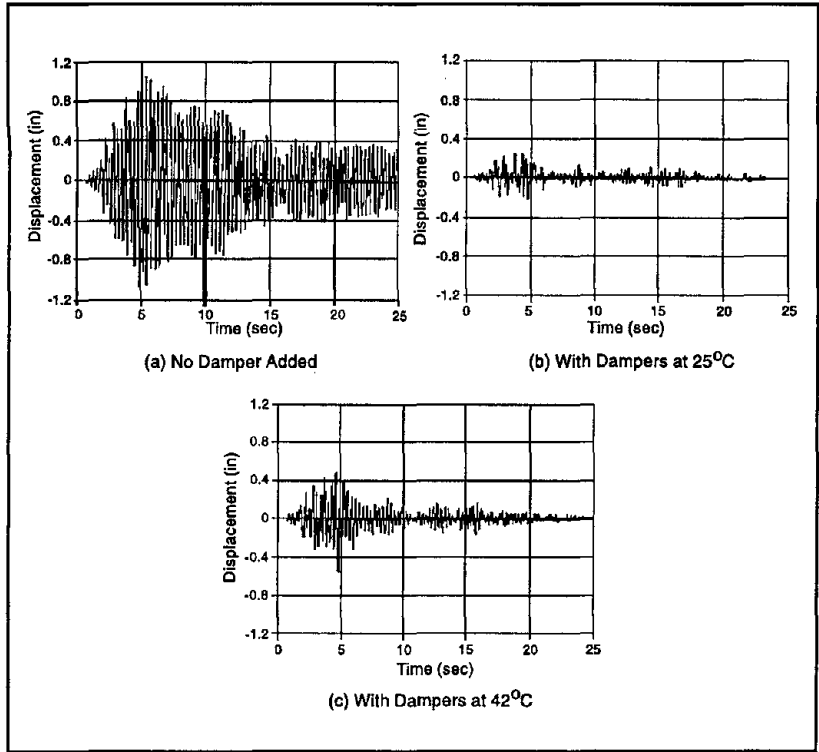
Chang et al., 1992

■ **Figure 4.19 Roof Displacement Time Histories**

(a) Simulated - No Damper

(b) Measured - With Dampers
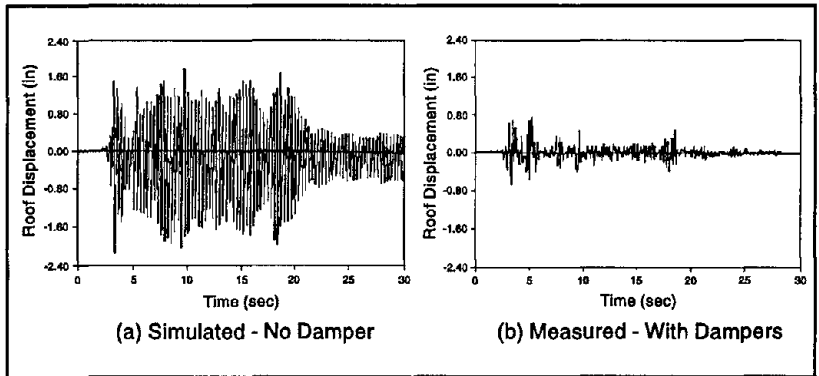
Chang et al., 1992

■ **Figure 4.20 Displacement Time History at Roof**

■ Table 4.2 Summary of Dynamic Response under 0.60g El Centro and Hachinohe
Earthquake Motions

Maximum Response	Floor Level	No Damper (Inelastic Analysis)		With Dampers (% Reduction of No-Damper Case)	
		El Centro (0.60g)	Hachinohe (0.60g)	El Centro (0.60g)	Hachinohe (0.60g)
Relative Floor Disp. (in)	5	2.150	3.490	0.766 (64.4)	0.823 (76.4)
	4	1.990	3.240	0.665 (66.6)	0.719 (77.8)
	3	1.650	2.700	0.529 (67.9)	0.579 (78.6)
	2	1.110	1.630	0.346 (68.8)	0.382 (76.6)
	1	0.390	0.470	0.143 (63.3)	0.148 (68.5)
Interstory Drift (in)	5-4	0.207	0.310	0.104 (49.8)	0.111 (64.2)
	4-3	0.365	0.599	0.137 (62.5)	0.146 (75.6)
	3-2	0.598	1.100	0.187 (68.7)	0.201 (81.7)
	2-1	0.721	1.185	0.214 (70.3)	0.234 (80.3)
	1-0	0.394	0.470	0.143 (63.7)	0.148 (68.5)

Chang et al., 1995

dampers under the scaled 0.6 g El Centro and Hachinohe earthquake ground motions are summarized in Table 4.2.

Figure 4.21a-d shows the envelope curves of the lateral displacement, interstory drift, cumulated story shear, and overturning moment of the model structure with and without added dampers under the 0.6 g El Centro earthquake. It can be seen that adding VE dampers to the structure reduces not only the deformation but also the base shear and overturning moment even when the structure without added dampers behaves inelastically. The VE dampers dissipate a significant amount of seismic input energy to prevent the structure from undergoing inelastic deformation. Similar results were obtained for the 0. 6 g Hachinohe earthquake.

1/3-Scale Three-story Concrete Frame

In this study, the seismic response of a scaled reinforced concrete structure using VE dampers as a means for seismic retrofit was investigated. Unlike steel structures, the seismic response of a reinforced concrete structure is by and large inelastic, which is often accompanied by permanent deformation and damage.
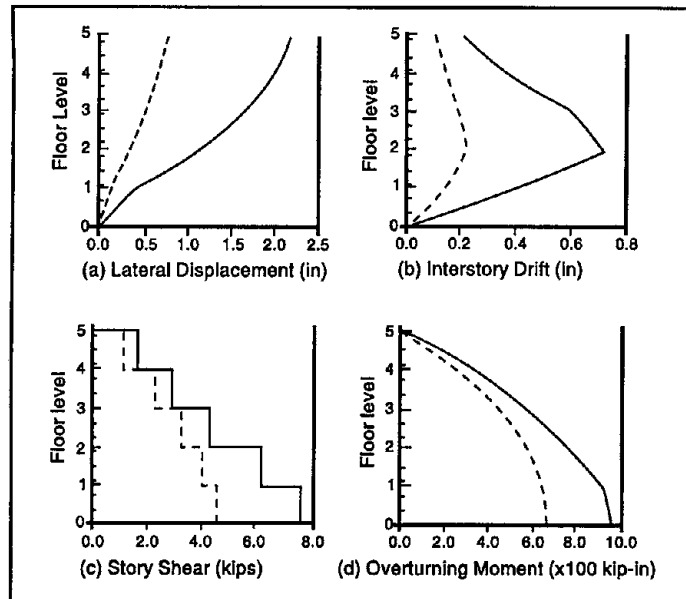
Chang et al., 1995

■ Figure 4.21 Response Envelopes: - - - - - - with Dampers, ——— without Dampers

The addition of viscoelastic dampers in this case can dissipate energy at the early stages of cracking of the concrete elements and reduce the development of damage. With proper selection of dampers, this damage can be substantially reduced or even eliminated. The quantification of the influence of viscous and elastic stiffness properties of dampers during the inelastic response of reinforced concrete structures was the subject of this investigation.

A one-third scale model of a three-story lightly reinforced concrete framed building was tested under simulated base motions using a shaking table (Lobo et al., 1993b; Chang et al., 1994). The structure was tested using a series of simulated ground motions obtained from the scaled 1952 Taft earthquake, N21E component, normalized for peak ground accelerations of 0.05 g, 0.20 g, and 0.30 g, representing minor, moderate, and severe ground motions. The structure, which was previously damaged in shaking table tests, was retrofitted by adding viscoelastic diagonal braces in the interior bay of each frame as shown in Figure 4.22. The viscoelastic dampers were similarly positioned as in the steel frame case. Some selected experimental results under the 0.2 g Taft earthquake are summarized here for one type of dampers tested from the viewpoint of energy dissipation.

(a) Elevation

(b) Viscoelastic Brace Dampers
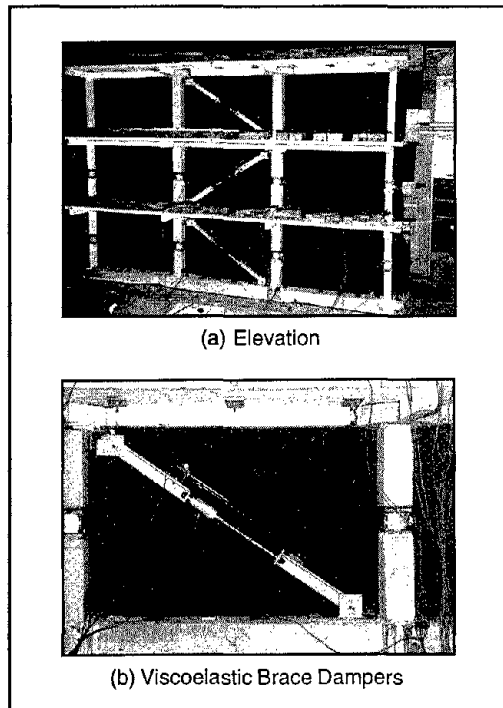
Lobo et al., 1993b

■ **Figure 4.22** Details of the R/C Model with Viscoelastic Braced Dampers

The interstory drifts and story shears in the columns are substantially reduced at all floors as indicated in Table 4.3. While the deformations are reduced approximately three times, the shear forces are reduced only twice. These forces are much smaller than the ultimate strength of the columns; moreover, they are smaller than their yielding strengths. A sample set of force-deformations at the first floor as shown in Figure 4.23 indicates that the column forces and deformations are substantially reduced, while most of the energy dissipation (area of hysteretic loops) is transferred from the columns to the viscoelastic dampers. Although some inelastic deformations are experienced by the columns in the presence of the viscoelastic braces, the column response is substantially improved.

■ **Table 4.3** Maximum Measured Interstory Response for 0.2g Taft Excitation

	Interstory Drifts (in)			Column Story Shears (kips)		
	First	Second	Third	First	Second	Third
Without Dampers	0.656	0.388	0.167	20.63	16.20	10.71
With Dampers	0.194	0.147	0.066	7.68	5.71	4.19

Lobo et al., 1993b
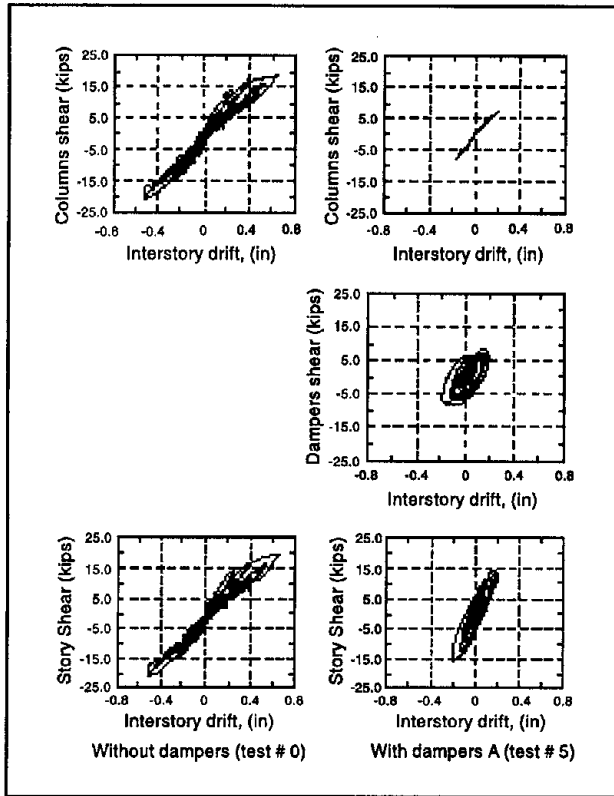
Lobo et al., 1993b

■ Figure 4.23 Force-deformation Curves under 0.2g Taft Earthquake

The VE dampers alter the overall energy balance as shown in Figure 4.24. For the 0.2 g Taft earthquake used in the experiment (Figures 4.24a,b), the total input energy is increased. However, the added VE dampers dissipate a majority of this energy, leaving only a small amount of hysteretic energy to be dissipated by the structural members. Similar energy calculations under some other earthquakes are also shown in Figure 4.24, showing that the overall energy input may vary depending on the match between the structural frequencies and the earthquake frequency content.

This series of experiments reveals that retrofitting reinforced concrete frames using viscoelastic dampers can reduce the overall response, but more importantly, can reduce the risk of developing a damaging mechanism near collapse. In particular, the hysteretic energy dissipation is transferred from the load bearing elements, such as the columns or beams, to non-load bearing devices that are not essentially damaged.
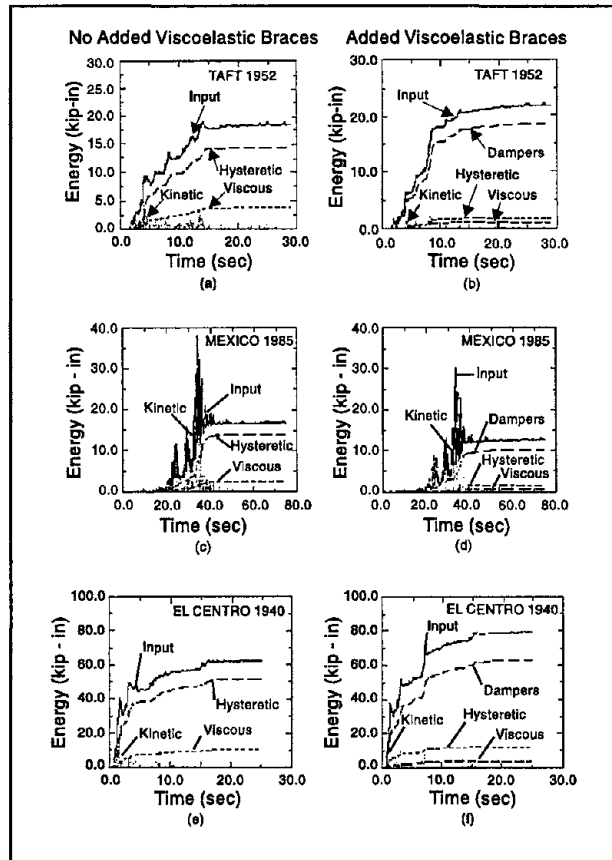
Lobo et al., 1993b

■ Figure 4.24 Contribution of Energy Terms

The analysis of a structure equipped with viscoelastic dampers is significantly simpler than those dealing with metallic or friction dampers. As seen from Eq. (3.12), the force-displacement relationship of a viscoelastic damper is linear in displacement and velocity. Thus, for a single-degree-of-freedom structure oscillating at frequency ω, the term Γx in Eq. (3.40) due to the addition of a viscoelastic damper with shear area A and thickness δ takes the form

$$\Gamma x = \beta \left[k'(\omega) + c'(\omega)\dot{x} \right] \tag{4.2}$$

where k' and c' are defined in Eq. (3.13a,b) and β is the position factor; $\beta = \cos^2\theta$ if the VE damper is installed diagonally at an inclination angle θ with the horizontal. Equation (4.2) strictly

applies only under harmonic motion at frequency ω. However, it represents a reasonable approximation for more general motions within a limited frequency band, provided that k' and c' are nearly constant throughout that band. Thus, unlike metallic or friction dampers, a linear structure with added VE dampers remains linear with the dampers contributing to increased viscous damping as well as lateral stiffness. This feature represents a significant simplification in the analysis of viscoelastically damped structures (Zhang et al., 1989; Zhang and Soong, 1992).

The extension of this analysis procedure to multi-degree-of-freedom structural systems is straightforward if proportional damping is assumed. The equations of motion for the modal displacements are decoupled in this case, and modifications to the modal damping and stiffness due to addition of VE dampers can be obtained by following the modal strain energy method (Soong and Lai, 1991). The ith modal damping ratio due to added VE dampers can be calculated as

$$\bar{\zeta}_i = \frac{\eta(\omega_i)}{2} \frac{E_v}{E_i} \tag{4.3}$$

where $\eta(\omega_i)$ is the loss factor of the VE material at modal frequency ω_i of the original structure, E_i is the ith modal strain energy of the system with dampers and E_v is the energy stored in the viscoelastic dampers. These energies are calculated from

$$E_v = \phi_i^T \bar{\bar{K}} \phi_i, \quad E_i = \phi_i^T (K + \bar{K}) \phi_i \tag{4.4}$$

where ϕ_i is the ith mode shape vector associated with ω_i, K is the original stiffness matrix without added dampers, and $\bar{K}$ is the stiffness matrix attributed to the added dampers. Eq. (4.3) can be written as

$$\bar{\zeta}_i = \frac{\eta(\omega_i)}{2} \left[\frac{\phi_i^T \bar{\bar{K}} \phi_i}{\phi_i^T (K + \bar{K}) \phi_i} \right] \tag{4.5a}$$

$$= \frac{\eta(\omega_i)}{2} \left[1 - \frac{\phi_i^T \bar{K} \phi_i}{\phi_i^T (K + \bar{K}) \phi_i} \right] \tag{4.5b}$$

The modified *i*th modal frequency is

$$\overline{\omega}_i = \left[\frac{\phi_i^T (\mathbf{K} + \overline{\mathbf{K}}) \phi_i}{\phi_i^T \mathbf{M} \phi_i} \right]^{1/2} \tag{4.6}$$

where **M** is the mass matrix of the structure.

If the change of the mode shapes due to added dampers can be neglected, Eq. (4.5) can be further simplified to (Chang et al., 1993a)

$$\overline{\zeta}_i = \frac{\eta(\omega_i)}{2} \left(1 - \frac{\omega_i^2}{\overline{\omega}_i^2} \right) \tag{4.7}$$

where ω_i is the *i*th modal frequency corresponding to the original structure.

4.4

VISCOELASTIC FLUID DAMPERS

    Damping devices based on the operating principle of high velocity fluid flow through orifices have found numerous applications in the shock and vibration isolation of aerospace and defense systems. These previous uses include the attenuation of weapons grade shock, including airburst, water surface, and underwater detonations; with applications including individual weapons or electronic systems, ship decks, and command, control and communications equipment for all branches of the military. Other previous aerospace/defense uses include the attenuation of aircraft, spacecraft and ship vibration, plus wind and airblast isolation on large rocket launch gantries, such as the Space Shuttle.

    In recent years, research and development of viscoelastic fluid dampers for seismic applications to civil engineering structures have been performed to accomplish three major objectives. The first was to demonstrate by analysis and experiment that fluid dampers can improve the seismic capacity of a structure by reducing damage and displacements and without increasing stresses.

The second was to develop mathematical models for these devices and demonstrate how these models can be incorporated in existing structural engineering software codes. Finally, the third was to evaluate the reliability and environmental stability of the dampers for structural engineering applications.

The approach used to adapt orificed viscoelastic fluid dampers for hazard mitigation applications began with computer simulations of structures incorporating this technology to establish parametric baselines for a series of experiments. Experiments were performed at the component level to verify proper performance. Shake table tests were then performed with steel moment frames (Constantinou and Symans, 1992, 1993) with a reinforced concrete building model (Reinhorn et al., 1995), and with an isolated bridge model (Tsopelas, et al., 1994). Mathematical models were then developed to analytically predict the observed response and to assist in the interpretation of the experimental results.

The construction of the orificed fluid dampers used in the experimental studies mentioned above is shown in Figure 3.16c. It consists of a stainless steel piston with bronze orifice head and an accumulator. It is filled with silicon oil. The piston head utilizes specially shaped passages which alter the flow characteristics with fluid speed so that the force output is proportional to $|\dot{u}|^{\alpha}$, where $\dot{u}$ is the piston rod velocity and α is a predetermined coefficient in the range of 0.5 to 2. A design with $\alpha = 1$ results in a linear viscous damper.

This behavior dominates for frequencies of motion below a predetermined cutoff frequency (related to the characteristics of the accumulator valves). Beyond this frequency, the fluid dampers exhibit strong stiffness in addition to substantial ability to dissipate energy. The existence of the cutoff frequency is sometimes desirable, since the lower modes of vibration are only damped while the higher ones are both damped and stiffened so that their contribution is completely suppressed.

The orifice flow may be compensated by a passive bi-metallic thermostat which allows operation of the device over a temperature range of -40°C to 70°C. The performance characteristics of the device are considered state-of-the-art. The described device with fluidic control orifices, bi-metallic thermostat and special silicon oil originated within products used in classified appli-

cations of the U.S. Air Force. Over 30,000 of these devices are currently in service in the United States.

The fluid dampers tested initially had all of the aforementioned characteristics and they were designed to behave as linear viscous dampers. Each had stroke of ±51 mm, length of 280 mm and weighed 20 N. They were used in the tested building model described in the sequel and a bridge model.

Figure 3.19 shows recorded loops of force vs. displacement of one damper at a temperature of 23°C. The purely viscous nature of the device is apparent. For frequencies above about 4 Hz, the damper exhibited stiffness. Figure 4.25 shows recorded data on the peak output force vs. peak velocity of input at temperatures of 0°, 25°, and 50°C. It may seem that the experimental results may be fitted with straight lines of slope C_o which represents the damping constant. The behavior of the device was completely unaffected by the amplitude of motion. The values of C_o in Figure 4.25 demonstrate the small dependency of the characteristics of the device on temperature.
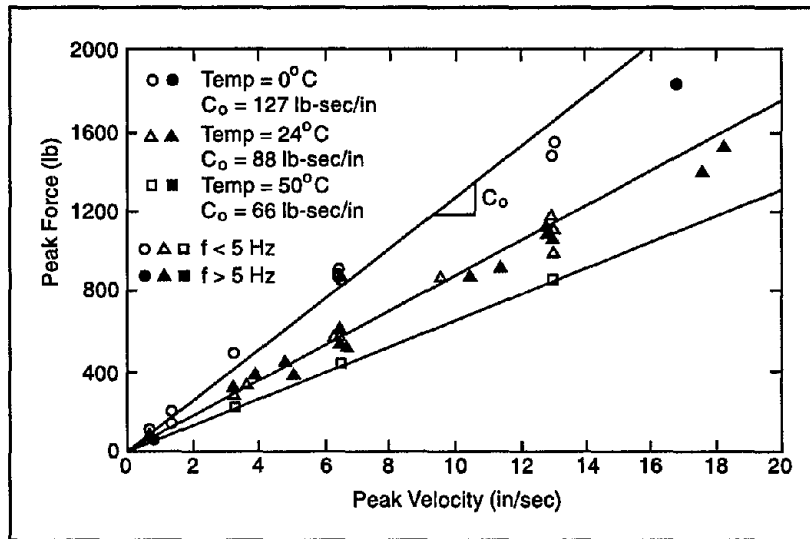
Constantinou and Symans, 1992, 1993

■ Figure 4.25 Peak Force vs. Peak Velocity at Various Temperatures

CHAPTER 4
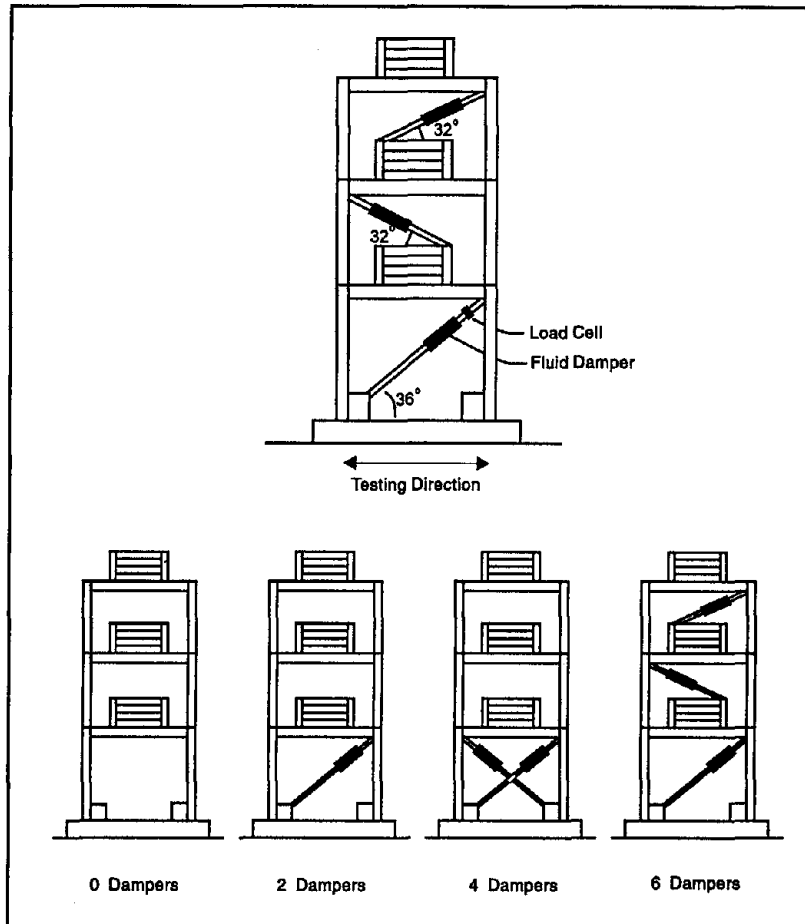
Constantinou and Symans, 1992, 1993

■ **Figure 4.26 Damper Configurations for Three-story Structure**

A series of earthquake simulation tests using five different earthquake records were performed on a three-story 1:4 scale steel frame model as shown in Figure 4.26 (Constantinou and Symans, 1992,1993). The total weight of the three-story model was 6300 lbs, equally distributed to each floor. The dampers were placed at the first story for the two- and four-damper cases and at all three stories for the six-damper case (see Figure 4.26). The dynamic characteristics of the structure were determined in small vibration amplitude tests and are listed in Table 4.4. As discussed earlier, the addition of fluid dampers had a primary effect of increasing damping while stiffening the higher modes.

■ Table 4.4 Properties of Three-story Structure

Frequency and Damping Ratio	Mode 1	Mode 2	Mode 3
No Dampers	2.00 Hz 0.017	6.60 Hz 0.008	12.20 Hz 0.003
2 Dampers	2.03 Hz 0.009	6.88 Hz 0.147	12.34 Hz 0.050
4 Dampers	2.11 Hz 0.177	7.52 Hz 0.319	12.16 Hz 0.113
6 Dampers	2.03 Hz 0.194	7.64 Hz 0.447	16.99 Hz 0.380

Constantinou and Symans, 1992, 1993

A comparison of responses of the structure without and with fluid dampers is presented in Figure 4.27 where the earthquake acceleration record was scaled by the percentage figures shown. The addition of fluid dampers resulted in overall significant reduction of accelerations, story shear forces and interstory drifts. Furthermore, the concentration of the fluid dampers at one
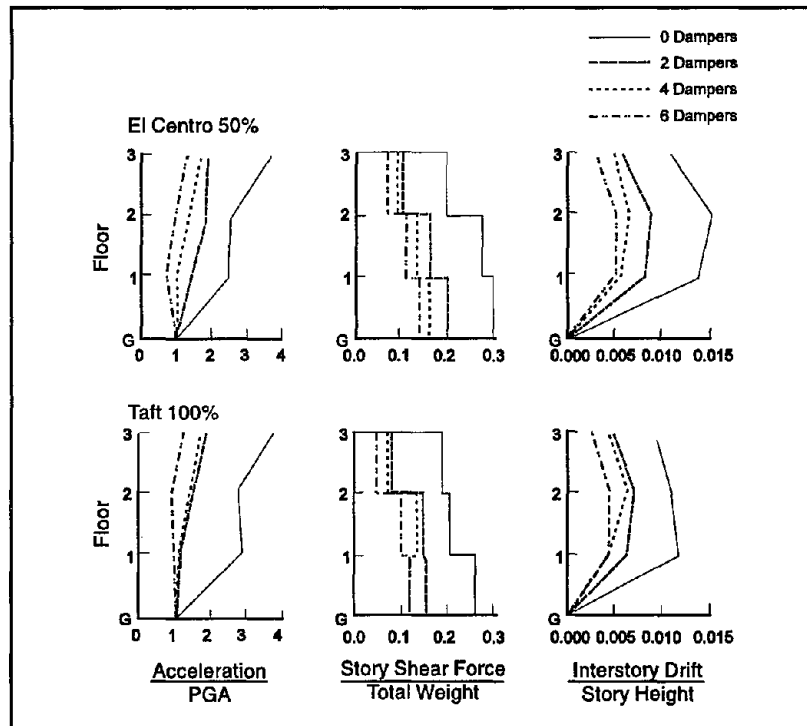
Constantinou and Symans, 1992, 1993

■ Figure 4.27 Acceleration, Story Shear and Interstory Drift Profiles of 3-story Structure

level did not have any adverse effect. A different comparison of responses is presented in Figure 4.28, which presents profiles of response of the structure without and with dampers at two different levels of the same earthquake. Evidently, the responses of the

Acceleration (g's)   Story Shear Force / Total Weight   Interstory Drift / Story Height

————— 0 Dampers, El Centro 33%
– – – – 6 Dampers, El Centro 100%
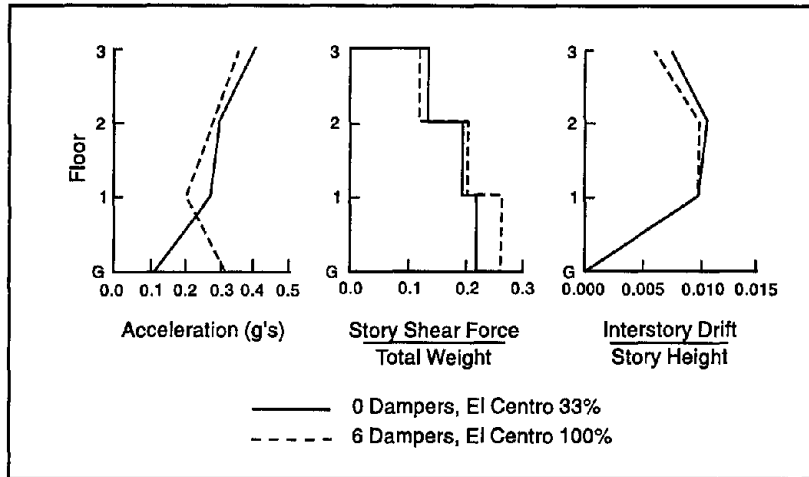
Constantinou and Symans, 1992, 1993

■ Figure 4.28 Comparison of Response Profiles for Two Different Levels of the Same Earthquake

3 - Story, 6 Dampers, Taft 300%
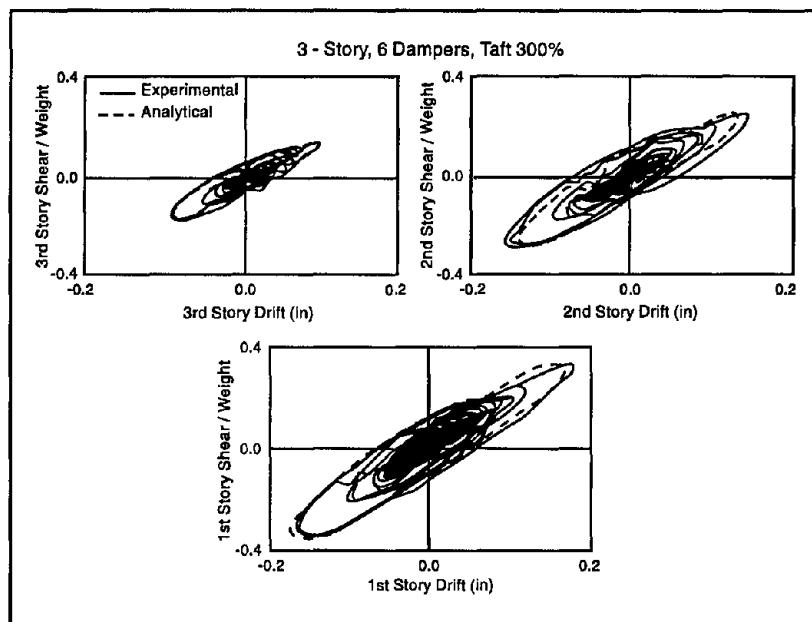
Constantinou and Symans, 1992, 1993

■ Figure 4.29 Comparison of Experimental and Analytical Results

two systems (in terms of acceleration, story shear force, and interstory drift) are approximately the same for two significantly different levels of the same earthquake which differ by a factor of three. Figure 4.29 compares experimental results with analytical results from time history dynamic analysis wherein the Maxwell model was used to define the damper behavior, showing good agreement.

Shaking table tests were also done using the 1/3-scale three-story concrete frame as described in Section 4.3 with fluid viscous dampers also positioned as diagonal braces (Reinhorn et al., 1995). Typical time-history responses under the El Centro earthquake scaled to 0.3 g are shown in Figures 4.30 and 4.31. It is seen that while the total displacements are reduced at all floors, the peak story absolute accelerations are not reduced; moreover, they are increased at the top floor. However, while the total base
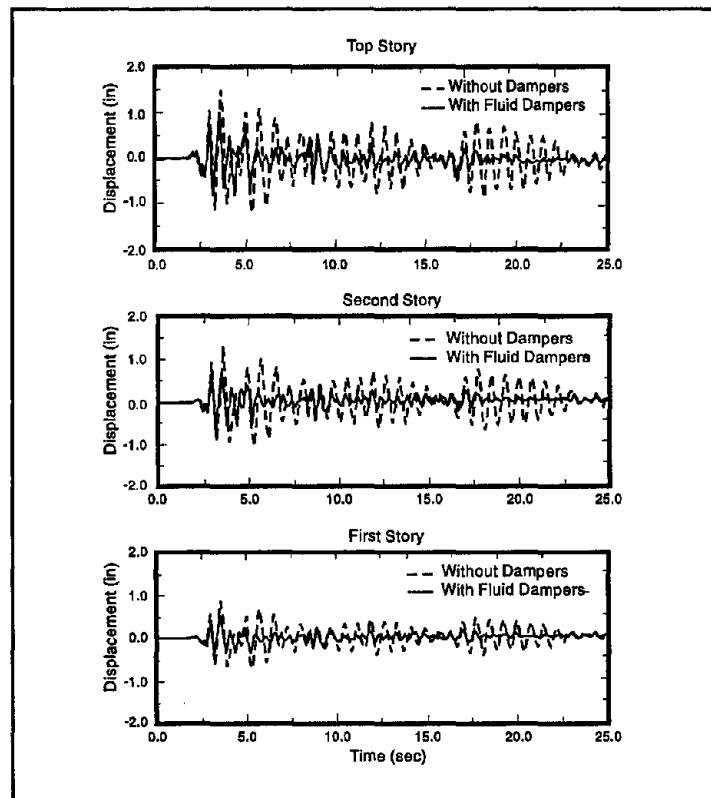
Reinhorn et al., 1995
■ Figure 4.30 Displacement Response Histories

Top Story

Second Story

First Story

Time (sec)
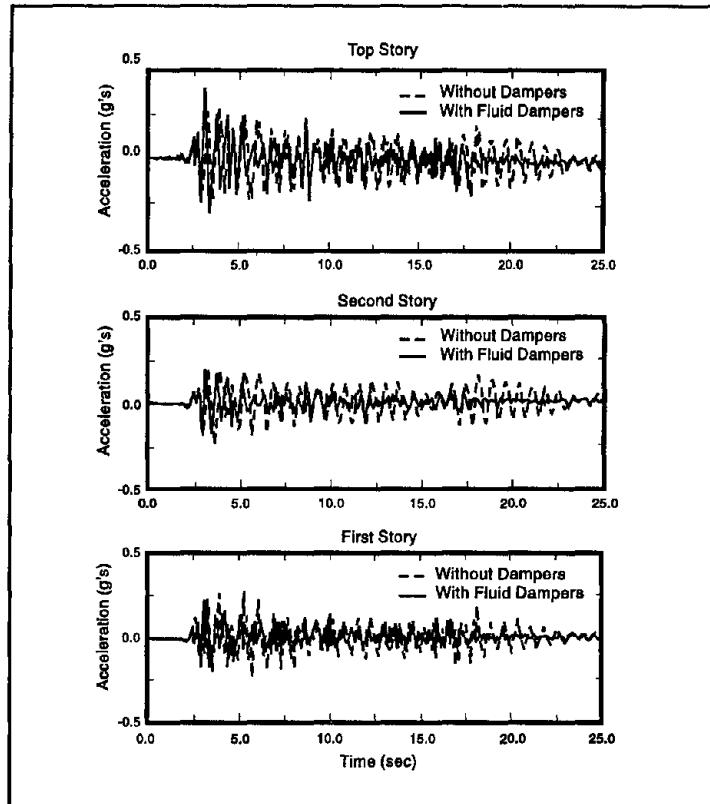
Reinhorn et al., 1995

■ Figure 4.31 Acceleration Response Histories

shear is increased, the maximum column shear force is somewhat reduced. The forces in the structural components are shown in Figure 4.32. The columns develop a maximum shear of only 14.0 kips with dampers, vs. 19.0 kips without dampers. The story drift is reduced from 1.45% to 0.83%. The total energy balance obtained from experimental data is displayed in Figure 4.33. While the total energy input is increased due to damping of the structure, the internal energy is redistributed such that 80% to 90% is taken by the supplemental dampers and dissipated, while hysteretic energy dissipation demand is reduced by 85% to 95% in the presence of dampers. These results are consistent with those predicted based upon time-history analyses employing the Maxwell damper model.
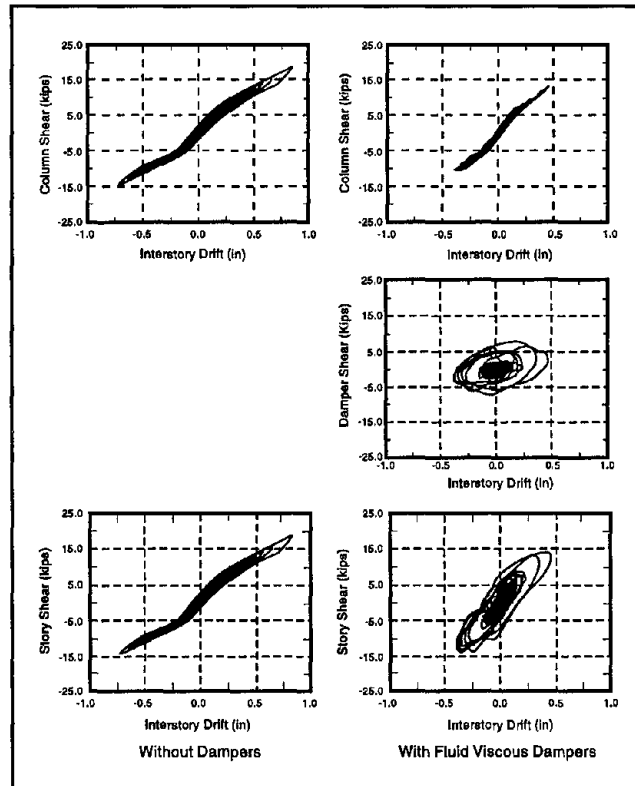
Reinhorn et al., 1995

■ Figure 4.32 Comparison of Forces in Structural Components at First Floor

A number of mathematical models were introduced in Section 3.2.2 to describe the force-displacement response of fluid dampers with different levels of accuracy and sophistication. The simplest case, of course, corresponds to the linear viscous model defined in Eq. (3.20). When this approximation is valid, the analysis of a structure incorporating orificed fluid dampers simplifies greatly. Of course, this is of significant benefit, since most of the general purpose structural analysis computer codes (e.g., SAP, DRAIN, ABAQUS, ADINA) already include all of the required capabilities. For analyses in which the primary structure remains elastic and the dampers are reasonably well distributed throughout the super-structure, the modal superposition methods discussed in Section 3.5.2 become attractive. Otherwise, the direct time domain approach of Section 3.5.3 can be employed. The time domain methods are also appropriate for the nonlinear models defined in Eq. (3.25) for preloaded fluid dampers.

Without Fluid Dampers

With Fluid Dampers

ELCENTRO
PGA: 0.3g

ELCENTRO
PGA: 0.3g

(a)

(b)

TAFT
PGA: 0.2g

TAFT
PGA: 0.2g

(c)

(d)
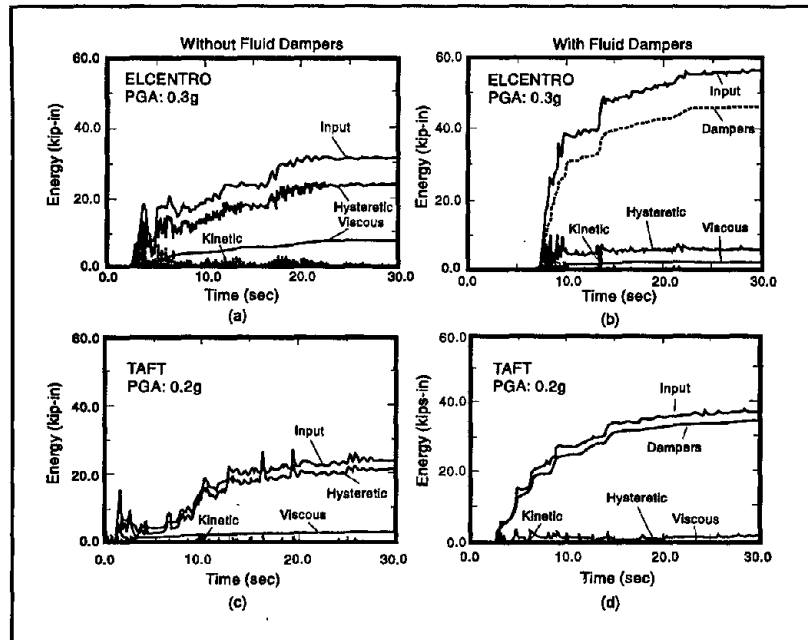
Reinhorn et al., 1995

■ Figure 4.33 Energy Distribution in Structure With and Without Fluid Viscous Dampers

4.5

TUNED MASS DAMPERS

The success of tuned mass dampers (TMDs) in reducing wind-excited structural vibrations is now well established. Recently, numerical and experimental studies have been carried out to examine the effectiveness of TMDs in reducing seismic response of structures. It is noted that a TMD can only be tuned to a single structural frequency. When the first mode of a multi-degree-of-freedom structure dominates the structural response, a TMD incorporated into such a structure is expected to be effective. Wirsching and Campbell (1974) investigated the minimum first-mode response as well as optimum absorber parameters for one-story, five-story and ten-story elastic structures. Results show that dimensionless response ratio σ_{yN} / σ_o, the ratio of root-mean-square (RMS) top-floor displacement with and without TMD, increases little as the number of stories increases. The optimum TMD stiffness becomes less sensitive to structural damping and mass

ratio when the number of stories increases and the optimum TMD damping is insensitive to structural damping even for one-story buildings. In their findings, mass ratio was defined as the ratio of the added mass to story mass of a uniform building. If this mass ratio is defined as the modal mass ratio, the above conclusions become even more obvious, i.e., all the previously discussed parameters are practically independent of the number of stories. This confirms the effectiveness of TMD in reducing the first-mode response of multi-story elastic structures and does not preclude the use of TMD design when the structural damping cannot be identified accurately. The optimum RMS response (σ_{yN} / σ_o) of the structure under random excitation at the base and the corresponding relative displacement RMS (σ_z / σ_o) of TMD for various structural damping ratios are shown in Figure 4.34 from which one can observe that σ_{yN} / σ_o decreases little but σ_z / σ_o decreases substantially as mass ratio μ increases within a practical range. Additionally, σ_{yN} / σ_o and σ_z / σ_o both increase as structural damping increases.
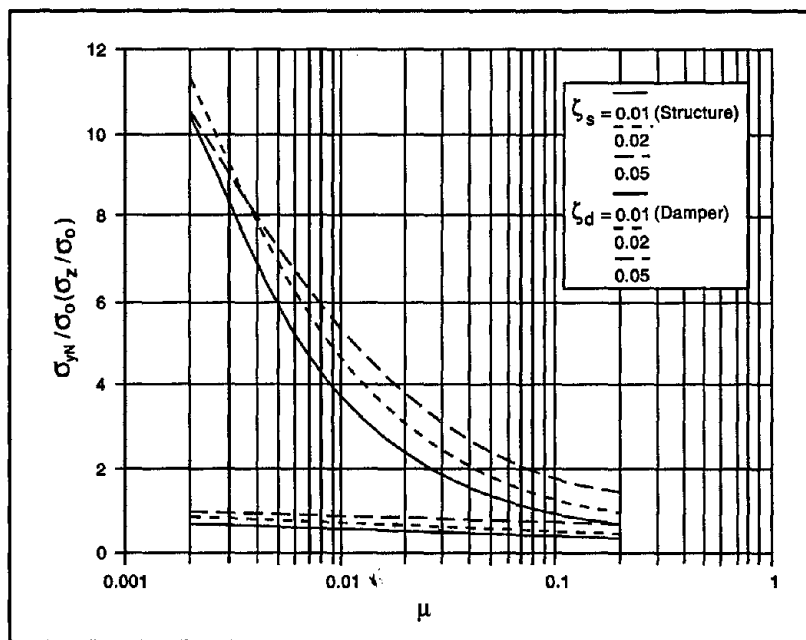
Wirsching and Campbell, 1974

■ Figure 4.34 σ_{yN} / σ_o and σ_z / σ_o as Functions of μ

While the first-mode response of a structure with TMD is proved to be substantially reduced, the higher mode response may in fact increase as the number of stories increases. For earthquake-type excitations, it has been demonstrated that, for shear structures up to 12 floors, the first mode response contributes more than 80% to the total motion (Wirsching and Yao, 1970). However, for a taller building on a firm ground, higher modal response may be a problem which needs further study. An attempt has been made by Chowdhury et al., (1987) to evaluate the higher-mode effect on TMD efficiency. A 25-story shear-flexure uniform building was considered for a sensitivity study of peak response ratio at the top-floor to the modal frequency ratio with and without dampers. It was demonstrated that the higher-mode response ratio may be greater than unity while the first-mode response is always less than unity around the tuning frequency. Unfortunately, since optimal damper parameters were not used, it is difficult to draw conclusions regarding the applicability of TMDs to control seismic response of structures.

In Villaverde (1994), three different structures were studied; the first is a two-dimensional ten-story shear building, the second a three-dimensional one-story frame building and the third a three-dimensional cable-stayed bridge, by using nine different kinds of real earthquake records. Numerical and experimental results show that the effectiveness of TMDs on reducing the response of the same structure under different earthquakes or of different structures under the same earthquake is significantly different; some cases give good performance and some have little or even no effect. It implies that there is a dependency of the attained reduction in response on the characteristics of the ground motion that excites the structure. This response reduction is large for resonant ground motions and diminishes as the dominant frequency of the ground motion gets further away from the structure's natural frequency to which the TMD is tuned.

For earthquake resistant design, a structure is permitted to experience inelastic deformation under strong earthquakes. Attempts to reduce structural response in this case using TMDs were made by a few investigators. When the structure experiences elastoplastic deformations, the 'frequency' of the system decreases so that the TMD may lose part of its effectiveness due to detuning effect.

In Kaynia et al., (1981), two quantities were introduced to measure the effectiveness of TMD in the case of inelastic structures, i.e., the ratio between cumulative yielding ductility in a 2-DOF and in a SDOF system and the ratio between the associated ductility ratios. The latter is actually the same as the peak response ratio.

The parameters of the SDOF elastic-perfectly plastic system consist of mass M, frequency of small-amplitude response ω_s, damping ratio ζ_s, and yielding displacement y_c; whereas the mass damper is identified as before by parameters μ, α and ζ_a For several combinations of ω_s and y_c, the sensitivity of cumulative yielding ductility ratio and ductility ratio to dimensionless damper parameters was investigated by using a set of historical earthquakes. The preliminary study showed that these two ratios have a weak dependence on the aforementioned parameters similar to that of peak response ratio in an elastic structure.

In order to overcome the frequency-related limitations of TMDs for seismic applications, more than one TMD in a given structure, each tuned to a different dominant frequency, can be used. The concept of multiple tuned mass dampers (MTMDs) together with an optimization procedure was proposed by Clark (1988). Since then, a number of studies have been conducted on the behavior of MTMDs connected in parallel to the main system (Xu and Igusa, 1992; Yamaguchi and Harnpornchai, 1993). Recently, a doubly-tuned mass damper (DTMD), consisting of two masses connected in series to the structure was proposed (Setareh, 1994). In this case, two different loading conditions were considered: harmonic excitation and zero-mean white-noise random excitation, and the efficiency of DTMDs on response reduction was evaluated. Analytical results show that DTMDs are more efficient than the conventional single mass TMDs over the whole range of total mass ratios, but are only slightly more efficient than TMDs over the practical range of mass ratios (0.01-0.05).

A nonlinear TMD may also improve the performance under earthquake excitations. Roberson (1952) considered the dynamic response of a structural system supporting a dynamic absorber with a linear plus cubic spring without damping. The suppression band in the nonlinear case was found to be wider than that in the linear case, indicating that the linear plus cubic spring absorber would suppress structural response excited by a wider

range of frequency components. This is superior to the conventional linear TMD in reducing the system response under excitations such as those due to earthquakes. However, the performance of a nonlinear TMD attached to a complex structure in which a few modes are activated needs to be further demonstrated before it can be applied in practice. Another alternative solution might be the use of an impact vibration absorber. This is defined as a system that has the added mass supported by neither a spring nor a damper but constrained to move unidirectionally in a container attached to the structural system. Its movement is limited by the bounds of the container. The vibration amplitude of the structural system is reduced by the momentum transfer between the structure and the added mass and by the conversion of mechanical energy into noise and heat. It was reported by Hunt (1979) that the maximum reduction in dynamic response can be achieved at all excitation frequencies as the impact vibration absorber is synchronized to the excitation frequency. The adverse impact of the damper on the acceleration response of a structural system, however, should be noted due to impulsive impacts.

Another promising approach to reducing the seismic response of a structural system is the application of a semi-active control concept, which will be discussed in more detail in Chapter 7. This will retain the benefits of an optimized active system but not pay the power and system complexity penalties associated with it (Hrovat et al., 1983). For a simple structure subjected to a periodic force consisting of four harmonic components, Hrovat et al., (1983) reported that the performance of a semi-active TMD was found to be similar to a fully active device. This device significantly reduced the RMS values of building displacement and acceleration as well as TMD stroke.

A hybrid mass damper or a TMD with active capability is another option to reduce the vibration induced by wind and earthquakes. In fact, these types of systems have been implemented in a number of tall buildings in recent years (Soong et al., 1994). Some examples of these hybrid systems are given in Chapter 7.

T U N E D   L I Q U I D   D A M P E R S

Similar in concept to a TMD, the tuned liquid damper (TLD) and tuned liquid column damper (TLCD) impart indirect damping to the system and thus improve structural performance (Kareem, 1990). A TLD absorbs structural energy by means of viscous actions of the fluid and wave breaking. In a TLCD, energy is dissipated by the passage of liquid through an orifice with inherent head loss characteristics. The performance of a single-degree-of-freedom structure with a TLD subjected to sinusoidal excitations was investigated by Sun (1991), along with its application to the suppression of wind-induced vibration by Wakahara et al., (1989). As a result of these and other studies, TLD has found practical applications in the area of structural control of wind-induced vibrations.

Fujino et al., (1988) and Welt and Modi (1989 a,b) were among the first to suggest the usage in buildings of a TLD to reduce overall response during strong wind or earthquakes. The behavior of rectangular or circular containers partially filled with water was studied by Fujino et al., (1988). The container studied by Welt and Modi (1989a,b) is geometrically the same as a nutation damper. Other types of tuned liquid dampers, not using liquid sloshing, have also been proposed. The simplest of them, known as tuned liquid column damper as mentioned earlier (Xu, et al., 1992a,b), consists of a tube filled with water. The fundamental frequency in this system is dependent only on the length of column of water, while the dissipation term, due to presence of the orifices, is nonlinear and depends on the coefficient of head loss. Another variety, similar to the tuned liquid column damper, has been proposed (Nakamura, et al., 1988), in which the dissipation is not attained through the presence of orifices, but rather by creating a nonlinearity with a gap between a mass and the damper unit itself.

Due to simplifications adopted by most of the investigators in describing motion of the fluid, experiments were in general performed to test the validity of these assumptions. Overall good agreement with the theory was found when the amplitude of os-

cillations was small. Welt and Modi (1989b) performed a series of experiments on partially filled torus shaped dampers. The results show that the damping ratio is very sensitive to the frequency ratio, with a maximum at about 1.0, where a reversal in sign of the added mass is observed. For an increase in the amplitude of oscillation, a decrease in damping is experienced. Modi and Welt (1987) tested structural models with the torus shaped damper in a wind tunnel. Using laminar and turbulent flows, several models with square or circular cross section were subjected to vortex induced resonance and galloping instability. The experiments showed a reduction of the induced oscillations in the models. Fujino et al., (1988) tested cylindrical shaped containers on a steel platform to simulate a flexible tower or a building. For this study, prototype size dampers were used, avoiding the need to satisfy similarity conditions. Results show that, for small amplitude oscillations, the added damping is highly dependent on the ratio of structure to sloshing frequencies, with maximum at a ratio of about one. For larger amplitudes, the additional damping in the system is reduced, and almost constant for any frequency ratios.

Later, Sun et al., (1989) performed shaking table tests on rectangular TLDs to verify the accuracy of the simplified theory developed. Additional experiments were carried out by Chaiseri et al., (1989) of a rectangular container on a single-degree-of-freedom platform. The first part of the experiment consisted of applying a harmonic force of constant amplitude, at the natural frequency of the platform, with varying water depths. The test showed that the minimum response corresponds to the tuned case. The second phase of the experiment was conducted by varying the excitation frequency. Similar results were obtained for a forward and backward sweep of frequency, which indicates that initial conditions on the structural response and waves are not significant.

As discussed earlier, tuned liquid dampers operate on the same basic principles as tuned mass dampers. However, some of the drawbacks of TMD systems are not present in TLDs. Due to the simple physical concepts on which the restoring force is provided in TLDs, no activation mechanism is required. Therefore, maintenance cost is minimized. The mechanism activating a TMD

must be set to a certain threshold level of excitation, while TLD systems are at all times active, avoiding problems due to an inadequate activation system.

Although the mathematical theory involved in accurately describing motion of a fluid in the container may be quite complicated, the hardware requirements are simple enough that minimum installation is required. The damper, in general, consists of a polypropylene tank, that may be commercially available, with several shallow layers of water. Maintenance of the system is practically nonexistent. Due to simplicity of installation, they may be used in existing buildings, even for temporary use if desired.

Due to the nature of the system, a small error may be expected when measuring the still water level, the parameter that controls the value of the fundamental sloshing frequency. Yet, another important advantage over TMD is that, for large amplitudes of oscillation, the system is not very sensitive to the actual frequency ratio between primary and secondary systems. Note that for small amplitudes of oscillation, proper tuning of the system may considerably influence the response. Therefore, the induced error due to measuring of the water height will not significantly modify the response during strong vibrations.

For structures with different fundamental frequencies in the two major directions, tuning may be accomplished by using rectangular tanks. With an adequate selection of the plan dimensions of the tank, both fundamental frequencies may be tuned. However, care should be taken in this situation since the theory was developed for tanks subjected only to a unidirectional excitation. For structures with the same fundamental frequencies in the principal directions, a circular tank may be used.

4.7

PHASE TRANSFORMATION DAMPERS

A brief mention was made in Section 3.3.3 of shape memory alloys (SMA), which have been considered for structural applications as a passive energy dissipation device. While no actual structural applications have taken place, some recent development in this area is briefly described below.

Shape memory alloys are one type of smart materials which have been studied recently in the context of civil engineering structural control. These smart materials can be incorporated into structural members or system components as embedded sensors and actuation elements, capable of modifying structural behavior in response to external stimuli. The existence of shape memory properties in certain alloys has been known since 1932 when it was first observed in a Gold-Cadmium (AuCd) alloy exhibiting a "rubberlike" behavior (Ölander, 1932). The shape memory effect (SME) of an alloy is generally referred to its ability to undergo reversible and diffusionless transformation between two crystalline phases known as austenite, the high-temperature phase of the alloy, and martensite, the low-temperature crystalline phase. This micromechanical transition process is illustrated in Figure 3.28 when the shape memory alloy (SMA) is cyclically loaded. Some promising characteristics of the martensitic and superelastic modes of SMA behavior include high stiffness for small strain levels (elastic loading), reduced stiffness for intermediate levels of strain (due to formation and/or reorientation of martensite), and high stiffness at large levels of strain (elastic loading of martensite). Also, since the superelastic state ideally displays a hysteretic effect with zero residual strain, an energy absorbing device made from this material would theoretically provide a self-centering mechanism. Other attractive properties associated with SMAs include their insensitivity to environmental temperature changes when properly heat treated, and their excellent fatigue and corrosion resistance properties.

Some analyses and small-scale experiments have been carried out with respect to the application of shape memory alloys to civil engineering structural control. In Aiken et al., (1992), the possible use of Nitinol as a passive energy dissipation device for structures was studied experimentally by incorporating small loops of Nitinol wire into diagonal braces in a three-story model structure. The structural model was six feet in height and weighed 3,000 lb. The results of the testing included two types of behavior of special interest: large strain behavior and cyclic superelastic behavior. Figure 4.35 shows the large strain behavior of Nitinol, which has three distinct phases. Initially, the material was stiff and elastic, then at 2% strain the crystalline structure changed. Here the Nitinol became softer while remaining elastic, which

corresponds to the nearly horizontal region of the hysteresis loop. This plateau continued until 6% strain was reached, then as the deformation continued, the additional deformation caused dislocation and permanent deformation in the crystalline structure, causing an increase in the stiffness. The advantage of this behavior is that, for low levels of seismic excitation, the structure behaves elastically; for moderate earthquakes, the Nitinol will dissipate large amounts of energy while remaining elastic and, for large earthquakes, the structure will stiffen and again dissipate large amounts of energy.
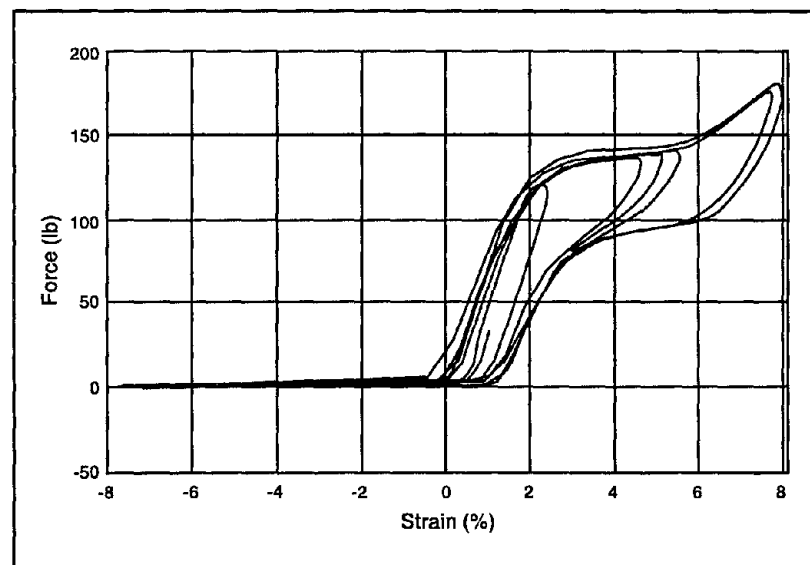
Aiken et al., 1992

■ Figure 4.35 Large Strain Behavior of Nitinol

Figure 4.36 shows the behavior that can be achieved during a moderate earthquake. The Nitinol wire loops were preloaded so that the hysteretic behavior was confined to the flat region of the hysteretic curve. During cyclic stretching and relaxation in the diagonal braces, the increase in the tensile force caused a change in the crystalline structure of the Nitinol and, when the tensile force decreased, the Nitinol reverted to its original crystalline structure. This cyclical change in crystalline structure dissipated a substantial amount of earthquake input energy. Significantly, the Nitinol did not sustain any dislocations in its crystal-

line structure to dissipate this energy and thus a Nitinol energy dissipator could perform in this controlled elastic manner for a large number of seismic cycles. This behavior is in contrast to that of normal metals which must be permanently deformed to dissipate large amounts of energy. It is also noted that this superelastic material is capable of sustaining strains in the range of 5% to 7%, while normal steels can only sustain strains of less than 0.2% without permanent deformation.
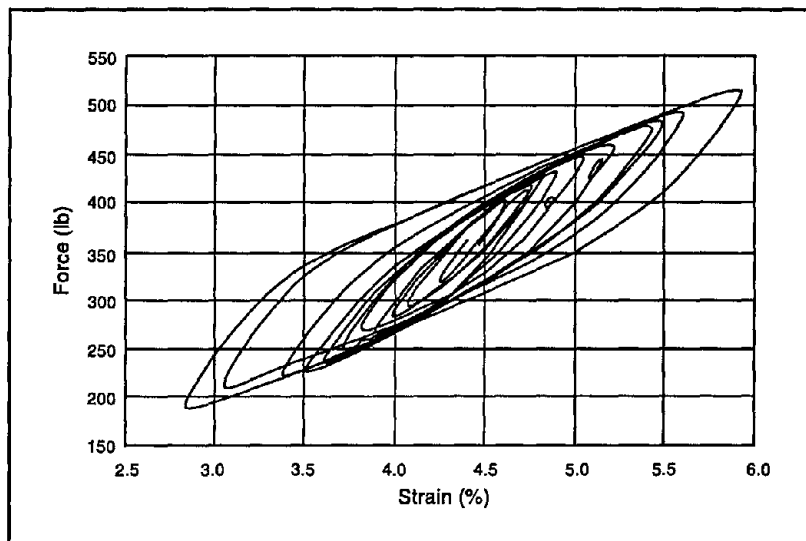
Aiken et al., 1992
■ Figure 4.36 Superelastic Behavior

The implementation of a tuned mass damper using Nitinol as an energy dissipation mechanism was studied analytically and experimentally by Inaudi et al., (1993a). The TMD consisted of a mass attached to a lightly damped structure with prestressed Nitinol cables. The cables were installed in the direction perpendicular to the motion of the points of attachment—both to the mass damper and to the structural system. This geometric configuration along with prestressing in the Nitinol cables introduced a resistance scheme which can be approximated by a bilinear relationship between the force acting on the TMD and the relative displacement between the mass damper and its support, leading to a triangular hysteresis loop. Results of this study show that this TMD scheme can improve the dynamic performance of the structure

with regard to its maximum deformation. However, no performance comparison with conventional TMDs was made and TMD parameters were not optimized in this study.

An experimental study using Cu-Zn-Al shape memory dampers installed as diagonal braces on a 2/5-scale steel frame model structure was carried out by Witting and Cozzarelli (1992). A torsion bar design of the SMA damper as shown in Figure 4.37
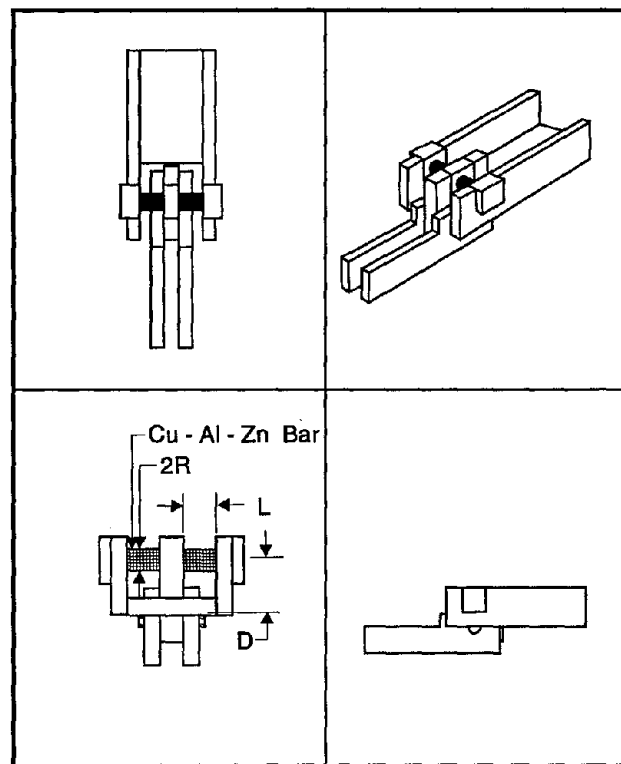
Witting and Cozzarelli, 1992
■ Figure 4.37 Torsional Bar Design

was used and the structure was subjected to several simulated ground motions supplied by a shaking table. Figures 4.38 and 4.39 show the maximum floor displacements and accelerations under, respectively, the simulated El Centro and Quebec ground motions scaled to 0.06g. These results demonstrate the sensitivity of damper effectiveness to the type of ground motions used. This observation can be partially explained by the fact that the SMA

damper stiffness decreases with larger material deformation, caus-
ing a decrease in the natural frequency of the structure. It is thus
expected to be more effective against earthquakes with energy
concentrated over the low-frequency range. Since the Quebec
earthquake has higher high-frequency content, the dampers did
not perform as well in this case as in the El Centro case. Test
results also showed that the SMA dampers were not as effective as
viscoelastic dampers operating under similar conditions.

No large-scale structural tests involving the use of SMA
energy dissipation devices have been carried out to date. Cost, in
addition to technical feasibility, will be another factor in assessing
potential applicability of SMA materials to civil engineering struc-
tural control.
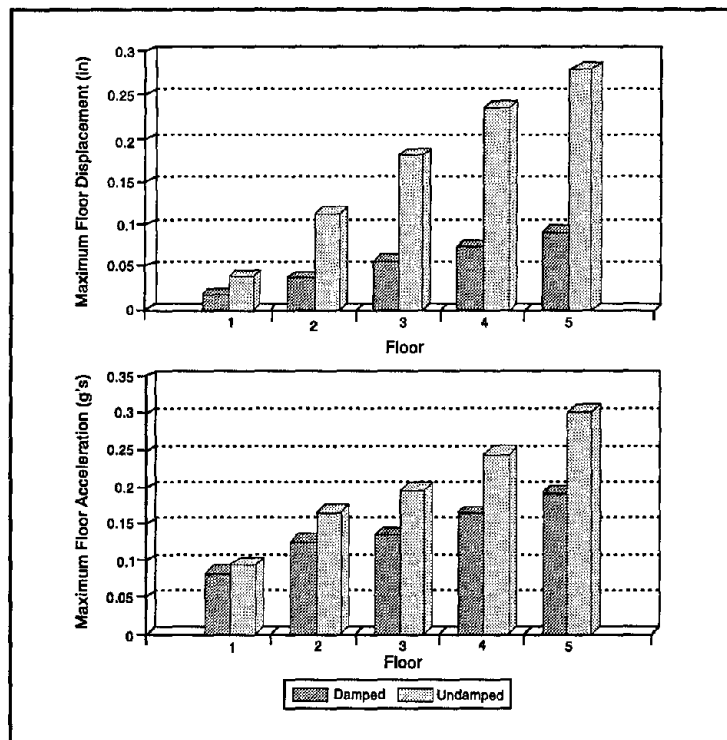
Witting and Cozzarelli, 1992
■ Figure 4.38 Maximum Floor Response (0.06g El Centro)
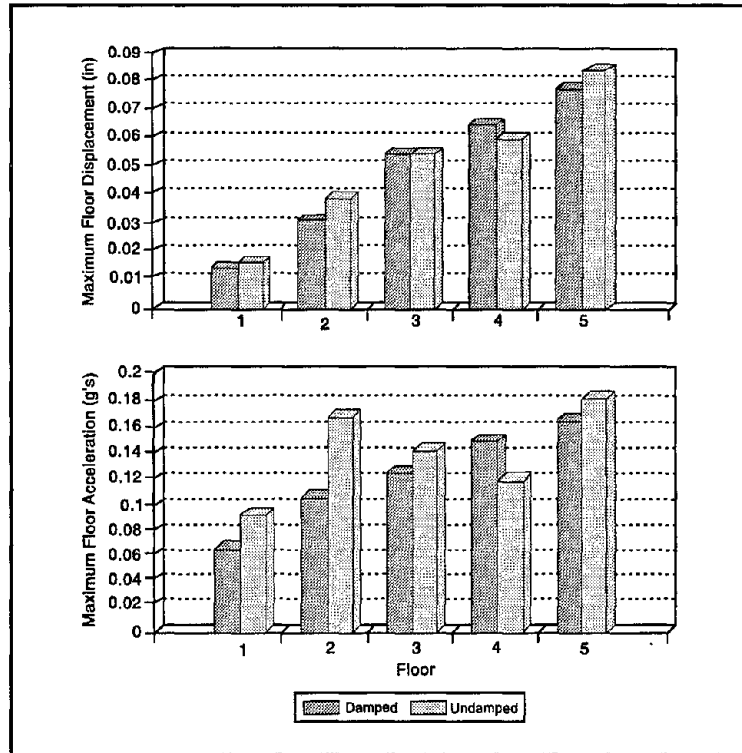
Witting and Cozzarelli, 1992

■ Figure 4.39 Maximum Floor Response (0.06g Quebec)

4.8

OTHER ENERGY DISSIPATORS

Other innovations which operate on similar passive energy dissipation principles have also been advanced in recent years. In order to reduce aerodynamic vibrations of bridge cables, a method of vibration suppression was proposed by which the protection tube surfaces of the cables are cut as V-stripes and U-stripes (Miyazaki, 1994). The results of wind tunnel tests show that the Reynold's number of the cable configured by V-stripes or U-stripes increases appreciably and aerodynamic vibrations could be significantly reduced by means of this technique.

A method was recently presented for controlling vibration in high-rise buildings during strong earthquakes by connecting two adjacent structures with dampers at the roofs (Kageyama et al., 1994). In this case, two structures are required to have different dynamical properties. When the mass ratio and stiffness ratio between the structures are optimized, the responses of both structures can be simultaneously reduced by using an optimum connecting damper. Another approach using a high-damping rubber damper was proposed by Fujita et al., (1992, 1993, 1994). A major component of the damper is unvulcanized rubber, which has low stiffness and high energy absorption ability compared with the vulcanized high damping rubber material usually used for laminated rubber bearings. The properties of the rubber damper are similar to those of VE dampers. Based on the experimental results, a design formula for the rubber damper was proposed and its viability was verified by full-size damper tests and response reduction analysis of a 40-story structural model with the full-size dampers (Fujita et al., 1994).

For cable-stayed bridges, a special rubber damper, called rubber composite damper, consisting mainly of a cable sleeve and a rubber washer has also been developed (Gu and Xiang, 1994). By studying vibration and control mechanisms of the cable, a practical design method of the rubber dampers for a cable-stayed bridge was presented, which mainly involves the calibration of the stiffness and damping ratio of the damper.

Finally, based on the concept of impact dampers, a particle damper has been developed by Papalou and Masri (1994). The damper consists of four-edge brackets. Experimental results performed on a particle damper attached to a randomly excited model structure show that the damper with a relatively small auxiliary mass can be effective in attenuating vibration of a lightly damped structure.

Review of Modern Applications

As can be seen from Chapter 4, serious efforts have been undertaken in recent years to develop the concept of energy dissipation or supplemental damping into a workable technology. As a result, a number of these devices have been installed in structures throughout the world, including Japan, New Zealand, Italy, Mexico, Canada, and the United States. Appendix A provides a summary of recent known installations in buildings and on bridges in North America. In what follows, some of these installations are discussed in some detail.

5.1 Metallic Dampers

After gaining confidence in the performance of metallic dampers based primarily on experimental evidence, implementation of these devices in full-scale structures has taken place. The earliest implementations of metallic dampers in structural systems occurred in New Zealand and Japan. A number of these interesting applications are reported in Skinner et al., (1980) and Fujita (1991). In New Zealand, the first implementation involved the use of a torsion beam steel damper for the piers of the Rangitikei Bridge. Transverse flexibility of the bridge is afforded by permitting rocking and uplift of the piers, while damping is provided by the first-generation metallic dampers. Meanwhile, tapered plate cantilever devices were employed at the base of a chimney at Christchurch and for the Dunedin Motorway Overbridge. Six 300 kN flexural beam dampers were used in the Cromwell Bridge, while lead extrusion dampers found application in two sloping highway bridges in Wellington. Additional implementations for metallic dampers as components in base isolation systems are discussed in Skinner et al., (1980).

Many other base isolation applications have appeared. However, the remainder of this section will concentrate on four examples in which metallic dampers are utilized as passive energy dissipators within the superstructure of a building (see Appendix A). All four utilize ADAS elements for the seismic upgrade of an existing structure. The first three of these occurred in Mexico City (Martinez-Romero, 1993) and the fourth in San Francisco (Perry et al., 1993).

The thirteen story Izazaga #38-40 building is shown in Figure 5.1. This is a reinforced concrete frame with brick infilled
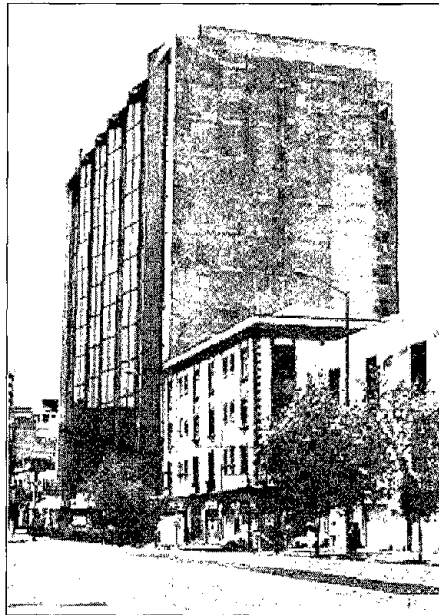
Martinez-Romero, 1993

■ Figure 5.1 Izazaga #38-40 Building, Mexico City

end walls constructed in the late 1970s. The building sustained moderate damage in the 1985 Mexico City earthquakes. An upgrade afterward was unsuccessful, since further damage occurred during earthquakes in 1986 and 1989. ADAS dampers were used for a second retrofit in which approximately 250 dampers were installed in the outer frame bays to permit continued building operation during construction. A view of a typical installation of a brace-damper subassembly is provided in Figure 5.2. Structural analysis indicated that the fundamental periods in the principal directions were reduced from 3.82 seconds and 2.33 seconds to, respectively, 2.24 seconds and 2.01 seconds with the addition of
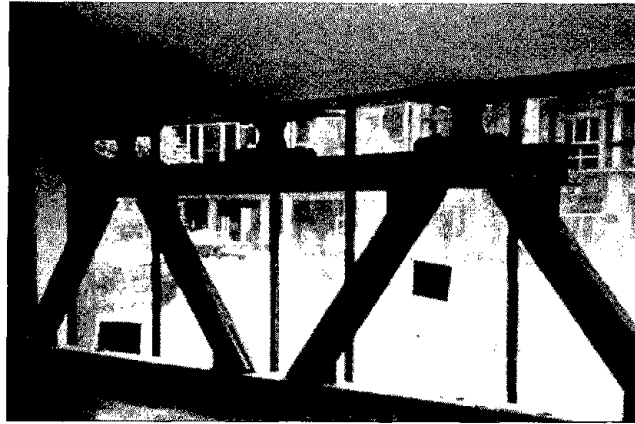
Martinez-Romero, 1993
■ Figure 5.2 Brace-Damper Assembly in Izazaga #38-40 Building

the ADAS elements. Calculations also showed a 40% reduction in interstory drift, while retaining the same base shear coefficient. Nonlinear time history DRAIN-2DX analyses were used to verify the final design.

The second Mexican application involves retrofit of the six-story Cardiology Hospital Building, built in the 1970s and damaged in the 1985 earthquake. The seismic upgrade of the reinforced concrete frame structure features a series of 18 external buttresses connected to the building via a total of 90 ADAS dampers. A front view with the buttresses in place is presented in Figure 5.3. This particular design permitted minimal interference with
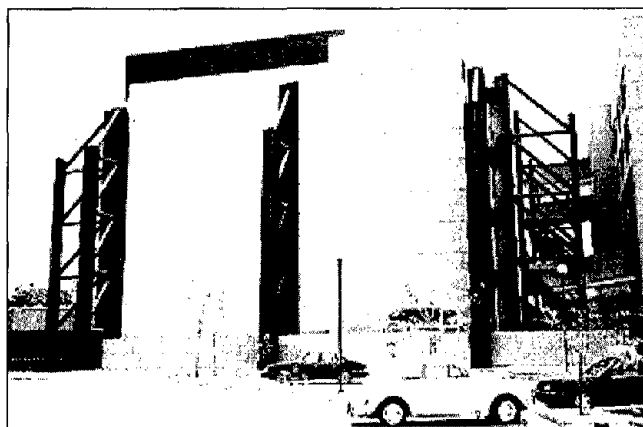
Martinez-Romero, 1993
■ Figure 5.3 Cardiology Hospital Building with Exterior Buttresses and ADAS Damper

hospital operation during retrofit construction. Nonlinear time history DRAIN-2D analyses were again employed extensively in the redesign process. However, in this case, the addition of the buttresses and ADAS dampers reduced both base shears and interstory drift.

Recently, the Reforma #476 buildings, which contain key operations of the Mexican Institute of Social Security (IMSS), underwent major seismic upgrade. This cluster of three ten-story buildings constructed in 1940 is listed in the National Register of Classical Buildings. An exterior view is provided in Figure 5.4.
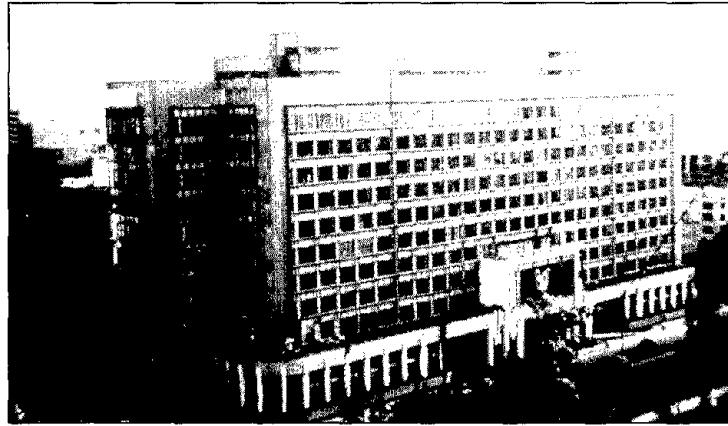
Martinez-Romero, 1993

■ **Figure 5.4 IMSS Reforma Building, Mexico City**

While the buildings sustained some significant damage during the 1957 earthquake, the more recent seismic events of 1985 had only minor effect. Through the years, the foundation has been improved to alleviate problems of differential settlement. Nevertheless, it was felt that the buildings remained vulnerable to future severe earthquakes. The most recent retrofit, discussed by Martinez-Romero (1993), involves the use of ADAS dampers with chevron bracing in 40 frame bays throughout the three structures. An example is shown in Figure 5.5. The buildings were analyzed in detail using the nonlinear DRAIN-2D program, along with four earthquake ground motions. Two dimensional analyses were performed on 13 different cross-sections. In order to assess the suitability of the revised design, comparisons were made among the bare frame, the structure with braces and ADAS dampers, and a

Martinez-Romero, 1993

■ Figure 5.5 Brace-Damper IMSS Reforma Building Retrofit Scheme from Outside

design using only the braces. The calculated response at one section of the central building is enumerated in Table 5.1 for one of the earthquakes, showing significant reduction of roof displacements and interstory drifts for the ADAS design. However, base shear, critical column force, and roof acceleration all increased, although not as much as would occur with the addition of only the bracing. In the final design, a floor diaphragm and several interior column strengths were increased to accommodate the elevated force levels. As in the other Mexican projects, the retrofit was completed while the complex remained in operation. It should be noted that in addition to describing the details of these three retrofit projects, Martinez-Romero (1993) relates many worthwhile observations concerning design and construction issues.

The final implementation of metallic dampers considered in this section involves the retrofit of the Wells Fargo Bank building in San Francisco, California (USA) discussed in Perry et al., (1993).The building is a two-story nonductile concrete frame structure originally constructed in 1967 and subsequently damaged in the 1989 Loma Prieta earthquake.The voluntary upgrade by Wells Fargo utilized chevron braces and ADAS damping elements. More conventional retrofit schemes were rejected due to an inability to meet the performance objectives while avoiding foundation work.

■ Table 5.1 Calculated Earthquake Response for IMSS Reforma Building

Building Condition		Deformations				
	Displacement at Roof (cm)	Story Drift (cm)		Story Drift Ratio		
		Max.	Avg.	Max.	Avg.	
Bare Frame	30.9	5.9	3.1	0.0147	0.0077	
Frame w/ADAS	25.8	3.5	2.6	0.0088	0.0064	
Frame w/Elastic Bracing	32.1	4.5	3.2	0.0113	0.0080	

Building Condition	Forces				
	Base Shear (tons)	Base Shear Coefficient	Force in Critical Column (tons)		Roof Acceleration (cm/sec²)
			Comp.	Ten.	
Bare Frame	455	0.11	317	58	178
Frame w/ADAS	652	0.13	477	272	230
Frame w/Elastic Bracing	680	0.14	556	340	340

Martinez-Romero, 1993

A plan view of the second floor including upgrade details is provided in Figure 5.6. A total of seven ADAS devices were employed, each with a yield force of 150 kips. Both linear and nonlinear analyses were used in the retrofit design process. For example, the three dimensional model shown in Figure 5.7 provided elastic modes and response spectrum analysis results for the original structure from the program SAP90. Additional three dimensional response spectrum analyses, using an approximate equivalent linear representation for the ADAS elements, furnished a basis for the redesign effort. The final design was verified with DRAIN-2D nonlinear time history analyses. A comparison of computed response before and after the upgrade is contained in Figure 5.8. The numerical results indicated that the revised design was stable and that all criteria were met. In addition to the introduction of the bracing and ADAS dampers, several interior columns and a shear wall were strengthened. The entire project, including design, permit approval, and construction were completed within a

3 @ 27' = 81'

2'-9"

2'-9"

3 @ 27' = 81'

(N) Brace, Typ.
4 Places
This Floor

(N) Steel
Jacket
2nd. Flr.
To Roof
Typ. 4 Places
This Floor
See

Relocate Glass
to Clear Brace
S.A.D.

Wall Location

(N) Shotcrete
Below

1'-6"

2'-2½"

1'-6"

(E) Wall
Below

Second Floor Plan
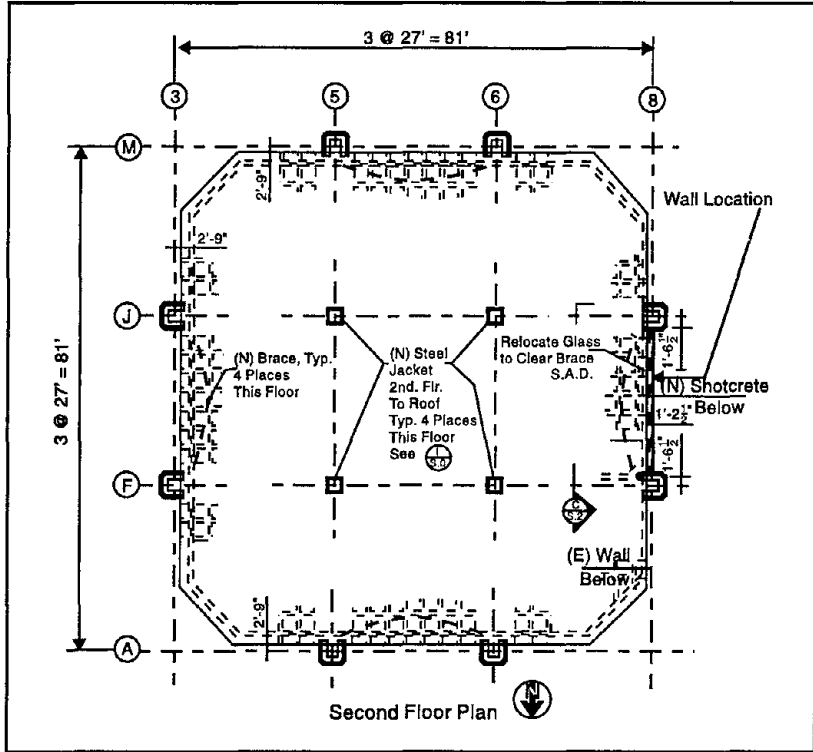
Perry et al., 1993

■ Figure 5.6 Wells Fargo Bank Building Retrofit Details

X-Dir

X-Dir

SAP90 Model

First Model Shape
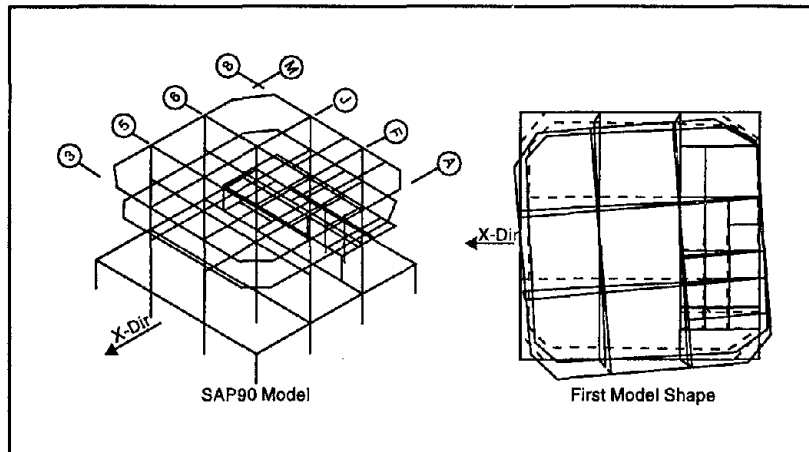
Perry et al., 1993

■ Figure 5.7 Structural Analysis Model for Wells Fargo Bank Building

Envelope of Response Values Due to SSR in X - Direction

Story Height

Displacement (inch)   Interstory Drift (inch)   Story Shear (kips)
                                                  Thousands

——— Frame Before Upgrade
— — — — Upgraded Frame With ADAS
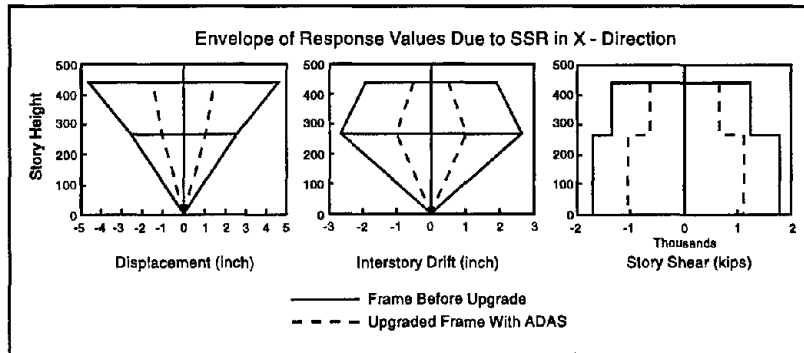
Perry et al., 1993

■ **Figure 5.8 Comparison of Computed Results for Wells Fargo Bank Building**

six-month period, in time for a February 1992 opening of the bank branch. Perry et al., (1993) also described the permit approval process, and suggested that the ADAS elements have many potential applications for both new and retrofit projects involving either concrete or steel framed structures.

5.2

FRICTION DAMPERS

In recent years, there have been a number of commercial applications of friction dampers aimed at providing enhanced seismic protection of new and retrofitted structures. As indicated in Appendix A, these include Pall friction dampers and slotted bolted connections in North America. In addition, three building projects in Japan, involving Sumitomo friction dampers, are briefly described in the report by Aiken and Kelly (1990). The first is the 31-story steel frame Sonic Office Building in Omiya City, constructed in 1988. A total of eight 22 kip dampers were utilized on each story, primarily to reduce the effect of ground-borne vibration and small earthquakes. A similar motivation led to the use of four 22 kip dampers per level in the Asahi Beer Azumabashi Building in Tokyo. This 22-story braced steel frame structure was completed in 1989. The third project mentioned involves the use of Sumitomo friction dampers as part of a base isolation system for a six-story reinforced concrete structure in Tokyo.

As documented in Pall and Pall (1996), several variations of Pall friction devices have been installed in thirteen buildings; six retrofits and seven new facilities. Several of these applications are described below in more detail. A typical configuration of the Pall friction device is given in Figure 5.9.
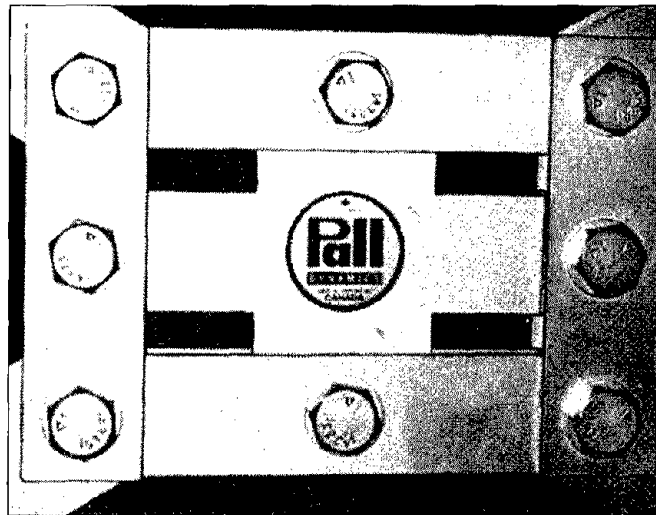
Pall et al., 1993
■ Figure 5.9 Pall Friction Dampers

The McConnel Library of the Concordia University in Montreal, Canada, consists of two buildings of six and ten stories interconnected by a galleria. An exterior view of the structure is shown in Figure 5.10. As discussed in Pall and Pall (1993), a total of 143 dampers were employed. Interestingly, the architects chose to expose sixty of the dampers to view due to their aesthetic appeal. A typical example is illustrated in Figure 5.11. A series of nonlinear DRAIN-TABS (Guendeman-Israel and Powell, 1977) analyses were utilized to establish the optimum slip load for the devices, which ranges from 600-700 kN depending upon the location within the structure. For the three-dimensional time history analyses, artificial seismic signals were generated with a wide range of frequency contents and a peak ground acceleration scaled to 0.18 g to represent expected ground motion in Montreal. Under this level of excitation, an estimate of the equivalent damping ratio for the structure with frictional devices is approximately 50%. In addition, for this library complex, the use of the friction damp-

■ Figure 5.10 McConnel Library at Concordia
University in Montreal

■ Figure 5.11 Exposed Friction Damper in McConnel Library Galleria

ers resulted in a net saving of 1.5% of the total building cost. The authors note that higher savings would be expected in more seismically vulnerable regions.

The application of friction dampers to the main headquarters building of the Canadian Space Agency Complex near Montreal is described in Vezina et al., (1992) and Pall et al., (1993). An aerial view of the entire complex is shown in Figure 5.12. The
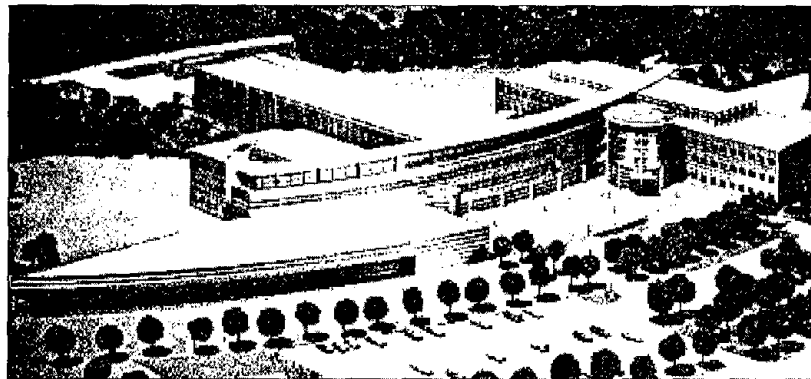
Pall et al., 1993
■ Figure 5.12 View of Canadian Space Agency Complex

headquarters building is a three-story steel framed structure clad with aluminum panels. Since it contains sensitive equipment and instrumentation, additional protection is required from the potentially damaging effects of earthquakes. Three-dimensional non-linear dynamic analyses were conducted using DRAIN-TABS to determine the suitability of employing friction dampers. Ground motions used in the analyses included several artificially generated seismic signals scaled to produce a peak ground acceleration of 0.18 g. Comparison with traditional braced and unbraced configurations indicated a superior performance for the friction damped design. Based upon these results, a total of 58 frictional devices were specified, each with a slip load of 500 kN. The cross braced frame bays with friction dampers are distributed evenly throughout the building, as illustrated for the first story in Figure 5.13. Several dampers were intentionally exposed for viewing purposes.

The three school buildings at Ecole Polyvalante near Montreal, pictured in Figure 5.14, were damaged in the 1988 Saguenay earthquake. The original structure, built in 1967, consists of precast concrete beams and columns with welded con-
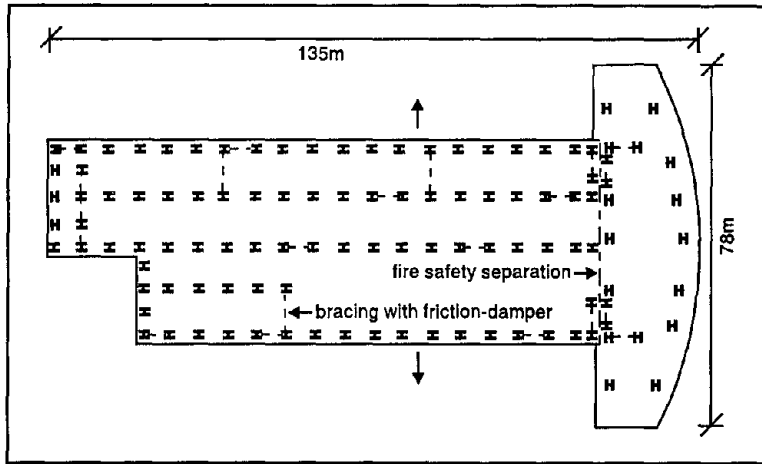
Pall et al., 1993

■ **Figure 5.13** Ground Floor Plan of Main Building in Canadian Space Agency
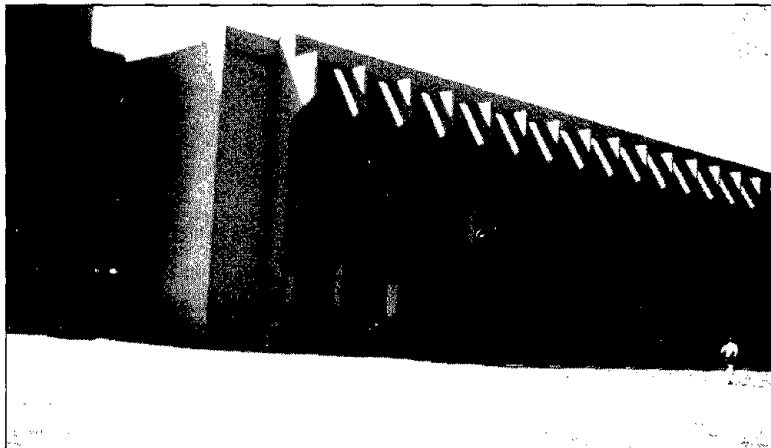
Pall and Pall, 1993

■ **Figure 5.14** Exterior View of Ecole Polyvalante, Sorel

nections. Floor and roof panels are also precast concrete. The result is a structure with little lateral resistance. In fact, analysis indicated that the existing structure could not withstand an earthquake with a peak acceleration of 0.05g. Two different retrofit schemes were considered; a conventional method using concrete shear walls, and an approach employing friction dampers. The latter was chosen because it resulted in a 40% reduction in retrofitting cost and a 60% reduction in construction time. Based upon

results from nonlinear time domain dynamic analyses, a total of 64 friction dampers were specified, along with 388 friction-based panel connectors. The project was completed during the summer break in 1990. Further details are provided in Pall and Pall (1993).

The eight story steel structure, shown in Figure 5.15, was originally constructed by the French government for EXPO'67 held in Montreal. After the exhibition, the building was donated to the city, and in 1992 a decision was made by Lotto-Quebec to rehabilitate the structure to house 'Casino de Montreal.' Preliminary analysis indicated that the building would no longer satisfy the seismic code requirements, which had been updated since the time of the original construction. Both conventional and friction-damped retrofit designs were considered. However, the former required considerable pile foundation work, which is expensive and time consuming. The friction-damped alternative employed 32 devices throughout the structure, based upon results from nonlinear dynamic analysis. In this case, a three-dimensional analysis was essential due to the eccentricities of the original structure. Additional information on this retrofit project can be found in Pasquin et al., (1994).
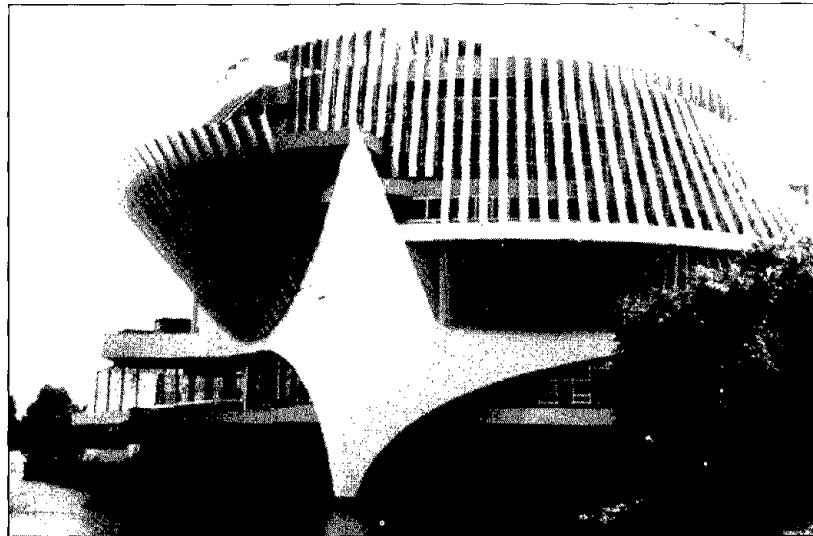
Pasquin et al., 1994
■ Figure 5.15   North View of Casino de Montreal

V I S C O E L A S T I C   D A M P E R S

As indicated in Appendix A, the first applications of viscoelastic (VE) dampers to structures were for reducing acceleration levels, or increasing human comfort, due to wind. In 1969, VE dampers were installed in the twin towers of the World Trade Center in New York, NY, as shown in Figure 5.16, as an integral

LVDT

World Trade Center
Damper in Place

Damper Position
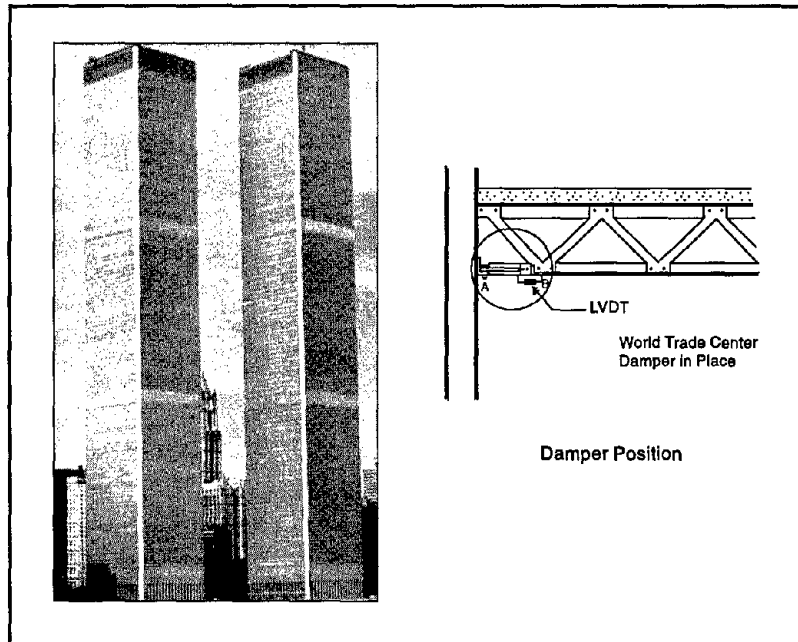
Courtesy of the 3M Co., St. Paul, MN
■ **Figure 5.16 Damper Installation in the World Trade Center, New York**

part of the structural system. They were designed to assist the tubular steel frame in limiting wind-induced building vibrations to levels below human perception (Mahmoodi, 1969; Mahmoodi et al., 1987).The selection, quantity, shape and location of the dampers were chosen based on the dynamics of the towers and required damping to achieve the performance objectives.

There are about 10,000 VE dampers in each tower, evenly distributed throughout the structure from the 10th to the 110th

floor. As shown in Figure 5.16, they are located between the lower chords of the horizontal trusses and the columns of the outside wall. The towers have experienced a number of moderate to severe wind storms over the last 28 years. The observed performance of the VE dampers has been found to agree well with theoretical values. After hurricane Gloria in 1978, the total damping of the building was calculated and found to be in the range of 2.5% to 3% of critical. The aging characteristics of the VE dampers have also been found to be excellent.

In 1982, VE dampers were incorporated into the 76-story Columbia SeaFirst Building in Seattle, as shown in Figure 5.17, against wind-induced vibrations (Keel and Mahmoodi, 1986). The building has a triangular plan and its lateral force resisting system consists of three composite columns interconnected with steel braced moment frames as shown in Figure 5.18 (Skilling et al., 1986). To reduce the wind-induced vibration, the design called for 260 dampers to be located alongside the main diagonal members in the building core as shown schematically in Figure 5.19. The addition of VE dampers to this building was calculated to increase its damping ratio in the fundamental mode from 0.8% to 6.4% for frequent storms and to 3.2% at design wind. Similar applications of VE dampers were made to the Two Union Square

■ Figure 5.17 The Columbia SeaFirst Building, Seattle

Building in Seattle, as seen in Figure 5.20, in 1988. In this case, 16 large VE dampers were installed parallel to four columns in one floor as shown in Figure 5.20.

Seismic applications of VE dampers to structures began only recently. A seismic retrofit project using VE dampers began in 1993 for the 13-story Santa Clara County building in San Jose, CA
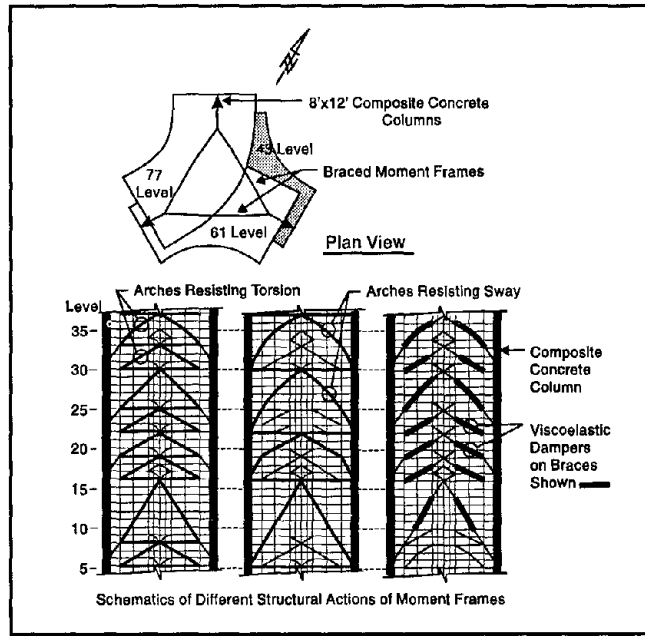
■ Figure 5.18 Plan View and Details of Wind Resisting System for Columbia SeaFirst Building
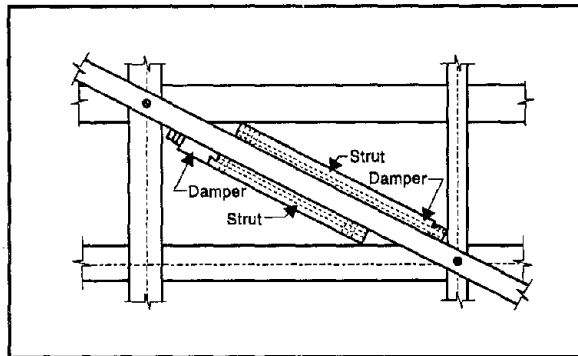
■ Figure 5.19 Damper Installation in the Columbia SeaFirst Building
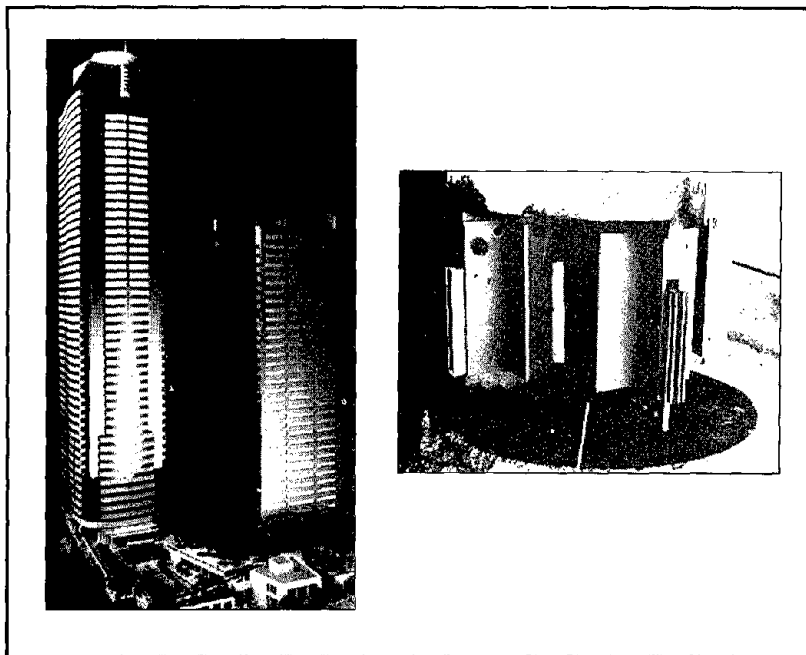
Courtesy of the 3M Co., St. Paul, MN

■ **Figure 5.20** Damper Installation in the Two Union Square Building, Seattle

(Crosby et al., 1994). Situated in a high seismic risk region, the building was built in 1976. As shown in Figure 5.21, it is approximately 64 meters in height and nearly square in plan, with 51 m x 51 m on typical upper floors. The exterior cladding consists of full-height glazing on two sides and metal siding on the other two sides. The exterior cladding, however, provides little resistance to structural drift. The equivalent viscous damping in the fundamental mode is less than 1% of critical.

The building has been extensively instrumented, providing invaluable response data obtained during a number of past earthquakes. A plan for seismic upgrade of the building was developed, in part, when the response data indicated large and long-duration response, including torsional coupling, to even moderate earthquakes. Initially, three different types of devices were considered. They were the steel-yielding ADAS device, the friction-slip energy dissipation restraints, and the VE dampers. The VE dampers were chosen primarily because they provided the structure with significantly increased damping for frequent low-level ground shaking, as well as for larger seismic events.
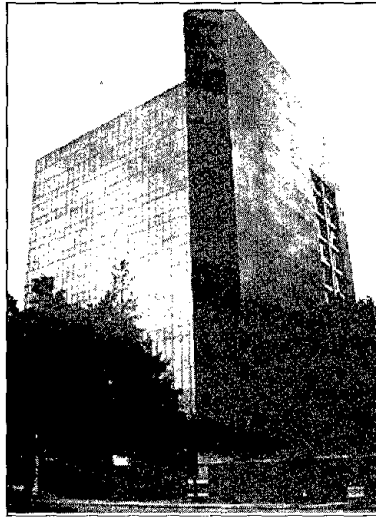
■ Figure 5.21 Santa Clara County Building, San Jose

The final design called for installation of two dampers per building face per floor level as shown in Figure 5.22, which would increase the equivalent damping in the fundamental mode of the building to about 17% of critical, providing substantial reductions to building response under all levels of ground shaking. A typical damper configuration is shown in Figure 5.23.

The structure shown in Figure 5.24 represents the first application of viscoelastic damper technology to a reinforced concrete structure for seismic upgrade. Located in San Diego, the building is a three-story structure with its plan and eleva-
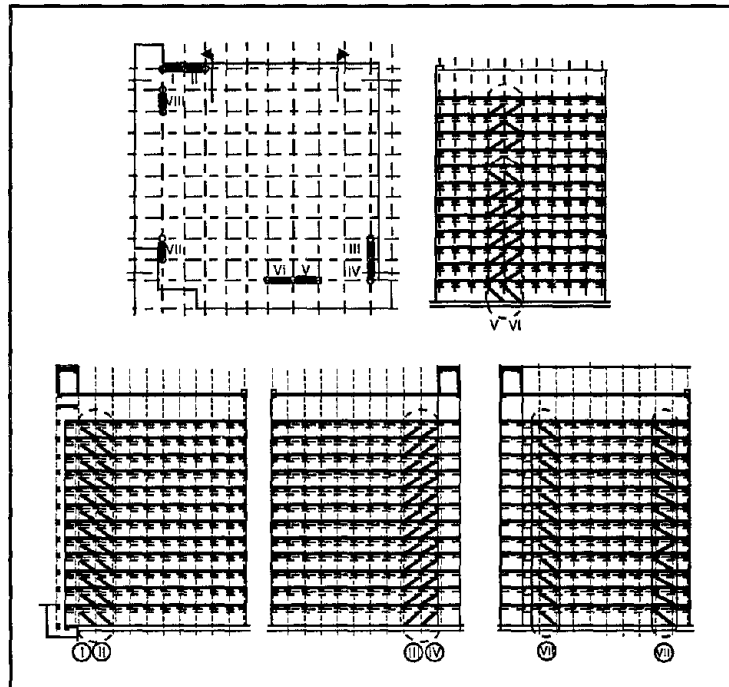
Courtesy of The Crosby Group, Redwood City, CA
■ Figure 5.22 Location of VE Dampers in Santa Clara County Building

■ Figure 5.23 Damper Configuration in Santa Clara County Building
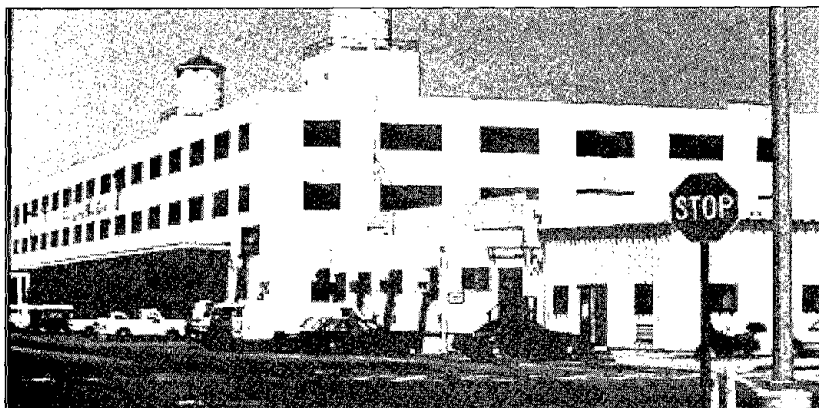
■ Figure 5.24 Building 116, Naval Supply Facility, San Diego

tion shown in Figure 5.25. Its lateral load resisting system consists of 8-inch reinforced concrete perimeter walls. There is a 4-inch separation joint at the center of the building, in the north/south direction. The second and third floor systems are 10-1/4 and 9-inch flat slabs, respectively, both with column capitals. The foundation consists of reinforced concrete wall footings at the exterior

(a) Front Elevation

(b) Floor Plan Showing Damper Locations (First Floor, North Half)
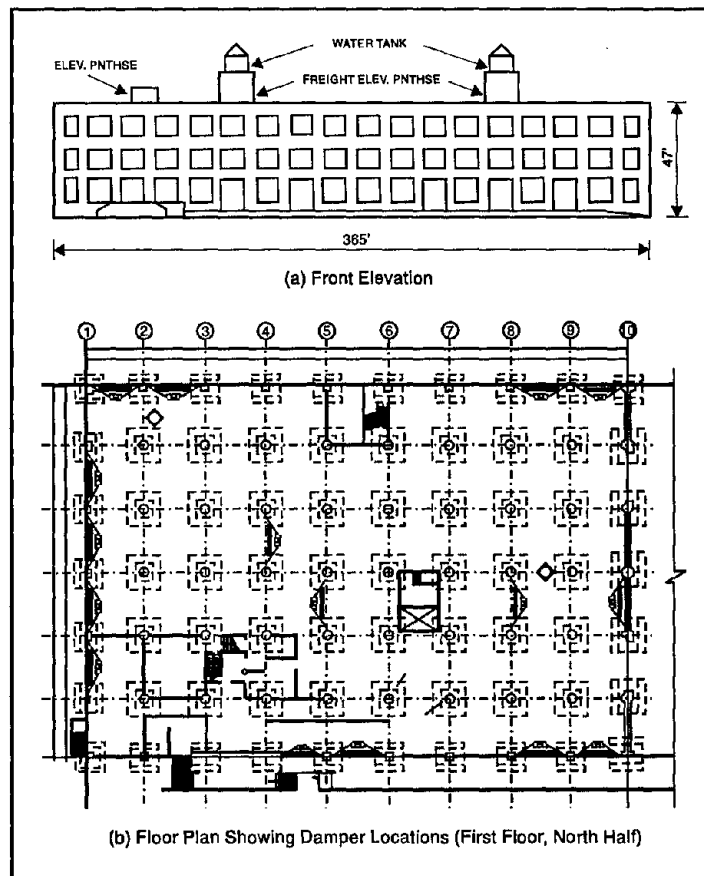
■ Figure 5.25 Elevation and Plan of Building 116

long wall, with all columns resting on the 6-inch slab on grade, which has 6 by 6 inch mesh of No. 6 wire for reinforcement. Results of extensive seismic evaluations show that the structure is not of sufficient quality to withstand the expected seismic loads. Appropriate reduction of interstory drifts was the primary objective of seismic upgrade and, based on nonlinear dynamic analysis, a total of 64 dampers were required to meet seismic demands on the structural elements in this case. As shown in Figure 5.26, each damper consists of four damper units incorporated into the structure in a K-brace configuration.
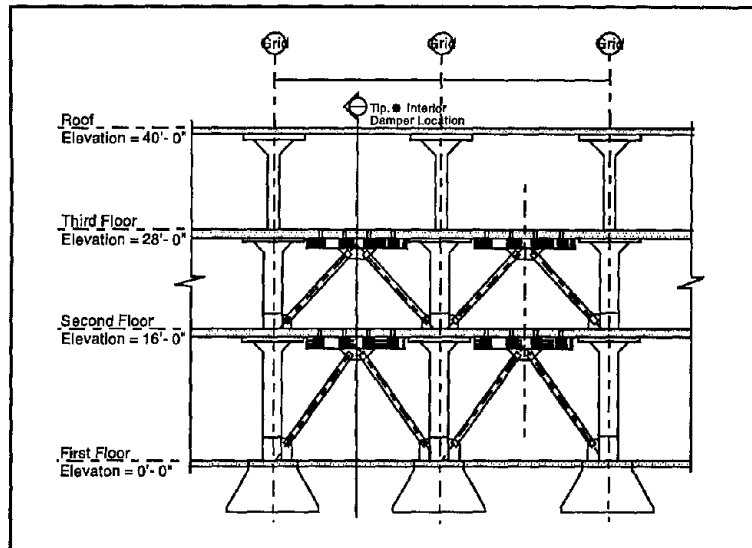
■ Figure 5.26 Damper Configuration in Building 116

5.4

VISCOELASTIC FLUID DAMPERS

Viscoelastic fluid (VF) dampers, widely used in aerospace and military applications, have in recent years been incorporated into civil engineering structures (see Appendix A). In several applications, they were used in combination with seismic isolation systems. For example, VF dampers have been applied in combination with helical steel springs for the combined vibration and seismic isolation of structures. The spring and damper system is placed at the foundation-superstructure interface to form a base isolation system as shown in Figure 5.27 from a small residential building in Los Angeles (Makris and Constantinou, 1992; Makris and Deoskar, 1996). The system for this building provided for a fundamental frequency of 1.6 Hz and damping of 23%. This frequency, which corresponds to the rocking mode of the isolated structure, is insufficient to produce a seismic isolation effect. Rather, the VF dampers enhance damping by reducing the amplitude of vibration and preventing any build-up of resonant vibrations.
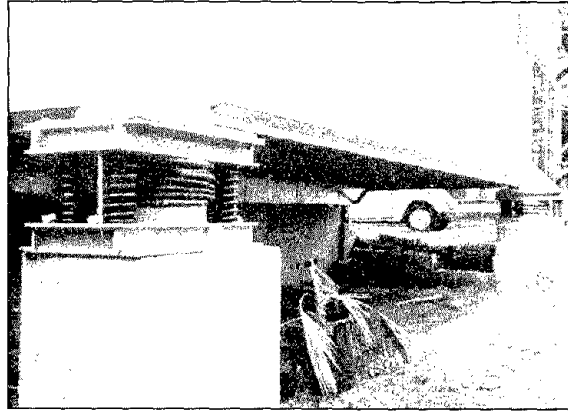
Courtesy of GERB Vibration Control, Inc., Downers Grove, IL

■ Figure 5.27 Spring and Viscous Damper System in Small Residential Building in Los Angeles

In 1995, viscous dampers were incorporated into base isolation systems for five buildings of the new San Bernardino Medical Center, as shown in Figure 5.28, located close to two major fault lines. The five buildings required a total of 184 dampers, each having an output force of 1400 kN and a stroke of ±600 mm. A layout of the damper-isolation system assembly is shown in Figure 5.29 and Figure 5.30 gives the dimensions of the VF dampers employed.

Several additional projects involving these orificed fluid dampers are described in Taylor and Constantinou (1996), and
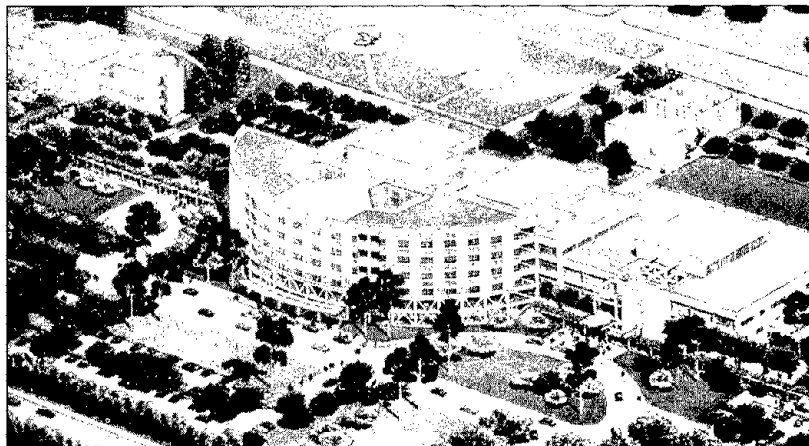
■ Figure 5.28 Architectural Drawing of San Bernardino Medical Center
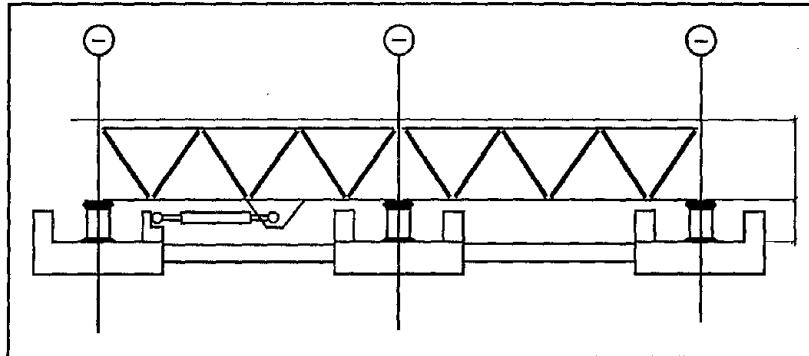
■ Figure 5.29 Damper-Base Isolator System Assembly for San Bernardino Medical Center
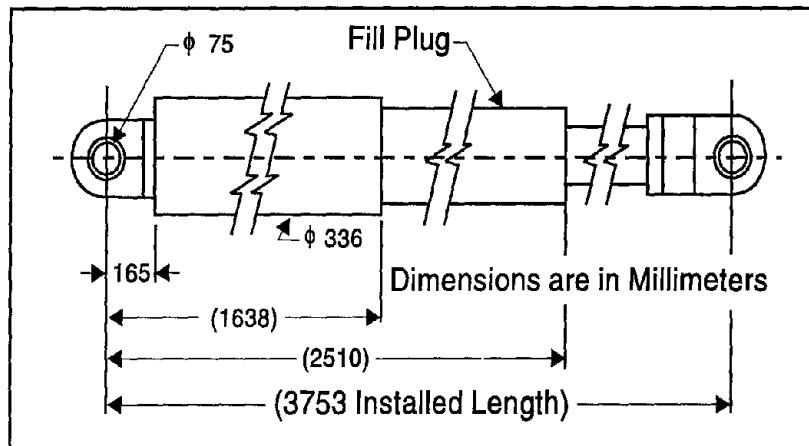
■ Figure 5.30 Dimensions of Viscous Fluid Damper for San Bernardino Medical Center

briefly summarized in the following. In Sacramento, California, Taylor fluid dampers were employed for seismic mitigation of the new three-story Pacific Bell North Area Operations Center, shown under construction in Figure 5.31 and completed in 1995. A total of 62 dampers each with a capacity of 130 kN and a stroke of ±50 mm were utilized within the steel braced frame. Figure 5.32 illustrates a typical installation of the fluid dampers. These damper-chevron brace assemblies are distributed throughout the structure, and sufficient supplemental damping is provided to maintain an elastic frame response even under a maximum level earthquake. This level of protection is necessary because the building serves as the central '911' facility for Northern California, and consequently must remain operational after seismic events.
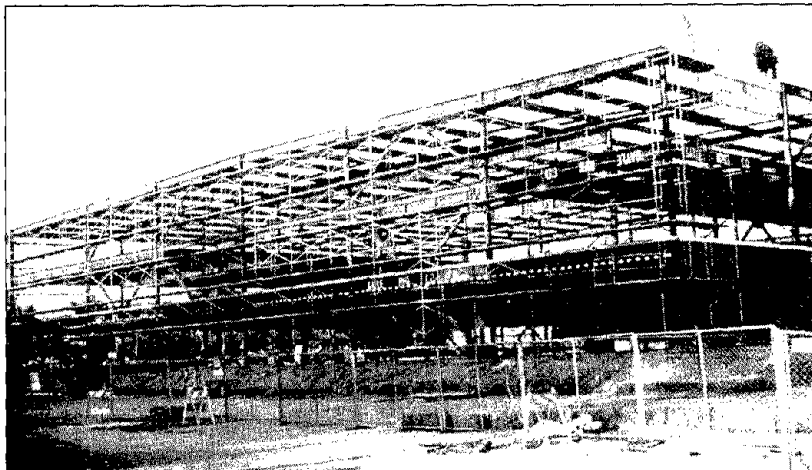
Courtesy of Taylor Devices, Inc., North Tonawanda, NY

■ Figure 5.31 Pacific Bell North Area Operations Center, Sacramento, under Construction
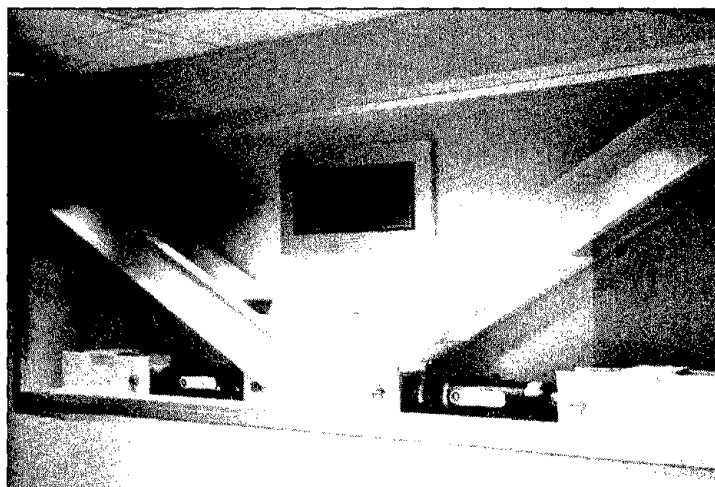
Courtesy of Taylor Devices, Inc., North Tonawanda, NY

■ Figure 5.32 Damper Installation in the Pacific Bell North Area Operations Center

A seismic retrofit of the Woodland Hotel, an historic masonry structure in Woodland, California, also employed Taylor fluid dampers. The four-story structure, originally constructed in 1927, is shown in Figure 5.33. In this case, a total of 16 450 kN dampers were utilized with chevron bracing for the project completed in

Courtesy of Taylor Devices, Inc., North Tonawanda, NY
■ Figure 5.33 Woodland Hotel, Woodland, California

1996. Another recent project involved the installation of a total of 40 orificed fluid dampers in the 35-story building in downtown Boston, MA. Each damper has a capacity of 670 kN and a stroke of ±25 mm. This 1996 retrofit is intended to improve the overall damping of the structure.

Viscous damping walls were recently used for aseismic protection in the newly constructed SUT-Building in Shizuka City, Japan, as described in Miyazaki and Mitsusaka (1992). The building consists of a 78 m 14-story above-ground steel frame structure, along with a two-story reinforced concrete basement. A total of 170 damping walls are employed within the steel frame to elevate the effective damping ratio of the building to approximately 27% at 20°C. A schematic illustrating the locations of the walls is provided in Figure 5.34. Notice the staggered arrangement. Based upon time history dynamic analyses, the damping walls reduced response by 70-80%. Consequently, no damage is expected for level-2 earthquakes having a maximum input velocity of 50 cm/s.
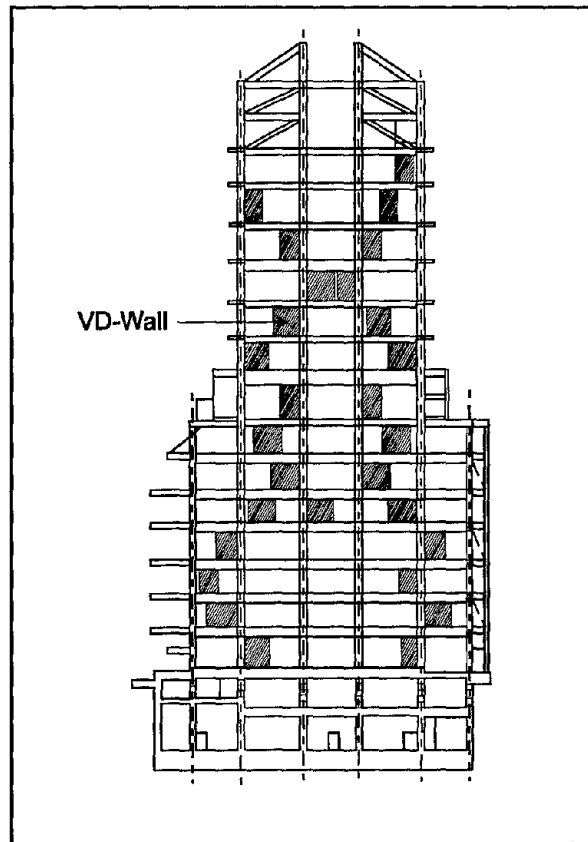
Miyazaki and Mitsusaka, 1992

■ Figure 5.34 Viscous Damping Wall Locations in SUT-Building, Shizuka
City, Japan

5.5
TUNED MASS DAMPERS

As in the case of viscoelastic dampers, early applications
of tuned mass dampers (TMDs) have been directed toward mitiga-
tion of wind-induced excitations. It appears that the first structure
in which a TMD was installed is the Centerpoint Tower in Sydney,
Australia (ENR, 1971; Kwok and MacDonald, 1987). The struc-
ture consists of a 150-ft-high (45.72 m) office building topped
with a 700-ft-high (213.36 m) tower as shown in Figure 5.35a.
Serving as the building water and fire protection supply, the tower's
water tank in conjunction with hydraulic shock absorbers was in-
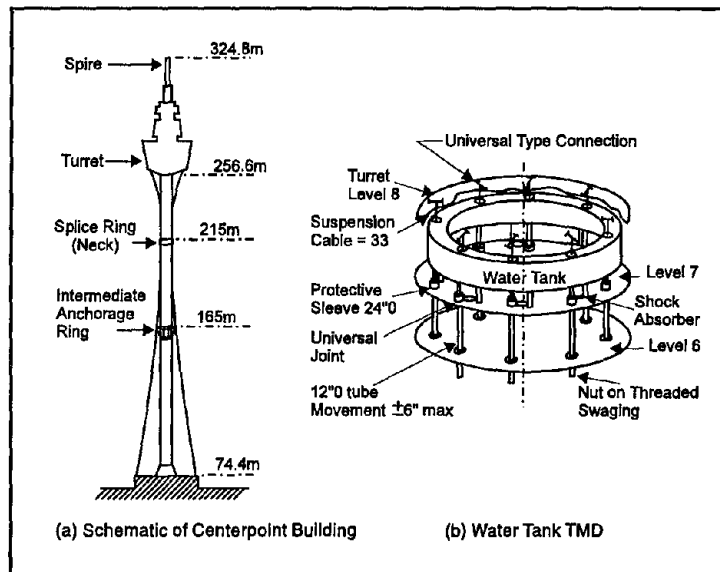
■ Figure 5.35 Water Tank TMD at Centerpoint Tower, Sydney, Australia

corporated into the design of the TMD to reduce wind-induced motions. The tank, 7-ft (2.13 m) deep and 7-ft (2.13 m) wide with a capacity of 35,000 gal (132.4 m³) hangs from the top radial members of the turret as shown in Figure 5.35b.

A 40-ton secondary mass was later installed on the intermediate anchorage ring to further increase damping in the second mode, which resulted in increases in the damping level from 1.0% to 1.2% and from 0.4% to 1.5% in the first and second mode, respectively. Results of acceleration measurements showed that the wind-induced acceleration response was reduced by 40% to 50% (Kwok, 1984; Kwok and MacDonald, 1990). Other examples of structures having pendulum-type TMDs include the 102 m steel antenna mast atop the 553 m CN Tower in Toronto, Canada, which has two doughnut-shaped TMDs to reduce the second and fourth modes of vibration, and the 157 m Crystal Tower in Osaka, which also makes use of water storage tanks at the top of the structure as pendulum TMDs.

One of only two buildings in the U.S. equipped with a TMD (see Appendix A), the 960-ft Citicorp Center (Figure 5.36) has a distributed mass of about 60,000 tons (64.6×10^6 kg), a first bending mode lateral natural frequency of about 0.16 Hz, and a

■ Figure 5.36 Citicorp Center, New York

damping ratio of 1% in its resonant response to wind gust force. The Citicorp TMD, as shown in Figure 5.37, is installed on the 63rd floor of the building. At this elevation, the building can be represented by a simple modal mass of approximately 20,000 tons (18.21×10^6 kg), to which the TMD is attached to form a 2-DOF system. The TMD system specifications are given in Table 5.2. Tests and actual observations have shown that the TMD produces an approximate effective damping of 4% as compared to the 1% original structural damping, which can reduce the building acceleration level by about 50%.

Involved in the design of the Citicorp TMD system are the linear gas spring, pressure balance supporting system, control actua-
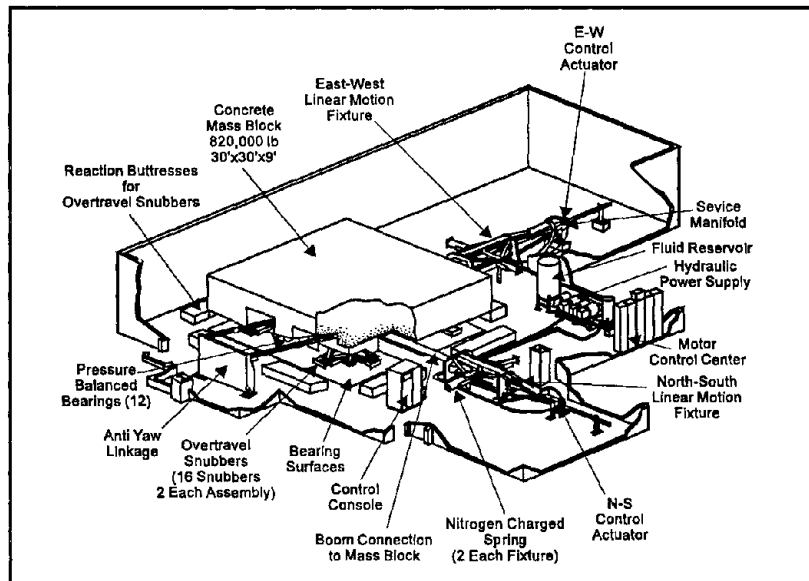
Petersen, 1980
■ Figure 5.37 TMD in Citicorp Center

■ Table 5.2 Tuned Mass Dampers in John Hancock Tower, Boston and Citicorp Center, New York

		John Hancock Boston, MA	Citicorp Center New York, NY
Typical floor size	(ft)	343 x 105	160 x 160
Floor area	(sq ft)	36,015	25,600
Building height	(ft)	800	920
Building modal weight	(tons)	47,000	20,000
Building period 1st mode	(sec)	7.00	6.25
Design wind storm	(years)	100	30
Mass block weight	(tons)	2 x 300	400
Mass block size	(ft)	18 x 18 x 3	30 x 30 x 8
Mass block material	(type)	lead/steel	concrete
TMD/AMD stroke	(ft)	± 6.75*	± 4.50*
Max spring force	(kips)	135	170
Max actuator force	(kips)	50	50
Max hydraulic supply	(gms)	145	190
Max operating pressure	(psi)	900	900
Operating trigger - acceleration	(g)	.002	.003
Max power	(HP)	120	160
Equivalent damping	(%)	4.0%	4.0%

* Including overtravel

tor, power supply and electronic control (Petersen, 1980; 1981). The passive spring was provided by a pair of opposed trunnion mounted and pneumatically precharged cylinders with connected piston rods. The 400-ton (363,000 kg) concrete block was supported on twelve pressure balanced bearings, each with a 22-in (55.9 cm) diameter. The individual bearings were hydraulically coupled together into three groups, each group containing its own height control valve. Fluid can flow between individual bearings to accommodate floor surface irregularities. The overall friction coefficient achieved due to the pressure balanced bearing installation was about 0.003, requiring about 2400 lbs (10,600 N) drive force to compensate for friction losses.

The biaxial motion of the mass block was controlled by two double-acting hydraulic actuators. Each control and spring actuator subassembly was mounted on a single linear guide assembly for each axis of the TMD. The mass block was restrained from rotational motion about its vertical axis (yaw) by a torsion box assembly mounted on the floor and connected to the mass block by two radius rods.

The same design principles were followed in the development of the TMD for installation in the John Hancock Tower, Boston (ENR, 1975). In this case, however, the TMD consisted of two 300-ton mass blocks as shown schematically in Figure 5.38. They move in phase to provide lateral response control and out-of-phase for torsional control. A comparison of the TMD and structural parameters of this system with those of the Citicorp TMD system is given in Table 5.2.
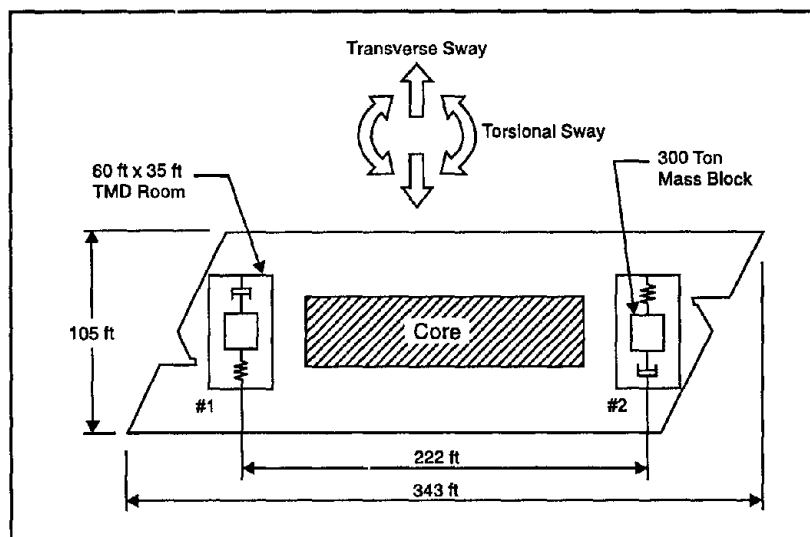
■ Figure 5.38 Dual TMD System in John Hancock Tower, Boston

In Japan, the first TMD was installed in Chiba Port Tower, Tokyo Bay, a 125-m-high steel structure. It has a rhombus plan with a side length of 15 m (Figure 5.39a). The TMD, as shown in Figure 5.39b, consists of a mass and two frames overlapping at right angle. The mass can move in X or Y direction but cannot rotate. Each frame has coil springs and a damping device. Pertinent values of the TMD and structural parameters are given in Table 5.3 (Kitamura et al., 1988; Mataki et al., 1989).

Figure 5.40 shows the wind-induced root-mean-square acceleration response under Typhoon 8719 (before tuned) and under strong wind Run 880205 (after tuned). The response due to Run 880205 is seen to have been reduced by 40% in the X-direction and by 50% in the Y-direction approximately.

An example of bridge applications of TMDs in Japan is the Funade Bridge Tower in Osaka. Wind tunnel tests of the tower

(a) Chiba Port Tower

Moving Mass (M1)

Oil buffer (X-direction)

Frame (M2)

Rack and Pinion (X-direction)

Oil Buffer (Y-direction)

Rail (Y-direction)

Roller Bearing (Y-direction)

Tension Spring (Y-direction)

Damping Device (X-direction)

y direction

x direction

Roller bearing (X-direction)

Rail (X-direction)

Base

Tension Spring (X-direction)

Rack and Pinion (Y-direction)

Oil Buffer (Y-direction)

Damping Device (Y-direction)
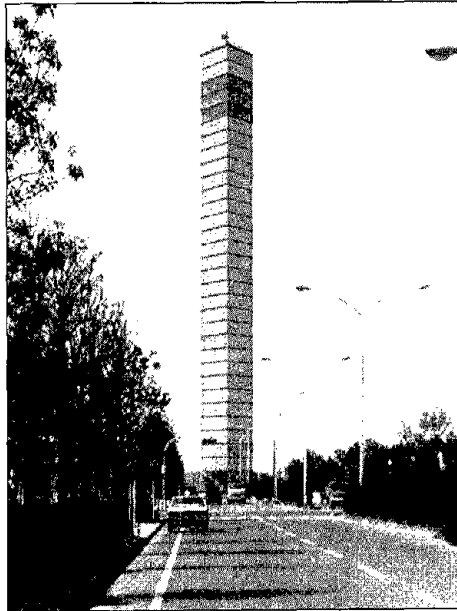
(b) TMD

Mataki et al., 1989

■ Figure 5.39 Chiba Tower, Tokyo Bay, Japan and TMD

■Table 5.3 TMD and Structural Parameters, Chiba Port Tower

			X-direction	Y-direction
Structure	1st mode effective weight (tons)		1200	
	Period	1st mode (sec)	2.25	2.70
		2nd mode (sec)	0.51	0.57
	Damping ratio (%)		0.005	
TMD	Weight (tons)		10.0	15.4
	Period (sec)		2.24	2.72
	Spring constant (tons/cm)		0.080	0.084
	Friction force (tons)		0.045	0.045
	Damping ratio (%)		0.15	

Kitamura et al., 1988
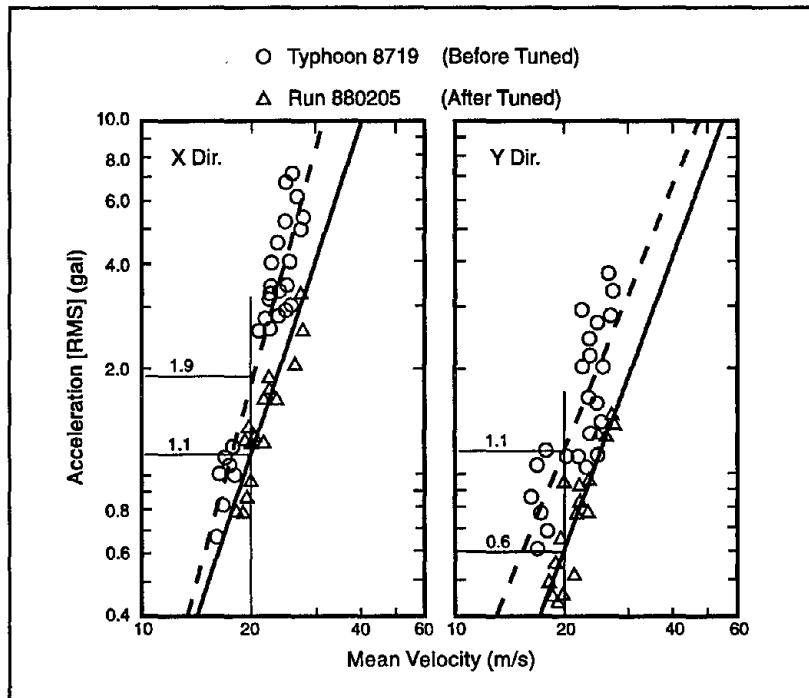
Mataki et al., 1989

■Figure 5.40 RMS Accelerations Without and With TMD, Chiba Port Tower

showed that galloping may occur at a wind speed of about 10 m/s. The SDOF equivalent weight of the tower is 8.09 tons with a fundamental frequency of 0.835 Hz. The air damper type TMD developed for the structure is shown in Figure 5.41. It is composed of a circular cylinder, a disc weighing 97.4 kg ($\mu = 1.2\%$) and coil springs. The TMD damping results from the passing of air through the narrow space between the disc weight and the cylinder. Fine adjustments in the damping coefficient could be made by varying the number of holes passing through the disc (Ueda et al., 1992).
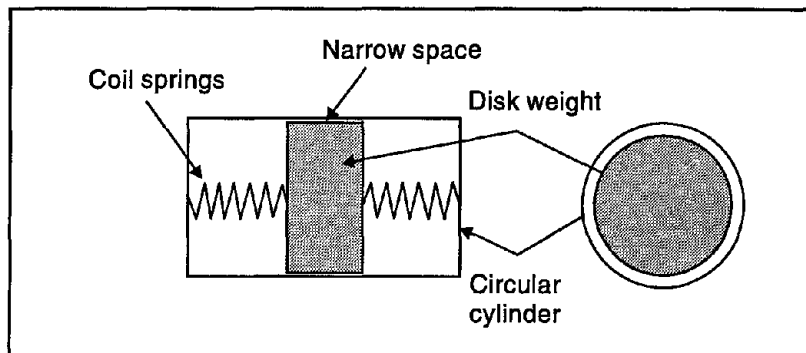
Ueda et al., 1992
■ Figure 5.41 TMD on Funade Bridge Tower, Osaka

Results of damped free vibration tests are shown in Figure 5.42. The logarithmic decrement increases from 0.046 to 0.26, phase lag is about 105 degrees, and the ratio of motion amplitudes of TMD and tower is about 6. The resonance frequency of the coupled motion is 0.86 Hz.
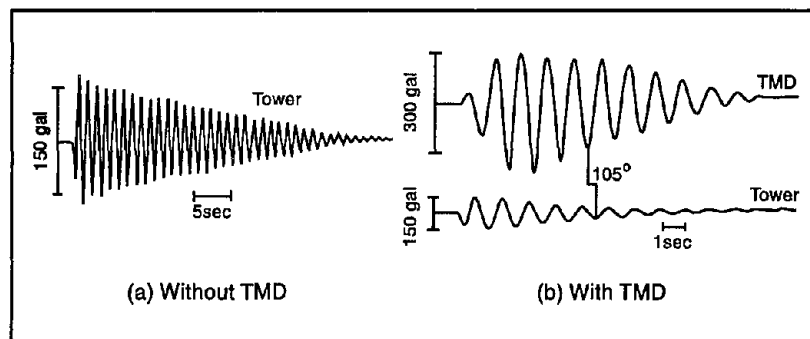
Ueda et al., 1992
■ Figure 5.42 Damped Free Vibrations Without and With TMD, Funade Bridge

All the TMD applications discussed above have been made toward suppression of wind-induced motion. The interest in using TMDs for vibration control of structures under earthquake loads has resulted in some innovative developments. An interesting approach is the use of a TMD with active capability, so called hybrid mass damper (HMD) or active tuned mass damper (ATMD). Systems of this type are best described as semi-active systems as mentioned in Chapter 1 and have been implemented in a number of tall buildings in recent years in Japan (Soong et al., 1994). Some examples of these semi-active systems are discussed in Chapter 7.

5.6

TUNED LIQUID DAMPERS

Tuned liquid dampers (TLDs), operating on similar principles as TMDs, have also been used for suppressing wind-induced vibrations of tall structures. In comparison with TMDs, the advantages associated with TLDs include low initial cost, virtually free maintenance and ease of frequency tuning.

It appears that TLD applications have taken place primarily in Japan. Examples of TLD-controlled structures include the Nagasaki Airport Tower, installed in 1987, the Yokohama Marine Tower, also installed in 1987, the Shin-Yokohama Prince Hotel, installed in 1992, and the Tokyo International Airport Tower, installed in 1993. Due to their similarities, only the TLD system installed in the Tokyo Airport Tower will be discussed below (Tamura et al., 1994, 1995).

The TLD installed in the 77.6 m air-traffic control tower consists of about 1400 vessels containing water, floating particles and a small amount of preservatives. The vessels, shallow circular cylinders 0.6 m in diameter and 0.125 m in height as shown in Figure 5.43, are stacked in six layers on steel-framed shelves (Figure 5.44). The total mass of the TLD is approximately 3.5% of the first-mode generalized mass of the tower and its sloshing frequency is optimized at 0.743 Hz. Floating hollow cylindrical polyethylene particles were added in order to optimize energy dissipation through an increase in surface area together with collisions between particles.
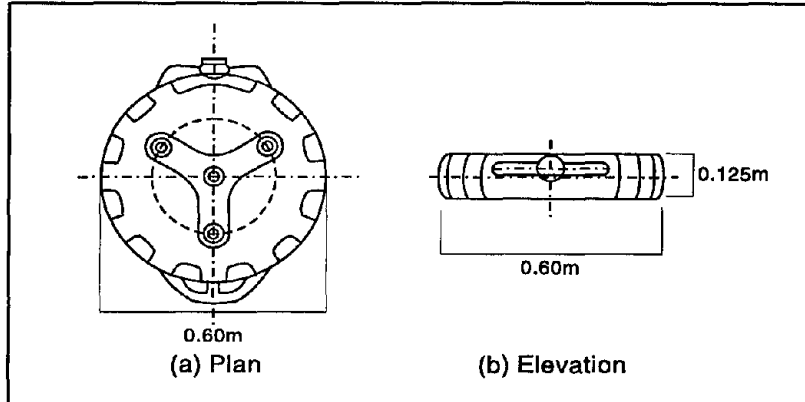
Tamura et al., 1995

■ **Figure 5.43 TLD Vessel, Tokyo Airport Tower**

The performance of the TLD has been observed during several storm episodes. In one of such episodes with a maximum
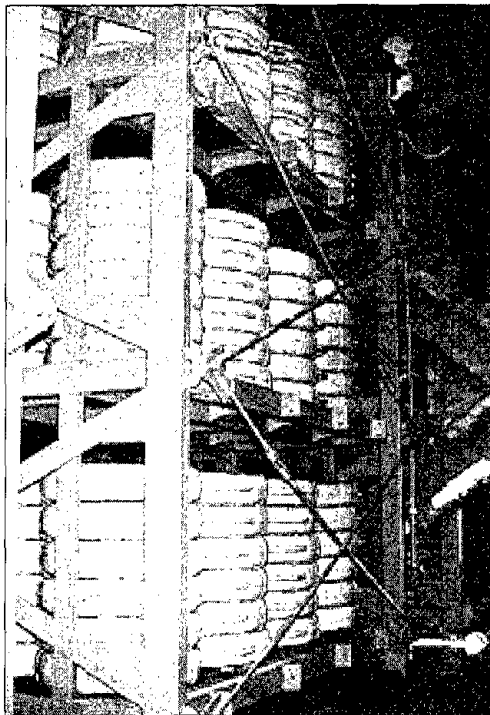
Tamura et al., 1995

■ **Figure 5.44 Installation of Vessels in TLD Room in Tower**

instantaneous wind speed of 25 m/s, the observed temporal variation of the root-mean-square (RMS) acceleration and damping ratio of the tower are given in Figure 5.45, showing that the damping ratio in the cross-wind direction (x-direction) reached the maximum value of 7.6% before the RMS acceleration recorded its maximum. Figure 5.46 shows a comparison of the x-direction RMS accelerations of the tower with and without TLD, indicating that the TLD reduced the response to about 60% of the RMS acceleration response of the tower without TLD.
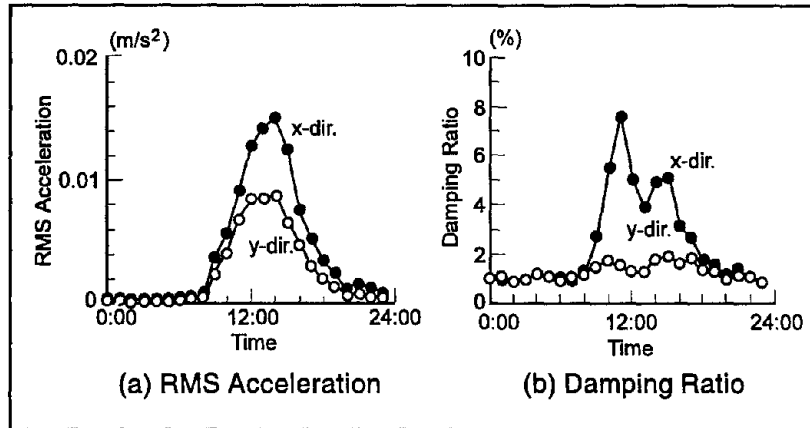
Tamura et al., 1995

■ **Figure 5.45** Temporal Variation of RMS Acceleration and Damping Ratio of Tower
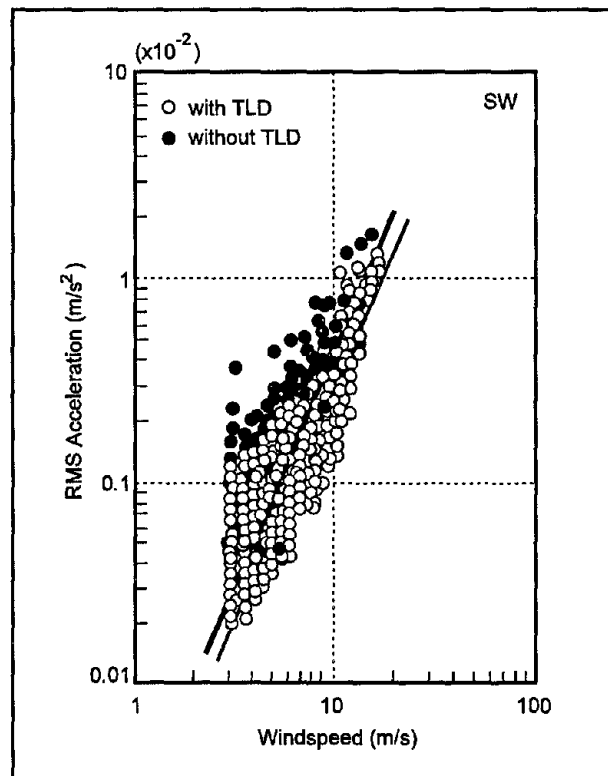
Tamura et al., 1995

■ **Figure 5.46** Comparisons of RMS Acceleration Responses of TIAT with/ without TLD (x-direction, ≈ across-wind)

GUIDELINES FOR ANALYZING STRUCTURES WITH PASSIVE ENERGY DISSIPATION SYSTEMS

Building activity in the United States is regulated by local governments by means of *building codes*. Building codes are generally established at the local or state level as a result of the constitutional framework in which powers not specifically granted to the Federal Government are reserved to the States. As a result of this framework, building activities are greatly fragmented. Certain organizations, such as the International Conference of Building Officials, the Building Officials and Code Administrators International and the Southern Building Code Congress, developed *model codes* that alleviate some of this fragmentation and raise the level of quality of codes. States and localities typically adopt one of these model codes. Available model codes include the Uniform Building Code (UBC), the Building Officials and Code Administrators Code (BOCA) and the Standard Building Code (SBC). Seismic provisions in these three model codes are not the same. However, there is currently an effort to consolidate the three into a single code by the year 2000, which will be called the International Building Code.

Several *resource documents* exist which provide detailed guidelines or specifications on specific topics. These documents typically represent the resource for model code development. Examples of such documents that contain seismic provisions are the *Blue Book* (Structural Engineers Association of California, 1995), the *1994 National Earthquake Hazard Reduction Program (NEHRP) Recommended Provisions for Seismic Regulations for New Buildings* (FEMA, 1995), and the recent *NEHRP Guidelines for the Seismic Rehabilitation of Buildings* (FEMA, 1997). This chapter presents a very brief description of various resource documents on passive energy dissipation systems. It is beyond the scope of this monograph to provide a critical review of these documents. So far, energy dissipation system design is not addressed in any model code.

6.1

TENTATIVE REQUIREMENTS OF SEAONC

The Energy Dissipation Working Group of the Base Isolation Subcommittee of the Seismology Committee of the Structural Engineers Association of Northern California (SEAONC) developed in 1993 a document on seismic design requirements for passive energy dissipation systems (Structural Engineers Association of Northern California, 1993). This document has remained in draft form and has not been reviewed or approved by the Structural Engineers Association of California.

This early document established a terminology for energy dissipation systems, classified systems as rate dependent (i.e., viscous and viscoelastic devices) or as rate independent (i.e., friction and metallic yielding devices), and prescribed analysis procedures for buildings and testing procedures for devices. Buildings incorporating rate dependent devices may be analyzed by equivalent linear procedures provided that all structural elements remain elastic. For buildings incorporating rate independent devices, nonlinear dynamic analysis is mandated. Moreover, the document promotes the use of dual lateral force resisting systems, consisting of the frame carrying the energy dissipation devices and a supplemental moment frame. The latter must be detailed as a special moment-resisting frame if the analysis predicts that the frame will experience inelastic deformations.

6.2

1994 NEHRP RECOMMENDED PROVISIONS

The 1994 edition of the *National Earthquake Hazard Reduction Program (NEHRP) Recommended Provisions for Seismic Regulations for New Buildings* (FEMA, 1995) contains an "Appendix on Passive Energy Dissipation Systems." The appendix is loosely based on the SEAONC Tentative Requirements. It requires nonlinear dynamic analysis for all buildings incorporating energy dissi-

pation devices except for the case of linear viscous devices and provided that the fundamental mode damping ratio is not more than 30% of critical. For buildings incorporating linear viscous devices with damping not more than 30% of critical, the equivalent lateral force procedure for seismic analysis is permitted. In accordance with this procedure, the seismic base shear is computed by the procedure applicable to the structural system exclusive of the energy dissipation system (that is, elastic response divided by response modification factor) and furthermore multiplied by a reduction factor for damping ratio larger than 5% of critical. This reduction factor is nearly equal to the inverse of the B_1 factor of Table 2-1. Moreover, the structural members that transmit forces from the energy dissipation devices to the foundation should be designed to remain elastic.

It is now recognized that this procedure is not appropriate since it will allow significant reduction in lateral forces due to both inelastic action in the building and viscous damping provided by the energy dissipation system. As demonstrated in Chapter 2, the lateral forces on a yielding system with energy dissipation devices may not reduce. Rather, certain actions in members of the structural frame are reduced since drift is reduced. The Technical Subcommittee 12 of the Building Seismic Safety Council is currently in the process of revising the "NEHRP Recommended Provisions on Passive Energy Dissipation Systems." Scheduled to be included as a subsection on "Provisions for Passive Energy Dissipation Systems," these revised provisions will appear in the *2000 NEHRP Recommended Provisions for Seismic Regulations for New Buildings.*

6.3

APPLIED TECHNOLOGY COUNCIL PROJECT 33

The Applied Technology Council (ATC) developed for the Building Seismic Safety Council *Guidelines and Commentary for the Seismic Rehabilitation of Buildings*. The 75-percent complete draft of this document has been available since November 1995 (Applied Technology Council, 1995). The complete ballot version of this document was made available in September 1996. The

document was approved in 1997, and is now available with the official title: *FEMA 273, NEHRP Guidelines for the Seismic Rehabilitation of Buildings* and *FEMA 274, NEHRP Commentary on the Guidelines for the Seismic Rehabilitation of Buildings* (FEMA, 1997).

A novelty of these guidelines is the option of selecting among ground motion criteria and performance objectives to achieve the desired intent of the user. This intent is described as the rehabilitation objective, which is a statement of the desired limits of damage for an earthquake of certain probability of occurrence. Statements of desired limits of damage are given as performance levels. Verification of the rehabilitation design requires, of course, analysis of the rehabilitated buildings. The analysis procedures include a nonlinear dynamic analysis procedure, a simplified nonlinear analysis procedure, an elastic dynamic response procedure and an equivalent lateral force procedure. Each of the analysis procedures may be acceptable for a particular rehabilitation design depending on the characteristics of the structural system, rehabilitation strategy and ground motion criteria.

The New Technologies Team of this project was responsible for the development of guidelines and commentary for seismic isolation and energy dissipation systems. Particularly, the simplified nonlinear analysis procedure of this document has been largely described in Chapter 2 of this monograph. This was done for the purpose of providing a theoretical background and some verifications of the procedure in this monograph.

7

SEMI-ACTIVE
CONTROL SYSTEMS

As described in Chapter 1, semi-active control systems are an extension of passive energy dissipation systems, which have received increasing attention in recent years because they offer a degree of adaptability under external loads. Referring to Figure 3.1a, the added feature of a semi-active device over a passive one is that the mechanical properties of the device element, Γ, can be adjusted in real time in response to the external load, or to the structural response, or to both. Semi-active systems require nominal amounts of energy to adjust their mechanical properties and, unlike fully active systems, they can not add energy to the structural system as no active forces are applied directly to the structure.

While semi-active control systems have long been studied, for example, in the automotive engineering field, their applications to the motion control of civil engineering structures subject to environmental loads have been investigated only recently. Examples of such devices are semi-active mass dampers (Hrovat et al., 1983; Higashino and Aizawa, 1993; Nishimura et al., 1993; Soong et al., 1994; Yoshida, 1996), friction devices with controllable friction (Akbay and Aktan, 1990, 1991; Dowdell and Cherry, 1994; Yang and Lu, 1994; Inaudi, 1997), semi-active fluid viscous dampers (Kawashima, et al., 1992; Mizuno, et al., 1992; Sack and Patten, 1993; Kobori, et al., 1993; Symans and Constantinou, 1995; Nagarajaiah, 1995; Kurino et al., 1996) and, more recently, semi-active devices employing smart materials such as shape memory alloys (Graesser and Cozzarelli, 1991b; Aiken et al., 1992; Witting and Cozzarelli, 1992; Inaudi, et al., 1993a), piezoelectric materials (Bailey and Hubbard, 1985; Baz and Ro, 1993; Shen, 1994) and electro- or magneto-rheological fluid dampers (Ehrgott and Masri, 1992; Gavin and Hanson, 1994; Makris et al., 1996; Spencer et al., 1996, 1997).

The semi-active concept can be illustrated by considering a semi-active mass damper. In comparison with a passive tuned

mass damper schematically shown in Figure 3.1b, the semi-active version proposed by Hrovat et al., (1983) has an added piston-cylinder combination supplemented by a control valve assembly, represented by the S/A unit in Figure 7.1 and shown schematically in Figure 7.2. In its passive mode of operation, the valve in the S/A actuator is stationary, which corresponds to the conventional
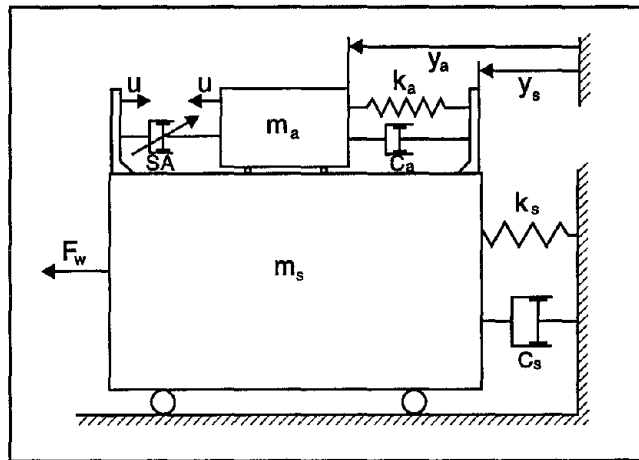
Hrovat et al., 1983
■ Figure 7.1 A Semi-Active Mass Damper
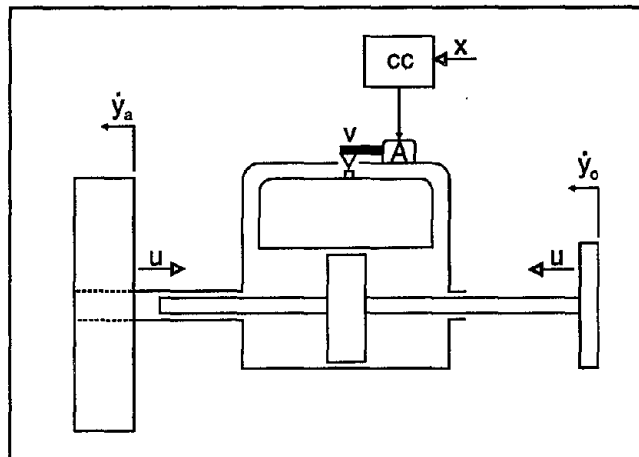
Hrovat et al., 1983
■ Figure 7.2 Schematic of Semi-Active Device

tuned mass damper. During the semi-active mode of operation, electrical signals from the control computer (CC in Figure 7.2) initiate control-value actuator action which in turn results in valve (V) executing upward and downward motion. If, at the same time, the piston is moving with respect to the cylinder, different levels of the damper force (u) are produced. The term "semi-active" is used as a consequence of the fact that the control valve action requires active energy; however, the amount of the required energy is usually small in comparison with the total energy dissipated by damping.

For a semi-active device, the active control force is designed as a function of the state of the structural system and/or the state of the external force as measured by sensors based upon a certain control strategy. It potentially offers reliable operation and can be viewed as fail-safe in that they become passive systems should the control hardware malfunction.

Of the four broad types of semi-active systems described above, semi-active mass dampers and semi-active fluid dampers have found applications in civil engineering structural control. These two areas are the focus of this chapter. The reader is referred to Soong and Dargush (1997) for an account of recent development in smart material research for structural applications.

7.1

SEMI-ACTIVE MASS DAMPERS

As discussed in Section 5.5, in an effort to extend the effectiveness of tuned mass dampers to counter moderate earthquake load as well as wind load, semi-active mass dampers or hybrid mass dampers (HMD) have been developed and implemented in a number of tall buildings, mostly in Japan, in recent years. This trend is clearly indicated in Appendix B, which summarizes recent installations of active and semi-active devices in Japan.

In some of these installations, active capabilities of the HMDs are supplied by electrohydraulic actuators. An example is an HMD system installed in the Sendagaya INTES building in Tokyo in 1992 (Building No. 3 in Appendix B). As shown in Figure 7.3, the hybrid mass damper was installed atop the 11th floor and consists of two masses to control transverse and torsional motions
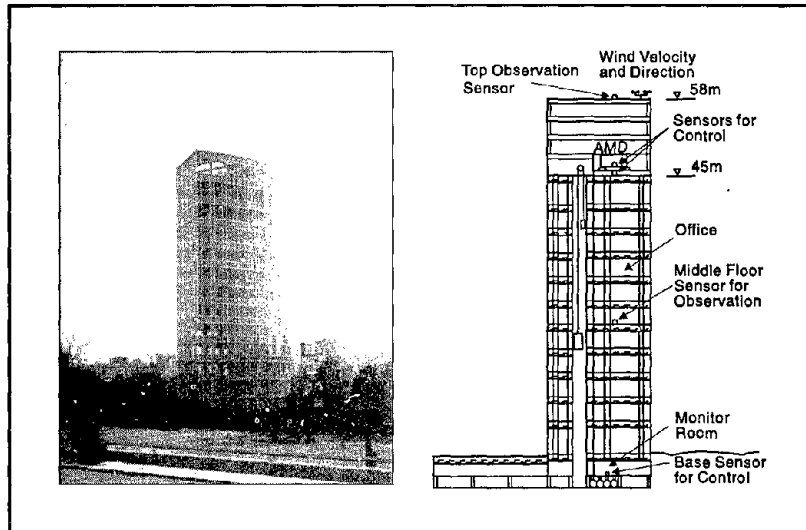
Higashino and Aizawa, 1993

■ Figure 7.3 Sendagaya INTES Building

of the structure while electrohydraulic actuators provide the active control capabilities. The top view of the control system is shown in Figure 7.4 where, as shown in Figure 7.5, ice thermal storage tanks are used as mass blocks so that no extra mass is introduced. The masses are supported by multi-stage rubber bearings intended for reducing the control energy consumed in the HMD and for insuring smooth mass movement (Higashino and Aizawa, 1993).
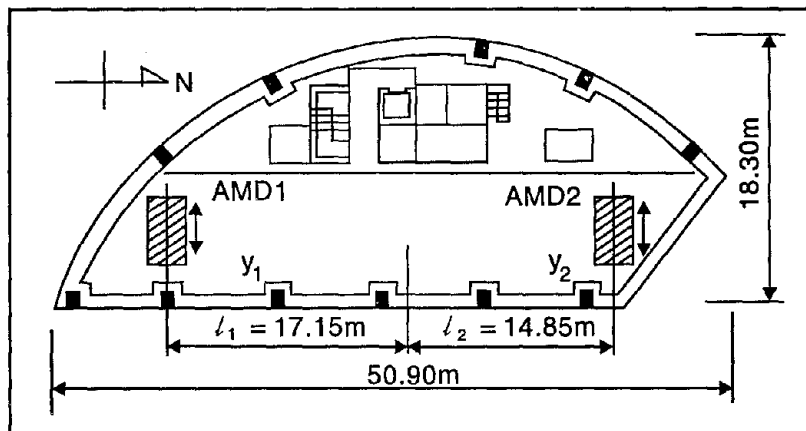
Higashino and Aizawa, 1993

■ Figure 7.4 Top View of AMD
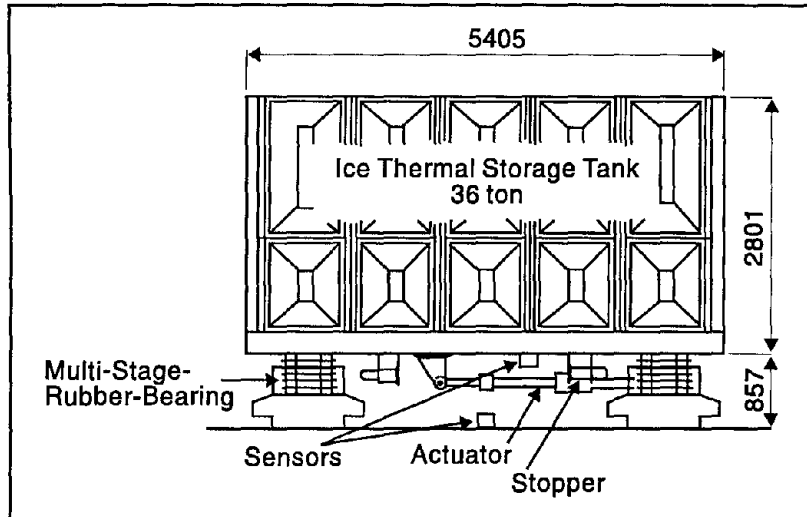
Higashino and Aizawa, 1993
■ Figure 7.5 Elevation of AMD

Sufficient data were obtained for evaluation of the AMD performance when the building was subjected to strong wind on March 29, 1993, with peak instantaneous wind speed of 30.6 m/sec. An example of the recorded time histories is shown in Figure 7.6, giving both the uncontrolled and controlled states. Their Fou-
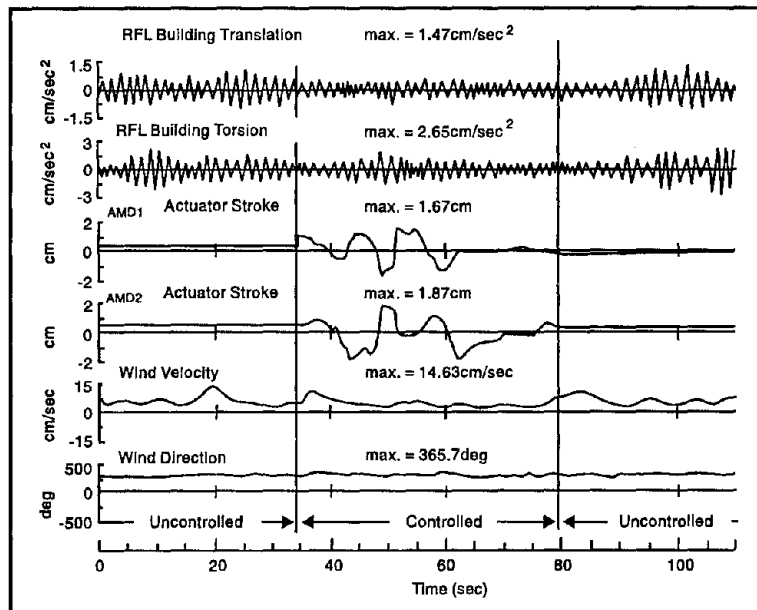
Higashino and Aizawa, 1993
■ Figure 7.6 Response Time Histories (March 29, 1993)

rier spectra using samples of 30-second duration are shown in Figure 7.7, again showing good performance in the low frequency range. The response at the fundamental mode was reduced by 18% and 28% for translation and torsion, respectively. Similar performance characteristics were observed during a series of earthquakes recorded in 1993.
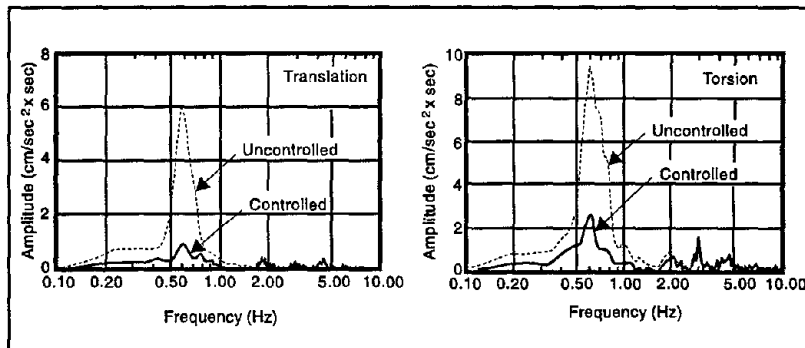
Higashino and Aizawa, 1993
■ Figure 7.7 Response Fourier Spectra (March 29, 1993)
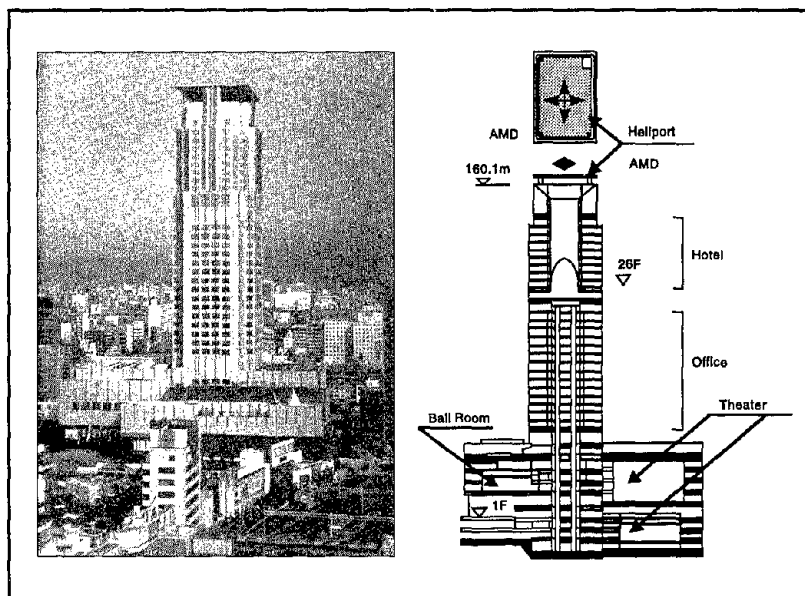
Higashino and Aizawa, 1993
■ Figure 7.8 Hankyu Chayamachi Building

The 160m 34-story Hankyu Chayamachi building (Figure 7.8) in Osaka, Japan (Building No. 4 in Appendix B), also uses an HMD system. In this case, the heliport at the roof top is utilized as the moving mass of the HMD, which weights 480 tons and is about 3.5% of the weight of the tower portion. The layout of the HMD is shown in Figure 7.9. The heliport is supported by six multi-stage rubber bearings. The natural period of rubber and heliport system was set to 3.6 seconds, slightly lower than that of the building (3.8 seconds). The active control mechanism used here has the same architecture as that of Sendagaya INTES, namely, scheme of the digital controller, servomechanism and the hydraulic design, except that two actuators of 5-ton thrusts are attached in horizontal orthogonal directions. Torsional control is not considered here.
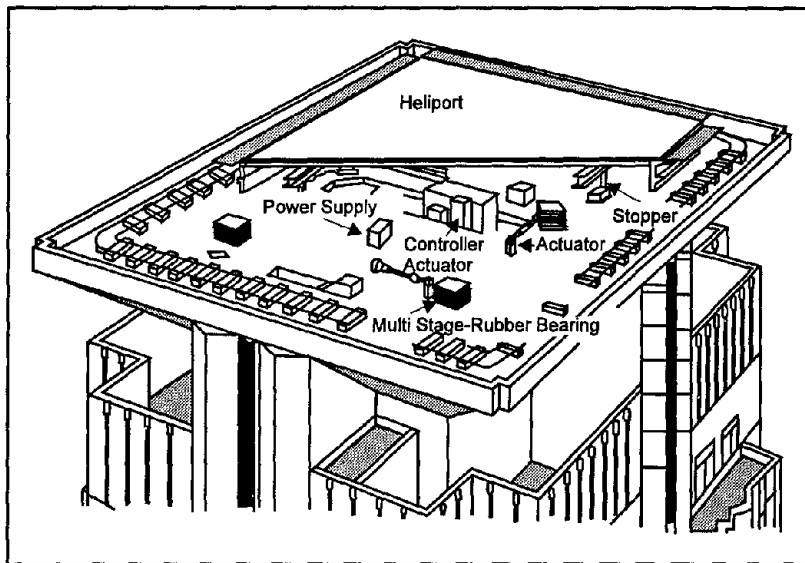
Higashino and Aizawa, 1993
■ Figure 7.9 Layout of HMD

Acceleration Fourier spectra during a recent typhoon are shown in Figure 7.10. Since the building in this case oscillated primarily in its fundamental mode, significant reductions in acceleration levels were expected.

The HMD system installed atop the Ando Nishikicho Building (Building No. 7 in Appendix B) is a dual-mass system, which has been called a DUOX system (Nishimura et al., 1993). It is the combination of an active mass damper (AMD) and a passive tuned
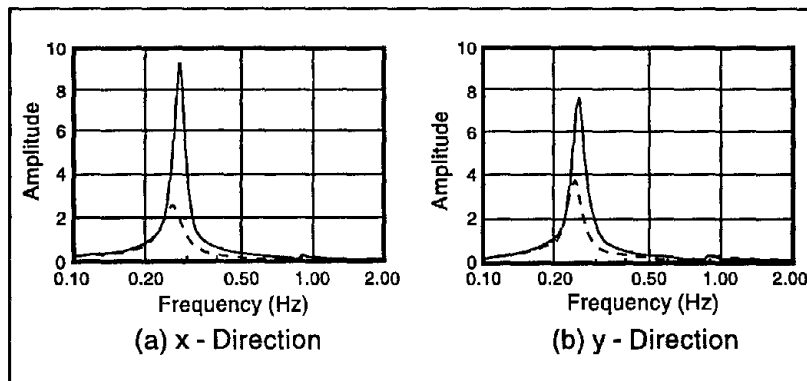
■ Figure 7.10 Acceleration Fourier Spectra

mass damper (TMD) as shown schematically in Figure 7.11. Active force is supplied to the TMD through the AMD driven by an AC servo motor and ball screws. The composition of the bi-direc-
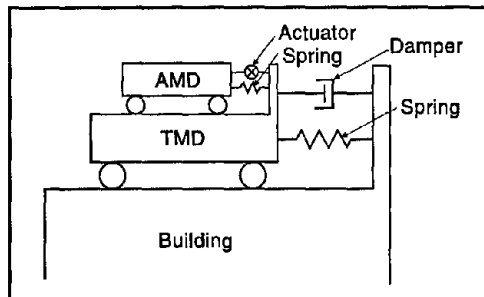
■ Figure 7.11 Principle of DUOX System

tion DUOX system used in this building is shown in Figure 7.12 (Sakamoto and Kobori, 1993). The weight of the device is about 0.8% of the building weight and the weight of the AMD is about 10% of the TMD weight or 0.08% of the building weight. The TMD consists of springs and hollow laminated rubber bearings that also serve as the device supports, and oil dampers that provide damping to the system.

Another variation of the HMD system is the pendulum type which has been installed, among others, in the 70-story Yokohama Land MarkTower (Building No. 8 in Appendix B), the tallest building in Japan (Abiru et al., 1992). Two pendulum systems as schematically shown in Figure 7.13 were installed on the same floor in 1993. Each moving mass is located in the center of a series of concentric steel frames which are connected to each other by ropes provided with natural period control adjustments. Only the outermost frame is fixed to the floor. This multi-stage arrangement is

Upper AMD
(6tf)

Lower AMD
(6tf)

TMD

Control Computer

Oil Damper

Hollow Laminated
Rubber Bearing

Ball Bearing Support

■ Figure 7.12 Composition of DUOX System

Multistage
Pendulum

Weight

Shear Connection
with Uplift Degree
of Freedom

Threaded
Rod

Guide

Electric
Motor
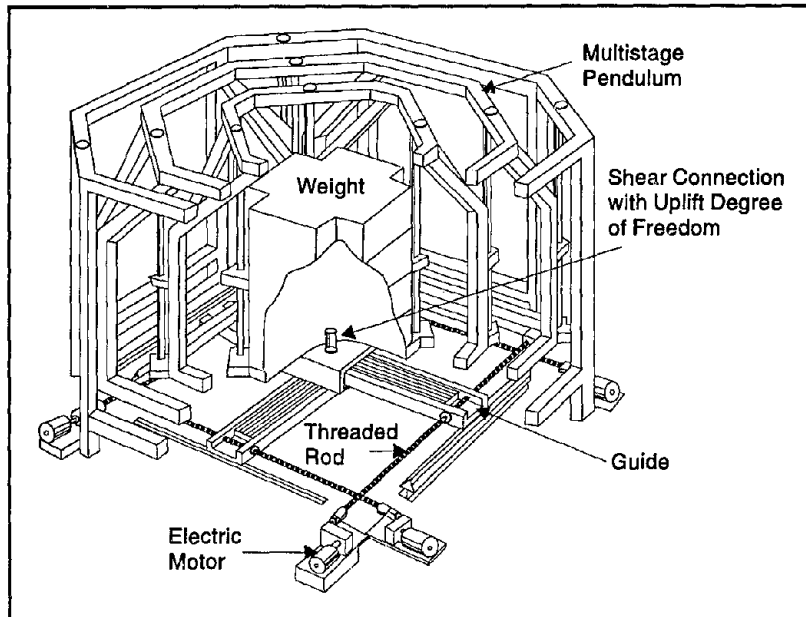
■ Figure 7.13 Pendulum-type HMD

depicted in Figure 7.14 and is used in place of a normal pendulum mechanism in order to decrease the height of the pendulum arm which, as shown in Figure 7.14, requires only 1/3 of the height of a conventional pendulum-type mass damper. The drive device is beneath the moving mass and consists of servomotors, ball screws, an XY-motion mechanism and a universal joint connecting the drive device to the moving mass.
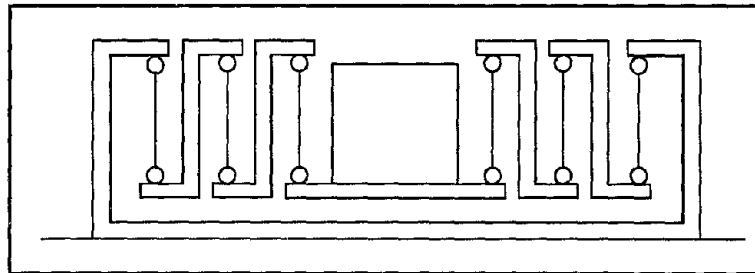
■ Figure 7.14 Multistage Pendulum Mass Damper

7.2

SEMI-ACTIVE FLUID DAMPERS

The semi-active fluid dampers studied by Symans and Constantinou (1995) are based on the design of the passive fluid damping device discussed in Section 4.4 and shown in Figure 3.16c. As a semi-active device, the passive damper was modified by including an external bypass loop containing a control valve as shown in Figure 7.15. Two semi-active damper systems were developed: a two-stage damper utilizing a solenoid valve; and a variable damper utilizing a direct-drive servovalve. Physical characteristics of the dampers include a cylinder length of about 19.0 cm, a stroke of ±7.62 cm, and a maximum output force of 8,900 N.

The damping characteristics of the two-stage damper are controlled by varying the amount of flow passing through the external bypass loop using an AC controlled solenoid valve. The solenoid valve can either be turned on (solenoid valve open) or off (solenoid valve closed). Therefore, only two levels of damping are available from the system. The control valve used on the variable

damper is a direct-drive servovalve which can be off (valve closed), full on (valve open), or between off and fully on (valve partially open). Therefore, a full range of damping levels is available from the system.
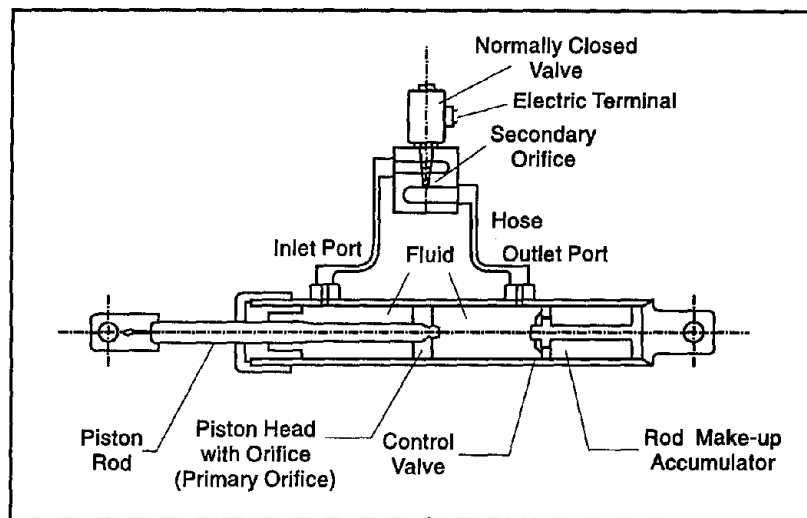
Symans and Constantinou, 1995

■ Figure 7.15 A Semi-Active Fluid Viscous Damper

The mechanical properties of the two-stage damper and the variable damper were obtained by subjecting the dampers to both sinusoidal and constant velocity motions. The relationship between peak velocity and peak force for the variable damper is shown in Figure 7.16 for three different command signal voltages. The data for each command signal voltage level can be fit with straight lines having a slope equal to the corresponding damping coefficient.

In the shaking table tests on a one-story model structure with semi-active control provided by two-stage dampers, the command signal was switched between off (digital 0) and on (digital 1). This is shown in Figure 7.17 for the one-story structure subjected to harmonic input motion and controlled according to the base shear coefficient control algorithm. Under this control algorithm, the valve is switched on (low damping) when the base shear coefficient exceeds a specified limit (BSCLIM) which, in this case, had a value of 0.08. One may note the interesting response of the
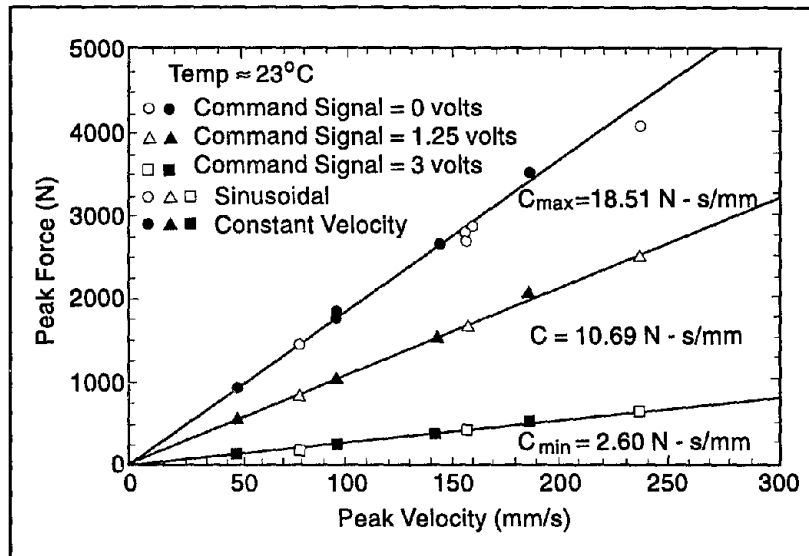
■ Figure 7.16 Experimental Values of Peak Force vs. Peak Velocity

structure in the test results shown in Figure 7.17. Apparently the response contains two distinct frequencies, one at the driving frequency of the input and the other at the natural frequency of the structure. This behavior can be explained by the observation that the drift time history builds up steadily (under high damping) and then, when the base shear coefficient exceeds 0.08, the valves open, initiating a bi-harmonic motion. The bi-harmonic motion is clearly present in the drift time history and in the Fourier amplitude spectrum of the drift. The two harmonics that are present in the response correspond to the driving frequency of the input (5 Hz) and the natural frequency of the structure (about 2.5 Hz). Apparently, the modification of damping during the semi-active control test initiated, in addition to the steady-state response at the frequency of the input, a transient response corresponding to the natural frequency of the structure. It has been shown analytically that this bi-harmonic motion is the result of time delays in the system (Symans and Constantinou, 1995). Interestingly, this behavior was not observed with any other input motion or control algorithm and it was eliminated when time delay compensation was used.
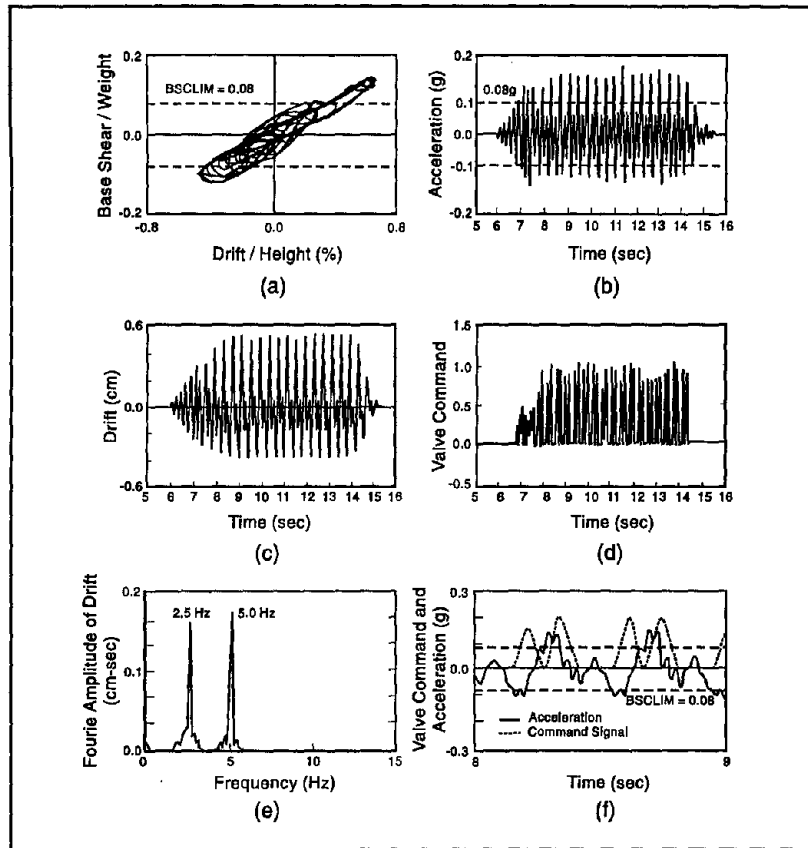
Symans and Constantinou, 1995

■ Figure 7.17 Test Results for Two-Stage Dampers

Two tests are compared in Figure 7.18 for the one-story structure with two-stage dampers subjected to 50% of the Hachinoche ground motion. In one case, the valves are closed to provide high damping while in the second case the base shear coefficient algorithm is employed with a base shear coefficient limit of 0.1. The peak base shear is reduced by about 6% while the peak drift is increased by about 6%. Therefore, the semi-active control was marginally effective in meeting the objective of reducing the peak base shear. However, a penalty is paid in terms of an increase in story drift. Note that time delay compensation was not utilized in the semi-active control test. Further, note that the effectiveness of the semi-active control system is being evaluated based on comparisons with a high damping passive control sys-
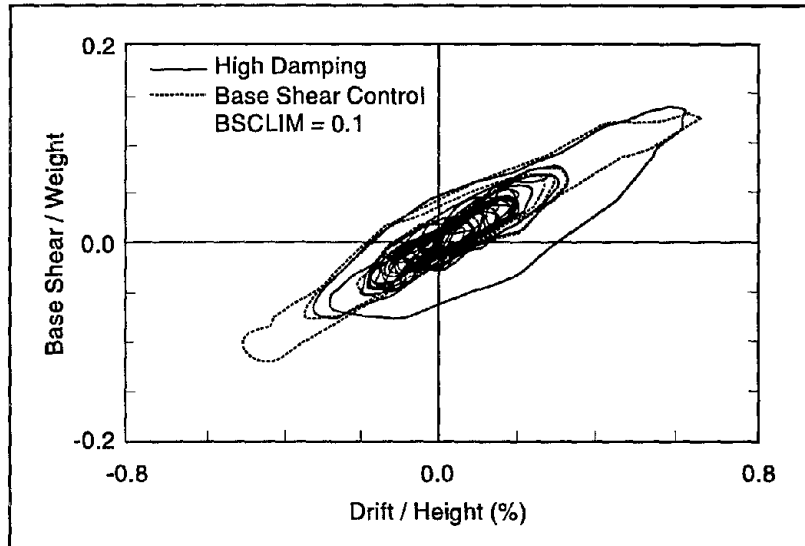
Symans and Constantinou, 1995

▓ Figure 7.18 Base Shear-Drift Loops for High Damping Passive Case and Base Shear Control Case

tem. When comparisons were made with the bare frame response, dramatic reductions in response were observed with the semi-active control system.

In shaking table testing of a three-story model structure with semi-active control provided by variable dampers, a variety of control algorithms were tested, all produced significant response reductions in comparison to the bare frame response. However, the response of the semi-actively controlled structure was nearly identical to the structure with a properly designed passive damping system. For example, Figure 7.19 compares the peak response of the structure subjected to 50% of the Hachinoche ground motion and controlled by various control systems (BF = bare frame, LD = passive low damping viscous system, HD = passive high damping viscous system, OPT = optimal control algorithm, SMC = sliding mode control algorithm).

Functionally similar to a semi-active fluid device, the active variable stiffness system (AVS) developed by Kobori et al., (1993) is designed to maintain nonresonant state of the structure under seismic excitations by altering the structural stiffness based on information provided by the seismic ground motions. For a three-story structure schematically shown in Figure 7.20a, the AVS

Excitation: 50% Hachinohe

a)

Floor

3
2
1
0

0.0   0.2   0.4

3
2
1
0

0.0 0.1   0.2 0.3

3
2
1
0

0.0 0.5 1.0 1.5

———— BF
- - - - - LD
·············· HD

b)

Floor

3
2
1
0

0.0   0.2   0.4

3
2
1
0

0.0 0.1   0.2 0.3

3
2
1
0

0.0 0.5 1.0 1.5

———— BF
- - - - - OPT
·············· SMC

c)

Floor

3
2
1
0

0.0   0.2   0.4
Acceleration (g)

3
2
1
0

0.0 0.1   0.2 0.3
Story Shear / Weight

3
2
1
0

0.0 0.5 1.0 1.5
Story Drift / Height (%)

———— HD
- - - - - OPT
·············· SMC
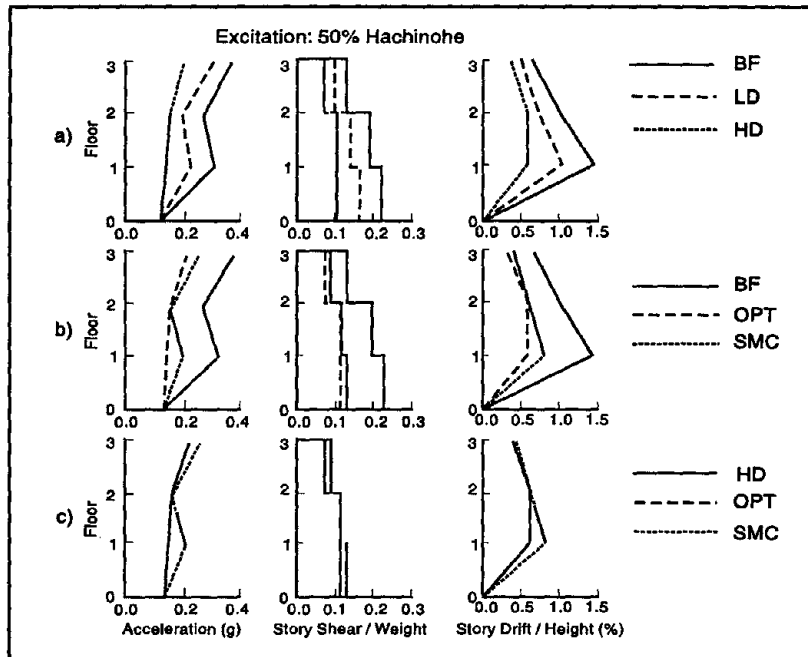
Symans and Constantinou, 1995

■ Figure 7.19   Comparison of Peak Response Profiles for Three-Story Structure

Beam

Bracket   Valve   Control Signal

Oil

Rod

Piston
Cylinder Tube

Brace

Detail A.

VSD

(a) AVS with Braces   (b) AVD System
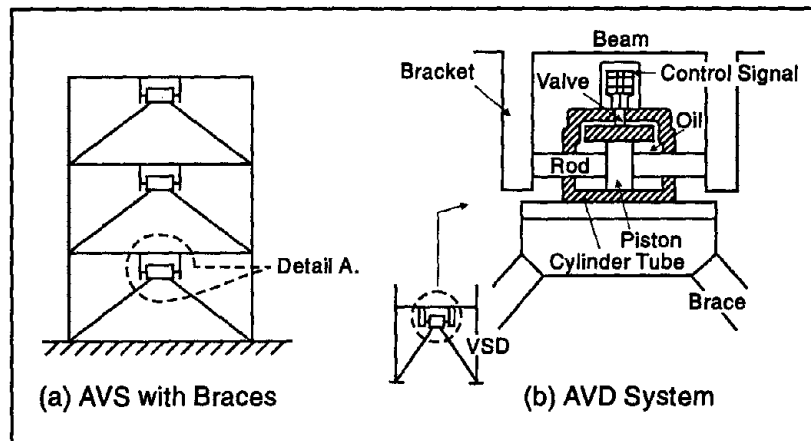
Kobori et al., 1993

■ Figure 7.20   A Semi-active Variable Stiffness System

device, connected between the inverted V-shaped bracing system
and the floor beams at each floor, is used to switch between two
different stiffness states according to the opening or closing of the
valve in a cylinder lock device as shown in Figure 7.20b. The switch-

ing action is taken based on real-time analysis of the seismic ground motion so that optimal stiffness is selected from within a range of structural stiffnesses in order to attain the lowest vibration level.

The AVS system was tested on a scaled three-story model structure and was subsequently installed in a full-scale building in Tokyo in 1990 (Building No. 2 in Appendix B) (Kobori et al., 1993). A view of the building is shown in Figure 7.21 and the overall AVS system configuration is shown in Figure 7.22, where AVS devices are installed on both sides of the structure in the longitudinal direction. The building underwent several recent earthquakes. The performance of the AVS system during a 1991 earthquake was good as the stiffness selection was appropriate for the earthquake;
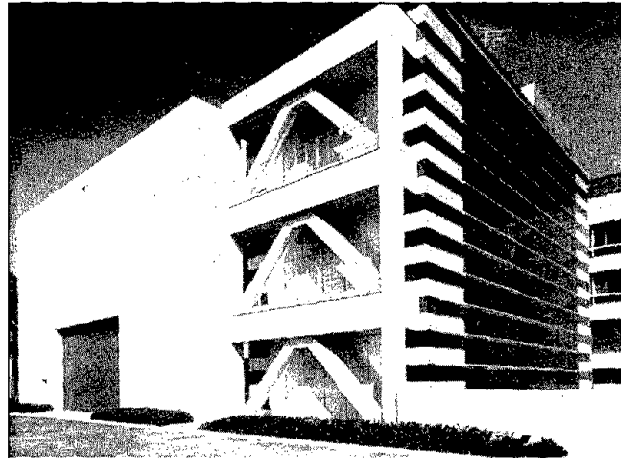
Kobori et al., 1993
■ Figure 7.21 KaTRI No. 21 Building

however, its performance during a 1992 earthquake was less satisfactory due to improper stiffness selection and impulsive nature of the earthquake. One of the major limitations of the AVS system as described by Yamada and Kobori (1995) is that abrupt switching between the two stiffness states induces impulsive forces, causing acceleration pulses which can be detrimental to the structure and its contents. Additionally, the AVS device dissipates energy due to the flow of oil within the hydraulic mechanism whenever the valve is opened or closed to disengage or engage the braces. The increased damping is inherent in this AVS device and thus cannot be independently controlled with respect to stiffness changes.
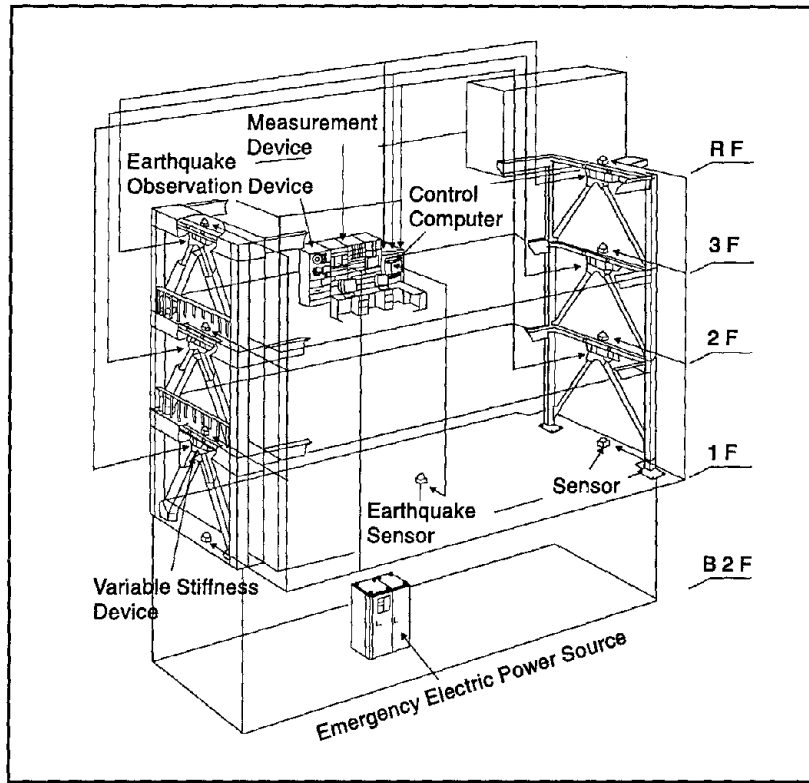
Kobori et al., 1993

■ Figure 7.22 AVS System Configuration

A more desirable variable stiffness system is clearly one in which the structural stiffness can be changed continuously. One such system is currently being developed (Nagarajaiah, 1995), which consists of a nonlinear spring in parallel with a passive friction damper. The nonlinearity of the spring is varied by a self equilibrating mechanical device which is controlled by a servo-motor perpendicular to its axis.

A variable damping system (AVD) has also been proposed (Kurino et al., 1996). The AVD device consists of a variable hydraulic damper and a digital damping force controller. The variable hydraulic damper controls the damping force by tuning the opening of a flow control valve between two chambers in a hydraulic cylinder. Since the controller directly controls the damping force using the information of actual valve opening and oil

pressure, the influences of oil temperature and excitation frequency are eliminated. The controller also has the advantage that characteristics of the AVD device can be easily adjusted by changing the control gain. A schematic diagram of the AVD device is shown in Figure 7.23 and it can be installed in a structure in a similar configuration as an AVS device as shown in Figure 7.20a.
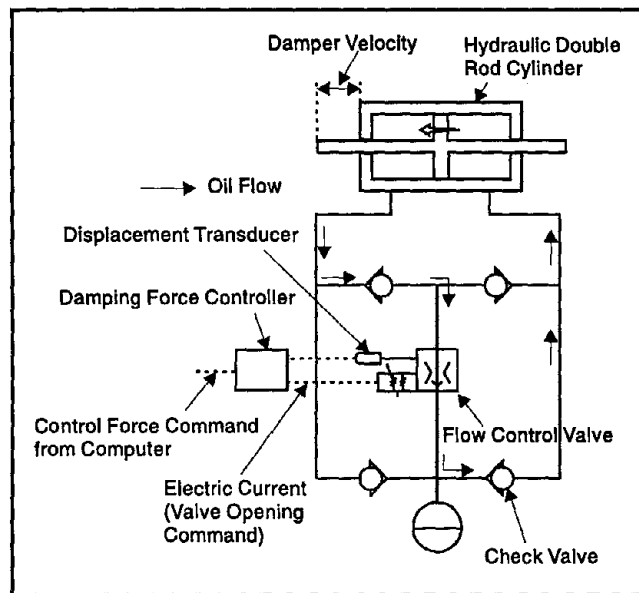
Kurino et al., 1996

■ Figure 7.23 AVD Device Configuration

An analytical and experimental study of a semi-active fluid damper was carried out by Sack and Patten (1993). As shown in Figure 7.24, the configuration of the damper includes a balanced piston rod and an external control valve containing an orifice which is modulated by a small motor. In Sack and Patten (1993), a control algorithm is described in which the control of the adjustable orifice involves the linearization of the damper dynamics. Through this process of dynamic linearization, the variable orifice is adjusted in such a way that the damper delivers a force which is directly proportional to the relative velocity of the piston, thus causing the damper to behave as a linear viscous damper.
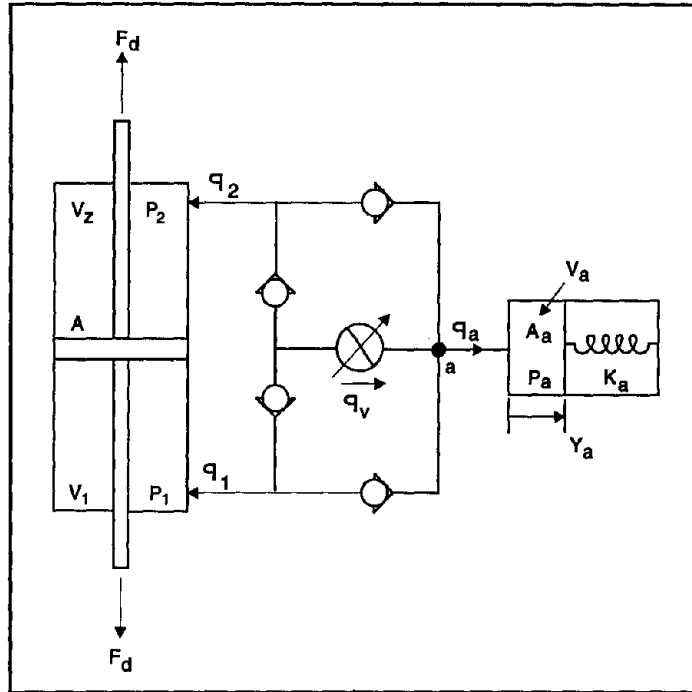
Sack and Patten, 1993

■ Figure 7.24 Schematic of a Semi-Active Fluid Damper

A modified version of this semi-active fluid damper was examined in connection with mitigating vibration of bridges under traffic loads (Patten et al., 1996). A simple bridge span with a generic truck travel on it is shown in Figure 7.25. Two dynamic models of the vehicle/bridge system were used. First, the model of the vehicle was treated as an assemblage of sprung and unsprung masses, interconnected with compliant chassis elements. Secondly, the dynamic effects of the truck's suspension were disregarded. Simulations were conducted using parameters for the bridge and truck that mimic a typical U.S. interstate bridge with deep steel beams and a composite concrete roadway. The results indicate that the control fixturing arms should be made as long as possible, and a double actuator assembly provides little advantage over a single actuator configuration.

Similar studies were conducted for a continuous two-span bridge with the same cross section. The simulations indicate that a
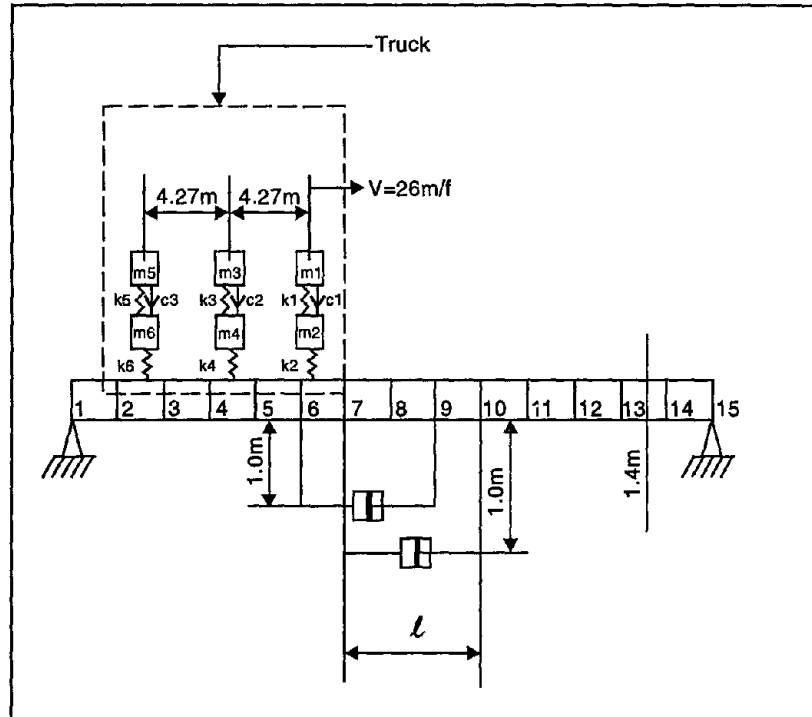
Patten et al., 1996

■ Figure 7.25 Single-Span Bridge with Compliant Truck Model and Double Actuator Arrangement

semi-active system using a bistate control scheme achieved a 60% reduction in deflection due to truck traffic. A comparison of simulations using both a traveling force model and a compliant suspension model revealed a similarity in plotted responses. A revealing result of the two-span study is shown in Figure 7.26. Note that the bistate control tends to decrease the magnitude below the first natural frequency and significantly shift the natural frequencies, especially the second and higher modes. These significant structural changes are not accomplished using a passive damper since the bistate control tends to add stiffness to the structure, which manifests itself in lesser response and a shift in the modal content of the system. This work has led to the installation of such a system on a two-lane segment of I-35 crossing the Walnut Creek in Oklahoma for the purpose of increasing load capacity and service life of the bridge under traffic loads.

■ Figure 7.26   Transfer Functions for a Continuous Two-Span Bridge with: (a) No Control, (b) Passive Damper, (c) Bistate Control

APPENDIX A

STRUCTURAL APPLICATIONS OF PASSIVE
ENERGY DISSIPATION IN NORTH AMERICA

■ Table A.1 Metallic Dampers

Name and Type of Structure	Location	Type and Number of Dampers	Date of Installation	Load	Additional Information
Cardiology Hospital Bldg. Reinforced concrete frames Five stories and basemat Constructed in 1970s	Mexico/ Mexico City	ADAS (yielding steel) Total: 90	1990	Seismic	Retrofit; damaged in 1985 earthquake Retrofit completed while allowing continuous operation of hospital Nonlinear time history dynamic analysis conducted
Izazaga #38-40 Bldg. Reinforced concrete frame with brick infilled end walls 12 stories + basement 1200m² plan Constructed late 1970s	Mexico/ Mexico City	ADAS (yielding steel) Total: approx. 200	1990	Seismic	Retrofit; damaged in 1985, 1986, & 1989 earthquakes 2D nonlinear time-history analysis for final verification Retrofit complete during building occupation Fundamental periods(analysis) Original: 3.82, 2.33s Upgraded: 2.24, 2.01s Maximum interstory drift reduced by 40%
IMSS Reforma #476 Bldg. Mexican Institute for Social Security Three bldg. complex Reinforced concrete frame 10 stories + basement Constructed in 1940s	Mexico/ Mexico City	ADAS (yielding steel) Total: approx. 400	1992	Seismic	Retrofit; significant damage in 1957 earthquake National Register of Classical Buildings 2D nonlinear time-history analysis

Name and Type of Structure	Location	Type and Number of Dampers	Date of Installation	Load	Additional Information
Wells Fargo Bank Bldg. Nonductile concrete frame Two-story; 14,000 ft^2 Constructed in 1967	CA/ San Francisco	ADAS (yielding steel) Total: 7 Design Yield Force: 150 kips	1992	Seismic	Retrofit; damaged in 1989 Loma Prieta earthquake Fundamental periods (analysis): Original: 0.84, 0.65, 0.36s Upgraded: 0.45, 0.44, 0.23s 3D elastic and 2D nonlinear analysis conducted

■ Table A.2 Friction Dampers

Name and Type of Structure	Location	Type and Number of Dampers	Date of Installation	Load	Additional Information
Gorgas Hospital	Panama	Friction Dampers Total: 2	1970s	Seismic	

McConnel Bldg.,
Concordia University
library complex,
RC frames w/flat slab
Interconnected
10 and 6-story bldgs.
Constructed in 1987-1991
	Canada/
	Montreal
		Pall Friction Dampers
		Total: 143
		Slip loads: 600-700 kN
			1987	Seismic	Equiv. damping ratio: 52%
					  for artificial 0.18g earthquake
					Net savings: 1.5% of total
					  bldg. cost of $65M
					3D nonlinear dynamic
					  analysis conducted

Residential House
2-story and basement
  wood stud, brick veneer
	Canada/
	Montreal
		Pall Friction Dampers
		Total: 15 friction
		  base isolators
			1988	Seismic	New construction

Ecole Polyvalante
3 precast concrete,
  three-story bldgs.
Constructed in 1967
	Canada/Sorel	Pall Friction Dampers
		Total: 64
		Slip loads: 225-335 kN
		
		Pall Friction Panel
		Connectors
		Total: 388
		Slip loads: 30-55 kN
			1990	Seismic	Retrofit; bldgs. damaged in
					  1988 Saguenay earthquake
					Design for 0.18g peak
					  ground acceleration
					Nonlinear time-history
					  dynamic analysis conducted
					Net savings: 40% in
					  retrofitting costs

Canadian Information and Travel Center 4-story steel frame Constructed in 1992	Canada/Laval	Pall Friction Dampers Slip load: 350 kN	1992	Seismic	New construction

Name and Type of Structure	Location	Type and Number of Dampers	Date of Installation	Load	Additional Information
Department of Defense 3-story concrete frame Constructed in 1992	Canada/Ottawa	Pall Friction Dampers Slip load: 500 kN	1992	Seismic	New construction
Canadian Space Agency Structural steel frames w/prefabricated aluminum panels, 3 stories, 135m x 78m plan Constructed in 1992	Canada/ St. Hubert (near Montreal)	Pall Friction Dampers Total: 58 Slip load: 500kN	1993	Seismic	Building houses sensitive and expensive equipment 40 dampers exposed to view for aesthetic purposes 3D nonlinear time history dynamic analysis conducted
Casino de Montreal former French Pavilion for Expo '67 8-story steel frame Constructed in 1967	Canada/ Montreal	Pall Friction Dampers Total: 32 Slip load: 700-1800 kN	1993	Seismic	Highly eccentric rigidity Retrofit to comply with current code standards
Building 610, Stanford University 1-story stucco/brick Constructed in 1915	CA/Palo Alto	Slotted Bolted Conn. Total: 80 Slip load: 12kips	1994	Seismic	Retrofit Damaged in 1989 Loma Prieta earthquake
Hoover Building, Stanford University 2-story+2-story basement Constructed in 1966	CA/Palo Alto	Slotted Bolted Conn. Total: 8	1994	Seismic	Retrofit Second level braced frame damaged in 1989 Loma Prieta earthquake

■ Table A.2 Friction Dampers (continued)

Name and Type of Structure	Location	Type and Number of Dampers	Date of Installation	Load	Additional Information
Maison 1 McGill 11-story RC frame Constructed in 1995	Canada/ Montreal	Pall Friction Dampers Total: 65 Slip load: 600-700 kN	1995	Seismic	New construction
Ecole Technologie Superieure Two steel frame bldgs. Constructed in 1949 and 1977	Canada/ Montreal	Pall Friction Dampers Total: 74 Slip load: 700 kN	1995	Seismic	Retrofit
Federal Building 4-story RC frame Constructed in 1950	Canada/ Sherbrooke	Pall Friction Dampers Total: 30 Slip load: 350 kN	1995	Seismic	Retrofit
Desjardin Life Ins. Bldg. 6-story RC frame Constructed in 1995	Canada/ Quebec	Pall Fricton Dampers Total: 30 Slip loads: 600-700 kN	1995	Seismic	New construction
Water Tank Overhead steel tower Constructed in 1950	WA/Beaux Arts	Pall Friction Dampers Total: 12 Slip load: 75 kN	1995	Seismic	Retrofit
St. Luc Hospital 5-story RC frame raised to 8 stories Constructed in 1975	Canada/ Montreal	Pall Friction Dampers Total: 34 Slip loads: 600-700 kN	1995	Seismic	Retrofit

Name and Type of Structure	Location	Type and Number of Dampers	Date of Installation	Load	Additional Information
Residence Maison-Neuve 6-story steel frame Constructed in 1972	Canada/ Montreal	Pall Friction Dampers Total: 42 Slip loads: 500 kN	1996	Seismic	Retrofit
Hamilton Courthouse 8-story steel frame Constructed in 1934	Canada/ Hamilton	Pall Friction Dampers Total: 73 Slip loads: 500-700 kN	1996	Seismic	Retrofit
Water Tanks, Univ. of CA at Davis Overhead 120-ft steel towers Constructed in 1958	CA/Davis	Pall Friction Dampers Total: 48 Slip loads: 135-160 kN	1996	Seismic	Retofit
Harry Stevens Building 3-story concrete frame building	Canada/ Vancouver	Pall Friction Dampers Total: 38 Slip loads: 350-500 kN	1996	Seismic	Built in 1957; rehabilitated in 1996
Justice Headquarters 8-story concrete frame building	Canada/ Ottawa	Pall Friction Dampers Total: 84 Slip loads: 500-700 kN	1996	Seismic	Built in 1951; rehabilitated in 1996
BCBC Selkirk Waterfront Office Buildings Two 5-story steel frame buildings	Canada/ Victoria	Pall Friction Dampers Total: 74 Slip loads: 700-1,400 kN	1997	Seismic	New
Maisons de Beaucours 6-story concrete frame building	Canada/ Quebec City	Pall Friction Dampers Total: 42 Slip loads: 500-600 kN	1997	Seismic	New
Maison Sherwin William 6-story concrete frame building	Canada/ Montreal	Pall Friction Dampers Total: 64 Slip loads: 400-500 kN	1997	Seismic	Built in 1950; rehabilitated in 1997

■ Table A.3 Viscoelastic Dampers

Name and Type of Structure	Location	Type and Number of Dampers	Date of Installation	Load	Additional Information
World Trade Center Tubular steel frame, twin towers 110 stories	NY/ New York City	3M Viscoelastic Dampers Total: approx. 20,000 Evenly distributed from 10th-110th floor	1969	Wind	Damping ratio with dampers: 2.5-3%
Columbia SeaFirst Bldg. Composite concrete columns with steel frame 76 stories	WA/Seattle	3M Viscoelastic Dampers Total: 260	1982	Wind	New construction
Two Union Square Bldg. Steel frame 60 stories	WA/Seattle	3M Viscoelastic Dampers Total: 16	1988	Wind	New construction
School Bldg. 2 stories	AZ/Phoenix	Viscoelastic Beam/ Column Connections	1992	Seismic	New construction
Santa Clara County Bldg. Steel frame 13 stories 51m x 51m plan Constructed in 1976	CA/San Jose	3M Viscoelastic Dampers Total: 96	1993	Seismic	Retrofit Damping ratio in fundamental mode Original: less than 1% Upgrade: approx 17%

Name and Type of Structure	Location	Type and Number of Dampers	Date of Installation	Load	Additional Information
Navy Office/Supply Bldg. Nonductile concrete 3 stories 121 ft x 365 ft plan	CA/San Diego	3M Viscoelastic Dampers Total: 64	1996	Seismic	Upgrade
Hall of Justice and Records 8-story steel frame Constructed in mid-1960's	CA/ Redwood City	3M Viscoelastic Dampers Total: 44	1996	Seismic	Upgrade
Los Angeles Police Dept. Recruit Training Center 4-story steel frame	CA/Los Angeles	3M Viscoelastic Dampers	1997	Seismic	Upgrade
3M Mexico Steel/Concrete Frame 8 stories	Mexico City, Mexico	3M Viscoelastic Dampers Total: 21	1998	Seismic	New construction

■ Table A.4 Viscoelastic Fluid Dampers

Name and Type of Structure	Location	Type and Number of Dampers	Date of Installation	Load	Additional Information
North American Air Defense Command	CO/Cheyenne Mountain	Spring mounted with Taylor Fluid Dampers	1984	Nuclear Shock	Classified
Rich Stadium	NY/ Buffalo	Taylor Fluid Dampers Total: 12 50 kN, ± 460mm stroke	1993	Wind	Dampers connect light poles to the stadium parapet wall
Pacific Bell North Area Operation Center 3-story steel braced frame	CA/ Sacramento	Taylor Fluid Dampers Total: 62 130 kN, ± 50mm stroke	1995	Seismic	New construction, three-story steel braced frame Devices used to dissipate seismic energy
San Bernardino County Medical Center 5 steel-frame buildings	CA/ San Bernardino	Taylor Fluid Dampers Total: 184 1,400 kN, ± 600mm stroke	1996	Seismic	New construction, devices used to enhance energy dissipation in rubber bearing isolation system
Woodland Hotel 4-story Non-Ductile RC frame/shear wall Constructed in 1927	CA/ Woodland	Taylor Fluid Dampers Total: 16 450 kN, ± 50mm stroke	1996	Seismic	Seismic upgrade of historic structure
San Francisco Opera House	CA/ San Francisco	Enidine Fluid Dampers Total: 16 400 kip, ±3 in stroke	1996	Seismic	Retrofit

Name and Type of Structure	Location	Type and Number of Dampers	Date of Installation	Load	Additional Information
Science Building II	CA/ Sacramento	Taylor Fluid Dampers Total: 40 200 kN, ±50mm stroke	1996	Seismic	New construction
Langenbach House	CA/Oakland	Taylor Fluid Dampers Total: 4 130 kN, ±150mm stroke	1996	Seismic	New construction, included in base isolation
Gerald Desmond Bridge	CA/Long Beach	Enidine Fluid Dampers Total: 258 50 kip, ±6 in stroke	1996	Seismic	Retrofit
28 State Street 35-story steel frame	MA/Boston	Taylor Fluid Dampers Total: 40 670 kN, ±25 mm stroke	1996	Wind	Retrofit
The Money Store 11-story steel frame	CA/Sacramento	Taylor Fluid Dampers Total: 120 1,290 kN, ±64 mm stroke 710 kN, ±64 mm stroke	1996	Seismic	New construction
Kaiser Data Center	CA/ Corona	Taylor Fluid Dampers Total: 16 425 kN, ±560 mm stroke	1996	Seismic	Seismic retrofit with dampers used to add energy disspation to rubber bearing isolation system
Civic Center Building	CA/ San Francisco	Taylor Fluid Dampers Total: 292 1,000 kN, ±100 mm stroke 550 kN, ±100 mm stroke	1997	Seismic	New construction

■ Table A.4 Viscoelastic Fluid Dampers (continued)

Name and Type of Structure	Location	Type and Number of Dampers	Date of Installation	Load	Additional Information
Hayward City Hall	CA/Hayward	Taylor Fluid Dampers Total: 15 1,400 kN, ±600 mm stroke	1997	Seismic	New construction; devices used to enhance energy dissipation in Friction Pendulum isolation system.
Quebec Iron and Titanium Smelter	Canada/ Tracy	Taylor Spring Dampers and Taylor Dampers Total: 22 450 kN, ±64 mm stroke 225 kN, ±100 mm stroke 130 kN, ±100 mm stroke	1997	Seismic/ Wind	Dual purpose spring dampers used for seismic and wind protection of two smelter buildings. Dampers used to prevent buildings from impacting during a seismic event.
CSULA Administration Building	CA/Los Angeles	Taylor Fluid Dampers Total: 14 1,100 kN, ±75 mm stroke	1997	Seismic	Seismic upgrade to office building. Dampers used in chevron bracing elements to dissipate seismic energy.
First Avenue South Bridge	WA/Seattle	Taylor Fluid Dampers Total: 4 600 kN, ±635 mm stroke	1997	Kinetic Energy of Moving Bridge	Retrofit of a bascule bridge to protect the bascule leafs from runaway motors and brake failures.
Alaska Commercial Building	Alaska	Taylor Fluid Dampers Total: 2 445 kN, ±64 mm stroke	1997	Seismic	Retrofit of a timber frame structure. Dampers used in diagonal bracing to dissipate earthquake energy.
Studio Parking Garage	CA/Los Angeles	Taylor Fluid Dampers Total: 2 150 kN, ±50 mm stroke	1997	Seismic	Dampers used to allow thermal motion, concrete expansion/contraction and creep, while controlling earthquake movement.

Name and Type of Structure	Location	Type and Number of Dampers	Date of Installation	Load	Additional Information
Rockwell Building 505	CA/ Newport Beach	Taylor Fluid Dampers Total: 6 320 kN, ±64 mm stroke	1997	Seismic	Retrofit of a long building with multiple expansion gaps. Dampers restrict relative movement between building sections.
Santiago Creek Bridge	CA	Enidine Fluid Dampers	1998	Seismic	New construction
3COM Corp. Data Center 4-story	CA	Enidine Fluid Dampers Total: 63 300 kips, ±2 in stroke	1998	Seismic	New construction
Los Angeles City Hall 28-story steel frame Constructed in 1927	CA/Los Angeles	Taylor Fluid Dampers Total: 68 1,400 kN, ±600 mm stroke 1,000 kN, ±115 mm stroke	Sched. 1998	Seismic	Retrofit; dampers used to enhance energy dissipation in elastomeric isolation system and as energy dissipation elements in the upper structure.
The Golden Gate Bridge	CA/ San Francisco	Fluid Dampers Total: approx. 40 650 kips, ±24 in stroke	To be determined	Seismic	Retrofit
Vincent Thomas Bridge	CA/ Long Beach	Enidine Fluid Dampers Total: 48 160-250 kips ±30 in, ±40 in stroke	1998-1999	Seismic	Retrofit
I-5/91 HOV Bridge	USA/Anaheim, CA	Taylor Fluid Dampers Total: 8 1,110 kN, ±200 mm stroke	To be installed 1998	Seismic	New bridge uses dampers to dissipate earthquake energy for reduced demands on the structure.

■ **Table A.4 Viscoelastic Fluid Dampers (continued)**

Name and Type of Structure	Location	Type and Number of Dampers	Date of Installation	Load	Additional Information
Sidney Lanier Bridge	GA/ Glynn County	Taylor Fluid Dampers Total: 4 2,200 kN, ±203 mm stroke	To be installed 1998	Seismic	New bridge utilizes dampers to control earthquake movement and distribute forces while allowing free thermal movement.
Maysville Bridge	KY/ Maysville	Taylor Fluid Dampers Total: 8 1,300 kN, ±305 mm stroke	To be installed 1998	Seismic	New bridge utilizes dampers to control earthquake movement and distribute forces while allowing free thermal movement.
Cape Girardeau Bridge	MO/ Cape Girardeau	Taylor Fluid Dampers Total: 16 6,700 kN, ±180 mm stroke	To be installed 1998	Seismic	New construction of a cable-stayed bridge. Dampers used to control longitudinal earthquake movement while allowing free thermal movement.
Ferry Street Bridge	OR/ Eugene	Taylor Fluid Dampers Total: 4 500 kN, ±40 mm stroke	To be installed 1998	Seismic	Retrofit of a bridge over the Willamette River. Dampers used to control earthquake movement while allowing free thermal movement.
UCLA-Knudsen Hall	CA/ Los Angeles	Taylor Dampers Total: 84 355 kN, ±100 mm stroke 245 kN, ±100 mm stroke	To be installed 1998	Seismic	Seismic upgrade of a University building. Dampers used in chevron bracing elements to dissipate earthquake energy.
San Francisco-Oakland Bay Bridge, East Span	CA/ San Francisco	Taylor Dampers Total: 6 890 kN, ±406 mm stroke	To be installed 1998	Seismic	Interim retrofit of East Bay 504 truss sections. Dampers used to dissipate seismic energy.

Name and Type of Structure	Location	Type and Number of Dampers	Date of Installation	Load	Additional Information
Tillamook Hospital	OR/ Tillamook	Taylor Fluid Dampers Total: 30 135 kN, ±50 mm stroke	To be installed 1998	Seismic	Retrofit of an existing hospital to meet current seismic protection code levels. Dampers used in chevron braces to dissipate earthquake energy.
New Pacific Northwest Baseball Park	WA/ Seattle	Taylor Fluid Dampers Total: 8 3,600 kN, ±381 mm stroke	To be installed 1998	Seismic	New baseball stadium utilizes dampers to dissipate earthquake energy in each of three movable roof sections.
New Pacific Northwest Baseball Park	WA/ Seattle	Taylor Fluid Dampers Total: 36 1,780 kN, 100 mm stroke 890 kN, 400 mm stroke	To be installed 1998	Wind/ Kinetic Energy	Dampers installed between three roof sections and at end stops to absorb energy from impact due to wind, kinetic energy, and motor drive.
Rio Vista Bridge	CA/ Rio Vista	Taylor Fluid Dampers Total: 8 685 kN, ±254 mm stroke	To be installed 1999	Seismic	Retrofit of a highway bridge to reduce forces and deflections by dissipating earthquake energy.
San Francisco International Airport - Rail Transit System Westside Guideway	CA/ San Francisco	Taylor Fluid Dampers Total: 10 4,225 kN, ±508 mm stroke 3,115 kN, ±508 mm stroke	To be installed 1999	Seismic	New Airport Rail Transit (ART) and Bay Area Rapid Transit (BART) structure implement dampers for earthquake energy dissipation.
San Francisco International Airport - South International Parking Garage Pedestrian Bridge	CA/ San Francisco	Taylor Fluid Dampers Total: 20 445 kN, ±254 mm stroke	To be installed 1999	Seismic	New pedestrian bridge utilizes dampers to dissipate earthquake energy and reduce movement.

■ Table A.5 Tuned Mass Dampers

Name and Type of Structure	Location	Type and Number of Dampers	Date of Installation	Load	Additional Information
CN Tower TV antenna Height: 553m	Canada/Toronto	Tuned Mass Damper	1973	Wind	New construction

John Hancock Tower
  Office building
Height: 244m
Plan: 3600m²
58-stories
	MA/Boston	MTS Tuned Mass
		  Damper
		Two 300-ton lead/
		  steel blocks
			1977	Wind	Retrofit
					Natural freq: 0.14 Hz
					Damping ratio with TMD: 4%

Citicorp Center
  Office building
Height: 280m
Plan: 2600m²
	NY/
	  New York City
		MTS Tuned Mass
		  Damper
		400-ton concrete block
			1978	Wind	New construction
					  Natural freq: 0.16 Hz
					Damping ratios:
					Original: 1%
					  w/TMD: 4%

APPENDIX B

STRUCTURAL APPLICATIONS OF ACTIVE AND SEMI-ACTIVE SYSTEMS IN JAPAN

■ Table B.1 Active and Semi-active Systems Installed in Buildings in Japan

Building Number/ Name/Year	Building Scale	Type[1], Manufacturer and Number	Mass	Support	Driver	Direction
1. Kyobash Seiwa Bldg. 1989	33m, 400 ton, 11 stories	AMD Kajima 2	5 ton	Pendulum	Hydraulic	S&T
2. Kajima Research Inst. Bldg. #21 1990	12m, 400 ton, 3 stories	AVS Kajima 6	——	——	Hydraulic	S
3. Sendagaya INTES Bldg. 1992	58m, 3280 ton, 11 stories	HMD Kayaba 2	72 ton	Rubber Bearing	Hydraulic	S&T
4. Hankyu Chayamachi Bldg. 1992	161m, 13943 ton, 34 stories	HMD Takenaka 1	480 ton	Rubber Bearing	Hydraulic	S&L
5. Kansai Int. Airport Control Tower 1992	86m, 2570 ton, 7 stories	HMD Mitsubishi H.I. 1	5 ton	Pendulum	Servo Motor	S&L
6. Osaka ORC 2000 1992	200m, 56680 ton, 50 stories	HMD Shimizu 2	200 ton	Rubber Bearing	Servo Motor	S&T

Building Number/ Name/Year	Building Scale	Type[1], Manufacturer and Number	Mass	Support	Driver	Direction
7. Ando Nishikicho Bldg. 1993	54m, 2600 ton, 14 stories	HMD Kajima 1	22 ton	Linear Spring	Servo Motor	S&L
8. Yokohama Land Mark Tower 1993	296m, 260610 ton, 70 stories	HMD Mitsubishi H.I. 2	340 ton	Pendulum	Servo Motor	S&L&T
9. Long Term Credit Bank of Japan 1993	30m, 40000 ton, 21 stories	HMD Takenaka 1	195 ton	Rubber Bearing	Hydraulic	S&L
10. Hotel Nikko Kanazawa 1993	131m, 10150 ton, 30 stories	HMD Takenaka 2	100 ton	Rubber Bearing	Hydraulic	S&T
11. Shinjyuku Park Tower 1994	227m, 130000 ton, 52 stories	HMD Ishikawajima H.I. 3	330 ton	Pendulum	Servo Motor	S
12. Hikarigaoka J. City Bldg. 1994	100m, 9360 ton, 24 stories	HMD Ishikawajima H.I. 2	44 ton	Pendulum	Servo Motor	S&L

■ Table B.1 Active and Semi-active Systems Installed in Buildings in Japan (continued)

Building Number/ Name/Year	Building Scale	Type[1], Manufacturer and Number	Mass	Support	Driver	Direction
13. Hamamatsu Act City 1994	212m, 107500 ton, 45 stories	HMD Mitsubishi H.I. 1	180 ton	Pendulum	Servo Motor	S&L&T
14. Riverside Sumida 1994	134m, 52000 ton, 33 stories	AMD Tokiko 2	30 ton	——	Servo Motor	S&T
15. Osaka World Trade Ctr. Bldg. 1994	256m, 80000 ton, 55 stories	HMD Mitsubishi H.I. 2	100 ton	Pendulum	Servo Motor	S&L&T
16. Miyazaki Phoenix Hotel Ocean 45 1994	154m, 83650 ton, 43 stories	HMD Shimizu 2	240 ton	Rubber Bearing	Servo Motor	S&T
17. MHI Yokomama Bldg. 1994	152m, 61800 ton	HMD Mitsubishi H.I. 1	60 ton	Pendulum	Servo Motor	S&L
18. NTT CRED Motomachi Bldg. 1994	150m, 83000 ton	HMD Mitsubishi H.I. 1	80 ton	Pendulum	Servo Motor	S&L

Building Number/ Name/Year	Building Scale	Type[1], Manufacturer and Number	Mass	Support	Driver	Direction
19. Dowa Kasai Phoenix Tower 1995	145m, 26000 ton, 29 stories	HMD Kajima 2	84 ton	Linear Spring	Servo Motor	S&L
20. Rinku Gate Tower North Bldg. 1995	255m, 56 stories	HMD Mitsubishi H.I. 2	160 ton	Pendulum	Servo Motor	S&L
21. Hirobe Miyake Bldg. 1995	31m, 273 ton, 9 stories	HMD Mitsubishi Steel 1	2.1 ton	Linear Spring	Servo Motor	S&L
22. Plaza Ichihara 1995	61m, 5760 ton, 12 stories	HMD Ishikawajima H.I. 2	14 ton	Pendulum	Servo Motor	S&T

Yoshida, 1996
1. AMD: Active Mass Damper
2. AVS: Active Variable Stiffness
3. HMD: Hybrid Mass Damper

REFERENCES

ABAQUS (1997), *Theory Manual*, Hibbitt, Karlsson & Sorensen, Inc., Pawtuckett, RI.

Abiru, H., Fujishino, M., and Matsumoto, T., (1992), "Modal Seismic Response Control of High Rise Building by Active Tuned Mass," *Proceedings of the Tenth World Conference on Earthquake Engineering*, Madrid, Spain, Vol. 4, pp. 2055-2060.

Aiken, I. D. and Kelly, J. M., (1990), *Earthquake Simulator Testing and Analytical Studies of Two Energy-Absorbing Systems for Multistory Structures*, Technical Report UCB/EERC-90/03, University of California, Berkeley, CA.

Aiken, I. D., Kelly, J. M., and Pall, A. S., (1988), *Seismic Response of a Nine-Story Steel Frame with Friction Damped Cross-Bracing*, Technical Report UCB/EERC-88/17, University of California, Berkeley, CA.

Aiken, I. D., Nims, D. K., and Kelly, J. M, (1992), "Comparative Study of Four Passive Energy Dissipation Systems," *Bulletin of the New Zealand National Society for Earthquake Engineering*, Vol. 25, No. 3, pp. 175-192.

Aiken, I. D., Nims, D. K., Whittaker, A. S., and Kelly, J. M., (1993), "Testing of Passive Energy Dissipation Systems," *Earthquake Spectra*, Vol. 9, No. 3, pp. 335-370.

Akbay, Z. and Aktan, H. M., (1991), "Actively Regulated Friction Slip Devices," *Proceedings of the Sixth Canadian Conference on Earthquake Engineering*, pp. 367-374.

Akbay, Z. and Aktan, H. M., (1990), "Intelligent Energy Dissipation Devices," *Proceedings of the Fourth U.S. National Conference on Earthquake Engineering*, Vol. 3, No. 4, pp. 427-435.

Anderson, E. et al., (1992), *LAPACK Users' Guide*, SIAM, Philadelphia, PA.

Applied Technology Council, (1995), *Guidelines and Commentary for the Seismic Rehabilitation of Buildings*, Project ATC-33, 75% complete draft, Redwood City, CA, October.

Arima, F., Miyazaki, M., Tanaka, H., and Yamazaki, Y., (1988), "A Study on Buildings with Large Damping Using Viscous Damping Walls," *Proceedings of the Ninth World Conference on Earthquake Engineering*, Tokyo, V, pp. 821-826.

Ashour, S. A. and Hanson, R. D., (1987), *Elastic Seismic Response of Buildings with Supplemental Damping*, Technical Report UMCE 87-01, The University of Michigan, Ann Arbor, MI.

Bagley, R. L. and Torvik, P. J., (1983), "Fractional Calculus - A Different Approach to the Analysis of Viscoelastically Damped Structures," *AIAA Journal*, Vol. 21, No. 5, pp. 742-748.

Bailey, T. and Hubbard, J. E., (1985), "Distributed Piezoelectric-polymer Active Vibration Control of a Cantilever Beam," *Journal of Guidance, Control and Dynamics*, Vol. 8, No. 5, pp. 605-611.

Bathe, K. J., (1996), *Finite Element Procedures*, Prentice-Hall, Englewood Cliffs, NJ.

Baz, A. and Ro, J., (1993), "Partial Treatment of Flexible Beams with Active Constrained Layer Damping," *Recent Developments in Stability, Vibration and Control of Structural Systems*, ASME/AMD, pp. 61-80.

Bergman, D. M. and Goel, S. C., (1987), *Evaluation of Cyclic Testing of Steel-Plate Devices for Added Damping and Stiffness*, Technical Report UMCE 87-10, The University of Michigan, Ann Arbor, MI.

Bergman, D. M. and Hanson, R. D., (1993), "Viscoelastic Mechanical Damping Devices Tested at Real Earthquake Displacements," *Earthquake Spectra*, Vol. 9, No. 3, pp. 389-418.

Bhatti, M. A., Pister, K. S., and Polek, E., (1978), *Optimal Design of an Earthquake Isolation System*, Technical Report UCB/EERC-78/22, University of California, Berkeley, CA.

Bracci, J. M., Kunnath, S. K., and Reinhorn, A. M., (1997), "Seismic Performance and Retrofit Evaluation of Reinforced Concrete Structures," *Journal of Structural Engineering*, ASCE, Vol. 123, No. 1, pp. 3-10.

Brock, J. E., (1946), "A Note on the Damped Vibration Absorber," *Journal of Applied Mechanics*, Vol. 13, No. 4, pp. A-284.

Chaiseri, P., Fujino, Y., Pacheco, B. M., and Sun, L. M., (1989), "Interaction of Tuned Liquid Damper and Structure: Theory, Experimental Verification and Application," *Structural Engineering/Earthquake Engineering*, JSCE, Vol. 6, No. 2, pp. 273s-282s.

Chang, K. C., Lai, M. L., Soong, T. T., Hao, D. S., and Yeh, Y. C., (1993a), *Seismic Behavior and Design Guidelines for Steel Frame Structures with Added Viscoelastic Dampers*, Technical Report NCEER-93-0009, National Center for Earthquake Engineering Research, Buffalo, NY.

Chang, K. C., Shen, K. L., Soong, T. T., and Lai, M. L., (1994), "Seismic Retrofit of A Concrete Frame with Added Viscoelastic Dampers," *Proceedings of the Fifth National Conference on Earthquake Engineering*, Chicago, IL.

Chang, K. C., Soong, T. T., Lai, M. L., and Nielsen, E. J., (1993b), "Development of a Design Procedure for Structures with Added Viscoelastic Dampers," *Proceedings of ATC-17-1 on Seismic Isolation, Energy Dissipation and Active Control*, San Francisco, CA, Vol. 2, pp. 473-484.

Chang, K. C., Soong, T. T., Lai, M. L., and Nielsen, E. J., (1993c), "Viscoelastic Dampers as Energy Dissipation Devices for Seismic Applications," *Earthquake Spectra*, Vol. 9, No. 3, pp. 371-388.

Chang, K. C., Soong, T. T., Oh, S-T, and Lai, M. L., (1995), "Seismic Behavior of Steel Frame with Added Viscoelastic Dampers," *Journal of Structural Engineering,* ASCE, Vol. 121, No. 10, pp. 1418-1426.

Chang, K. C., Soong, T. T., Oh, S-T., and Lai, M .L., (1992), "Effect of Ambient Temperature on a Viscoelastically Damped Structure," *Journal of Structural Engineering,* ASCE, Vol. 118, No. 7, pp. 1955-1973.

Chang, K. C., Soong, T. T., Oh, S-T, and Lai, M. L., (1991), *Seismic Response of a 2/5 Scale Steel Structure with Added Viscoelastic Dampers,* Technical Report NCEER-91-0012, National Center for Earthquake Engineering Research, Buffalo, NY.

Chopra, A. K., (1995), *Dynamics of Structures,* Prentice Hall, Englewood Cliffs, NJ.

Chowdhury, A. H., Iwuchukwu, M. D., and Garske, J. J., (1987), "The Past and Future of Seismic Effectiveness of Tuned Mass Dampers," *Structural Control,* (Leipholz, H.H.E., Editor), Martinus Nijhoff Publishers, pp. 105-127.

Civil Engineering Research Center, (1992), *Manual of Menshin Design Method for Highway Bridges,* Ministry of Construction, Japan (in Japanese).

Clark, A. J., (1988), "Multiple Passive Tuned Mass Damper for Reducing Earthquake Induced Building Motion," *Proceedings of the Ninth World Conference on Earthquake Engineering,* Tokyo/Kyoto, Japan, Vol. 5, pp. 779-784.

Clough, R. W. and Penzien, J., (1975), *Dynamics of Structures,* McGraw-Hill, New York.

Cofie, N. G. and Krawinkler, H., (1985), "Uniaxial Cyclic Stress-Strain Behavior of Structural Steel," *Journal of Engineering Mechanics,* ASCE, Vol. 111, No. 9, pp. 1105-1120.

Constantinou, M. C. and Symans, M. D., (1993), "Experimental Study of Seismic Response of Buildings with Supplemental Fluid Dampers," *Structural Design of Tall Buildings,* Vol. 2, No. 2, pp. 93-132.

Constantinou, M. C. and Symans, M. D., (1992), *Experimental and Analytical Investigation of Seismic Response of Structures with Supplemental Fluid Viscous Dampers,* Technical Report NCEER-92-0032, National Center for Earthquake Engineering Research, Buffalo, NY.

Constantinou, M. C., Symans, M. D., Tsopelas, P., and Taylor, D. P., (1993), "Fluid Viscous Dampers in Applications of Seismic Energy Dissipation and Seismic Isolation," *Proceedings of ATC 17-1 on Seismic Isolation, Energy Dissipation and Active Control,* San Francisco, CA, Vol. 2, pp. 581-591.

Crosby, P., Kelly, J. M., and Singh, J., (1994), "Utilizing Viscoelastic Dampers in the Seismic Retrofit of a Thirteen Story Steel Frame Building," *Proceedings of the Structures Congress XII,* Atlanta, GA, pp. 1286-1291.

Dafalias, Y. F. and Popov, E. P., (1975), "A Model of Nonlinearly Hardening Materials for Complex Loading," *Acta Mechanica,* Vol. 21, pp. 173-192.

Dargush, G. F. and Soong, T. T., (1995), "Behavior of Metallic Plate Dampers in Seismic Passive Energy Dissipation Systems," *Earthquake Spectra,* Vol. 11, No. 4, pp. 545-568.

Den Hartog, J. P., (1956), *Mechanical Vibrations*, Fourth Edition, McGraw-Hill, New York.

Dowdell, D. J. and Cherry, S., (1994), "Semi-active Friction Dampers for Seismic Response Control of Structures," *Proceedings of the Fifth U.S. National Conference on Earthquake Engineering*, Chicago, IL, Vol. 1, pp. 819-828.

Earthquake Engineering Research Institute, (1995), *Northridge Earthquake of January 17, 1994 Reconaissance Report*, Supplement C to Vol. 11, Oakland, California.

Ehrgott, R. C. and Masri, S. F., (1992), "Use of Electro-rheological Materials in Intelligent Systems," *Proceedings of the US/Italy/Japan Workshop on Structural Control and Intelligent Systems*, Naples, Italy, pp. 87-100.

ENR, (1995), "Hospital Isolated from Big One," *Engineering News-Record*, September 11.

ENR, (1975), "Hancock Tower Now to Get Dampers," *Engineering News-Record*, Oct. 30, p. 11.

ENR, (1971), "Tower Cables Handle Wind, Water Tank Dampens It," *Engineering News-Record*, Dec. 9, 23.

Erdelyi, A., Magnus, W., Oberhettinger, F., and Tricomi, F. G., (1954), *Tables of Integral Transforms*, II, McGraw-Hill, New York.

Federal Emergency Management Agency, (1997), *NEHRP Guidelines for the Seismic Rehabilitation of Buildings*, Report No. FEMA-273, and *NEHRP Commentary on the Guidelines for the Seismic Rehabilitation of Buildings*, Report No. FEMA-274, Washington, D.C., October.

Federal Emergency Management Agency, (1995), *1994 NEHRP Recommended Provisions for Seismic Regulations for New Buildings*, Report No. FEMA 222A, Washington, D.C.

Ferry, J. D., (1980), *Viscoelastic Properties of Polymers*, John Wiley, New York.

Filiatrault, A. and Cherry, S., (1988), "Comparative Performance of Friction Damped Systems and Base Isolation Systems for Earthquake Retrofit and Aseismic Design," *Earthquake Engineering Structural Dynamics*, Vol. 16, pp. 389-416.

Filiatrault, A. and Cherry, S., (1987), "Performance Evaluation of Friction Damped Braced Frames Under Simulated Earthquake Loads," *Earthquake Spectra*, Vol. 3, No. 1, pp. 57-78.

FitzGerald, T. F., Anagnos, T., Goodson, M., and Zsutty, T., (1989), "Slotted Bolted Connections in Aseismic Design for Concentrically Braced Connections," *Earthquake Spectra*, Vol. 5, No. 2, pp. 383-391.

Foutch, D. A., Wood, S. L., and Brady, P. A., (1993), "Seismic Retrofit of Nonductile Reinforced Concrete Frames using Viscoelastic Dampers," *Proceedings of ATC-17-1 on Seismic Isolation, Passive Energy and Active Control*, San Francisco, CA, Vol. 2, pp. 605-616.

Fujino, Y., Pacheco, B. M., Chaiseri, P., and Sun, L. M., (1988), "Parametric Studies on Tuned Liquid Damper (TLD) Using Circular Containers by Free Oscillation Experiments," *Structural Engineering/Earthquake Engineering*, JSCE, Vol. 5, No. 2, pp. 381s-391s.

Fujino, Y., Sun, L., Pachero, B. M., and Chaiseri, P., (1992), "Tuned Liquid Damper (TLD) for Suppressing Horizontal Motion of Structures," *Journal of Engineering Mechanics*, Vol. 118, No. 10, pp. 2017-2030.

Fujita, T. (Editor), (1991), "Seismic Isolation and Response Control for Nuclear and Non-Nuclear Structures," *Special Issue for the Exhibition of Eleventh International Conference on SMiRT*, Tokyo, Japan.

Fujita, S., Fujita, T., Furuya, O., Morikawa, S., Suizu, Y., Teramoto, T., and Kitamura, H., (1992), "Development of High Damping Rubber Damper for Vibration Attenuation of High-Rise Building," *Proceedings of the Tenth World Conference on Earthquake Engineering*, Madrid, Spain, Vol. 4, pp. 2097-2101.

Fujita, S., Fujita, T., Suizu, Y., Kasahara, Y., Furuya, O., Teramoto, T., and Kitamura, H., (1993), "Energy Dissipation Characteristics of High Damping Rubber Damper for Vibration Control of High-Rise Buildings," *Transactions of the Twelfth SMiRT*, Vol. A, pp. 243-248.

Fujita, S., Furuya, O., Fujita, T., Suizu, Y., Kasahara, Y., Teramoto, T., and Kitamura, H., (1994), "Dynamic Tests on High-Damping Rubber Damper for Vibration Control of Tall Buildings," *Proceedings of the First World Conference on Structural Control*, Los Angeles, CA, Vol. 2, pp. TP3-107 -TP3-116.

Gavin, H. P. and Hanson, R. D., (1994), *Electrorheological Dampers for Structural Vibration Suppression*, Technical Report UMCEE 94-35, Department of Civil and Environmental Engineering, The University of Michigan, Ann Arbor, MI.

Gemant, A., (1936), "A Method of Analyzing Experimental Results Obtained from Elastoviscous Bodies," *Physics*, Vol. 7, No. 8, pp. 311-317.

Graesser, E. J. and Cozzarelli, F. A., (1991a), *A Multidimensional Hysteretic Model for Plastically Deforming Metals in Energy Absorbing Devices*, Technical Report NCEER-91-0006, National Center for Earthquake Engineering Research, Buffalo, NY.

Graesser, E. J. and Cozzarelli, F. A., (1991b), "Shape-memory Alloys as New Materials for Aseismic Isolation," *Journal of Engineering Mechanics*, ASCE, Vol. 117, No. 11, pp. 2590-2608.

Graesser, E. J. and Cozzarelli, F. A., (1989), *Multidimensional Models of Hysteretic Material Behavior for Vibration Analysis of Shape Memory Energy Absorbing Devices*, Technical Report NCEER-89-0018, National Center for Earthquake Engineering Research, Buffalo, NY.

Grigorian, C. E., Yang, T. S., and Popov, E. P., (1993), "Slotted Bolted Connection Energy Dissipators," *Earthquake Spectra*, Vol. 9, No. 3, pp. 491-504.

Gu, Q. and Xiang, H. F., (1994), "Vibration Control of Stay Cables in Cable-Stayed Bridges," *Proceedings of the First World Conference on Structural Control*, Los Angeles, CA, Vol. 1, pp. WA4-3 - WA4-12.

Guendeman-Israel, R. and Powell, G. H., (1977), *DRAIN-TABS - A Computerized Program for Inelastic Earthquake Response of Three Dimensional Buildings*, Technical Report UCB/EERC 77-08, University of California, Berkeley, CA.

Hanson, R. D., (1993), "Supplemental Damping for Improved Seismic Performance," *Earthquake Spectra*, Vol. 9, No. 3, pp. 319-334.

Higashino, M. and Aizawa, S., (1993), "Application of Active Mass Damper System in Actual Buildings," *Proceedings of the International Workshop on Structural Control*, (G. W. Housner and S. F. Masri, Editors), Honolulu, HI, August 5-7, USC Publication Number CE-9311, pp. 194-205.

Hrovat, D., Barak, P., and Rabins, M., (1983), "Semi-active versus Passive or Active Tuned Mass Dampers for Structural Control," *Journal of Engineering Mechanics*, ASCE, Vol. 109, No. 3, pp. 691-705.

Huerta, A. and Liu, W. K., (1988), "Viscous Flow with Large Free Surface Motion," *Computer Methods in Applied Mechanics and Engineering*, Vol. 69, pp. 277-324.

Huffmann, G. K., (1985), "Full Base Isolation for Earthquake Protection by Helical Springs and Viscodampers," *Nuclear Engineering Design*, Vol. 84, No. 2, pp. 331-338.

Hunt, J. B., (1979), *Dynamic Vibration Absorbers*, Mechanical Engineering Publications Ltd., London.

Hussain, S. M., Asher, J. W., and Ewing, R. D., (1993), "Seismic Base Isolation Design for the San Bernardino County Medical Center Replacement Project," *Proceedings of the Structures Congress 1993*, Irvine, California, Vol. 1, pp. 760-765.

Inaudi, J. A., (1997), "Modulated Homogeneous Friction, Semi-active Damping Strategy," *Earthquake Engineering and Structural Dynamics*, Vol. 26, pp. 361-376.

Inaudi, J. A., Kelly, J. M., Taniwangsa, W., and Krumme, R., (1993a), "Analytical and Experimental Study of a Mass Damper Using Shape Memory Alloys," *Proceedings of Damping '93*, San Francisco, CA, Vol. 3.

Inaudi, J. A., Kelly, J. M., and To, C. W. S., (1993b), "Statistical Linearization Method in the Preliminary Design of Structures with Energy Dissipating Devices," *Proceedings of ATC-17-1 on Seismic Isolation, Energy Dissipation, and Active Control*, San Francisco, CA, Vol. 2, pp. 509-520.

International Association for Structural Control, (1994), *Proceedings of the First World Conference on Structural Control*, Los Angeles, CA.

International Conference of Building Officials (ICBO), (1994), Uniform Building Code, Whittier, CA.

Iwan, W. D. and Gates, N. C., (1979), "Estimating Earthquake Response of Simple Hysteretic Structures," *Journal of Engineering Mechanics*, ASCE, Vol. 105, No. EM3, pp. 391-405.

Jara, J. M., Gómez-Soberón, C., Vargas, E., and Gonzàlez, R., (1993), "Seismic Performance of Buildings with Energy Dissipating Systems," *Proceedings of ATC-17-1 on Seismic Isolation, Energy Dissipation, and Active Control,* San Francisco, CA, Vol. 2, pp. 663-673.

Kageyama, M., Yoshida, O., and Yasui, Y., (1994), "A Study on Optimal Damping Systems for Connected Double Frame Structures," *Proceedings of the First World Conference on Structural Control,* Los Angeles, CA, Vol. 1, pp. WP4-32 - WP4-39.

Kanaan, A. E. and Powell, G. H., (1973), *DRAIN-2D - A General Purpose Computer Program for Dynamic Analysis of Inelastic Plane Structures,* Technical Report UCB/EERC 73-06, University of California, Berkeley, CA.

Kareem, A., (1994), "The Next Generation of Tuned Liquid Dampers," *Proceedings of the First World Conference on Structural Control,* Los Angeles, CA, pp. FP5-19 to FP5-28.

Kareem, A., (1990), "Reduction of Wind Induced Motion Utilizing a Tuned Sloshing Damper," *Journal of Wind Engineering and Industrial Aerodynamics,* Vol. 36.

Kasai, K., Munshi, J. A., Lai, M. L., and Maison, B. F., (1993), "Viscoelastic Damper Hysteretic Model: Theory, Experiment and Application," *Proceedings of ATC-17-1 on Seismic Isolation, Energy Dissipation, and Active Control,* San Francisco, CA, Vol. 2, pp. 521-532.

Kawashima, K. and Unjoh, S., (1994) "Menshin Design of Highway Bridges in Japan," *Proceedings of the Third US-Japan Workshop on Earthquake Protective Systems for Bridges,* (I. G. Buckle and I. M. Friedland, Editors), Berkeley, CA, Technical Report NCEER-94-0009, National Center for Earthquake Engineering Research, Buffalo, NY.

Kawashima, K., Unjoh, S., and Shimizu, K., (1992), "Experiments on Dynamic Characteristics of Variable Damper," *Proceedings of the Japan National Symposium on Structural Response Control,* Tokyo, Japan, Vol. 121.

Kaynia, A. M., Veneziano, D., and Biggs, J. M., (1981), "Seismic Effectiveness of Tuned Mass Dampers," *Journal of the Structural Division,* ASCE, Vol. 107, pp. 1465-1484.

Keel, C. J. and Mahmoodi, P., (1986), "Designing of Viscoelastic Dampers for Columbia Center Building," *Building Motion in Wind,* (N. Isyumov and T. Tschanz, Editors), ASCE, NY, pp. 66-82.

Keightley, W. O., (1977), "Building Damping by Coulomb Friction," *Sixth World Conference on Earthquake Engineering,* New Delhi, India, pp. 3043-3048.

Kelly, J. M., (1993), *Earthquake-Resistant Design with Rubber,* Springer-Verlag, London.

Kelly, J. M., (1988), *Base Isolation in Japan, 1988,* Technical Report UCB/EERC 88/20, University of California, Berkeley, CA.

Kelly, J. M., Skinner, R. I., and Heine, A. J., (1972), "Mechanisms of Energy Absorption in Special Devices for Use in Earthquake Resistant Structures," *Bulletin of the New Zealand National Society for Earthquake Engineering,* Vol. 5, pp. 63-88.

Kirekawa, A., Ito, Y., and Asano, K., (1992), "A Study of Structural Control using Viscoelastic Material," *Proceedings of the Tenth World Conference on Earthquake Engineering*, Madrid, Spain, Vol. 4, pp. 2047-2054.

Kitamura, H., Fujita, T., Teramoto, T., and Kihara, H., (1988), "Design and Analysis of a Tower Structure with a Tuned Mass Damper," *Proceedings of the Ninth World Conference on Earthquake Engineering*, Tokyo, Japan, Vol. 8, pp. 415-420.

Kobori, T., Takahashi, M., Nasu, T., Niwa, N., and Ogasawara, K., (1993), "Seismic Response Controlled Structure with Active Variable Stiffness System," *Earthquake Engineering and Structural Dynamics*, Vol. 22, pp. 925-941.

Krieg, R. D., (1975), "A Practical Two Surface Plasticity Theory," *Journal of Applied Mechanics*, ASME, Vol. E42, pp. 641-646.

Kurino, H., Kobori, T., Takahashi, M., Niwa, N., Kurata, N., and Mizuno, T., (1996), "Development and Modeling of Variable Damping Unit for Active Variable Damping System," *Proceedings of the Eleventh World Conference on Earthquake Engineering*, Acapulco, Mexico.

Kwok, K. C. S., (1984), "Damping Increase in Building with Tuned Mass Damper," *Journal of Engineering Mechanics*, ASCE, Vol. 110, No. 11, pp. 1645-1649.

Kwok, K. C. S. and MacDonald, P. A., (1990), "Full-scale Measurements of Acceleration Response of Sydney Tower," *Engineering Structures*, Vol. 12, pp. 153-162.

Kwok, K. C. S. and MacDonald, P. A., (1987), "Wind-induced Response of Sydney Tower," *Proceedings of the First National Structural Engineering Conference*, pp. 19-24.

Lai, M. L., Chang, K. C., Soong, T. T., Hao, D. S., and Yeh, Y. C., (1995), "Full-scale Viscoelastically Damped Steel Frame," *Journal of Structural Engineering*, ASCE, Vol. 121, No. 10, pp. 1443-1447.

Lepelletier, T. G. and Raichlen, F., (1988), "Nonlinear Oscillations in Rectangular Tanks," *Journal of Engineering Mechanics*, Vol. 114, pp. 1-23.

Liang, Z. and Lee, G. C., (1991), *Damping of Structures: Part 1 - Theory of Complex Damping*, Technical Report NCEER-91-0004, National Center for Earthquake Engineering Research, Buffalo, NY.

Lin, R. C., Liang, Z., Soong, T. T., and Zhang, R. H., (1991), "An Experimental Study on Seismic Structural Response with Added Viscoelastic Dampers," *Engineering Structures*, Vol. 13, pp. 75-84.

Lin, R. C., Liang, Z., Soong, T. T., and Zhang, R. H., (1988), *An Experimental Study of Seismic Structural Response with Added Viscoelastic Dampers*, Technical Report NCEER-88-0018, National Center for Earthquake Engineering Research, Buffalo, NY.

Lobo, R. F., Bracci, J. M., Shen, K. L., Reinhorn, A. M., and Soong, T. T., (1993a), *Inelastic Response of Reinforced Concrete Structures with Viscoelastic Braces*, Technical Report NCEER-93-0006, National Center for Earthquake Engineering Research, Buffalo, NY.

Lobo, R. F., Bracci, J. M., Shen, K. L., Reinhorn, A. M., and Soong, T. T., (1993b), "Inelastic Response of R/C Structures with Viscoelastic Braces," *Earthquake Spectra,* Vol. 9, No. 3, pp. 419-446.

Mahmoodi, P., (1969), "Structural Dampers," *Journal of the Structural Division,* ASCE, Vol. 95, pp. 1661-1672.

Mahmoodi, P., Robertson, L. E., Yontar, M., Moy, C., and Feld, I., (1987), "Performance of Viscoelastic Dampers in World Trade Center Towers," *Dynamic of Structures, Structures Congress '87,* Orlando, FL.

Makris, N., (1992), *Theoretical and Experimental Investigation of Viscous Dampers in Applications of Seismic and Vibration Isolation,* Ph.D. Dissertation, State University of New York at Buffalo, NY.

Makris, N. and Constantinou, M. C., (1993), "Models of Viscoelasticity with Complex Order Derivatives," *Journal of Engineering Mechanics,* ASCE, Vol. 119, Vol. 7, pp. 1453-1464.

Makris, N. and Constantinou, M. C., (1992), "Spring-Viscous Damper Systems for Combined Seismic and Vibration Isolation," *Earthquake Engineering and Structural Dynamics,* Vol. 21, pp. 649-664.

Makris, N. and Constantinou, M. C., (1991), "Fractional-Derivative Maxwell Model for Viscous Dampers," *Journal of Structural Engineering,* ASCE, Vol. 117, No. 9, pp. 2708-2724.

Makris, N. and Constantinou, M. C., (1990), *Viscous Dampers: Testing, Modeling and Application in Vibration and Seismic Isolation,* Technical Report NCEER-90-0028, National Center for Earthquake Engineering Research, Buffalo, NY.

Makris, N. and Deoskar, H. S., (1996), "Prediction of Observed Response of Base-Isolated Structure," *Journal of Structural Engineering,* Vol. 122, No. 5, pp. 485-493.

Makris, N., Burton, S., Hill, D., and Jordan, M., (1996), "Analysis and Design of an Electrorheological Damper for Seismic Protection of Structures," *Journal of Engineering Mechanics,* ASCE, in press.

Makris, N., Constantinou, M. C., and Dargush, G. F., (1993), "Analytical Model of Viscoelastic Fluid Dampers," *Journal of Structural Engineering,* ASCE, Vol. 119, No. 11, pp. 3310-3325.

Makris, N., Dargush, G. F., and Constantinou, M. C., (1995), "Dynamic Analysis of Viscoelastic Fluid Dampers," *Journal of Engineering Mechanics,* ASCE, Vol. 121, No. 10, pp. 1114-1121.

Marquardt, D. W., (1963), "An Algorithm for Least-Squares Estimation of Nonlinear Parameters," *Journal of the Society for Industrial and Applied Mathematics,* Vol. 11, No. 2, pp. 431-441.

Martinez-Romero, E., (1993), "Experiences on the Use of Supplemental Energy Dissipators on Building Structures," *Earthquake Spectra,* Vol. 9, No. 3, pp. 581-624.

Mataki, Y., Ohkuma, T., Kanda, J., Kitamura, H., Kawabata, S., and Ohtake, K., (1989), *Full-scale Measurement of Wind Actions on Chiba Port Tower*, Takenaka Technical Research Report No. 42.

Mayes, R. L. and Mowbray, N. A., (1975), "The Effect of Coulomb Damping on Multidegree of Freedom Elastic Structures," *Earthquake Engineering and Structural Dynamics*, Vol. 3, pp. 275-286.

Mei, C. C., (1983), *The Applied Dynamics of Ocean Waves*, John Wiley, New York.

Mizuno, T., Kobori, T. Hirai, J., Matsunaga, Y., and Niwa, N., (1992), "Development of Adjustable Hydraulic Dampers for Seismic Response Control of Large Structure," *ASME PVP Conference*, PVP-229, pp. 163-170.

Miyazaki, M., (1994), "Aerodynamic Control Method for Vibration of Bridge Cables," *Proceedings of the First World Conference on Structural Control*, Los Angeles, CA, Vol. 1, pp. WA4-13 - WA4-22.

Miyazaki, M. and Mitsusaka, Y., (1992), "Design of a Building with 20% or Greater Damping," *Tenth World Conference on Earthquake Engineering* , Madrid, Spain, pp. 4143-4148.

Modi, V. J. and Welt, F., (1987), "Vibration Control using Nutation Dampers," *International Conference on Flow Induced Vibrations*, Bowness on Windermere, England, pp. 369-376.

Nagarajaiah, S., (1995), *Development of Novel Semi-active Continuous Variable Stiffness Device, Application in SDOF Cantilever Model and Shake Table Tests*, Internal Report, Department of Civil Engineering, University of Missouri, Columbia, MO.

Nakamura, Y., Watanabe, H., and Kawamata, S., (1988), "Seismic Response of Structures by Accelerated Liquid Mass Damper," *Proceedings of the Ninth World Conference on Earthquake Engineering*, Tokyo-Kyoto, Japan, Vol. V, pp. 785-790.

Newmark, N. M. and Hall, W. J., (1982), *Earthquake Spectra and Design*, Earthquake Engineering Research Institute, Oakland, CA.

Nims, D. K., Richter, P. J., and Bachman, R. E., (1993a), "The Use of the Energy Dissipating Restraint for Seismic Hazard Mitigation," *Earthquake Spectra*, Vol. 9, No. 3, pp. 467-489.

Nims, D. K., Inaudi, J. A., Richter, P. J., and Kelly, J. M., (1993b), "Application of the Energy Dissipating Restraint to Buildings," *Proceedings of ATC-17-1 on Seismic Isolation, Energy Dissipation, and Active Control*, San Francisco, CA, Vol. 2, pp. 627-638.

Nishimura, I., Kobori, T., and Sakamoto, M., (1993), "Active Passive Composite Tuned Mass Damper," *Proceedings of ATC-17-1 Seminar on Active Isolation, Passive Energy Dissipation and Active Control*, San Francisco, CA, Vol. 2, pp. 737-748.

Okamoto, T. and Kawahara, M., (1990), "Two-dimensional Sloshing Analysis by Lagrangian Finite Element Method," *International Journal for Numerical Methods in Fluids*, Vol. 11, pp. 453-477.

Ölander, A., (1932), "An Electrochemical Investigation of Solid Cadmium-Gold Alloys," *Journal of the American Chemical Society,* Vol. 54, pp. 3819-3833.

Oldham, K. B. and Spanier, J., (1974), *The Fractional Calculus,* Academic Press, New York.

Özdemir, H., (1976), *Nonlinear Transient Dynamic Analysis of Yielding Structures,* Ph.D. Dissertation, University of California, Berkeley, CA.

Pall, A. S. and Marsh, C., (1982), "Response of Friction Damped Braced Frames," *Journal of the Structural Division,* ASCE, Vol. 108, No. ST6, pp. 1313-1323.

Pall, A. S., Marsh, C., and Fazio, P., (1980), "Friction Joints for Seismic Control of Large Panel Structures," *Journal of the Prestressed Concrete Institute,* Vol. 25, No. 6, pp. 38-61.

Pall, A. S. and Pall, R., (1996), "Friction-Dampers for Seismic Control of Buildings: A Canadian Experience," *Proceedings of the Eleventh World Conference on Earthquake Engineering,* Acapulco, Mexico.

Pall, A. S. and Pall, R., (1993), "Friction-Dampers Used for Seismic Control of New and Existing Building in Canada," *Proceedings of the ATC-17-1 Seminar on Isolation, Energy Dissipation and Active Control,* San Francisco, CA, Vol. 2, pp. 675-686.

Pall, A., Vezina, S., Proulx, P., and Pall, R., (1993), "Friction-Dampers for Seismic Control of Canadian Space Agency Headquarters," *Earthquake Spectra,* Vol. 9, No. 3, pp. 547-557.

Papalou, A. and Masri, S. F., (1994), "An Experiment Study on Particle Dampers under Random Excitation," *Proceedings of the First World Conference on Structural Control,* Los Angeles, CA, Vol. 3, pp. FP2-18 - FP2-24.

Pasquin, C., Pall, A., and Pall, R., (1994), "High-Tech Seismic Rehabilitation of Casino de Montreal," *Structures Congress, 1994,* Atlanta, Georgia, Vol. 2, pp. 1292-1297.

Patten, W. N., Sack, R. L., and He, Q., (1996), "Controlled Semiactive Hydraulic Vibration Absorber for Bridges," *Journal of Structural Engineering,* ASCE, Vol. 122, No. 2, pp. 187-192.

Paulay, T. and Priestly, M. J. N., (1992), *Seismic Design of Reinforced Concrete and Masonry Buildings,* J. Wiley & Sons, New York.

Pekcan, G., Mander, J. B., and Chen, S. S., (1995), "The Seismic Response of a 1:3 Scale Model R.C. Structure with Elastomeric Spring Dampers," *Earthquake Spectra,* Vol. 11, No. 2, pp. 249-267.

Perry, C. L., Fierro, E. A., Sedarat, H., and Scholl, R. E., (1993), "Seismic Upgrade in San Francisco Using Energy Dissipation Devices," *Earthquake Spectra,* Vol. 9, No. 3, pp. 559-579.

Petersen, N. R., (1981), "Using Servohydraulics to Control High-rise Building Motion," *Proceedings of the National Convention on Fluid Power,* Chicago, IL, pp. 209-213.

Petersen, N. R., (1980), "Design of Large Scale TMD," *Structural Control,* North Holland, pp. 581-596.

Pong, W. S., Tsai, C. S., and Lee, G.C., (1994), *Seismic Study of Building Frames with Added Energy-absorbing Devices,* Technical Report NCEER-94-0016, National Center for Earthquake Engineering Research, Buffalo, NY.

Press, W. H., Teukolsky, S. A., Vetterling, W. T., and Flannery, B. P., (1992), *Numerical Recipes in FORTRAN,* Cambridge University Press, Cambridge, UK.

Reinhorn, A. M., Li, C., and Constantinou, M. C., (1995), *Experimental and Analytical Investigation of Seismic Retrofit of Structures with Supplemental Damping Part I: Fluid Viscous Damping Devices,* Technical Report NCEER-95-0001, National Center for Earthquake Engineering Research, Buffalo, NY.

Reinhorn, A. M., Soong, T. T., Lin, R. C., Riley, M. A., Wang, Y. P., Aizawa, S., and Higashino, M., (1992), *Active Bracing System: A Full Scale Implementation of Active Control,* Technical Report NCEER-92-0020, National Center for Earthquake Engineering Research, Buffalo, NY.

Richter, P. J., Nims, D. K., Kelly, J. M., and Kallenbach, R. M., (1990), "The EDR - Energy Dissipating Restraint, A New Device for Mitigation of Seismic Effects," *Proceedings of the 1990 Structural Engineers Association of California (SEAOC) Convention,* Lake Tahoe, NV.

Rivlin, R. S., (1981), "Some Comments on the Endochronic Theory of Plasticity," *International Journal of Solids and Structures,* Vol. 17, pp. 231-248.

Roberson, R. E., (1952), "Synthesis of a Non-linear Dynamic Vibration Absorber," *Journal of the Franklin Institute,* Vol. 254, pp. 205-220.

Roik, K., Dorka, U., and Dechent, P., (1988), "Vibration Control of Structures Under Earthquake Loading by Three-Stage Friction-Grip Elements," *Earthquake Engineering Structural Dynamics,* Vol. 16, pp. 501-521.

Sack, R. L. and Patten, W., (1993), "Semiactive Hydraulic Structural Control," *Proceedings of the International Workshop on Structural Control,* (G. W. Housner and S.F. Masri, Editors), Honolulu, HI, August 5-7, USC Publication Number CE-9311, pp. 417-431.

Sakai, F., (1989), "Tuned Liquid Column Damper-New Type Device for Suppression of Building Vibrations," *Proceedings, International Conference on High Rise Buildings,* Nanjing, China.

Sakamoto, M. and Kobori, T., (1993), "Practical Applications of Active and Hybrid Response Control Systems," *Proceedings of the International Workshop on Structural Control,* (G. W. Housner and S. F. Masri, Editors), Honolulu, HI, August 5-7, USC Publication Number CE-9311, pp. 432-446.

Sakurai, T., Shibata, K., Watanabe, S., Endoh, A., Yamada, K., Tanaka, N., and Kobayashi, H., (1992), "Application of Joint Damper to Thermal Power Plant Buildings," *Proceedings of the Tenth World Conference on Earthquake Engineering,* Madrid, Spain, Vol. 7, pp. 4149-4154.

Scholl, R. E., (1993), "Design Criteria for Yielding and Friction Energy Dissipators," *Proceedings of ATC-17-1 on Seismic Isolation, Energy Dissipation, and Active Control,* San Francisco, CA, Vol. 2, pp. 485-495.

Seleemah, A. A. and Constantinou, M. C., (1997), *Investigation of Seismic Response of Buildings with Linear and Nonlinear Fluid Viscous Dampers,* Technical Report NCEER-97-0004, National Center for Earthquake Engineering Research, Buffalo, NY.

Setareh, M., (1994), "Use of the Doubly-Tuned Mass Dampers for Passive Vibration Control," *Proceedings of the First World Conference on Structural Control,* Los Angeles, CA, Vol. 1, pp. WP4-12 - WP4-21.

Shen, I. Y., (1994), "Bending-vibration Control of Composite and Isotropic Plates through Intelligent Constrained-layer Treatments," *Smart Materials and Structures,* Vol. 3, No. 1, pp. 59-70.

Shen, K. L. and Soong, T. T., (1995), "Modeling of Viscoelastic Dampers for Structural Applications," *Journal of Engineering Mechanics,* ASCE, Vol. 121, No. 6, pp. 694-701.

Shen, K. L., Soong, T. T., Chang, K. C., and Lai, M. L., (1995), "Seismic Behavior of Reinforced Concrete Frame with Added Viscoelastic Dampers," *Engineering Structures,* Vol. 17, No. 5, pp. 372-380.

Shimizu, T. and Hayama, S., (1987), "Nonlinear Response of Sloshing Based on the Shallow Water Wave Theory," *JSME International Journal,* Vol. 30, pp. 806-813.

Skilling, J. B., Tschanz, T., Isyumov, N. Loh, P., and Davenport, A. G., (1986), "Experimental Studies, Structural Design and Full-scale Measurements for the Columbia SeaFirst Center," *Building Motion in Wind,* (N. Isyumov and T. Tschanz, Editors), ASCE, New York, pp. 1-22.

Skinner, R. I., Kelly, J. M., and Heine, A. J., (1975), "Hysteresis Dampers for Earthquake-Resistant Structures," *Earthquake Engineering and Structural Dynamics,* Vol. 3, pp. 287-296.

Skinner, R. I., Robinson, W. H., and McVerry, G. H., (1993), *An Introduction to Seismic Isolation,* J. Wiley & Sons, Chistester, England.

Skinner, R. I., Tyler, R. G., Heine, A. J., and Robinson, W. H., (1980), "Hysteretic Dampers for the Protection of Structures from Earthquakes," *Bulletin of the New Zealand Society of Earthquake Engineering,* Vol. 13, No. 1, pp. 22-36.

Soong, T. T., (1990), *Active Structural Control: Theory and Practice,* Longman, London, and Wiley, New York.

Soong, T. T. and Constantinou, M. C., (Editors), (1994), *Passive and Active Structural Vibration Control in Civil Engineering,* Springer-Verlag, Wien-New York.

Soong, T. T. and Dargush, G. F., (1997), *Passive Energy Dissipation Systems in Structural Engineering,* Wiley, Chichester, UK and New York, NY.

Soong, T. T. and Grigoriu, M., (1993), *Random Vibration of Mechanical and Structural Systems,* Prentice Hall, Englewood, NJ.

Soong, T. T. and Lai, M. L., (1991), "Correlation of Experimental Results With Predictions of Viscoelastic Damping of a Model Structure," *Proceedings of Damping 1991*, San Diego, CA, pp. FCB.1-FCB.9.

Soong, T. T., Reinhorn, A. M., Aizawa, S., and Higashino, M., (1994), "Recent Structural Applications of Active Control Technology," *Journal of Structural Control*, Vol. 1, No. 2, pp. 5-21.

Spencer, B. F., Jr., Dyke, S. J., Sain, M. K., and Carlson, J. D., (1997), "Phenomenological Model of a Magnetorheological Damper," *Journal of Engineering Mechanics*, ASCE, Vol. 123, No. 3, pp. 230-238.

Spencer, B. F., Jr. Dyke, S. J., Sain, M. K., and Carlson, J. D., (1996), "Idealized Model of a Magnetorheological Damper," *Analysis and Computation*, (F. K. Cheng, Editor), ASCE, New York, pp. 361-370.

Structural Engineers Association of California, (1995), *Recommended Lateral Force Requirements and Commentary*, Sixth Edition, Sacramento, CA.

Structural Engineers Association of Northern California, (1993), *Tentative Seismic Design Requirements for Passive Energy Dissipation Systems*, Draft, San Francisco, CA.

Su, T. C., Lou, Y. K., Flipse, J. E., and Bridges, T. J., (1982), *A Nonlinear Analysis of Liquid Sloshing in Rigid Containers*, Department of Transportation, DOT/RSPA/DMA-50/82/1.

Su, Y-F. and Hanson, R. D., (1990), *Seismic Response of Building Structures with Mechanical Damping Devices*, Technical Report UMCE 90-02, The University of Michigan, Ann Arbor, MI.

Sun, L. M., (1991), *Semi-Analytical Modeling of the Tuned Liquid Damper with Emphasis on Damping of Liquid Sloshing*, Ph.D. Dissertation, University of Tokyo, Japan.

Sun, L. M., Fujino, Y., Chaiseri, P., and Pacheco, B. M., (1995), "The Properties of Tuned Liquid Dampers Using a TMD Analogy," *Earthquake Engineering and Structural Dynamics*, Vol. 24, pp. 967-976.

Sun, L. M., Fujino, Y., Pacheco, B. M., and Isobe, M., (1989), "Nonlinear Waves and Dynamic Pressures in Rectangular Tuned Liquid Damper (TLD) - Simulation and Experimental Verification," *Structural Engineering/Earthquake Engineering*, JSCE, Vol. 6, No. 2, pp. 251s-262s.

Symans, M. D. and Constantinou, M. C., (1995), *Development and Experimental Study of Semi-active Fluid Damping Devices for Seismic Protection of Structures*, Technical Report NCEER-95-0011, National Center for Earthquake Engineering Research, Buffalo, NY.

Tamura, Y., Fujii, K., Ohtsuki, T., Wakahara, T., and Koshaka, R., (1995), "Effectiveness of Tuned Liquid Dampers and Wind Excitations," *Engineering Structures*, Vol. 17, No. 9, pp. 609-621.

Tamura, Y., Shimada, K., Sasaki, A., Koshaka, R., and Fujii, K., (1994), "Variation of Structural Damping Ratios and Natural Frequencies of Tall Buildings During Strong Winds," *Proceedings of the Ninth International Conference on Wind Engineering,* New Delhi, India, Vol. 3, pp. 1396-1407.

Taylor, D. P. and Constantinou, M. C., (1996), "Fluid Dampers for Applications of Seismic Energy Dissipation and Seismic Isolation," *Proceedings of the Eleventh World Conference on Earthquake Engineering,* Acapulco, Mexico.

Taylor, D. P. and Constantinou, M. C., (1995), "Testing Procedures for High Output Fluid Viscous Dampers Used in Building and Bridge Structures to Dissipate Seismic Energy," *Shock and Vibration,* Vol. 2, No. 5, pp. 373-381.

Tezcan, S. and Civi, A., (1979), "Reduction in Earthquake Response of Structures by Means of Vibration Isolators," *Proceedings of the Second U.S. National Conference on Earthquake Engineering,* Earthquake Engineering Research Institute, Stanford University, CA, pp. 433-442.

Tsai, C. S. and Lee, H. H., (1993), "Application of Viscoelastic Dampers to High-Rise Buildings," *Journal of Structural Engineering,* ASCE, Vol. 119, No. 4, pp. 1222-1233.

Tsai, C. S. and Tsai, K. C., (1995), "TPEA Device as Seismic Damper for High-Rise Buildings," *Journal of Engineering Mechanics,* ASCE, Vol. 121, No. 10, pp. 1075-1081.

Tsai, K. C., Chen, H. W., Hong, C. P., and Su, Y. F., (1993), "Design of Steel Triangular Plate Energy Absorbers for Seismic-Resistant Construction," *Earthquake Spectra,* Vol. 9, No. 3, pp. 505-528.

Tsopelas, P. and Constantinou, M. C., (1994), *NCEER-Taisei Corporation Research Program on Sliding Seismic Isolation Systems for Bridges: Experimental and Analytical Study of a System Consisting of Sliding Bearings and Fluid Restoring Force/Damping Devices,* Technical Report NCEER-94-0014, National Center for Earthquake Engineering Research, Buffalo, NY.

Tsopelas, P., Constantinou, M. C., Okamoto, S., Fujii, S., and Ozaki, D., (1996), "Experimental Study of Bridge Seismic Sliding Isolation Systems," *Engineering Structures,* Vol. 18, No. 4, pp. 301-310.

Tsopelas, P., Okamoto, S., Constantinou, M. C., Ozaki, D., and Fujii, S., (1994), *NCEER-Taisei Corporation Research Program on Sliding Isolation Systems for Bridges: Experimental and Analytical Study of Systems Consisting of Sliding on Bearings, Rubber Restoring Force Devices and Fluid Dampers,* Technical Report NCEER-94-0002, National Center for Earthquake Engineering Research, Buffalo, NY.

Tyler, R. G., (1985), "Test on a Brake Lining Damper for Structures," *Bulletin of the New Zealand National Society for Earthquake Engineering,* Vol. 18, No. 3, pp. 280-284.

Uang, C-M and Bertero, V. V., (1988), *Use of Energy as a Design Criterion in Earthquake-Resistant Design,* Technical Report UCB/EERC-88/18, University of California, Berkeley, CA.

Ueda, T., Nakagaki, R., and Koshida, K., (1992), "Suppression of Wind Induced Vibration by Dynamic Dampers in Tower-like Structures," *Proceedings of the Eighth International Conference on Wind Engineering*, (A. G. Davenport et al., Editors), London, Ontario, Canada, pp. 1907-1918.

Valanis, K. C., (1971), "A Theory of Viscoplasticity without a Yield Surface," *Archives of Mechanics*, Vol. 23, pp. 517-534.

Valles, R. E., Reinhorn, A. M., Madan, A., and Barron, R., (1997), *Seismic Evaluation of a Low-Rise RC Building in the Vicinity of the New Madrid Seismic Zone*, Technical Report NCEER-xx-xxxx, National Center for Earthquake Engineering Research, Buffalo, NY, (to be published).

Vezina, S., Proulx, P., Pall, R., and Pall, A., (1992), "Friction-Dampers for Aseismic Design of Canadian Space Agency," *Proceedings of the Tenth World Conference on Earthquake Engineering*, Madrid, Spain, pp. 4123-4128.

Villaverde, R., (1994), "Seismic Control of Structures with Damped Resonant Appendages," *Proceedings of the First World Conference on Structural Control*, Los Angeles, CA, Vol. 1, pp. WP4-113 - WP4-122.

Wakahara, T., Ohyama, T., and Fujii, K., (1989), "Suppression of Wind-induced Vibration of a Tall Building Using Tuned Liquid Damper," *Proceedings of the Symposium on Serviceability of Buildings*, Tokyo.

Warburton, G. B., (1982), "Optimal Absorber Parameters for Various Combinations of Response and Excitation Parameters," *Earthquake Engineering and Structural Dynamics*, Vol. 10, pp. 381-401.

Welt, F. and Modi, V. J., (1989a), "Vibration Damping Through Liquid Sloshing: Part I - A Nonlinear Analysis," *Proceedings of Diagnostics, Vehicle Dynamics and Special Topics*, ASME, *Design Engineering Division (DE)*, Vol. 18-5, pp. 149-156.

Welt, F. and Modi, V. J. (1989b), "Vibration Damping Through Sloshing: Part II - Experimental Results," *Proceedings of Diagnostics, Vehicle Dynamics and Special Topics*, ASME, *Design Engineering Division (DE)*, Vol. 18-5, pp. 157-165.

Whittaker, A. S., Bertero, V., Alonso, J., and Thompson, C., (1989), *Earthquake Simulator Testing of Steel Plate Added Damping and Stiffness Elements*, Technical Report EERC-89/02, University of California, Berkeley, CA.

Whittaker, A. S., Bertero, V. V., Thompson, C. L., and Alonso, J. L., (1991), "Seismic Testing of Steel Plate Energy Dissipation Devices," *Earthquake Spectra*, Vol. 7, No. 4, pp. 563-604.

Williams, M. L., (1964), "Structural Analysis of Viscoelastic Materials," *AIAA Journal*, Vol. 2, No. 5, pp. 785-808.

Wirsching, P. H. and Campbell, G. W., (1974), "Minimal Structural Response under Random Excitation Using the Vibration Absorbers," *Earthquake Engineering Structural Dynamics*, Vol. 2, pp. 303-312.

Wirsching, P. H and Yao, J. T. P., (1970), "Modal Response of Structures," *Journal of the Structural Division*, ASCE, Vol. 96, No. 4, pp. 879-883.

Witting, P. R. and Cozzarelli, F. A., (1992), *Shape Memory Structural Dampers: Material Properties, Design and Seismic Testing,* Technical Report NCEER 92-0013, National Center for Earthquake Engineering Research, Buffalo, NY.

Xia, C. and Hanson, R. D., (1992), "Influence of ADAS Element Parameters on Building Seismic Response," *Journal of Structural Engineering,* ASCE, Vol. 118, No. 7, pp. 1903-1918.

Xu, K. and Igusa, T., (1992), "Dynamic Characteristics of Multiple Substructures with Closely Spaced Frequencies," *Earthquake Engineering and Structural Dynamics,* Vol. 21, pp. 1059-1070.

Xu, Y. L., Kwok, K. C. S., and Samali, B., (1992a), "Control of Wind Induced Tall Building Vibration by Tuned Mass Dampers," *Journal of Wind Engineering and Industry Aerodynamics,* Vol. 40, No. 1 , pp. 1-32.

Xu, Y. L., Samali, B., and Kwok, K. C. S., (1992b), "Control of Along Wind Response of Structures by Mass and Liquid Dampers," *Journal of Engineering Mechanics,* ASCE, Vol. 118, No. 1, pp. 20-39.

Yamada, K. and Kobori, T., (1995), "Control Algorithm for Estimating Future Responses of Active Variable Stiffness Structure," *Earthquake Engineering Structural Dynamics,* Vol. 24, pp. 1085-1099.

Yamaguchi, H. and Harnpornchai, N., (1993), "Fundamental Characteristics of Multiple Tuned Mass Dampers for Suppressing Harmonically Forced Oscillations," *Earthquake Engineering Structural Dynamics,* Vol. 22, pp. 51-62.

Yang, C. and Lu, L. W., (1994), "Seismic Response Control of Cable-stayed Bridges by Semi-active Friction Damping," *Proceedings of the U.S. National Conference Earthquake Engineering,* Chicago, IL, Vol. 1, pp. 911-920.

Yoshida, K., (1996), "Research Trends on Active Vibration Control and Smart Structures in Japan," *Proceedings of the US/Japan Workshop on Smart Structures Technology,* Silver Spring, MD.

Zhang, R. H. and Soong, T. T., (1992), "Seismic Design of Viscoelastic Dampers for Structural Applications," *Journal of Structural Engineering,* ASCE, Vol. 118, No. 5, pp. 1375-1392.

Zhang, R. H., Soong, T. T., and Mahmoodi, P., (1989), "Seismic Response of Steel Frame Structures with Added Viscoelastic Dampers," *Earthquake Engineering and Structural Dynamics,* Vol. 18, pp. 389-396.

Zienkiewicz, O. C. and Taylor, R. L., (1989), *The Finite Element Method,* Volumes 1 and 2, Fourth Edition, McGraw-Hill, London.

A U T H O R I N D E X

STRUCTURES INDEX

S U B J E C T   I N D E X

CONTRIBUTORS

Dr. Michael C. Constantinou
Professor
Department of Civil Engineering
132 Ketter Hall
State University of New York at Buffalo
Buffalo, NY 14260
constan1@eng.buffalo.edu

Dr. Gary F. Dargush
Research Associate Professor
Department of Civil Engineering
234 Ketter Hall
State University of New York at Buffalo
Buffalo, NY 14260
gdargush@eng.buffalo.edu

Dr. Tsu-Teh Soong
Samuel P. Capen Professor of Civil Engineering
Department of Civil Engineering
238 Ketter Hall
State University of New York at Buffalo
Buffalo, NY 14260
tsoong@eng.buffalo.edu

MONOGRAPHS AND SPECIAL PUBLICATIONS

Economic Consequences of Earthquakes: Preparing for the Unexpected, *edited by Barclay G. Jones*

Passive Energy Dissipation Systems for Structural Design and Retrofit, *by M. C. Constantinou, T. T. Soong, and G. F. Dargush*

Engineering and Socioeconomic Impacts of Earthquakes: An Analysis of Electricity Lifeline Disruptions in the New Madrid Area, *edited by M. Shinozuka, A. Rose, and R. T. Eguchi*